

การประเมินผลและการคาดการณ์เชิงพื้นที่ของปรากฏการณ์เกาะความร้อน
ในเขตเมืองบริเวณกรุงเทพมหานครและปริมณฑล

นางสาววิลาวัลย์ ประสมทรัพย์

วิทยานิพนธ์นี้เป็นส่วนหนึ่งของการศึกษาตามหลักสูตรปริญญาวิทยาศาสตรดุษฎีบัณฑิต
สาขาวิชาภูมิสารสนเทศ

มหาวิทยาลัยเทคโนโลยีสุรนารี

ปีการศึกษา 2560

**SPATIAL EVALUATION AND PREDICTION OF URBAN
HEAT ISLAND PHENOMENA IN BANGKOK
AND ITS VICINITY**

Wilawan Prasomsup

**A Thesis Submitted in Partial Fulfillment of the Requirements for the
Degree of Doctor of Philosophy in Geoinformatics**

Suranaree University of Technology

Academic Year 2017

**SPATIAL EVALUATION AND PREDICTION OF URBAN HEAT
ISLAND PHENOMENA IN BANGKOK AND ITS VICINITY**

Suranaree University of Technology has approved this thesis submitted in partial fulfillment of the requirements for the Degree of Doctor of Philosophy.

Thesis Examining Committee



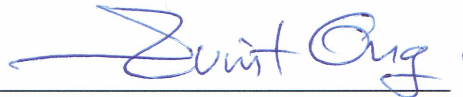
(Assoc. Prof. Dr. Sura Pattanakiat)

Chairperson



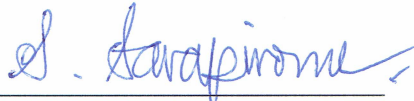
(Assoc. Prof. Dr. Songkot Dasananda)

Member (Thesis Advisor)



(Assoc. Prof. Dr. Suwit Ongsomwang)

Member



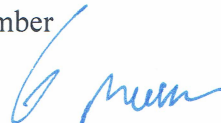
(Asst. Prof. Dr. Sunya Sarapirome)

Member



(Asst. Prof. Dr. Omprapa Pummakarnchana Robert)

Member



(Asst. Prof. Dr. Worawat Meevasana)



(Prof. Dr. Santi Maensiri)

Vice Rector for Academic Affairs
and Internationalisation

Dean of Institute of Science

วิลาวัณย์ ประสมทรัพย์ : การประเมินผลและการคาดการณ์เชิงพื้นที่ของปรากฏการณ์เกาะความร้อนในเขตเมืองบริเวณกรุงเทพมหานครและปริมณฑล (SPATIAL EVALUATION AND PREDICTION OF URBAN HEAT ISLAND PHENOMENA IN BANGKOK AND ITS VICINITY) อาจารย์ที่ปรึกษา : รองศาสตราจารย์ ดร.ทรงกต ทศานนท์, 264 หน้า.

การประยุกต์ใช้ข้อมูลอุณหภูมิพื้นผิวดินจากข้อมูลดาวเทียมเพื่อการวิจัยเชิงลึกเกี่ยวกับปรากฏการณ์เกาะความร้อนในเขตเมือง (UHI) ในประเทศไทยยังมีค่อนข้างน้อย ข้อมูลอุณหภูมิพื้นผิวดินส่วนใหญ่ถูกนำไปใช้ในการศึกษาปรากฏการณ์เกาะความร้อนในเขตเมือง การประเมินคุณภาพอากาศและการตรวจหาจุดความร้อนของไฟฟ้า ดังนั้น ในการศึกษาครั้งนี้จึงได้ออกแบบแผนการวิจัยเพื่อทำการประเมินและคาดการณ์เชิงพื้นที่ของปรากฏการณ์เกาะความร้อนในเขตเมืองอย่างเป็นระบบ วัตถุประสงค์หลักของการศึกษาคือ (1) เพื่อค้นหาปัจจัยที่มีอิทธิพลต่อรูปแบบของอุณหภูมิของประเทศไทย (2) เพื่อระบุวิธีการภูมิสถิติ (Geostatistical method) ที่เหมาะสมสำหรับการประมาณค่าในช่วงของอุณหภูมิเฉลี่ยจากข้อมูลภาคสนาม (3) เพื่อสกัดและคาดการณ์อุณหภูมิพื้นผิวดินจากแบนด์ความร้อนของข้อมูล Landsat สำหรับการศึกษาปรากฏการณ์เกาะความร้อนในเขตเมือง และ (4) เพื่อประเมินและคาดการณ์ปรากฏการณ์เกาะความร้อนในเขตเมืองและการเปลี่ยนแปลงระหว่างปี พ.ศ. 2549 ถึง 2569 องค์ประกอบหลักของวิธีการวิจัยประกอบด้วย การรวบรวมและเตรียมข้อมูล การค้นหาปัจจัยที่มีอิทธิพลต่อรูปแบบของอุณหภูมิ วิธีการภูมิสถิติที่เหมาะสมสำหรับการประมาณค่าในช่วงของอุณหภูมิเฉลี่ย การสกัดและการคาดการณ์อุณหภูมิพื้นผิวดินจากข้อมูลดาวเทียม และการประเมินผลและการคาดการณ์ปรากฏการณ์เกาะความร้อนในเขตเมือง

จากผลการศึกษาปัจจัยที่มีอิทธิพลในระดับท้องถิ่นต่อรูปแบบของอุณหภูมิ พบว่า ปัจจัยที่มีอิทธิพลอย่างมีนัยสำคัญต่อรูปแบบของอุณหภูมิในประเทศไทย ประกอบด้วย ปัจจัยด้านชีวภาพ (NDVI, NDBI, Elevation และ MNDWI) และปัจจัยด้านสิ่งแวดล้อม (PM₁₀, CO และ SO₂) วิธีการที่เหมาะสมที่สุดสำหรับประมาณค่าในช่วงอุณหภูมิเฉลี่ยรายเดือนในประเทศไทยจากข้อมูลของกรมอุตุนิยมวิทยา ได้แก่ Universal kriging (UK) ในขณะที่ ผลการศึกษาในการประเมินและคาดการณ์ปรากฏการณ์เกาะความร้อนในเขตเมือง พบว่า พื้นที่เมืองของกรุงเทพมหานครและปริมณฑลมีการเพิ่มขึ้นอย่างต่อเนื่อง ความเข้มข้นของเกาะความร้อนเฉลี่ยแบบถ่วงน้ำหนัก (WAI) มีความเข้มข้นสูงมากระหว่างปี 2549 ถึง 2565 และมีความเข้มข้นสูงระหว่างปี 2567 ถึง 2569 ใน

ขณะเดียวกัน ดัชนีสัดส่วนเกาะความร้อนในเขตเมือง (URI) ซึ่งแสดงระดับการพัฒนาของปรากฏการณ์เกาะความร้อนในเขตเมือง พบว่า เพิ่มขึ้นในปี พ.ศ. 2553 และ 2559 และลดลงอย่างรวดเร็วในปี พ.ศ. 2561 และเพิ่มขึ้นอย่างต่อเนื่องระหว่างปี พ.ศ. 2563 ถึง 2569 นอกจากนี้ การเปลี่ยนแปลงโดยรวมของดัชนีการเปลี่ยนแปลงระดับอุณหภูมิ (TGCI) ในเขตเมืองเก่า (old urban) และพื้นที่การขยายของเขตเมือง (urban expansion) ในคาบเวลา 2 ปีระหว่างปี พ.ศ. 2549 ถึง 2557 พบว่า ในเขตเมืองเก่า แนวโน้มการเพิ่มขึ้นของการเปลี่ยนแปลงระดับอุณหภูมิน้อยกว่าแนวโน้มการลดลงเกือบทุกคาบเวลา ยกเว้น ระหว่างปี พ.ศ. 2553 ถึง 2555 และ 2559 ถึง 2561 ในทางตรงกันข้าม ในพื้นที่การขยายของเขตเมือง แนวโน้มการเพิ่มขึ้นของการเปลี่ยนแปลงระดับอุณหภูมิมากกว่าแนวโน้มการลดลงเกือบทุกคาบเวลา ยกเว้น ระหว่างปี พ.ศ. 2563 ถึง 2565

จากผลการศึกษาสรุปได้ว่า สามารถนำการวิเคราะห์ปัจจัย (factor analysis) มาใช้เป็นเครื่องมือในการค้นหาปัจจัยที่มีอิทธิพลอย่างมีนัยสำคัญต่อรูปแบบของอุณหภูมิของประเทศไทยได้อย่างมีประสิทธิภาพ นอกจากนี้ สามารถนำดัชนี WAI URI และ TGCI มาใช้ประเมินและคาดการณ์ปรากฏการณ์เกาะความร้อนในเขตเมืองของกรุงเทพมหานครและปริมณฑลได้อย่างมีประสิทธิภาพ โดยอาศัยการสกัดและคาดการณ์ข้อมูลอุณหภูมิพื้นผิวดินและพื้นที่เขตเมืองและมีใช้เขตเมืองจากข้อมูลดาวเทียม

สาขาวิชาการรับรู้จากระยะไกล
ปีการศึกษา 2560

ลายมือชื่อนักศึกษา วิศวะกรณ์ ประสงค์ทรัพย์

ลายมือชื่ออาจารย์ที่ปรึกษา ทนายธรรม

ลายมือชื่ออาจารย์ที่ปรึกษาร่วม วิศวะกรณ์

WILAWAN PRASOMSUP : SPATIAL EVALUATION AND
PREDICTION OF URBAN HEAT ISLAND PHENOMENA IN BANGKOK
AND ITS VICINITY. THESIS ADVISOR : ASSOC. PROF. SONGKOT
DASANANDA, Ph.D. 264 PP.

FACTOR ANALYSIS/ TEMPERATURE PATTERN/ URBAN HEAT ISLAND/
WAI/ URI/ TGCI/ BANGKOK AND ITS VICINITY

In Thailand, applications of satellite-based LST data to advanced research on urban heat island (UHI) are still relatively low. Most of LST data are applied to study UHI, air-quality assessment, and to detect active forest fire hotspots. Thus, systematic research scheme on spatial evaluation and prediction of urban heat island phenomena was here conducted in more details in this study. Main objectives of the study are (1) to determine local principal influential factors on temperature pattern of Thailand, (2) to identify an optimum geostatistical method for in situ mean temperature interpolation, (3) to extract and predict land surface temperature from thermal band of Landsat data for UHI phenomena study, and (4) to evaluate and predict UHI phenomena and their changes during 2006 to 2026. Main components of research methodology consisted of data collection and preparation, influential factors on temperature pattern identification, optimum geostatistical method for mean temperature interpolation, satellite-based LST extraction and prediction, and UHI phenomena evaluation and prediction.

As results of the local influential factors on temperature pattern, the significant influential factors on temperature pattern in Thailand consisted of biophysical (NDVI, NDBI, elevation, and MNDWI) and environmental (PM₁₀, CO, and SO₂) factors. The

most suitable method for monthly mean temperature interpolation in Thailand from TMD data was Universal kriging (UK). Meanwhile, results of UHI phenomena evaluation and prediction showed that urban areas of Bangkok Metropolitan and its vicinity had been continuously increased. Weighted Average Heat Island Intensity (WAI) were very strong between 2006 and 2022 and became strong between 2024 and 2026. Meanwhile, Urban Heat Island Ratio Index (URI) as degree of UHI development increased in 2010 and 2016 and suddenly decreased in 2018 and continuously increased between 2020 and 2026. In addition, overall change of Temperature Grade Change Index (TGCI) in old urban and urban expansion of 2 years period between 2006 and 2026 showed that increasing trend of temperature grade change was weaker than decreasing trend in old urban in almost periods, except during 2010 to 2012 and 2016 to 2018. On contrary, increasing trend of temperature grade change was stronger than decreasing trend in urban expansion in almost period, except during 2020 to 2022.

In conclusion, it appears that factor analysis can be used as an efficiently tools to extract significant local influential factors on temperature pattern for Thailand. In addition, WAI, URI, and TGCI can be effectively used to evaluate and predict UHI phenomena of Bangkok Metropolitan and its vicinity based on extracted and predicted satellite-based LST data and urban and non-urban areas.

School of Remote Sensing

Academic Year 2016

Student's Signature Nilanon Prasomsup

Advisor's Signature S. Dasananda

Co-advisor's Signature Savit Ong

ACKNOWLEDGEMENTS

I would like to express my deep gratitude to my advisor, Assoc. Prof. Dr. Songkot Dasananda in help, guidance, and discussion on many concerned problems.

I would like to appreciate the co-advisor, Assoc. Prof. Dr. Suwit Ongsomwang for his supervision, advice, helps with valuable instructions, guidance and suggestions during the study periods at Suranaree University of Technology (SUT). Without his constructive devotion and support, this thesis would not be finished successfully.

I am also very grateful to the chairperson and other committees, Assoc. Prof. Dr. Sura Pattanakiat, Asst. Prof. Dr. Sunya Sarapirome, and Asst. Prof. Dr. Ornprapa Pummakarnchana Robert, for always being interested in the progress of my work, and for all valuable suggestions and critical comments. I am also very thankful to Dr. Pantip Piyatadsananon and Dr. Siripon Kamontum for valuable comments on my work. I am also very grateful to Suranaree University of Technology for providing scholarship.

Thank are also extended to Thai Meteorological Department and Pollution Control Department for giving the data collected at the station. I extend my thanks to all the staffs and all of my friends at School of Remote Sensing for their helps and supports during my study here, especially Mrs. Pimprapai Piphatnawakul, Miss Warunee Aunphoklang, Mr. Athiwat Phinyoyang, and Miss Salisa Saraisamrong.

Finally, I would like to express my special thanks to my family for their financial supports, great love, care, and patience during my study.

Wilawan Prasomsup

CONTENTS

	Page
ABSTRACT IN THAI.....	I
ABSTRACT IN ENGLISH	III
ACKNOWLEDGEMENTS.....	V
CONTENTS.....	VI
LIST OF TABLES.....	XII
LIST OF FIGURES	XIX
CHAPTER	
I INTRODUCTION.....	1
1.1 Background problems and significance of the study	1
1.2 Research objectives.....	3
1.3 Scope of the study.....	4
1.4 Limitation of the study.....	5
1.5 Study area.....	5
1.6 Benefit of the study	8
1.7 Outline of the thesis	8
II BASIC CONCEPT AND LITERATURE REVIEWS.....	11
2.1 Local influential factor on temperature	11
2.2.1 Latitude or insolation	11
2.1.2 Altitude or elevation.....	12

CONTENTS (Continued)

	Page
2.1.3 Land use and land cover (LULC).....	16
2.1.4 Proximity to sea (distance to the sea).....	17
2.1.5 Ocean current/prevaling wind.....	19
2.1.6 Habitat.....	20
2.1.7 Air pollutants.....	22
2.2 Geostatistics methods for spatial interpolation.....	26
2.2.1 Ordinary kriging.....	29
2.2.2 Simple kriging.....	29
2.2.3 Universal kriging.....	29
2.2.4 Co-Kriging.....	29
2.3 Conversion of LST from satellite data.....	30
2.4 UHI phenomena: Definition, cause, consequence and mitigation.....	35
2.4.1 Definition of UHI.....	35
2.4.2 Cause of UHI.....	36
2.4.3 Impacts of UHI.....	39
2.4.4 Mitigation Strategies for UHI Effects.....	42
2.5 Literature review.....	44
2.5.1 Geostatistical interpolation method.....	44
2.5.2 Satellite-based LST extraction and UHI effect.....	47

CONTENTS (Continued)

	Page
III RESEARCH METHODOLOGY	53
3.1 Data collection and preparation	53
3.2 Influential factors on temperature pattern identification.....	57
3.2.1 Variables selection of factor analysis.....	57
3.2.2 Component extraction of factor analysis.....	59
3.2.3 Development of local influential factor on temperature	59
3.3 Optimum geostatistical method for mean temperature interpolation	64
3.4 Satellite-based LST extraction and prediction	67
3.5 UHI phenomena evaluation and prediction.....	69
3.5.1 Urban and non-urban extraction.....	69
3.5.2 Urban and non-urban prediction	71
3.5.3 Urban BT grade classification.....	71
3.5.4 UHI phenomena evaluation and prediction.....	72
IV LOCAL PRINCIPAL INFLUENTIAL FACTORS ON TEMPERATURE PATTERN	75
4.1 Local principal influential factors on temperature by factor analysis.....	75
4.1.1 Standardization of variable values for factor analysis	88
4.1.2 Variables selection for factor analysis	93
4.1.3 Component extraction by factor analysis	94

CONTENTS (Continued)

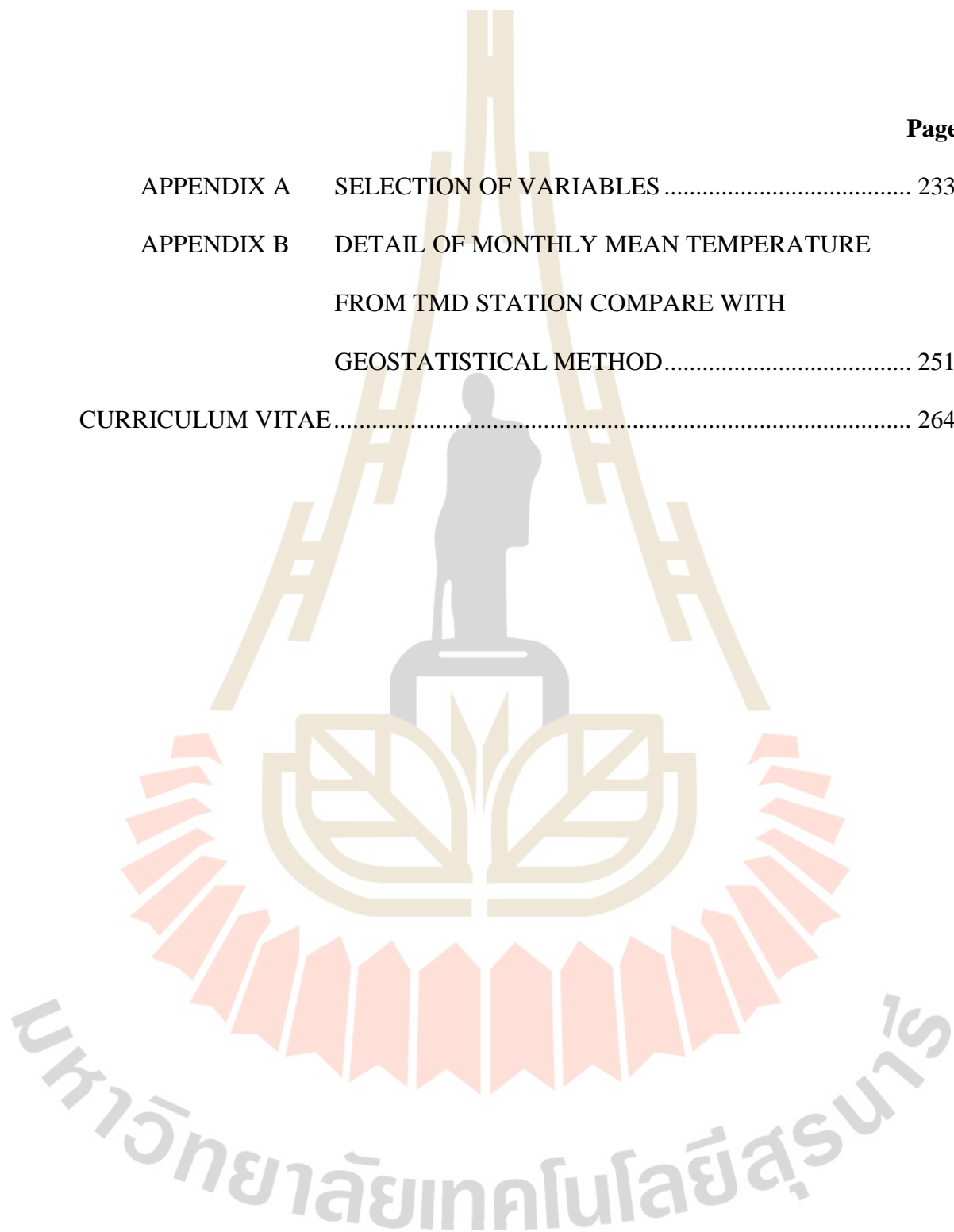
	Page
4.2 Top three influential factors on temperature pattern using spatial simple linear regression analysis.....	117
4.2.1 Top three influential factors on temperature pattern in November	119
4.2.2 Top three influential factors on temperature pattern in December	120
4.2.3 Top three influential factors on temperature pattern in January ...	121
4.2.4 Top three influential factors on temperature pattern in February .	122
4.2.5 Top three influential factors on temperature pattern in March	123
4.2.6 Top three influential factors on temperature pattern in April	124
V OPTIMUM GEOSTATISTICAL METHOD FOR IN SITU MEAN TEMPERATURE INTERPOLATION.....	127
5.1 Optimum univariate geostatistical method for monthly mean temperature interpolation	128
5.2 Optimum multivariate geostatistical method for monthly mean temperature interpolation	134
5.3 Optimum geostatistical method for monthly mean temperature interpolation	141
VI LAND SURFACE TEMPERATURE EXTRACTION AND PREDICTION	143
6.1 Satellite-based LST extraction	143
6.1.1 Conversion of LST	144

CONTENTS (Continued)

	Page
6.1.2 Refine of LST using simple regression analysis.	148
6.2 LST prediction	156
VII UHI PHENOMENA EVALUATION AND PREDICTION.....	160
7.1 Urban and non-urban area extraction.....	160
7.2 Urban and non-urban area prediction.....	167
7.3 Temperature grade classification	171
7.4 Urban heat island intensity and its severity.....	184
7.5 Quantitative analysis of UHI.....	187
7.5.1 Quantitative analysis of UHI in different urban regions	187
7.5.2 Overall analysis of UHI change	210
VIII CONCLUSION AND RECOMMENDATION	213
8.1 Conclusion	213
8.1.1 Local principal influential factors on temperature pattern	213
8.1.2 Optimum geostatistical method for in situ mean temperature interpolation.	213
8.1.3 Land surface temperature extraction and prediction	214
8.1.4 UHI phenomena evaluation and prediction.....	214
8.2 Quantitative analysis of UHI.....	215
REFERENCES	217
APPENDICES	232

CONTENTS (Continued)

	Page
APPENDIX A SELECTION OF VARIABLES	233
APPENDIX B DETAIL OF MONTHLY MEAN TEMPERATURE FROM TMD STATION COMPARE WITH GEOSTATISTICAL METHOD.....	251
CURRICULUM VITAE.....	264



LIST OF TABLES

Table		Page
2.1	Comparison of Landsat 5, Landsat 7 and 8 specifications.....	32
2.2	Thermal constant of K_1 , K_2 value.	34
2.3	Summary of geostatistics methods comparison for spatial interpolation	46
3.1	List of data collection and preparation of each component	55
3.2	Pairwise of input data for urban and non-urban areas prediction between 2018 and 2026.....	71
4.1	Descriptive statistical data of 16 variables before s normalization.....	89
4.2	Descriptive statistical data of 16 variables after normalization	91
4.3	Summary of suitable variable selection of six months datasets for factor analysis.....	94
4.4	Factor loading matrix by factor analysis of November 2015 dataset	95
4.5	Factor loading matrix by factor analysis of December 2015 dataset.....	99
4.6	Factor loading matrix by factor analysis of January 2016 dataset.....	102
4.7	Factor loading matrix by factor analysis of February 2016 dataset.....	106
4.8	Factor loading matrix by factor analysis of March 2016 dataset.....	109
4.9	Factor loading matrix by factor analysis of April 2016 dataset.....	112
4.10	Highest significant variable in each component with percent of variance and cumulative percent of variance in each month (November to April).....	115

LIST OF TABLES (Continued)

Table	Page
4.11 Spatial regression analysis between factor map from November 2015 and MODIS LST data.....	120
4.12 Spatial regression analysis between factor map from December 2015 and MODIS LST data.....	121
4.13 Spatial regression analysis between factor map from January 2016 and MODIS LST data.....	122
4.14 Spatial regression analysis between factor map from February 2016 and MODIS LST data.....	123
4.15 Spatial regression analysis between factor map from March 2016 and MODIS LST data.....	124
4.16 Spatial regression analysis between factor map from April 2016 and MODIS LST data.....	125
4.17 Monthly top three significant influential factors on temperature pattern of MODIS data.....	126
5.1 Basic statistical data of the interpolated monthly mean temperature of univariate methods.....	128
5.2 Correlation coefficient of monthly mean temperature among three univariate methods.....	132
5.3 Accuracy assessment of monthly mean temperature interpolation by univariate geostatistical method using MAE, MRE, and RMSE.....	133

LIST OF TABLES (Continued)

Table	Page
5.4 Basic statistical data of the interpolated monthly mean temperature of multivariate methods.....	134
5.5 Correlation coefficient of monthly mean temperature among three multivariate methods.....	138
5.6 Accuracy assessment of monthly mean temperature interpolation by multivariate geostatistical method using MAE, MRE, and RMSE	140
5.7 Accuracy assessment of monthly mean temperature interpolation based on geostatistical method using AIC	142
6.1 List of selected Landsat data for LST extraction over Bangkok and its vicinity	144
6.2 Basic statistical data of LST	148
6.3 Temperature station in the study area from TMD	149
6.4 Independent and dependent variables for simple linear regression analysis.	150
6.5 List of linear equations and its R and R ² coefficients values of simple linear regression analysis.....	150
6.6 Basic statistical data of LST refinement with masking cloud.....	155
6.7 Basic statistical data of predicted LST between 2018 and 2026 with masking cloud.....	159
7.1 Pixel value of representative land covers.....	161
7.2 Accuracy assessment of urban and non-urban areas in 2006	164

LIST OF TABLES (Continued)

Table	Page
7.3 Accuracy assessment of urban and non-urban areas in 2008	164
7.4 Accuracy assessment of urban and non-urban areas in 2010	165
7.5 Accuracy assessment of urban and non-urban areas in 2012	165
7.6 Accuracy assessment of urban and non-urban areas in 2014	165
7.7 Accuracy assessment of urban and non-urban areas in 2016	165
7.8 Area and percentage of urban and non-urban area between 2006 and 2026	170
7.9 Basic statistics of normalized LST data in Bangkok Metropolitan and its vicinity between 2006 and 2026	172
7.10 Basic statistics of normalized LST data in urban areas of Bangkok Metropolitan and its vicinity between 2006 and 2026.....	175
7.11 Area of brightness temperature grade in Bangkok and its vicinity between 2006 and 2026	181
7.12 Percent of brightness temperature grade in Bangkok and its vicinity between 2006 and 2026	181
7.13 WAI and URI calculation of Bangkok and its vicinity between 2006 and 2026.....	185
7.14 Classification of heat island intensity Based on WAI	186
7.15 Transition matrix of difference BT grade in old urban areas in 2006-2008 .	188
7.16 Transition matrix of difference BT grade in urban expansion region in 2006-2008	188

LIST OF TABLES (Continued)

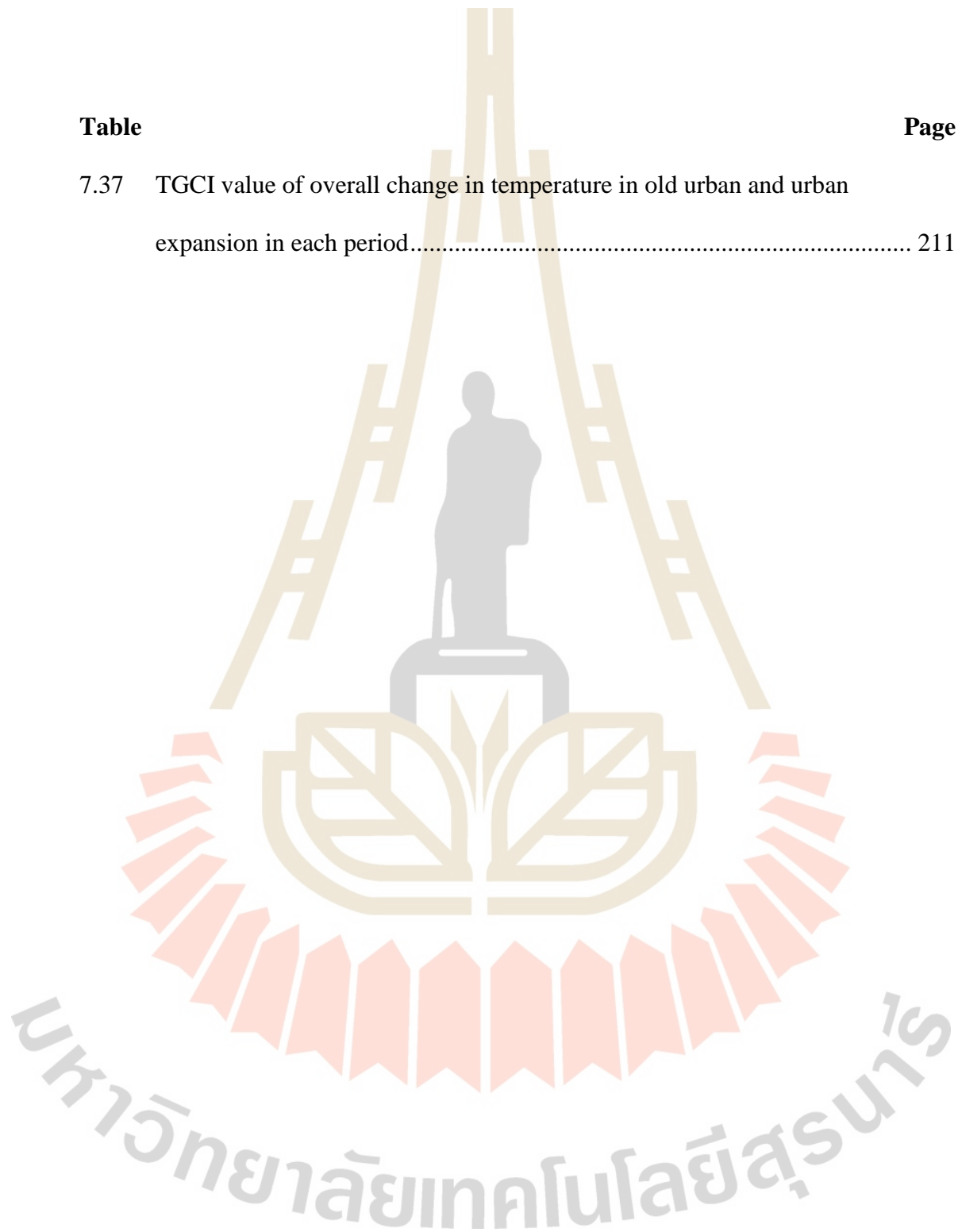
Table		Page
7.17	Transition matrix of difference BT grade in old urban region in 2008-2010	189
7.18	Transition matrix of difference BT grade in urban expansion region in 2008-2010	189
7.19	Transition matrix of difference BT grade in old urban region in 2010-2012	189
7.20	Transition matrix of difference BT grade in urban expansion region in 2010-2012	189
7.21	Transition matrix of difference BT grade in old urban region in 2012-2014	190
7.22	Transition matrix of difference BT grade in urban expansion region in 2012-2014	190
7.23	Transition matrix of difference BT grade in old urban region in 2014-2016	190
7.24	Transition matrix of difference BT grade in urban expansion region in 2014-2016	190
7.25	Transition matrix of difference BT grade in old urban region in 2016-2018	191
7.26	Transition matrix of difference BT grade in urban expansion region in 2016-2018	191

LIST OF TABLES (Continued)

Table	Page
7.27 Transition matrix of difference BT grade in old urban region in 2018-2020	191
7.28 Transition matrix of difference BT grade in urban expansion region in 2018-2020	191
7.29 Transition matrix of difference BT grade in old urban region in 2020-2022	192
7.30 Transition matrix of difference BT grade in urban expansion region in 2020-2022	192
7.31 Transition matrix of difference BT grade in old urban region in 2022-2024	192
7.32 Transition matrix of difference BT grade in urban expansion region in 2022-2024	192
7.33 Transition matrix of difference BT grade in old urban region in 2024-2026	193
7.34 Transition matrix of difference BT grade in urban expansion region in 2024-2026	193
7.35 Area and percentage of unchanged, increase and decrease of BT grades in old urban in each period.....	193
7.36 Area and percentage of unchanged, increase and decrease of BT grades in urban expansion in each period	194

LIST OF TABLES (Continued)

Table		Page
7.37	TGCI value of overall change in temperature in old urban and urban expansion in each period.....	211



LIST OF FIGURES

Figure	Page
1.1 In situ station and terrain characteristic of Thailand.....	6
1.2 Location map and terrain characteristic of Bangkok Metropolitan and its vicinity	7
1.3 Structure of the thesis.....	10
2.1 Daily insolation at the top of the atmosphere in Wm^{-2} for three locations....	13
2.2 Examples of latitude influence on mean monthly temperature as seen on the mean monthly temperatures of five Northern Hemisphere locations with different latitudes.	14
2.3 Relationship between mean monthly net radiation and surface air temperature for Singapore.....	14
2.4 Elevation influence on mean monthly temperature.	15
2.5 LULC pattern and LST distribution in the China's Pearl River Delta region	17
2.6 Temperature change with distance to the sea in summer and winter season..	18
2.7 Variation of the average LST data with distances from the Thai Gulf.....	18
2.8 Major ocean currents at present (warm/cold).	19
2.9 Urban and rural population of the world, 1950-2030.....	21
2.10 Increased city size and number of habitants cause increase in temperature ...	21
2.11 The densely populated zone compared the LST pattern.....	22
2.12 Variogram example.....	28

LIST OF FIGURES (Continued)

Figure	Page
2.13 The principle of Kriging.....	28
2.14 Bandpass wavelengths for Landsat 8 OLI and TIRS sensor, compared to Landsat 7 ETM+ sensor.....	31
2.15 Typical temperature profile represents the UHI phenomenon.....	36
2.16 Typical diurnal variations of air temperature under calm/clear air.....	38
2.17 Atmospheric conditions inside and outside urban area in winter	39
2.18 Concept of countermeasures to UHIs	43
3.1 Overview of methodology framework according to objectives.....	54
3.2 Workflow of influential factors on temperature pattern identification.....	60
3.3 Flow diagram for insolation extraction under function of Area Solar Radiation.....	62
3.4 Workflow of optimum geostatistical method for mean temperature interpolation.....	66
3.5 Workflow satellite-based LST extraction and LST prediction.....	68
3.6 Workflow of UHI phenomena evaluation and prediction.....	70
4.1 Biophysical factors as static data in 2014.....	76
4.2 Average monthly insolation during November 2015 to April 2016.....	77
4.3 Average monthly wind speed during November 2015 to April 2016.....	78
4.4 NDVI during November 2015 to April 2016.....	79
4.5 NDBI during November 2015 to April 2016.....	80

LIST OF FIGURES (Continued)

Figure	Page
4.6 MNDWI during November 2015 to April 2016	81
4.7 Demographic factors as static data in 2015	82
4.8 Average monthly particulate matter (PM ₁₀) during November 2015 to April 2016	83
4.9 Average monthly carbon monoxide (CO) during November 2015 to April 2016	84
4.10 Average monthly nitrogen dioxide (NO ₂) during November 2015 to April 2016	85
4.11 Average monthly sulfur dioxide (SO ₂) during November 2015 to April 2016	86
4.12 12 Average monthly ozone (O ₃) during November 2015 to April 2016.....	87
4.13 Factor map of November 2015 dataset by factor analysis	98
4.14 Factor map of December 2015 dataset by factor analysis	101
4.15 Factor map of January 2016 dataset by factor analysis	105
4.16 Factor map of February 2016 dataset by factor analysis	108
4.17 Factor map of March 2016 dataset by factor analysis	111
4.18 Factor map of April 2016 dataset by factor analysis	114
4.19 Monthly MODIS LST during November 2015 to April 2016.....	118
5.1 Monthly mean temperature interpolation using OK	129
5.2 Monthly mean temperature interpolation using SK.....	130

LIST OF FIGURES (Continued)

Figure	Page
5.3 Monthly mean temperature interpolation using UK	131
5.4 Monthly mean temperature interpolation using OCK	135
5.5 Monthly mean temperature interpolation using SCK	136
5.6 Monthly mean temperature interpolation using UCK	137
6.1 Land surface temperature from Landsat-5 in January 2006	145
6.2 Land surface temperature from Landsat-7 in January 2008	145
6.3 Land surface temperature from Landsat-7 in November 2010.....	146
6.4 Land surface temperature from Landsat-7 in February 2012	146
6.5 Land surface temperature from Landsat-8 in November 2014.....	147
6.6 Land surface temperature from Landsat-8 in April 2016	147
6.7 Distribution of TMD location over Bangkok and its vicinity.....	149
6.8 Simple linear regression between LST extraction from Landsat data and TMD station during 2006 to 2016	151
6.9 Refinement of land surface temperature in January 2006	152
6.10 Refinement of land surface temperature in January 2008	153
6.11 Refinement of land surface temperature in November 2010.....	153
6.12 Refinement of land surface temperature in February 2012	154
6.13 Refinement of land surface temperature in November 2014.....	154
6.14 Refinement of land surface temperature in April 2016	155
6.15 Distribution of urban and non-urban areas in 2018	156

LIST OF FIGURES (Continued)

Figure	Page
6.16 Distribution of urban and non-urban areas in 2020	157
6.17 Distribution of urban and non-urban areas in 2022	157
6.18 Distribution of urban and non-urban areas in 2024	158
6.19 Distribution of urban and non-urban areas in 2026	158
6.20 Comparison of basic statistical data of LST between 2006 and 2026	159
7.1 Distribution of urban and non-urban areas in 2006	161
7.2 Distribution of urban and non-urban areas in 2008	162
7.3 Distribution of urban and non-urban areas in 2010	162
7.4 Distribution of urban and non-urban areas in 2012	163
7.5 Distribution of urban and non-urban areas in 2014	163
7.6 Distribution of urban and non-urban areas in 2016	164
7.7 Distribution of sampling points for accuracy assessment of urban and non-urban area	166
7.8 Distribution of predicted urban and non-urban areas in 2018	167
7.9 Distribution of predicted urban and non-urban areas in 2020	168
7.10 Distribution of predicted urban and non-urban areas in 2022	168
7.11 Distribution of predicted urban and non-urban areas in 2024	169
7.12 Distribution of predicted urban and non-urban areas in 2026	169
7.13 Urban and non-urban areas change between 2006 and 2026.....	171
7.14 Normalized LST data	173

LIST OF FIGURES (Continued)

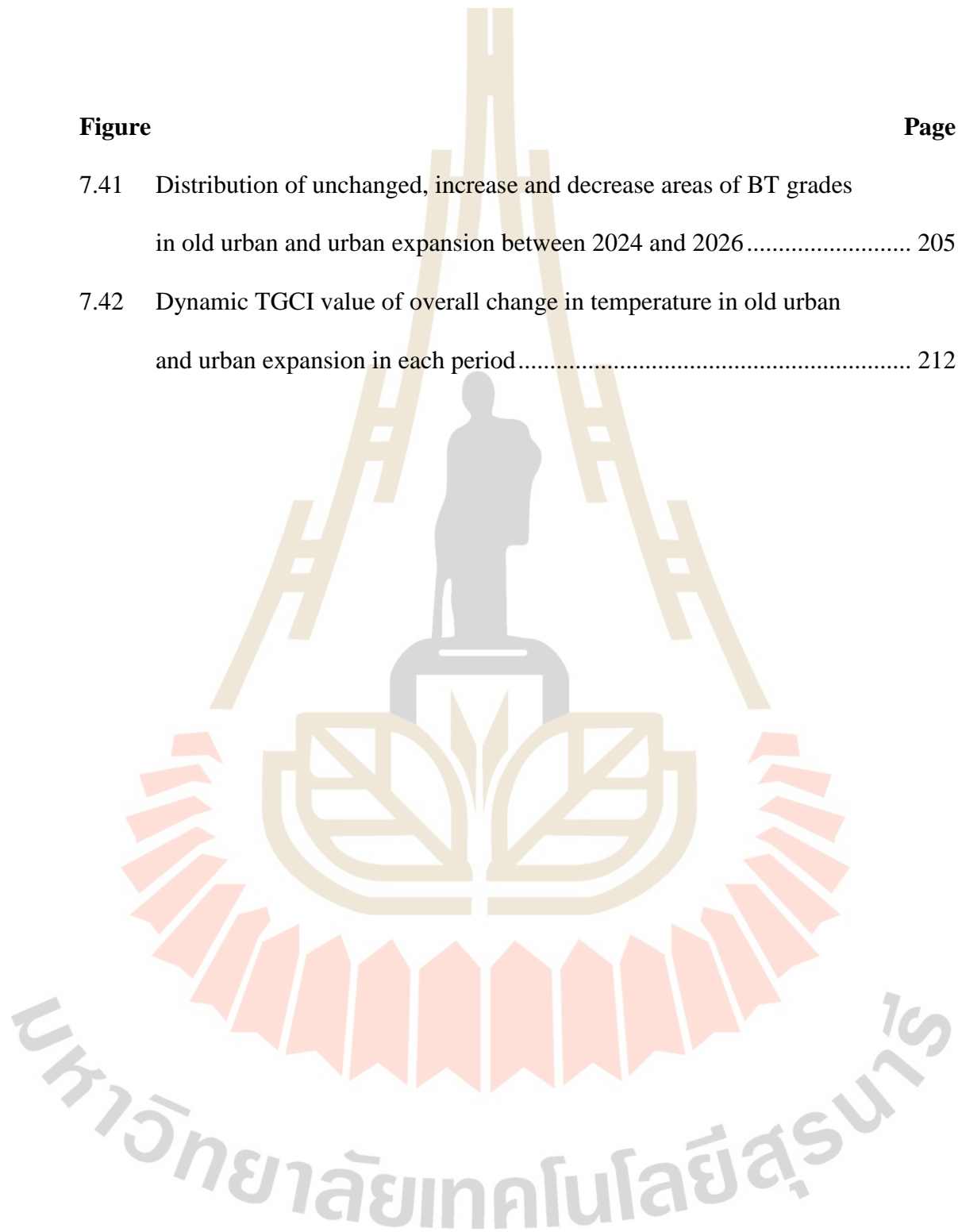
Figure	Page
7.15 Distribution BT grade classification of Bangkok and its vicinity in 2006 ...	175
7.16 Distribution BT grade classification of Bangkok and its vicinity in 2008 ...	176
7.17 Distribution BT grade classification of Bangkok and its vicinity in 2010 ...	176
7.18 Distribution BT grade classification of Bangkok and its vicinity in 2012 ...	177
7.19 Distribution BT grade classification of Bangkok and its vicinity in 2014 ...	177
7.20 Distribution BT grade classification of Bangkok and its vicinity in 2016 ...	178
7.21 Distribution BT grade classification of Bangkok and its vicinity in 2018 ...	178
7.22 Distribution BT grade classification of Bangkok and its vicinity in 2020 ...	179
7.23 Distribution BT grade classification of Bangkok and its vicinity in 2022 ...	179
7.24 Distribution BT grade classification of Bangkok and its vicinity in 2024 ...	180
7.25 Distribution BT grade classification of Bangkok and its vicinity in 2026 ...	180
7.26 Dynamic change of proportional area of BT grade in Bangkok and its vicinity between 2006 and 2026	182
7.27 Comparison of BT grade classification pattern and LST pattern in 2014 and 2016.....	183
7.28 Dynamic change of WAI between 2006 and 2026	186
7.29 Dynamic change of URI between 2006 and 2026	187
7.30 Comparison of percentage of unchanged, increase and decrease of BT grades in old urban in each period	194

LIST OF FIGURES (Continued)

Figure	Page
7.31 Comparison of percentage of unchanged, increase and decrease of BT grades in urban expansion in each period	195
7.32 Distribution of unchanged, increase and decrease areas of BT grades in old urban and urban expansion between 2006 and 2008	196
7.33 Distribution of unchanged, increase and decrease areas of BT grades in old urban and urban expansion between 2008 and 2010	197
7.34 Distribution of unchanged, increase and decrease areas of BT grades in old urban and urban expansion between 2010 and 2012	198
7.35 Distribution of unchanged, increase and decrease areas of BT grades in old urban and urban expansion between 2012 and 2014	199
7.36 Distribution of unchanged, increase and decrease areas of BT grades in old urban and urban expansion between 2014 and 2016	200
7.37 Distribution of unchanged, increase and decrease areas of BT grades in old urban and urban expansion between 2016 and 2018	201
7.38 Distribution of unchanged, increase and decrease areas of BT grades in old urban and urban expansion between 2018 and 2020	202
7.39 Distribution of unchanged, increase and decrease areas of BT grades in old urban and urban expansion between 2020 and 2022	203
7.40 Distribution of unchanged, increase and decrease areas of BT grades in old urban and urban expansion between 2022 and 2024	204

LIST OF FIGURES (Continued)

Figure	Page
7.41 Distribution of unchanged, increase and decrease areas of BT grades in old urban and urban expansion between 2024 and 2026.....	205
7.42 Dynamic TGCI value of overall change in temperature in old urban and urban expansion in each period.....	212



CHAPTER I

INTRODUCTION

1.1 Background problem and significance of the study

Land surface temperature (LST) is an important parameter that is typically used as an indicator of thermal radiation intensity over an area. Knowledge of LST data is crucial for the research and study in many fields, such as, meteorology, climatology, hydrology, natural hazard/disaster observation and monitoring (e.g. forest fire or volcanic eruption detection/monitoring) (Li et al., 2013 and Land Surface Analysis Satellite Applications Facility, Online, 2015). At present, the LST has also played a critical role in the analysis of global climate change called global warming phenomenon which has become a highly concerned environmental issue for scientific community and governments worldwide (Chiras, 2014).

According to several reports published by the Intergovernmental Panel on Climate Change (IPCC), the observed global average near-surface air temperature has increased faster in recent decades than the natural changes found in previous millennia due to the dramatic increase of greenhouse gas concentration in lower atmosphere from human activities (from the anthropogenic source), especially carbon dioxide (CO₂) (IPCC, Online, 2002). Associated impacts of the global warming effect on human and nature as a whole expect to be immense but varying from region to region. These include, for examples, sea level rise, intense melting of snow/ice, more humidity, change in occurrence pattern of precipitation, and earlier arrival of spring events, e.g.,

the flowering of plants. Other anticipated effects include more frequency of the extreme weather events e.g. heat waves, droughts, heavy rainfall/snowfall. Notable effects to humans include, for examples, threat to food security, more prevalent of warm-climate diseases, and changes in quantity and quality of the natural ecosystem (Lake et al., 2012).

Through, information of the LST data is well acknowledged and required for research in many fields as stated earlier. However, the availability of these data in the past was still limited due to low number of the in situ ground-based measuring stations that can generate the accurate LST mapping (Puangporn Puntumakoo, 2001). Contrary to the ground-based measurements that mostly record the near surface air temperature data, the satellite-based thermal radiometers are able to detect LST data at larger spatial coverage (but with less temporal frequency) than typical in-situ measurements. Notable examples of these devices are the thermal infrared (TIR) sensors operating on Landsat satellites and those working as part of MODIS instruments aboard NASA's Terra and Aqua satellites. These measurements can give better spatial LST characterization over an area of interest and provide a continuous and simultaneous view of the whole region which is of prime importance for the detailed investigation of LST variation both in space and time at every considered spatial scale from local to global level (Mendelsohn, Kurukulasuriya, Basist, Kogan, and Williams, 2007).

In Thailand, applications of satellite-based LST data to advanced research are still relatively low. Most of LST data are applied to analyze the urban heat island (UHI) phenomenon in crowded cities (like Bangkok, and Chiang Mai), air-quality assessment between LST and impervious surface, and the detection/mapping of active forest fire hotspots (Chowdhury and Hassan, 2015, Pathompong Sukthong, 2008, Potapov,

Hansen, Stehman, Loveland, and Pittman, 2008). Therefore, systematic research scheme is here conducted in more details since the great advance of the TIR sensors and more availability of their archival data for public uses. In this study, local influential factors on temperature pattern of Thailand is firstly examined using factor analysis and spatial regression analysis, and three primary influential factors on temperature pattern are further examined with Co-Kriging geostatistical methods for mean temperature interpolation. Meanwhile, series data of Landsat thermal band during 2006 to 2016 are used to extract LST data for UHI phenomena evaluation using Weighted Average Heat Island Intensity (WAI) and Urban Heat Island Ratio Index (URI). In addition, future UHI phenomena during 2018 to 2026 are predicted using CA- Markov model. Additionally, Brightness Temperature Grade Change Index (TGCI) are also extracted to reveal the overall change in temperature in different periods during 2006-2026.

1.2 Research objectives

Two main goal of the study are to identify significant influential biophysical, demographic and environmental factors on temperature pattern in Thailand and to evaluation and prediction of urban heat island effect in Bangkok and its vicinity using geoinformatics technology. The specific research objectives of the study are as follows:

1.2.1 To determine local principal influential factors on temperature pattern of Thailand,

1.2.2 To identify an optimum geostatistical method for in situ mean temperature interpolation,

1.2.3 To extract and predict land surface temperature from thermal band of Landsat data for UHI phenomena study,

1.2.4 To evaluate and predict UHI phenomena and their changes during 2006 to 2026.

1.3 Scope of the study

1.3.1 Significant biophysical, demographic and environmental factors on mean temperature pattern, which include (1) elevation, (2) aspect, (3) slope, (4) insolation, (5) wind speed, (6) distance to the sea, (7) NDVI, (8) NDBI, (9) MNDWI, (10) population density at district level, (11) household density at district level, and (12) air pollutants (PM₁₀, CO, NO₂, SO₂, and O₃), are identified using factor analysis and spatial regression analysis. Herein, factor analysis is firstly applied to create influential factors map and then compared with LST pattern map of MODIS data to identify significant factors (components) on mean temperature pattern using spatial regression analysis.

1.3.2 Standard geostatistical method of univariate (OK, SK, and UK) and multivariate (SCK, OCK, and UCK) methods are here examined to identify an optimum geostatistical method based on model-based inference method for monthly mean temperature interpolation (November, December, January, February, March and April) from 2015/16.

1.3.3 LST data from thermal band of Landsat data during November to April between 2006 and 2016 are firstly extracted using standard conversion method and then refined with in situ mean temperature of TMD stations over Bangkok and its vicinity using simple linear regression analysis.

1.3.4 Development of urban and built-up areas series data are extracted based on Built-Up index (BUI) which is derived from corresponding Landsat data with relative radiometric correction.

1.3.5 The WAI and URI and its change during 2006 to 2026, which are spatially extracted and predicted using CA-Markov model, are here applied to characterize UHI phenomena in Bangkok and its vicinity.

1.3.6 The TGCI of Bangkok and its vicinity during 2006 to 2026 are extracted to quantify the overall change in temperature (increase or decrease) in different periods.

1.4 Limitation of the study

1.4.1 Availability of Landsat 5, Landsat 7 and 8 data during November to April from 2006, 2008, 2010, 2012, 2014, and 2016 depends on downloadable data and percent of cloud cover under USGS's service.

1.4.2 Because no Landsat data exist between 2018 and 2026 for UHI study, Trend Analysis function of MS Excel and ASCII to Image function of ERDAS Imagine software are here applied for creating the predicted LST during 2018 to 2026.

1.5 Study area

Thailand and Bangkok Metropolitan and its vicinity include Nakhon Pathom, Nonthaburi, Pathumthani, Sumut Prakarn, and Samut Sakhon provinces are selected as two study sites. The whole Thailand territory is used as study area for influential factors on temperature pattern investigation (objective 1 and 2) meanwhile Bangkok Metropolitan and its vicinity was selected as study area for UHI phenomena study (objective 3 and 4). Location map with DEM of two study sites are separately displayed in Figure 1.1 and 1.2.

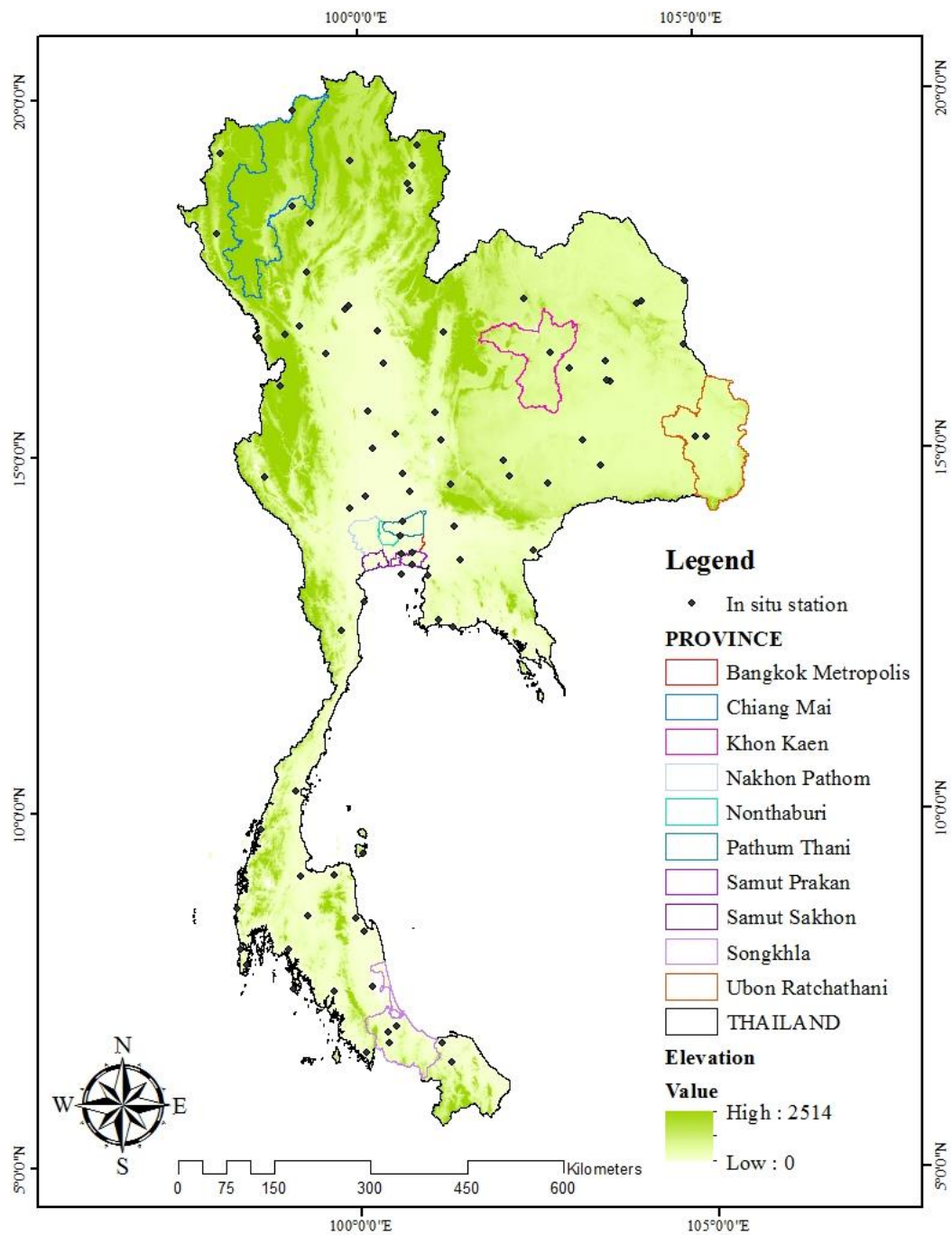


Figure 1.1 In situ station and terrain characteristic of Thailand.

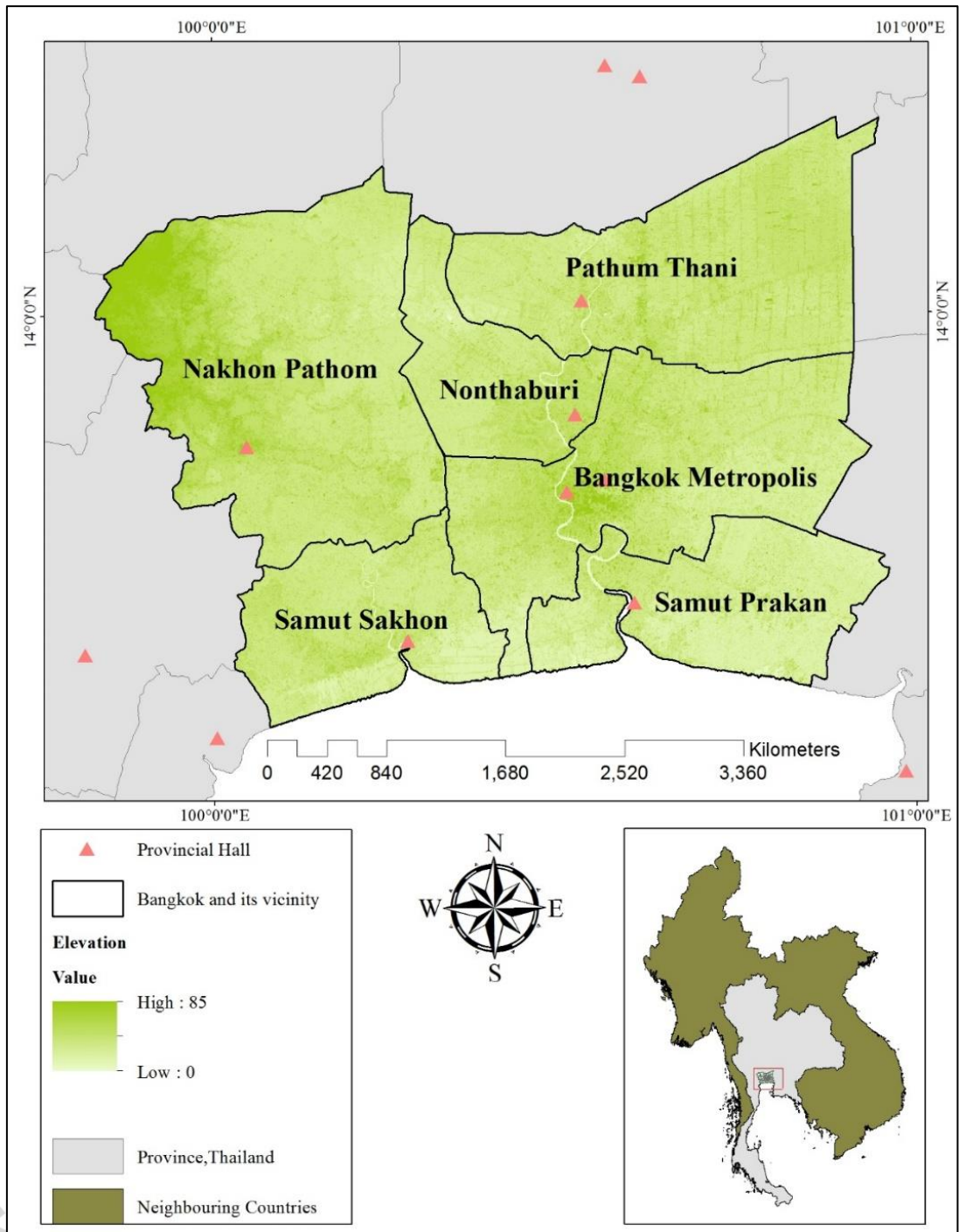


Figure 1.2 Location map and terrain characteristic of Bangkok Metropolitan and its vicinity.

1.6 Benefits of the Study

The specific benefits of the study are as follows:

1.6.1 Top three dominate influential factors on temperature pattern.

1.6.2 Optimum geostatistical method for monthly mean temperature interpolation.

1.6.3 Series of LST data during November to April from 2006, 2008, 2010, 2012, 2014 and 2016.

1.6.4 Monthly UHI intensity and its change during 2006-2026.

1.6.5 Monthly UHI severity and its change during 2006-2026.

1.6.6 Series of brightness temperature grade change by TGCI during 2006-2026.

1.7 Outline of the thesis

The thesis is structured in two parts and it follows a hierarchical organization as shown in Figure 1.3. Key information of each chapter in each part is summarized in the following section.

The first part includes Chapters I “Introduction”, Chapter II “Basic Concepts and Literature Reviews” and Chapter III “Research Methodology”. Chapter I contains background problem and significance of the study, research objectives, scope of the study, limitations of the study, study area, benefits of the study and outline of the thesis. Chapter II consists of local influential factor on temperature, geostatistics methods for spatial interpolation, conversion of LST from satellite data, UHI phenomena and relevant literatures. Meanwhile, Chapter III presents details of research methodology

including (1) data collection and preparation, (2) influential factors on temperature pattern identification, (3) optimum geostatistical method for mean temperature interpolation, (4) satellite-based LST extraction, and (5) UHI phenomena evaluation and prediction.

The second part consists of four chapters of the results with discussion, which separately describe according to objectives and one chapter presents conclusion and recommendation. Chapter IV “Local Principal Influential Factors on Temperature Pattern” contains (1) local principal influential factors on temperature by factor analysis and (2) top three influential factors on temperature pattern using spatial linear regression analysis. Chapter V “Optimum Geostatistical Method for In Situ Mean Temperature Interpolation” consists of (1) optimum univariate geostatistical method for monthly mean temperature interpolation, (2) optimum multivariate geostatistical method for monthly mean temperature interpolation and (3) optimum geostatistical method for monthly mean temperature interpolation. Meanwhile, Chapter VI “Land Surface Temperature Extraction for UHI Phenomena Evaluation and Prediction” contain (1) satellite-based LST extraction, (2) urban and non-urban area extraction, (3) urban and non-urban area prediction, (4) LST prediction, and (5) temperature grade classification for UHI evaluation, (6) calculation of heat island intensity and severity, and (7) quantitative analysis of UHI. Chapter VII “Conclusion and Recommendation” comprises conclusion of the study and recommendation.

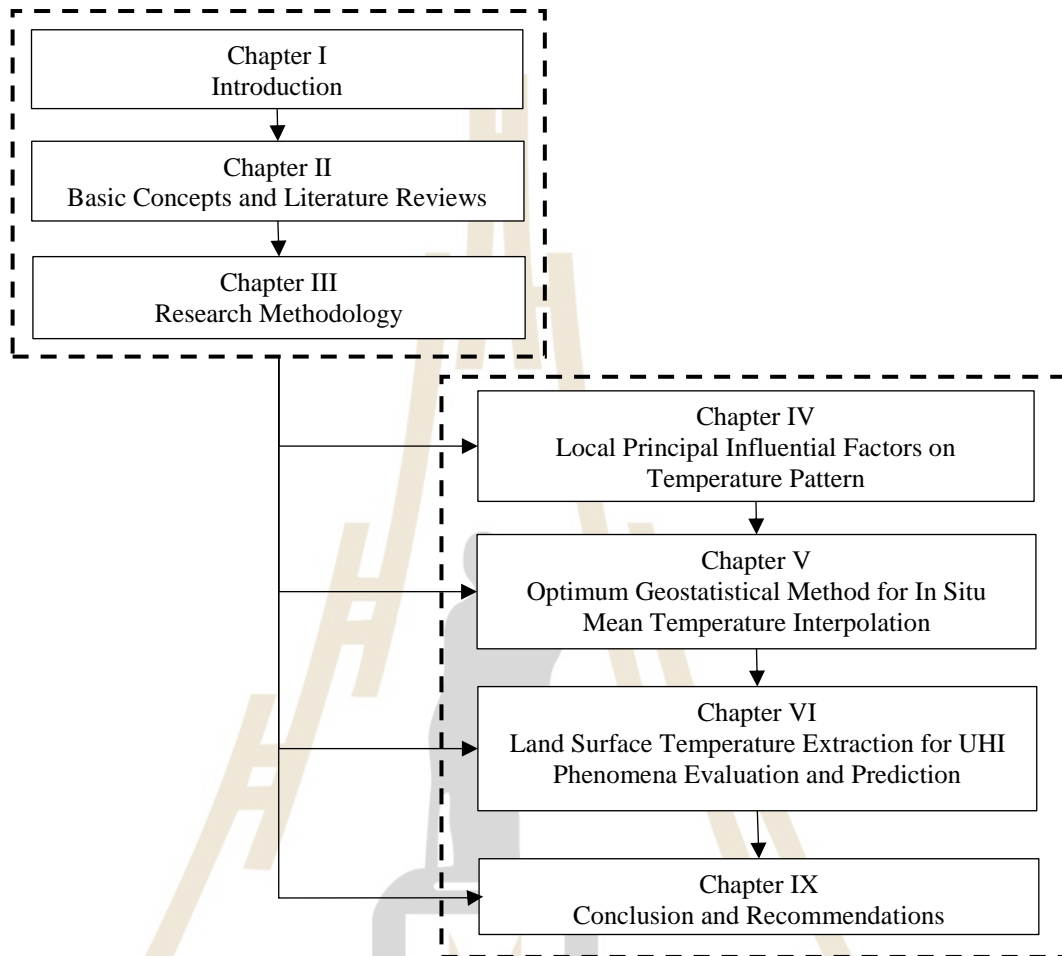


Figure 1.3 Structure of the thesis.

CHAPTER II

BASIC CONCEPTS AND LITERATURE REVIEWS

Under this chapter, basic concepts and theories related to the research including (1) local influential factor on temperature, (2) geostatistics methods for spatial interpolation, (3) conversion of LST from satellite data, (4) UHI phenomena: definition, cause, consequence and mitigation and (5) literature reviews are here summarized.

2.1 Local influential factor on temperature

Ambient air temperature over a particular area on the Earth can dramatically vary in a short period (e.g. during a day/night cycle) but its mean temperature on long-term basis depends on several factors. The most prominent factors typically include amount of the solar radiation, geographic location (latitude, proximity from sea or ocean), topography (altitude and aspect), effects of the ocean current (warm/cold) and prevailing wind, and land surface characteristics. Comprehensive details of each factor and its influence are summarized in the following section.

2.1.1 Latitude or insolation

The surface air temperature on the Earth is a direct result of heat budget at each location that varies over time (e.g. day/night). Some factors might positively influence the budget by increasing heat (converted from the input energy) and

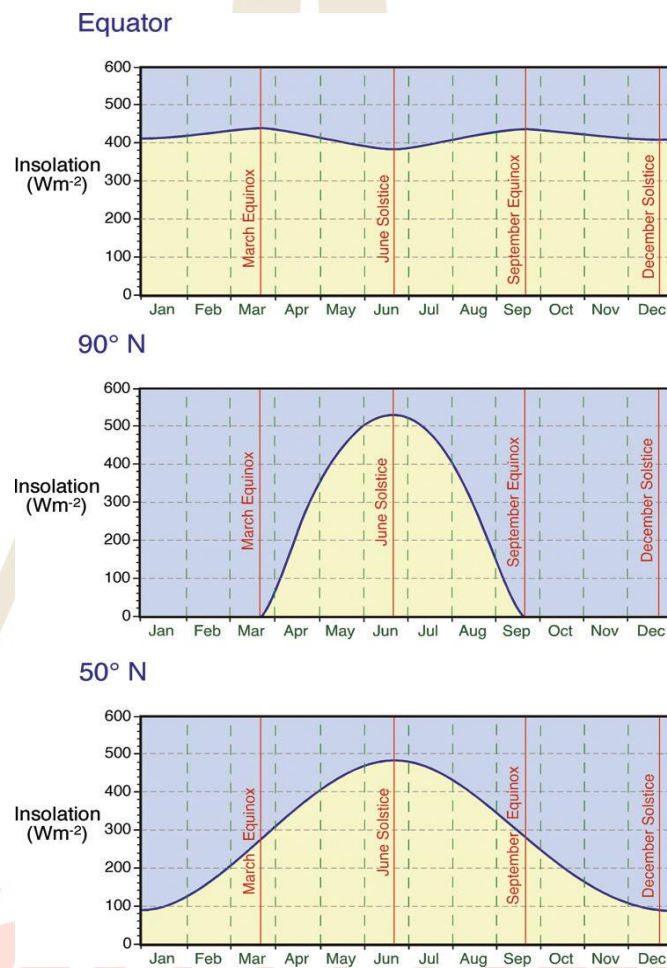
temperature. However, some act to reduce temperature by decreasing the input of heat energy, or by taking away heat energy from the atmosphere. Among the positive factors, the most important one is solar radiation input to the Earth's atmosphere whose amount is largely controlled by intensity and duration of the insolation. As the result of these two elements, the quantity of incoming solar radiation available at the surface varies annually with latitude (Figure 2.1). Typically, day length and incidence angle become greater with increasing latitude, which makes the seasonal changes in surface air temperature also become more extreme when it approaches the poles (Figure 2.2). Highest temperatures tend to occur in summer when day lengths are longest and sun angles are maximum. With shortest day-length and minimum sun angles (in winter), the lowest temperatures occur. Places near equator have only small variations in solar input annually because seasonal changes in day length and incidence angle are relatively low (Figure 2.3). Consequently, variations in temperature over period of one calendar year also are minor (Aguiar, Oliveira, and Goncalves, 2002). Solar radiation and LST are important parameters for analysis of urban thermal behavior.

2.1.2 Altitude or elevation

Surface air temperatures tend to cool gradually with altitude, which is well known to anyone living in a mountainous region. Temperature is usually higher at the mountain's base and decreasing with height above ground. Above this boundary, temperatures are cold enough to maintain snow and ice in a frozen state (subzero temperature). Below the snow line, average temperatures are above freezing.

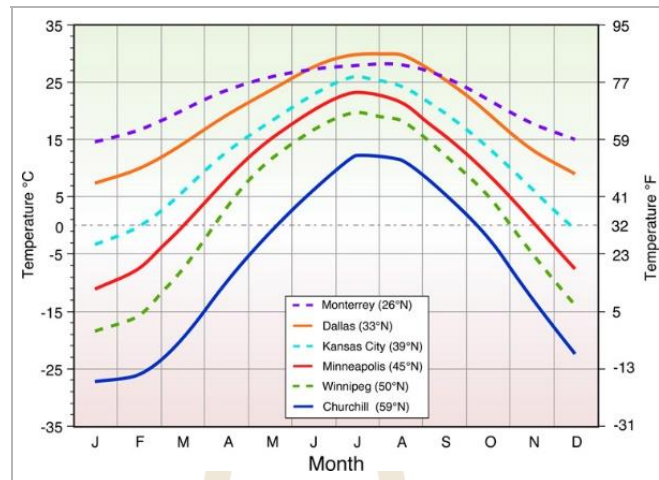
Figure 2.4 shows monthly mean temperatures for four locations in equatorial Columbia with similar latitudes but different elevations from which rate of temperature was found to be about 6.1°C per 1,000 m (3.3°F per 1,000 ft.). This drop

in temperature is related to the fact that the atmosphere becomes less dense with altitude. In general, the elevation of land above the sea level has also a great influence on the temperature, which decreases about 1°F for every 300 ft of ascent (Ahrens and Henson, 2015).



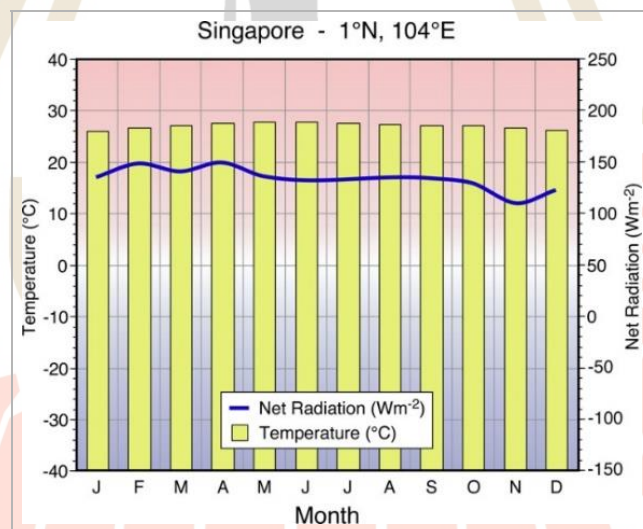
Source: Pidwirny (Online, 2014).

Figure 2.1 Daily insolation at the top of the atmosphere in Wm^{-2} for three locations: equator, 50°N , and 90°N . At the Equator, little annual variation in insolation occurs because of consistent 12-hour days and relatively high Sun angles all year long. 90°N experiences six months of darkness from the September equinox to the March equinox. A location at 50°N would show large seasonal variations in insolation that peak in the June solstice. Lowest quantities of insolation are received during the December solstice.



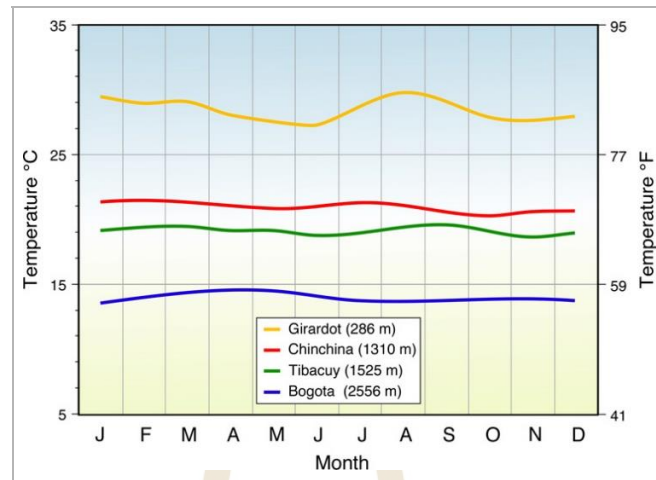
Source: Pidwirny (Online, 2014).

Figure 2.2 Examples of latitude influence on mean monthly temperature as seen on the mean monthly temperatures of five Northern Hemisphere locations with different latitudes.



Source: Pidwirny (Online, 2014).

Figure 2.3 Relationship between mean monthly net radiation and surface air temperature for Singapore. The air temperature data were for period 1877 to 1988. Average mean monthly net radiation data were from the Global Energy Balance Archive (GEBA).



Source: Pidwirny (Online, 2014).

Figure 2.4 Elevation influence on mean monthly temperature. Comparison of mean monthly temperature patterns for four locations in Columbia with different elevations: Girardot (286 m, 938 ft.), Chinchina (1,310 m, 4,298 ft.), Tibacuy (1,525 m, 5,003 ft.), and Bogota (2,556 m, 8,386 ft.). These locations are found within 200 kilometers (125 miles) of each other at a latitude of about 5° north of the equator.

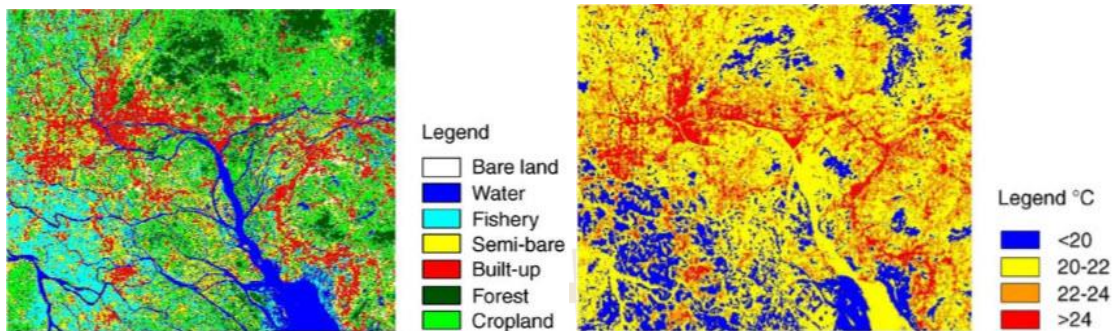
The density of air influences both the heating and cooling of the atmosphere near the Earth's surface. At high elevation, less of the incoming shortwave radiation is absorbed and reflected by particles in the atmosphere lying overhead. This results in more incoming radiation available for conversion into heat energy. The most obvious outcome of having more heat energy available is a rather rapid rise in daytime air temperature in high elevation locations. A thin atmosphere also causes less of the outgoing longwave radiation to be reradiated back to Earth's surface where it can be converted into heat energy again. This greenhouse effect is dependent on the availability of water and other greenhouse gases. When the air becomes thinner, the quantity of these atmospheric substances declines. The net effect of a weaker

greenhouse effect is a rapid and intense nighttime cooling. Magnitude of this nighttime cooling is usually greater than the additional heat created by more intense solar radiation. Therefore, daily, monthly, and annual mean temperatures generally decrease as altitude increases (Ahrens and Henson, 2015).

2.1.3 Land use and land cover (LULC)

Characteristics of the land surface itself can also dictate the appearance of local temperature over the area due mainly to the differences in some properties of the surface material, like absorption/reflection ability, and LULC aspect of an area. For instance, the crowded urban area is normally having higher temperature than the surrounding green or agricultural area nearby due to their difference in prime LULC components (building/ street/ residence for urban area and tree/ plant/ water for agriculture area) and the differences in their absorption/reflection ability (EPA, Online, 2008).

Recent investigations have also shown that climate forcing from LULC change also significantly impacts the temperature trends (Wichansky, Steyaert, Walko, and Weaver, 2008, Roy et al., 2007). Consequently, attention has been increasingly given to impact of LULC change on climate. For example, it has been reported that land use changes due to agriculture lead to the decrease in surface temperatures (Lobell and Bonfils, 2008). LULC change can greatly influence climatological variables such as maximum, minimum and diurnal temperature range (Hale, Gallo, and Loveland, 2008). Figure 2.5 shows examples of LULC pattern and LST distribution in the China's Pearl River Delta region on November 1, 2000.



Source: Chen, Zhao, Li, and Yin (2006).

Figure 2.5 LULC pattern and LST distribution in the China's Pearl River Delta region on November 1, 2000 (based on Landsat TM and ETM+ data).

LULC pattern is regarded as an important determinant of ecosystem function, and can be considered as the representative of landscape pattern in in situ area (Bain and Brush, 2004). LULC categories are linked to distinct behaviors of urban thermal environment (Voogt and Oke, 1997).

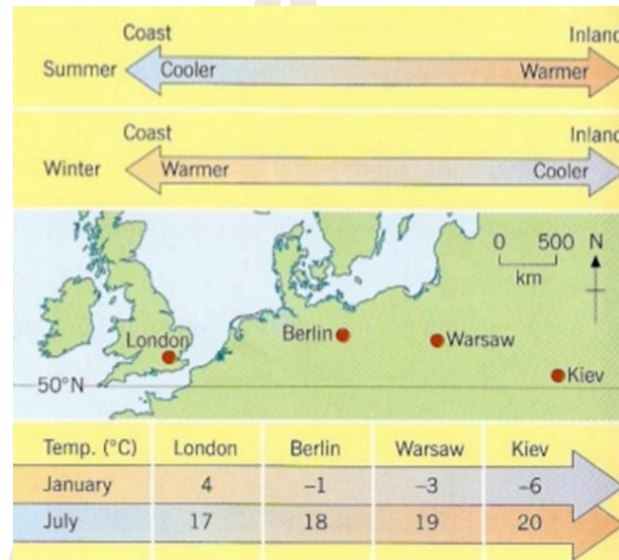
Positive correlation between LST and impervious surface clearly indicates temperature increase in the sprawled area (Bhatta, 2010).

The severity of the intensity of urban heat depends on a city's location and characteristics (Mirzaei and Haghghat, 2010). Typically, individual characteristics include size and density of population, level of industrialization, seasonality of the climate, and traffic pattern and density.

2.1.4 Proximity to sea (distance to the sea)

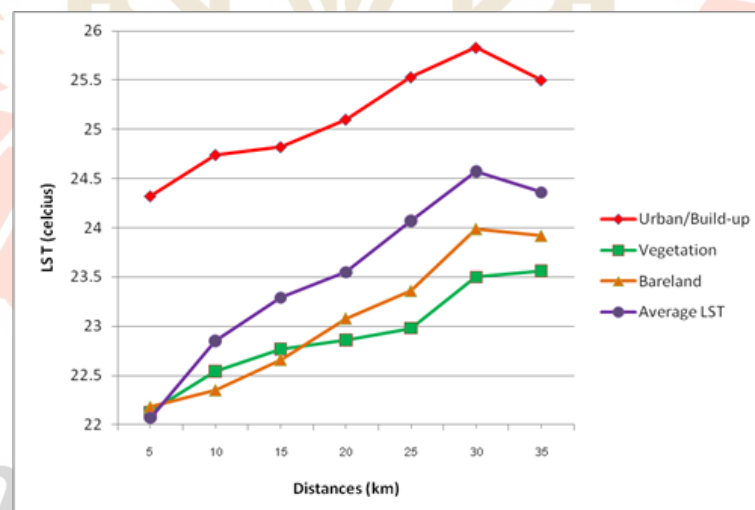
Temperature changes with distance from the sea as the sea makes coastal climates temperature. The oceans heat up and cool down much more slowly than land. This means that coastal locations tend to be cooler in summer and warmer in winter

than places inland at the same latitude and altitude (Price, Michaelides, Pashiardis, and Alpert, 1999) (see Figures 2.6 and 2.7 for example).



Source: <http://www.slideshare.net/maggiesalgado/factors-affecting-temperatures>.

Figure 2.6 Temperature change with distance to the sea in summer and winter season.



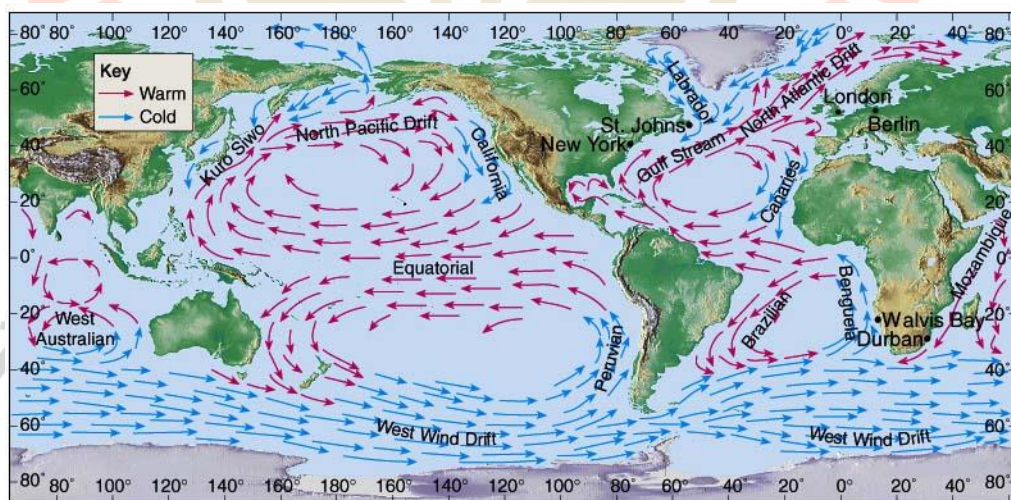
Source: Parinya Chayapong (2010).

Figure 2.7 Variation of the average LST data with distances from the Thai Gulf.

During summer, the sea or ocean water gets heat and cools down more slowly in comparison to land. In comparison with water, land gets heat faster and cools down fast. As the distance to the sea or ocean increases, the temperature increases. During winter, with less insolation, the water shall absorb more sun heat than land. Therefore, when distance to the sea or ocean increases, the temperature gradually decreases as land cools down fast (ECN, Online, 2016).

2.1.5 Ocean current/prevaling wind

The inherent temperature of major ocean currents is also regarded as being crucial factor in controlling land temperature nearby whereas the warm current from the equator (e.g., the Gulf Stream) can substantially warm up the proximate coastal land when passing by meanwhile cold current (like the Peruvian) shall induce opposite outcome (ECN, Online, 2016). Figure 2.8 illustrates major ocean currents known nowadays. Similarly, strong prevailing wind with distinctive nature of its temperature (cold/warm) can greatly affect local temperature of the associated land while it is moving over.



Source: Lutgens and Tarbuck (1998).

Figure 2.8 Major ocean currents at present (warm/cold).

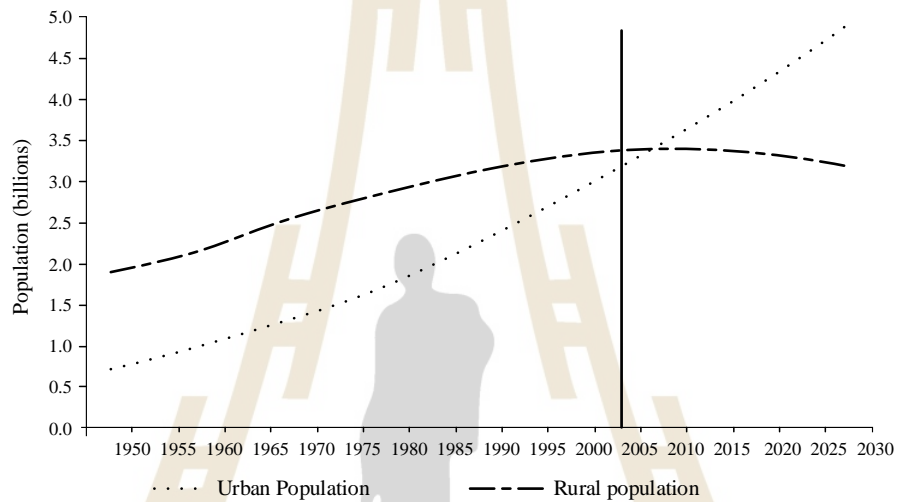
2.1.6 Habitat

In the recent time, the movement of people from rural to urban area within the country (internal migration) is most significant. According to the United Nations report (United Nation, 2006), the number and proportion of urban dwellers will continue to rise quickly in Figure 2.9. Urban global population will grow to 4.9 billion by 2030. At the global level, all future population growth will thus be in towns and cities; most of which will be in developing countries. The urban population of Africa and Asia is expected to be double between 2000 and 2030 (United Nation, 2006). Although very insignificant comparing the movement of people within the country, international migration is also increasing. In general, cities are perceived as places where one could have a better life, because of better opportunities, higher salaries, better services, and better lifestyles. The perceived better conditions attract poor people from rural areas. People move into urban areas mainly to seek economic opportunities. International migration includes labour migration, refugees and undocumented migrants. Both internal and international migrations contribute to urban growth. The number of habitant is decisive factor conditioning the occurrence of urban heat island. Figure 2.10 show increased city size (represented by circles) with increasing number of habitants is responsible for increasing urban temperature (Bhatta, 2010).

Previously, Arnfield (2003) noted that study on UHI has focused on single season analysis due to lack of multi-temporal data. However, multi-seasonal monitoring of urban heat remains a relevant requisite to understanding the implication of LULC types to yearlong urban heat and energy balance.

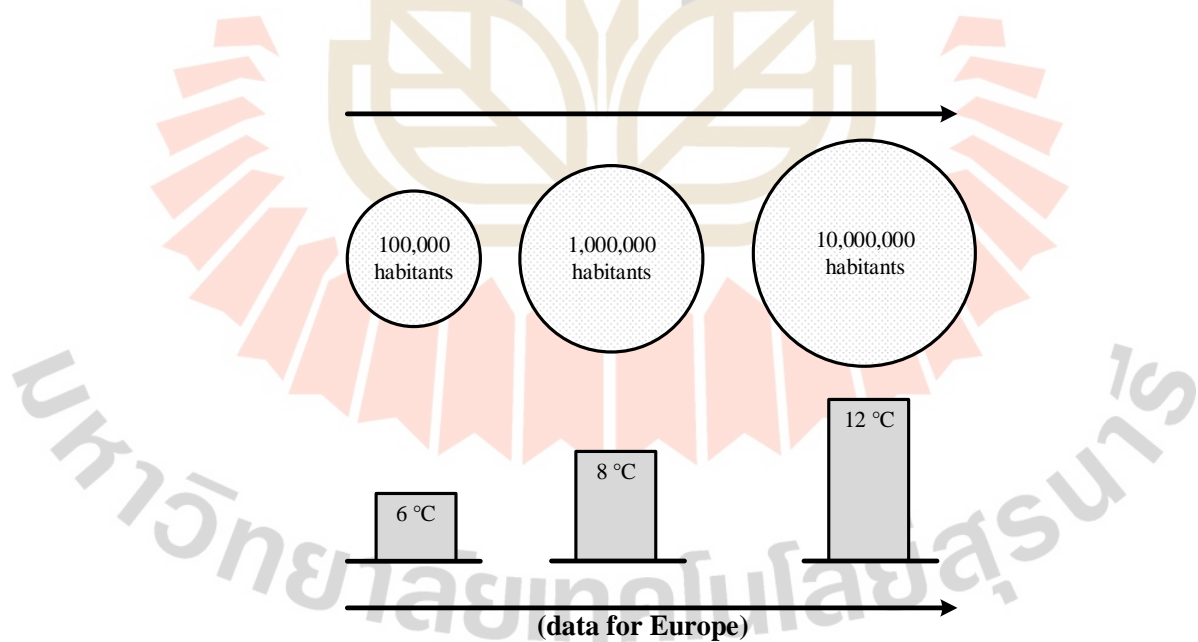
The relationship between LST and population from the main campus area of Prince of Songkla University on the eastern part of the city, a large part of which is

still covered by plants, the LST distribution tends to follow the population density. The relationship between communities and LST distribution in Figure 2.11 shows that more than 88.5% of the 139 communities in Hat Yai face high temperature.



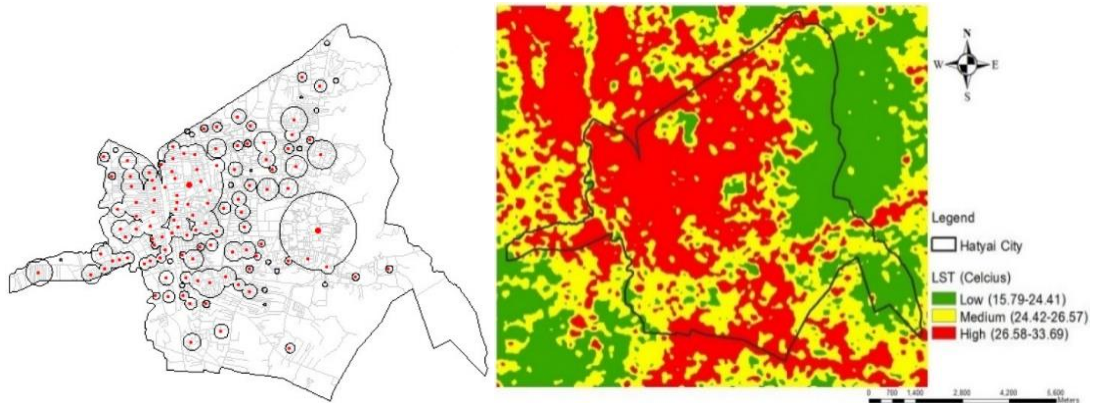
Source: United Nations (2006).

Figure 2.9 Urban and rural population of the world, 1950-2030.



Source: <http://www.mpimet.mpg.de/en/science/imprs-esm.html>.

Figure 2.10 Increased city size and number of habitants cause increase in temperature.



Source: Poonyanuch Ruthirako, Rotchanatch Darnsawasdi, and Wichien Chatupote, 2014.

Figure 2.11 The densely populated zone compared the LST pattern.

2.1.7 Air pollutants

Air pollutant can be found in every big city. The uniqueness of tropical cities is probably the relatively high ambient air temperature and relative humidity throughout the year. It is believed that atmospheric pollutant can be aggravated by the accumulation of smog that is related to the combination of the higher temperature and the presence of air pollutants (Wong and Chen, 2009).

In general, six standard air pollutants that have been extensively studied in urban populations are sulfur dioxide (SO₂), ozone (O₃), nitrogen dioxide (NO₂), carbon monoxide (CO), fine particulate matter (PM_{2.5}), and particulates (PM₁₀). The impact of some air pollutants on health is more evident during the summer or during high temperatures (Castellsague, Sunyer, Saez, and Anto, 1995; Bobak and Roberts, 1997; Hajat, Haines, Goubet, Atkinson, and Anderson, 1999).

In addition, surface temperature inversions play a major role in air quality, especially during the winter when these inversions are the strongest. The warm air

above cooler air acts like a lid, suppressing vertical mixing and trapping the cooler air at the surface. As pollutants from vehicles, fireplaces, and industry are emitted into the air, the inversion traps these pollutants near the ground, leading to poor air quality. The strength and duration of the inversion will control AQI levels near the ground. A strong inversion will confine pollutants to a shallow vertical layer, leading to high AQI levels, while a weak inversion will lead to lower AQI levels. A large contributor to poor air quality during the winter is residential wood burning. Wood smoke contains much higher amounts of particulate pollution than smoke from oil- or gas-fired furnaces (CIESE, 2017). Cold air is heavier than warm air, so temperature inversions limit vertical mixing and trap pollutants near Earth's surface. Such conditions are often found at night and during the winter months. Stagnation events characterized by weak winds are frequent during summer and can lead to accumulation of pollutants over several days (Annenberg Foundation, 2017).

SO₂ is a gas formed when sulfur is exposed to oxygen at high temperatures during fossil fuel combustion, oil refining, or metal smelting. SO₂ is toxic at high concentrations, but its principal air pollution effects are associated with the formation of acid rain and aerosols. SO₂ dissolves in cloud droplets and oxidizes to form sulfuric acid (H₂SO₄), which can fall to Earth as acid rain or snow or form sulfate aerosol particles in the atmosphere (Murphy, 2005). The relationship between SO₂ and total and cardiovascular mortality in Valencia (Ballester, Corella, Pérez Hoyos, and Hervás, 1996) and Rome, Italy (Michelozzi, Forastiere, Fusco, Tobias, and Anto, 1998), was found to be stronger during hot periods than during winter. However, Moolgavkar, Luebeck, Hall, and Anderson (1995) stated that SO₂ had the strongest health effects in spring, autumn, and winter in Philadelphia.

O₃ is the major pollution in tropical cities and it can be easily formed through a photochemical reaction of nitrogen oxides and volatile organic compounds (VOC) (Wong and Chen, 2009). High temperatures on sunny days makes ground-level O₃ (a major component of smog) form much more readily. An EPA study looking at more than 20 years of measurements across most of the rural areas in the eastern U.S. found that harmful O₃ concentrations increased nearly linearly as temperatures increased. Also of concern are days with stagnant air that allow air pollutants to build up and not be flushed out of an area by wind. Stagnant air has been shown to drive up concentrations of both O₃ and particulate matter, unlike temperature, which only directly affects ozone (Climate central, 2017). Touloumi et al. (1997) mentioned that increases in daily mortality and morbidity (indicated by hospital admissions) are associated with high O₃ levels on hot days in many cities.

Nitrogen oxides (NO) and NO₂, referred together as NO_x are highly reactive gases formed when oxygen and nitrogen react at high temperatures during combustion or lightning strikes. Nitrogen presents in fuel can also be emitted as NO_x during combustion. Emissions are dominated by fossil fuel combustion at northern mid-latitudes and by biomass burning in the tropics. In the atmosphere, NO_x reacts with VOCs and carbon monoxide to produce ground-level O₃ through a complicated chain reaction mechanism. It is eventually oxidized to nitric acid (HNO₃). Like sulfuric acid, nitric acid contributes to acid deposition and to aerosol formation (Annenberg Foundation, 2017).

CO is an odorless, colorless gas formed by incomplete combustion of carbon in fuel. The main source is motor vehicle exhaust, along with industrial processes and biomass burning. It binds to hemoglobin in red blood cells, reducing their

ability to transport and release oxygen throughout the body. Low exposures can aggravate cardiac ailments, while high exposures cause central nervous system impairment or death. It also plays a role in the generation of ground-level ozone (Annenberg Foundation, 2017).

In addition to gases, the atmosphere contains solid and liquid particles that are suspended in the air. These particles are referred to as aerosols or particulate matter (PM). Aerosols in the atmosphere typically measure between 0.01 and 10 micrometers in diameter, a fraction of the width of a human hair. Most aerosols are found in the lower troposphere, where they have a residence time of a few days. They are removed when rain or snow carries them out of the atmosphere or when larger particles settle out of suspension due to gravity. Large aerosol particles (usually 1 to 10 micrometers in diameter) are generated when winds blow sea salt, dust, and other debris into the atmosphere. Fine aerosol particles with diameters less than 1 micrometer are mainly produced when precursor gases condense in the atmosphere. Major components of fine aerosols are sulfate, nitrate, organic carbon, and elemental carbon. Sulfate, nitrate, and organic carbon particles are produced by atmospheric oxidation of SO₂, NO_x, and VOC. Elemental carbon particles are emitted by combustion, which is also a major source of organic carbon particles (Annenberg Foundation, 2017).

One important research challenge is learning more about organic aerosols, which typically account for a third to half of total aerosol mass. These include many types of carbon compounds with diverse properties and environmental impacts. Organic aerosols are emitted to the atmosphere directly by inefficient combustion. Automobiles, wood stoves, agricultural fires, and wildfires are major sources in the United States. Atmospheric oxidation of VOCs, both anthropogenic and biogenic, is

another major source in summer. The relative importance of these different sources is still highly uncertain, which presently limits our ability to assess anthropogenic influence and develop strategies for reducing concentrations (Annenberg Foundation, 2017).

2.2 Geostatistics methods for spatial interpolation

Spatial interpolation methods including geostatistics have been developed and applied to various disciplines. They are data-specific or even variable-specific. Many factors including sample size, sampling design and data properties affect the estimations of the methods. In geostatistics, the methods that are capable of using secondary information are often referred to as “multivariate”, while the methods that do not use the secondary information are called “univariate” methods. Geostatistics includes several methods that use kriging algorithms for estimating continuous attributes (Li and Heap, 2014).

In general, geostatistics methods can be categorized into two groups: univariate and multivariate methods. Method accounting for a single variable: Ordinary Kriging (OK), Simple Kriging (SK), and Universal Kriging (UK), is univariate while method accounting for secondary information: Simple Co-Kriging (SCK), Ordinary Co-Kriging (OCK), and Universal Co-Kriging (UCK), is multivariate (Li and Heap, 2014).

Kriging interpolation starts with the recognition that the spatial variation of a continuous attribute is often too irregular to be modelled by a simple function. The variation can be better described by a stochastic surface with an attribute known as a regionalized variable.

The regionalized variable theory assumes that the value of a random variable Z at (x)

$$Z(x) = m(x)\varepsilon'(x) + \varepsilon'' \quad (2.1)$$

Where $m(x)$ is a deterministic function describing a structural component of Z at x , $\varepsilon'(x)$ is a random spatially correlated component and ε'' is a residual non-spatially correlated term, or noise (Nugget variance).

When structural effects have been accounted for and the variation is homogenous in its variation, the semivariance $\gamma(h)$ can be estimated as:

$$\gamma(h) = \frac{1}{2n} \sum_{i=1}^n \{z(x_i) - z(x_i + h)\}^2 \quad (2.2)$$

Where n is number of pairs of sample points of observations of the values of attribute z separated by distance h .

A plot of $\gamma(h)$ against h is called a semivariogram and it gives a quantitative description of the regionalized variation (see Figure 2.12). An important factor of the variogram is the range, which describes the distance when the data points become spatially independent. The variogram can be used to estimate the optimal weights λ_i needed for interpolation. The value $\hat{Z}(x)$ for an unsampled point is then calculated with following equation:

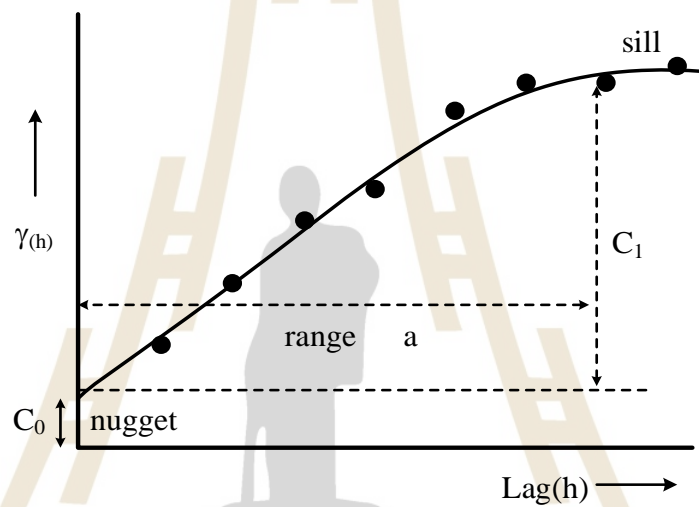
$$\hat{Z}(x_0) = \sum_{i=1}^n \lambda_i * Z(x_i) \quad (2.3)$$

The principle is show in Figure 2.13 (Burrough and McDonnell, 1998).

In general, Kriging is a relatively fast interpolator that is flexible with input and output data: many outputs can be generated besides the prediction maps like predictions

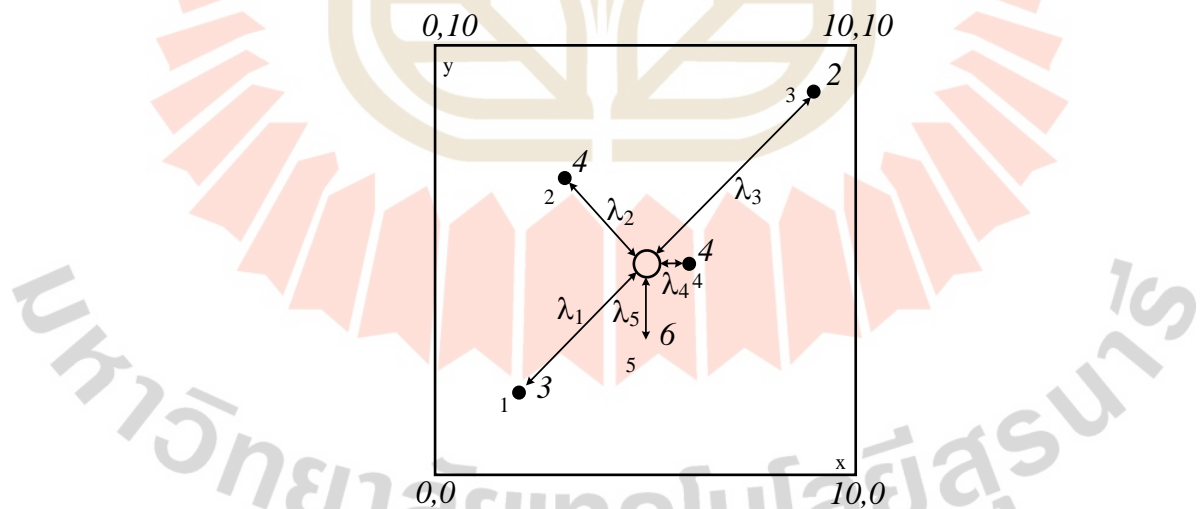
errors and probabilities. Drawback of the flexibility is that it may require a lot of decision-making. Measure of success is through the prediction errors or through cross validation.

Characteristics of each sub-type of univariate and multivariate methods are summarized based on Sluiter (2009) as follows.



Source: Burrough and McDonnell (1998).

Figure 2.12 Variogram example.



Source: Burrough and McDonnell (1998).

Figure 2.13 The principle of Kriging.

2.2.1 Ordinary kriging

Ordinary kriging (OK) is the basic form of kriging. The prediction by OK is a linear combination of the measured values. The spatial correlation between the data, as described by variogram, determines the weights. As the mean is unknown, fewer assumptions are made. The method assumes intrinsic stationary, unfortunately meteorological variables are often not stationary. In some case, this problem can be eliminated by using different sizes and shapes of the search neighbourhood. OK is frequently applied in meteorology.

2.2.2 Simple kriging

Simple Kriging (SK) is OK with a known mean. Therefore, it is slightly more powerful than OK, however the mean is often difficult to derive.

2.2.3 Universal kriging

Universal Kriging (UK) is also known as “Kriging with a trend/external drift”. It uses a regression model as part of the kriging process to model the mean value expressed as a linear or quadratic trend.

2.2.4 Co-Kriging

Co-Kriging (CK) is an extension of standard Kriging using a multivariate variogram or covariance model and multivariate (ancillary) data. With CK, the estimations on a location are based on a linear weighted sum of all examined variables. When more than one co-variable is considered, the method may become highly complex.

In meteorology, CK is often applied. Schuurmans, Bierkens and Pebesma (2007) used CK to combine station data with precipitation radar data (as well as Kriging with an external drift).

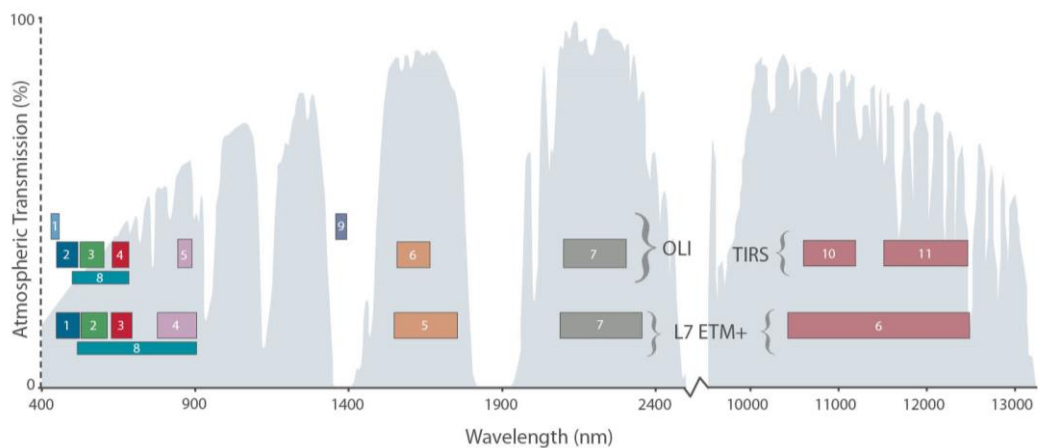
In general, CK gives better results when the number of covariables are (much) higher than the variable of interest and when the spatial correlation between variables and covariables is high. The assumptions are the same as for ordinary Kriging plus assumptions with respect to cross-variogram model estimation.

2.3 Conversion of LST from satellite data

The Landsat 8 satellite is the near-polar, sun-synchronous, 705 km circular orbit and in position as the recently decommissioned Landsat 5 satellite. Landsat 8 data are acquired in 185 km swaths and segmented into 185×180 km scenes using the second World-wide Reference System (WRS-2) with path (ground track parallel) and row (latitude parallel) as same as Landsat 4, 5, and 7 satellites (Arvidson, Gasch, and Goward, 2001). Landsat 8 has a 16 day repeat cycle, each WRS-2 path/row is overpassed every 16 days and may be acquired a maximum of 22 or 23 times per year for any scene. Combined, the Landsat 8 and 7 sensors provide the capability to acquire any WRS-2 path/row every 8 days at the Equator and more frequent coverage at higher latitudes due to the pole ward convergence of the Landsat orbits (Kovalskyy and Roy, 2013).

Prior to Landsat 8, the LST from Landsat can be derived without use of ancillary data from only one thermal wavelength band. The two thermal TIRS bands of Landsat 8 are spectrally similar to two thermal bands of MODIS and enable, for the first time, atmospheric correction of Landsat thermal imagery using split-window technique. This provides simpler and more accurate retrieval of surface temperature and emissivity than was possible with previous Landsat sensor data. Landsat 8 instruments represent an evolutionary advance in technology. Operational Land Imager (OLI) improves on the

past Landsat sensors using a technical approach demonstrated by a sensor flown on NASA's experimental EO-1 satellite. OLI is a pushbroom sensor with a four-mirror telescope and 12-bit quantization. OLI collects data for visible, near infrared, and short wave infrared spectral bands as well as a panchromatic band. It has a five-year design life. Figure 2.14 compares the OLI spectral bands to Landsat 7's ETM+ bands. OLI provides two new spectral bands, one tailored especially for detecting cirrus clouds and the other for coastal zone observations. Additionally, the bandwidth has been refined for six of the heritage bands. The Thermal Instrument (TIRS) carries two additional thermal infrared bands. Table 2.1 compares spectral characteristic of Landsat 7 and 8.



Source: <http://landsat.gsfc.nasa.gov/?p=3186>.

Figure 2.14 Bandpass wavelengths for Landsat 8 OLI and TIRS sensor, compared to Landsat 7 ETM+ sensor.

Table 2.1 Comparison of Landsat 5, Landsat 7 and 8 specifications.

Landsat 5			Landsat 7			Landsat 8		
Band	Wavelength (μm)	Resolution (m)	Band	Wavelength (μm)	Resolution (m)	Band	Wavelength (μm)	Resolution (m)
Band 1 - Blue	0.450-0.515	30	Band 1 - Blue	0.441-0.514	30	Band 1 – Coastal/Aerosol	0.43-0.45	30
Band 2 - Green	0.525-0.605	30	Band 2 - Green	0.519-0.601	30	Band 2 - Blue	0.45-0.51	30
Band 3 - Red	0.630-0.690	30	Band 3 - Red	0.631-0.692	30	Band 3 - Green	0.53-0.59	30
Band 4 - NIR	0.750-0.900	30	Band 4 - NIR	0.772-0.898	30	Band 4 - Red	0.64-0.67	30
Band 5 - SW-1IR	1.55-1.75	30	Band 5 - SW-1IR	1.547-1.749	30	Band 5 - NIR	0.85-0.88	30
Band 7 - SWIR-2	2.08-2.35	30	Band 7 - SWIR-2	2.064-2.345	30	Band 6 – SWIR-1	1.57-1.65	30
Band 8 - Pan	0.52-0.90	15	Band 8 - Pan	0.515-0.896	15	Band 7 – SWIR-2	2.11-2.29	30
Band 6 - TIR	10.4-12.5	60	Band 6 - TIR	10.31-12.36	60	Band 8 - Pan	0.50-0.68	15
						Band 9 - cirrus	1.36-1.38	30
						Band 10 - TIR-1	10.60-11.19	100
						Band 11 - TIR-2	11.50-12.51	100

Source: <http://landsat.gsfc.nasa.gov/?p=3186>.

In practice, the conversion of brightness value to LST from thermal band Landsat-8 divides into three basic steps:

(1) Conversion to TOA Radiance

The digital number (DN) of thermal band (Band 6 for Landsat-5 and Landsat-7, and Band 10 for Landsat 8) are converted to spectral radiance at top of atmosphere (TOA) with metadata file using following equation (USGS, Online, 2016).

$$L_{\lambda} = M_L Q_{cal} + A_L \quad (2.4)$$

Where L_{λ} is TOA spectral radiance (watts/ (m²•srad•μm)), M_L is band specific multiplicative rescaling factor from the metadata, A_L is band specific additive rescaling factor from the metadata and Q_{cal} is quantized and calibrated standard product pixel values (DN).

(2) Conversion to at satellite brightness temperature

The derived spectral radiance at TOA is converted to brightness temperature (BT) based on uniform emissivity (ϵ) assumption with constant value given in metadata file using following equation (USGS, Online, 2016)

$$BT = \frac{K_2}{\ln\left(\frac{K_1}{L_{\lambda}} + 1\right)} \quad (2.5)$$

Where BT = At – Satellite brightness temperature in Kelvin (K)

L_{λ} = TOA spectral radiance (watts/ (m²•ster•μm))

K_1, K_2 = Band specific thermal conversion from the metadata (See Table 2.2).

Table 2.2 Thermal constant of K_1 , K_2 value.

Thermal constant	Landsat 8		Landsat 7	Landsat 5
	Band 10	Band 11	Band 4	Band 6
K_1	774.89	480.89	666.09	607.76
K_2	1321.08	1201.14	1282.71	1260.56

(3) Correction for spectral emissivity

The temperature values obtained above are referenced to a black body. Therefore, corrections for spectral emissivity (ϵ) became necessary according to the nature of land cover. The emissivity corrected land surface temperatures (LST) were computed as follows (Artis and Carnahan, 1982):

$$LST = \frac{BT}{1 + (\lambda \cdot BT / \rho) \ln \epsilon} \quad (2.6)$$

Where λ is wavelength of emitted radiance, ρ is hc/σ (1.438×10^{-2} m K), σ is Boltzmann constant (1.38×10^{-23} J/K), h is Planck's constant (6.626×10^{-34} J s), and c is velocity of light (2.998×10^8 m/s).

In this study, Band 6 of Landsat 5, Band 6 of Landsat 7 and Band 10 of Landsat 8 are used to calculate LST. According to Yu, Guo, and Wu (2014), Band 10 of Landsat 8 can provide accuracy in term of RMSE higher than Band 11 when LST was inverted from the radiative transfer equation-based method.

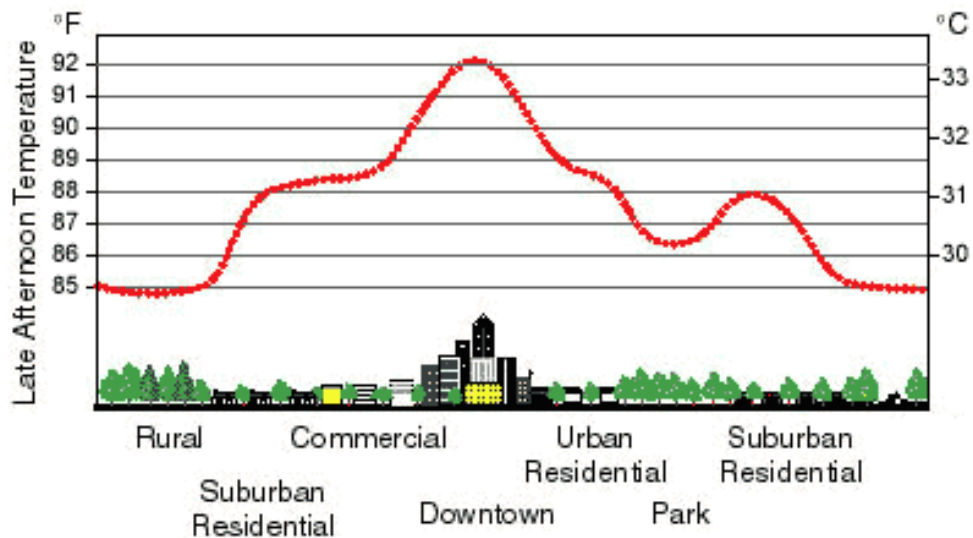
2.4 UHI phenomena: Definition, cause, consequence and mitigation

2.4.1 Definition of UHI

The UHI is created when naturally, vegetated surfaces e.g. grass and trees are replaced with non-reflective, water-resistant impervious surfaces that absorb a high percentage of incoming solar radiation (Taha, 1997). Magee, Curtis and Wendler (1999) defined the UHI is the temperature found at a given location within the city subtracted from the temperature that would be measured at that same location without the presence of the city. While, Roth (2013) defined the UHI is a phenomenon whereby urban regions experience warmer temperatures than their rural, undeveloped surroundings. Likewise, EPA (Online, 2016) defined the UHI describes built up areas that are hotter than nearby rural areas. Like, Voogt (2002) defined the UHI refers to the observed temperature difference between urban environments and the surrounding rural areas.

Parinya Chayapong (2010) claimed that the UHI is a phenomenon that has been known for long time by the climatologists in western countries and being evidenced globally at present, especially over large and crowded megacities. Outstanding feature of this incidence is a notable increase of the urban temperatures compared to those of the surrounding rural/suburban area that makes the obvious temperature gap between the two areas.

Figures 2.15 displays the typical temperature profile represents the UHI phenomenon.



Source: http://www.eoearth.org/article/Heat_island.

Figure 2.15 Typical temperature profile represents the UHI phenomenon.

2.4.2 Cause of UHI

Main cause of the UHI is strong absorption of sunlight by buildings and other hard surfaces, like road or open paved space, during daytime. Part of this absorbed heat shall then be released back to the atmosphere afterwards through the thermal radiation process, which can substantially increase local ambient temperature experienced in the urban area. This process shall keep urban lands warmer than surrounding areas during both daytime and nighttime (see Figure 2.16). Intensity of the UHI incidence (ΔT) is commonly measured by amount of the temperature differences between referred urban locations and some referred rural sites, or,

$$UHI\ Intensity(\Delta T) = T_{urban} - T_{rural(reference)} \quad (2.7)$$

The UHI are persistent zones with above average LST (Senanayake, Welivitiya, and Nadeeka, 2013). The intensity of the UHI is defined by the difference

between average temperature of UHI areas and that of rural areas (Ma, Kuang, and Huang, 2010) by the following condition equations:

$$LST > \mu + 0.5 * \sigma \quad (2.8)$$

This phenomenon represents UHI area exists in the study area.

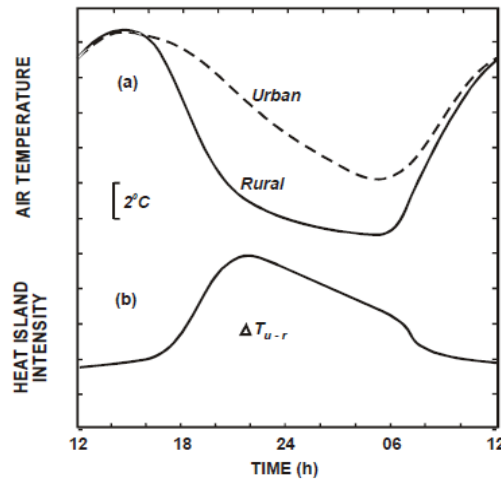
On contrary,

$$0 < LST \leq \mu + 0.5 * \sigma \quad (2.9)$$

This phenomenon represents non-UHI area exists in the study area.

Where, μ is mean temperature in the study area and σ is standard deviation of temperature in the study area.

It is well known that the progressive replacement of natural surfaces by built surfaces, through urbanization, constitutes the main cause of the UHI formation. Natural surfaces are often composed of vegetation and moisture-trapping soils. Therefore, they utilize a relatively large proportion of the absorbed radiation in the evapotranspiration process and release water vapour that contributes to cool the air in their vicinity. In contrast, built surfaces are composed of a high percentage of non-reflective and water-resistant construction materials. As consequence, they tend to absorb a significant proportion of the incident radiation, which is released as heat.



Source: Oke (1987).

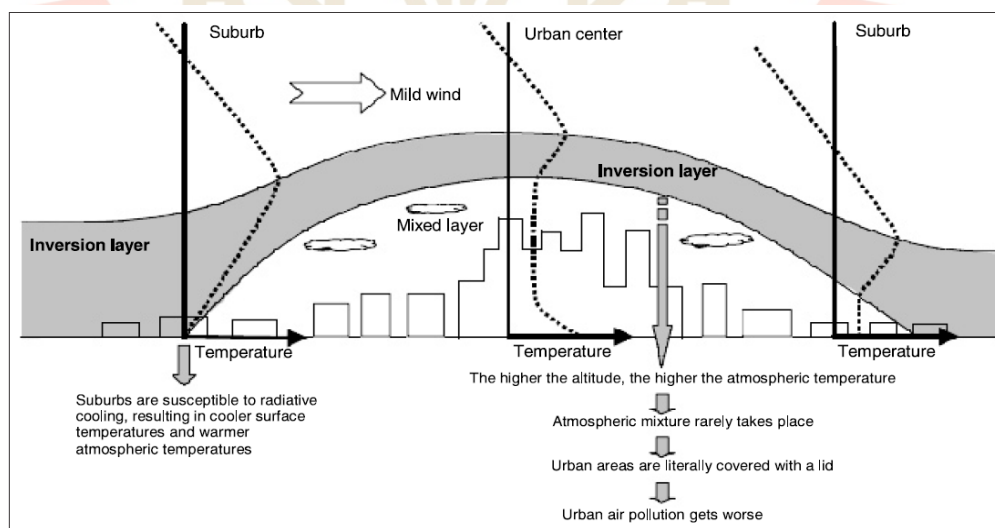
Figure 2.16 Typical diurnal variations of air temperature under calm/clear air: (a) air temperature in urban/rural area and (b) the resulting heat island intensity (ΔT_{u-r}) under ideal weather conditions.

Vegetation intercepts radiation and produces shade that also contributes to reduce urban heat release. The decrease and fragmentation of large vegetated areas such as parks, not only reduces these benefits, but also inhibits atmospheric cooling due to horizontal air circulation generated by the temperature gradient between vegetated and urbanized areas (i.e. advection), which is known as the park cool island effect. On the other hand, the narrow arrangement of buildings along the city's streets form urban canyons that inhibit the escape of the reflected radiation from most of the three-dimensional urban surface to space. This radiation is ultimately absorbed by the building walls (i.e. reduced sky view factor), thus enhancing the urban heat release. Additional factors, which include the scattered and emitted radiation from atmospheric pollutants to the urban area, the production of waste heat from air conditioning and

refrigeration systems, industrial processes and motorized vehicular traffic (i.e. anthropogenic heat), and the obstruction of rural air flows by the windward face of the built-up surfaces, have been recognized as additional causes of the UHI effect (Kumar, Bhaskar, and Padmakumari, 2012).

2.4.3 Impacts of UHI

Yamamoto (2006) described the UHI impact according to season: winter and summer. Winter impact, inversion layers form by radiative cooling on clear, calm winter nights. Ascending air currents created by warm urban areas are trapped under inversion layers, forming mixed layers (dust domes) that exacerbate air pollution (see Figure 2.17). Meanwhile, summer impacts, urban areas are becoming uncomfortable places to live because of higher temperatures during daytime and an increasing number of sweltering nights. Higher temperatures boost demand for air conditioning, resulting in increased energy consumption. They also contribute to localized torrential downpours and the production of photochemical oxidants.



Source: Yamamoto (2006).

Figure 2.17 Atmospheric conditions inside and outside urban area in winter.

Giguère (Online, 2009) stated that the UHI can have adverse impacts on (1) the environment and (2) on health during the summer. For impacts on the environment, the impact of the UHI on air quality arises due to increased temperatures as well as through the indirect effects that greater energy demand has on increasing emissions. Increased temperatures have been correlated with the elevated production of ground level ozone (O_3), also referred to as photochemical smog. Ozone is a respiratory irritant and is known to exacerbate a number of cardiopulmonary diseases including asthma and chronic bronchitis. Studies have also linked ozone to impaired lung function and development in children (Chan, Lebedeva, Otero, and Richardson, Online, 2007). The UHI can also indirectly contribute to poor air quality by increasing cooling demand and air-conditioning use. In addition, warmer surface and air temperatures during both the day and evening create an increased demand for energy. This demand is further increased by construction of urban environments with high albedo surfaces that increase the absorption of solar radiation by buildings (Forkes, Online, 2010). Increased energy demand results from the subsequent increase in air-conditioning use in order to keep buildings at safe and comfortable temperatures. While the warmer temperatures also lower requirements for heating in the winter months, it has been demonstrated that in cities with warm summers, the high-energy requirements for cooling outweigh the winter heating savings (Yow, 2007). It has been estimated that 5-10% of community electricity demand results from the need to compensate for the UHI effect (EPA, Online, 2008). Especially, greater air-conditioning use is concerning as it corresponds to increased peak energy demand. Peak energy demand describes the point within a 24-hour period where the demand for electricity is highest. Increases in peak energy

demand may compromise the security and stability of power supplies during extreme heat events. This may result in reduced transmission efficiency or compromise the power supply entirely, leading to temporary blackouts. Additionally, heat islands likely cause an increase in demand for potable water, for cooling (e.g. swimming pools and fountains) or for watering plants (Balling, Gober, and Jones, 2008).

Meanwhile, for impacts on health, periods of high temperatures, the effects of which are magnified by UHI, can cause heat stress for the population. Some individuals may be more vulnerable to the effects of UHI, such as people with chronic diseases, people who are socially isolated, very young children, outdoor workers, persons of low socioeconomic status, people who engage in strenuous outdoor exercise and the mentally ill (EPA, Online, 2008). However, more severe illnesses may develop as bodies lose water and vital minerals. These illnesses include heat cramps, heat rash, heat edema, fainting, heat exhaustion, and heat stroke (Forkes, Online, 2010).

In addition, the periods of high temperatures associated with the UHI can cause discomfort, weakness, disturbances of consciousness, cramps, fainting, heat stroke, and even exacerbate pre-existing chronic diseases such as diabetes, respiratory failure, and cardiovascular, cerebrovascular, neurological and renal diseases, to the point of causing death (Luber and McGeehin, 2008). On the recommendation of the World Health Organization, health agencies around the world, including in Québec, have instituted various programs to mitigate the effects of intense heat and prevent the UHI.

2.4.4 Mitigation Strategies for UHI Effects

Sailor (Online, 2006) reviewed the current and possible the future UHI mitigation strategies, including albedo modifications, tree planting, and “ecoroofs”. As in other reports on eco or green roofs, this one described the benefits for urban hydrology and energy use in the building with the roof without being able to say much about the effect of green roofs on general urban climate. Sailor also described the functions of U. S. national governmental and nonprofit organizations, as well as activities on mitigating UHIs in other countries.

The UHI mitigation strategies have an impact on both local and global climates. In addition to environmental benefits, these mitigation strategies also help in reducing the energy consumption for cooling and increase the thermal comfort of the poor people who suffer most in the heating summers. To counterbalance the impact of the phenomenon, important research has been carried out to develop proper mitigation technologies able to decrease ambient and surface temperatures in cities. Mitigation of the UHI leads to energy and energy expenditure savings, improves urban air quality and ambient conditions, and help to counter global warming. Many implementation technologies exist and are used in parallel, many scientific and administrative activities support the implementation of the UHI mitigation technologies (Moriyama and Tanaka, 2012).

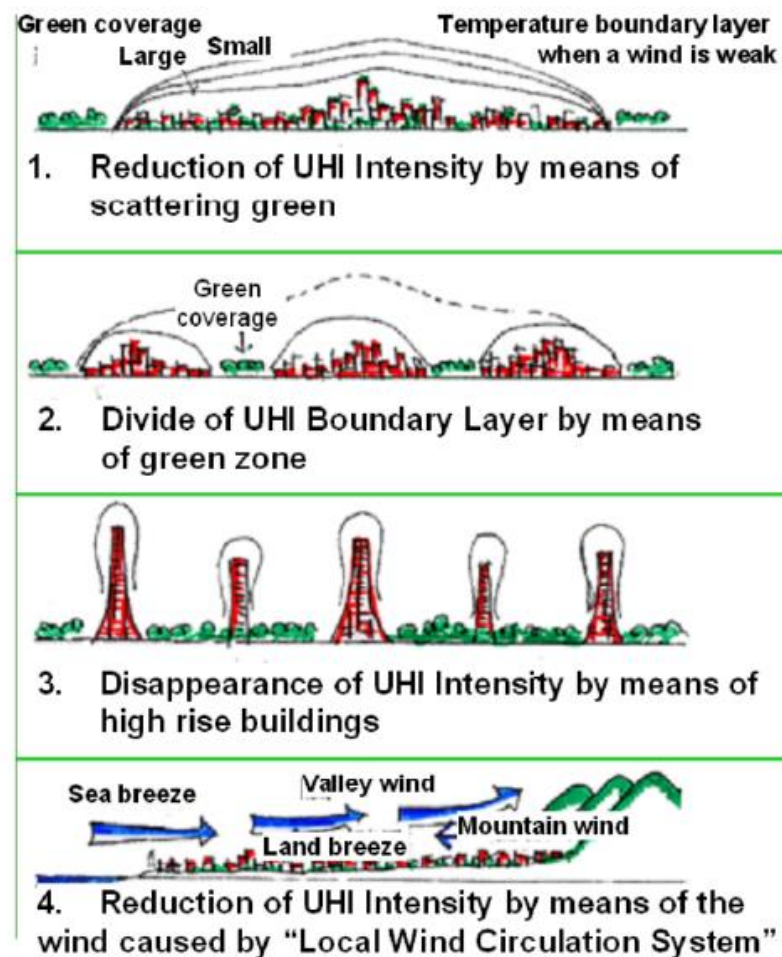
Generally, the UHI intensity depends on the city size. The UHI phenomenon means the air temperature boundary layer covered over a city. Moriyama and Tanaka (2012) suggested that there are four methods to reduce the intensity of the boundary layer over the city as shown in Figure 2.18.

(1) Reduction of UHI Intensity by means of creating green spaces, cool roofs and cool pavements.

(2) Dividing of UHI boundary layer by means of green belts or water surfaces such as rivers, and lakes.

(3) Disappearance of UHI phenomenon by the combination of high-rise buildings and the natural earth surface at the ground level.

(4) Reduction of UHI phenomenon by means of the wind caused by local wind circulation system.



Source: Moriyama and Tanaka (2012).

Figure 2.18 Concept of countermeasures to UHIs.

2.5 Literature review

Relevant literature reviews that are directly related with main research objectives are reviewed and summarized into two groups, namely, geostatistical method and satellite-based LST and UHI effect.

2.5.1 Geostatistical interpolation method

Chang, Dai, and Chen (2004) applied the Kriging interpolation, a geostatistical method, to meteorology. They compare the interpolation technique between Inverse Distance to a Power (IDP), Spline and OK and UK. The accuracy of the IDP method would be almost the same as the Kriging's if four sampling points around the points to be estimated. This result showed that there are the same interpolation weights for the Kriging and IDW method. When using the whole sampling points of the field instead of only eight sampling points to interpolation, the accuracy of UK method is not as good as that of spline. It is due to the complexity of the global drift that cannot be expressed by a second-order polynomial function. The interpolation of the OK method may be improved and is better than the UK method for most cases studies if the drift is removed by some preprocess, but it must remember that the improvement depends on the preprocess and the property of the field to be interpolated.

Tewelde, Beza, Costa, and Painho (2010) stated that the selection of the best interpolation technique for each particular situation is a key factor. The major objective of the study is to assess the spatial variability of annual average temperature in the southern region of Eritrea by comparing different interpolation procedures. The temperature data were interpolated using a deterministic method (Inverse square distance) and three geostatistical methods (OK, UK and SK). The performance of the

different techniques was compared through error statistics computed using Jackknife cross-validation. The error statistics of the different interpolation methods reveal that all techniques have a similar performance. IDW is slightly less accurate and more biased than the kriging methods as expectation.

Relevant previous work of geostatistics methods comparison for spatial interpolation is summarized in Table 2.3.

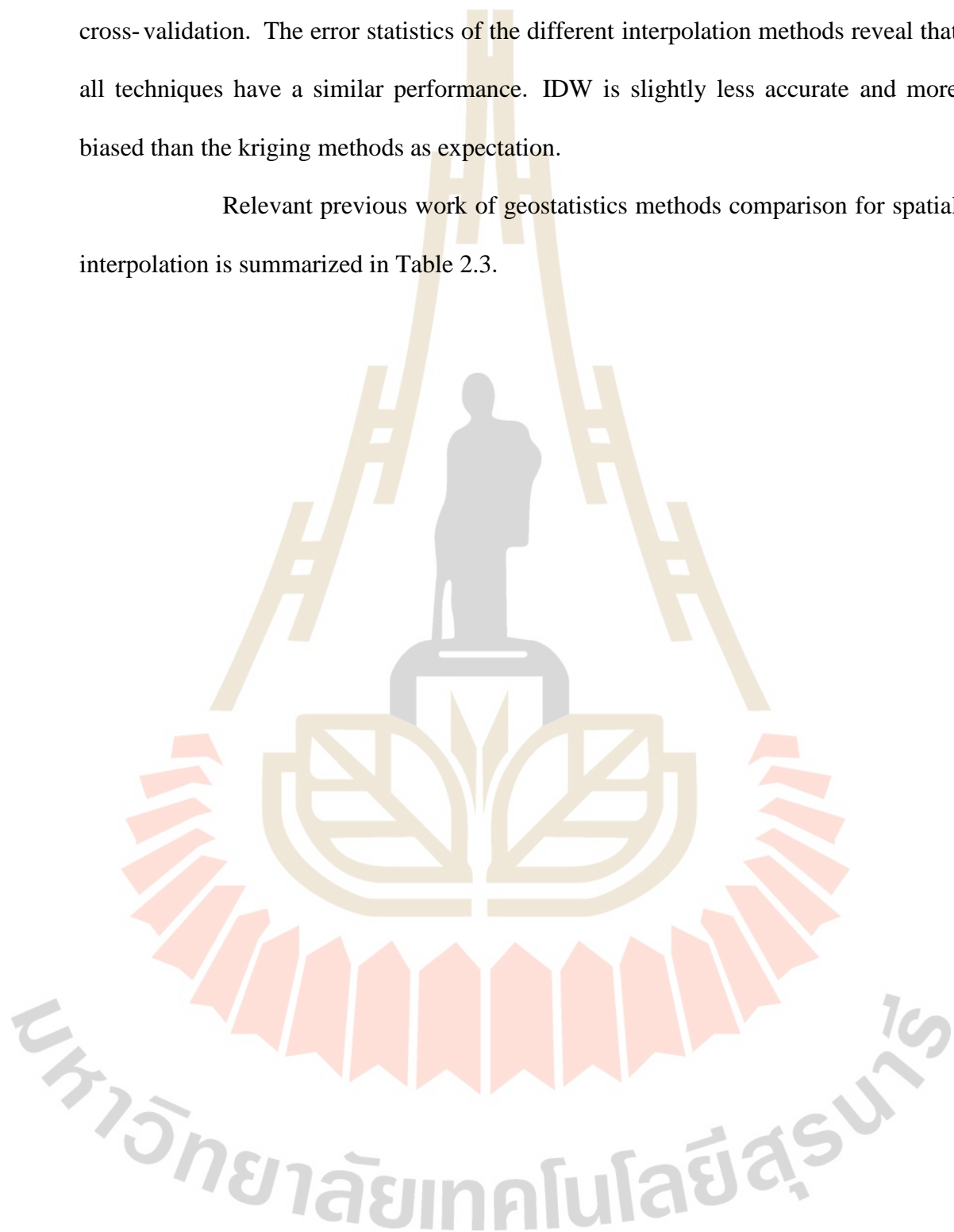


Table 2.3 Summary of geostatistics methods comparison for spatial interpolation.

No	Methods compared	Result	Reference
1	IDS, OK, OCK & OK combined with LMR	OK combined with LMR the best.	Li, Cheng, and Lu, 2005
2	IDW, Spline, Kriging-exponential, Kriging-spherical and Kriging-Gaussian,	Kriging-exponential and Kriging spherical have the best interpolation precision	Cao, Hu, and Yu, 2009.
3	IDW, GPI, LPI, RBF, OK, OCK, UK, UCK, SK, SCK, DK, DCK	For mean monthly temperature all Co-Kriging technique have more effectiveness than other interpolation techniques	Yaowaret Jantakat and Suwit Ongsomwang, 2010.
4	IDW, TPS ,GP, LP OK, and UK	OK and UK the best	Eldrandaly, and Abu-Zaid, 2011
5	IDW, OK	Ok better	Panudda Tiengrod and Waranyu Wongseree, 2013

Note:

Simple Kriging (SK)	Simple Co-Kriging (SCK)	Thin-Plate Spline (TPS)
Ordinary Kriging (OK)	Ordinary Co-Kriging (OCK)	Global Polynomial (GP)
Disjunctive Kriging (DK)	Disjunctive Co-Kriging (DCK)	Local Polynomial (LP)
Universal Kriging (UK)	Universal Co-Kriging (UCK)	Temperature Lapse Rate method (TLR)
Global Polynomial Interpolation (GPI)	Local Polynomial Interpolation (LPI)	Radial Basic Function (RBF)
Inverse Distance Weigth (IDW),	linear model of regionalization (LMR)	

2.5.2 Satellite-based LST extraction and UHI effect

Thanakrit Teanmanee (2002) examined the UHI and physical environment. High temperature and UHI phenomena particularly appear on areas highly dense with complex constructions and human activities. These areas included of living areas, business areas, locations of commercial activities and areas with heavy traffic. Low temperature appeared on areas with low density and on public park area with green areas as predominant characteristics. These findings further suggested that in order to avoid the UHI phenomena, direction of regional wind should be taken into a careful consideration and long successive blocks of buildings should be discouraged to allow continuous flow of wind.

Chen, Zhao, Li, and Yin (2006) had investigated relationship between UHI and land use/cover changes based on the found relationships between temperature and several LULC indices, including NDVI, NDWI, NDBaI and NDBI. It was concluded that correlations between NDVI, NDWI, NDBaI and temperature are negative when NDVI is limited in range, but positive correlation is shown between NDBI and temperature.

Kanokwan Komonveeraket (2008) analyzed effects of land cover on UHI in Bangkok Metropolis. Surface radiant temperature, the Transformed Vegetation Index (TVI), and LULC type derived from Landsat-TM data were introduced for UHI assessment throughout Bangkok Metropolis. Results showed an inverse relationship between TVI and surface temperature and the variation of these values on different land surface properties. The high TVI and low surface temperature corresponded to vegetation area, while the low TVI and high surface temperature corresponded to the

built up surface and bare soil. The study showed that the presence of vegetation could cool down the surface temperature in such land covers type. The decreasing of vegetation and the extension of built-up area can raise surface temperature when considered difference between TVI and surface temperature with respect to urban and rural area.

Pathompong Sukthong (2008) applied thermal remote sensing on UHI study at Pathumthani urban areas. The result indicated that there is a strong linear relationship between thermal infrared (band 12) of TERRA (ASTER) digital data and the in-situ surface temperature. It was found that the UHI phenomenon in Pathumtani urban area differs from other cities or metropolis because of its unique urban land use pattern, whereas the urbanized area is intermittently separated with scattered agricultural plots. Occurrence of UHI phenomenon is directly related to the urban land use pattern such as commercial and industrial areas.

Xiao et al. (2008) identify quantification of statistical relationship between LST and land use land cover parameters as a relatively neglected field of research in the field of thermal remote sensing. They quantitatively analyzed LST variations in context of biophysical and demographic variables. It was found that LST is positively correlated with built up area and population density, while negative association exists between LST and percentage of forest, farmland and water bodies. Positive relationship between LST and fraction of impervious surface, and negative association between LST and fraction of green vegetation cover has been collaborated by the findings of Weng, Liu, and Lu (2007), Buyantuyev and Wu (2010), and Li et al. (2014).

Parinya Chayapong (2010) analyzed spatial analysis of UHI phenomenon and its relationship to LULC and electrical energy consumption in Bangkok metropolitan area (BMA). Information from the derived LST maps indicated strong UHI phenomenon over BMA region. In central Bangkok, only Bang Krajae sub-district is still not experienced much of the severe UHI. Negative correlation was seen between LST data and their corresponding NDVI data at pixel scale (R^2 of 0.408) while strong positive correlations were found between LST and percent of impervious surface cover (ISC) or NDBI (with R^2 of 0.836 and 0.734, respectively). The strong positive correlation between percent of ISC and NDBI was also found (R^2 of 0.922). All three chosen public parks expressed different degrees of influences on ambient temperature data from which the largest park generated most obvious impact with temperature dropping of about 4°C over the distance of about 1.6 km away from its center. Strong positive correlation was evidenced between monthly electrical loading data and mean air temperature over the BMA region, especially for the residential and small general service sections (with R^2 of 0.937 and 0.843, respectively).

Ma, Kuang, and Huang (2010) applied coupling urbanization analyses to explore urban thermal environment and its interplay with biophysical one. Results indicated that area ratio of impervious surface in Guangzhou significantly increased; however, the intensity of the UHI was not always enlarged in observed years. In addition, geostatistical analyses showed that the mean-center of the impervious surface was moving towards the northwest during 1990-2005. While, correlation analyses revealed that, at the pixel-scale, the association of LSTs to other two variables (vegetation abundance and percent of impervious surface) was not straightforward,

while LSTs had strong positive correlation with percent of impervious surfaces and negative correlation with vegetation abundances at the regional-scale, respectively.

Dan, Xu, Xue, He, and Dan (2010) had conducted research on the comparison and analysis of research method for UHI effects based on Landsat TM band 6, at Guang'an and Nanchong in the middle of Sichuan Basin. They compared and analyzed five methods including the highest and lowest temperature, average temperature urban and rural, difference of highest and lowest temperature in urban and rural area, heat island area and low temperature area, and heat island area index. They concluded that (1) Mean-Standard Deviation method can classify the grade of temperature and avoid the difference in different time phases; (2) the heat island index method that was based on "Mean-Standard Difference Classification" has strong applicability. Comparison of urban and rural average temperature was second to it. Comparison of highest and lowest temperature is the worst.

Jaruwan Thongmeesang (2011) studied the UHI phenomenon in Chiang Mai city. Air temperature measuring stations comprising stationary and mobile units were installed to collect temperature variations and compared in 3 areas, including Suthep, Chang Khlan, and Nimmanhaemin Roads compared with Hang Dong as reference station during the summer (March-May 2011) and winter (February). The results showed that the city has a risk level of the UHI in terms of the UHI intensity (UHII). UHII average temperature of 2.8°C and mean UHII temperature of 3.23°C, which can be primarily concluded that the city has heat island phenomena. It was also discovered that high traffic congestion, consumption of electricity, population density,

and dense construction area are major sources of higher air temperature. These parameters are interrelated and affect heat island phenomena.

Li, Zhanga, and Kainz (2012) studied patterns of the UHI of the fast-growing Shanghai Metropolis, China using time-series of Landsat TM/ETM + data. The results showed that dramatic changes in LULC had occurred, with loss of cropland, forest and shrub to urban use that made the built-up land increased by 219.50%. In contrast, bare land, cropland, fallow land, forest and shrub were decreased. Consequently, these drastically altered the land surface characteristics and spatiotemporal patterns of UHI.

Xu, Chen, Dan, and Qiu (2011) demonstrated about how to use multi-temporal thermal infrared remote sensing data and dynamically monitor and evaluate UHI. This reseach took Luzhou City in Sichuan Province, China as an example and explored methods to monitoring and evaluating UHI based on Landsat-5 TM data and Landsat-7 ETM+ data. The main conclusions are as following

- 1) It is feasible to dynamically monitor and evaluate UHI Effects using thermal infrared remote sensing data.
- 2) In Luzhou City, WAI increased 0.34°C the increase rate was not large. The proportion of URI declined, which demonstrate that the development degree of heat island has reduced.
- 3) In old urban region, from 1988 to 2002, the area of the region that BT grade do not change was 710.37 hectares, and accounted for 87.50% of old urban region.

4) In urban expansion region, the area of the region that brightness temperature grade increased was 810.27 hectares, and accounted for 64.68% of urban expansion region.

5) TGCI in urban expansion region was 0.938, which demonstrated that UHI enhanced in 1988-2002. This was because this part region evolved from suburbs into urban region. TGCI in old urban region was 0.043, which demonstrated that UHI slightly increased in 1988-2002, which was consistent with calculation results of WAI.

Qiu, Xu, and He (2014) studied on the difference of the UHI defined by BT and LST retrieved by remote sensing technology. The result showed the UHI intensity defined by LST was slightly higher than that was defined by BT and the intensity value was determined by the heat island area index method or WAI.

Kachar, Vafsiyan, Modiri, Enayati, and Safdari Nezhad (2015) evaluated the spatial and temporal distribution changes of LST using Landsat 7 and 8 satellite images to analyze the changes in Tehran, Iran. The NDVI threshold method was applied to extract the LST; then the changes in spatial and temporal distribution of LST over the period 1999 to 2014 were evaluated by URI. It can reveal the intensity of the UHI within the urban area. The calculation of the index was based on the ratio of the UHI area to urban area. The greater the index, the more intense the UHI was.

CHAPTER III

RESEARCH METHODOLOGY

The research methodology framework according to the research objectives consists of data collection and preparation and four main components including (1) influential factors on temperature pattern identification, (2) optimum geostatistical method for mean temperature interpolation, component, (3) satellite-based LST extraction and prediction, and (4) UHI phenomena evaluation and prediction (Figure 3.1). Details of each component with major tasks are separately described in the following sections.

3.1 Data collection and preparation

The list of data collection and preparation of each component is summarized in Table 3.1.

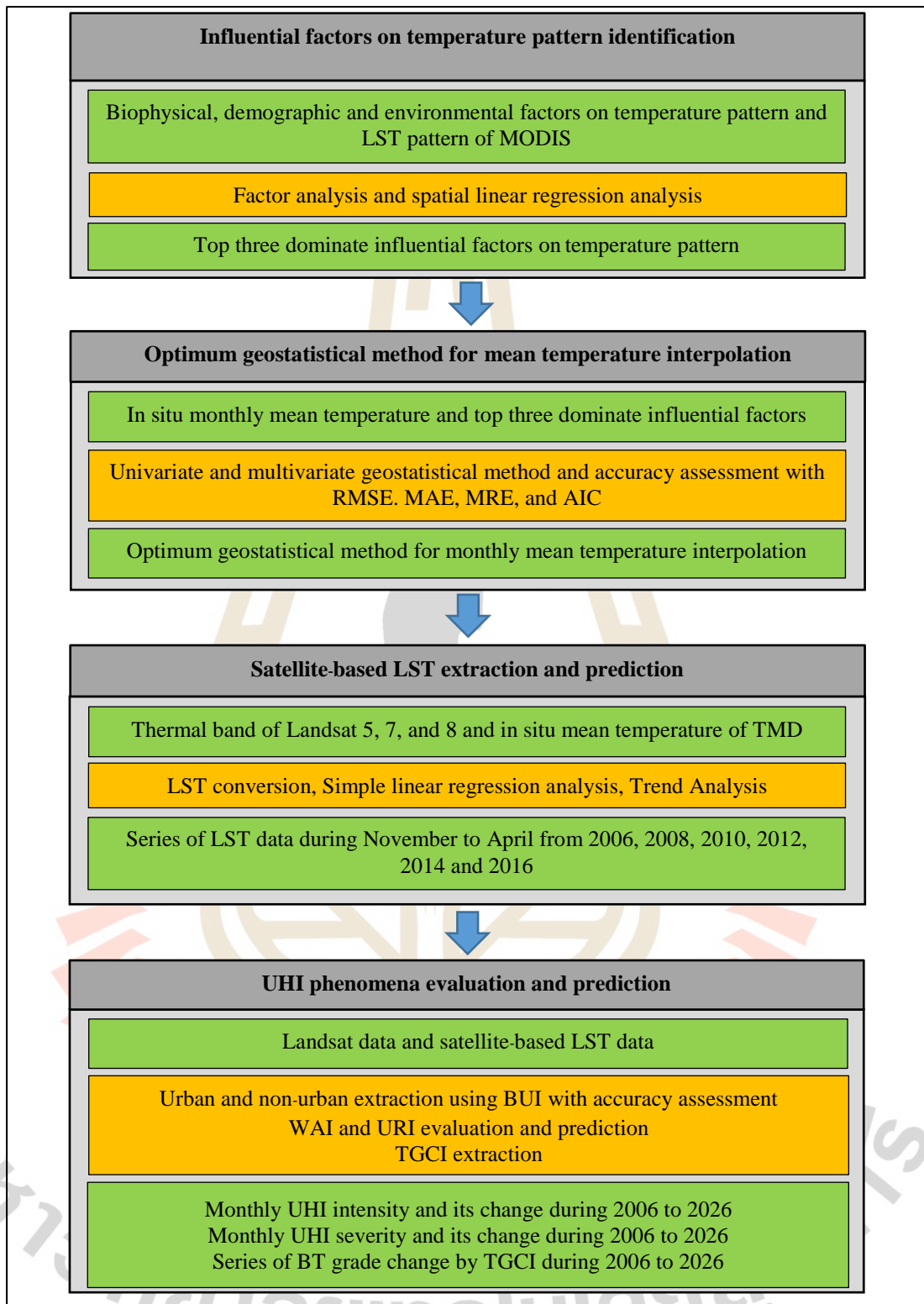


Figure 3.1 Overview of methodology framework according to objectives.

Table 3.1 List of data collection and preparation of each component.

Component	Data collection	Data preparation	Scale	Source	
1	DEM	Completeness Check	1 km resolution	USGS	
	Elevation (m)	Reading from DEM	1 km resolution	USGS	
	Aspect (degrees)	Extract from DEM	1 km resolution	USGS	
	Slope (degrees)	Extract from DEM	1 km resolution	USGS	
	Insolation (WH/m ²)	Extract from DEM	1 km resolution	USGS	
	Wind speed (km/hours)	Interpolate from TMD stations	1 km resolution	TMD	
	Distance to the sea (m)	Euclidean distance calculation	1 km resolution	RTSD	
	NDVI	Extract from MODIS data	1 km resolution	USGS	
	NDBI	Extract from MODIS data	1 km resolution	USGS	
	MNDWI	Extract from MODIS data	1 km resolution	USGS	
	PM ₁₀ (microgram/ m ³)	Interpolate from PCD station using Simple Cokring with elevation	1 km resolution	PCD	
	CO (ppm)	Interpolate from PCD station using Simple Cokring with elevation	1 km resolution	PCD	
	NO ₂ (ppb)	Interpolate from PCD station using Simple Cokring with elevation	1 km resolution	PCD	
	SO ₂ (ppb)	Interpolate from PCD station using Simple Cokring with elevation	1 km resolution	PCD	
	O ₃ (ppb)	Interpolate from PCD station using Simple Cokring with elevation	1 km resolution	PCD	
	Population density (people/sq.km)	Extract from population data at district level	people/sq.km	DOPA	
	Household density (household/sq.km)	Extract from household data at district level	Houses/sq. km	DOPA	
	LST data of MODIS	Download from USGS website	1 km resolution	USGS	
	2	In situ mean temperature	Convert ASCII data to Shape file (point data)	none	TMD
		Top three influential factors	Derived top three influential factor from Component 1		

Table 3.1 (Continued).

Component	Data collection	Data preparation	Scale	Source
3	Band 6 of Landsat 5: in 2006	LST conversion in Celsius	90 m resolution	USGS
	Band 6 of Landsat 7: in 2008, 2010, and 2012	LST conversion in Celsius	90 m resolution	USGS
	Band 10 of Landsat 8: in 2014 and 2016	LST conversion in Celsius	90 m resolution	USGS
	In situ mean temperature	Convert ASCII data to spreadsheet file for linear regression analysis	none	TMD
4	NDBI	Extract from Landsat data	90 m resolution	
	NDVI	Extract from Landsat data	90 m resolution	
	Built-up area and outskirt area	Extract from NDBI and NDVI	90 m resolution	
	Band 6 of Landsat 5: in 2006	Derived LST pattern from Component 3	90 m resolution	
	Band 6 of Landsat 7: in 2008, 2010, and 2012	Derived LST pattern from Component 3	90 m resolution	
	Band 10 of Landsat 8: in 2014 and 2016	Derived LST pattern from Component 3	90 m resolution	
	Temperature grade classification	Classify based on average (μ) and standard deviation (σ) values from the derived LST pattern from Component 3	90 m resolution	

Note: DOPA department of Provincial Administration, PCD, Pollution Control Department, RTSD, Royal Thai Survey Department, TMD, Thai Meteorological Department, USGS United State Geological Survey

3.2 Influential factors on temperature pattern identification

Workflow of the influential factors on temperature pattern identification is schematically displayed in Figure 3.2. Under this component, the selected influential factors on temperature pattern in raster format with cell size of 1 km including (1) elevation, (2) aspect, (3) slope, (4) insolation, (5) wind, (6) distance to the sea, (7) NDVI, (8) NDBI, (9) MNDWI, (10) population density at district level, (11) number of household at district level, and (12) air pollutants (PM_{10} , CO, NO_2 , SO_2 , and O_3), were firstly normalized any particular value (X) into a standardized normal distribution with Z-score based on Mean (μ) and Standard deviation (σ) as:

$$Z = (X - \mu) / \sigma \quad (3.1)$$

Then, all normalized influential factors were converted into ASCII file for factor analysis under SPSS statistics software. In principle, factor analysis attempts to explain the covariance (or correlation) among a large number of variables in terms of a smaller number of factors (Mukhopadhyay, 2009). In practice, major steps of factor analysis are as follows:

3.2.1 Variables selection of factor analysis

The test of data appropriation for factor analysis includes Bartlett's test of sphericity (measuring of sampling adequacy and anti-image correlation matrix) and the Kaiser-Meyer-Olkin (KMO) (measure of sampling adequacy) were firstly applied in this study (Habing, Online, 2003; Friel, Online, 2010).

For Bartlett's test of sphericity, the process started by calculating the determinant of the matrix of sums of products and cross-products (S) from which the inter-correlation matrix is derived. After that, the determinant of the matrix, S was

converted to a chi-square statistic and tested for significance. The null hypothesis is that the inter-correlation matrix comes from a population in which the variables are non-collinear (Friel, Online, 2010). Li and Weng (2007) suggested that the significant level of Bartlett's test should be less than 0.1.

Meanwhile, Kaiser-Meyer-Olkin (KMO) is the one method of orthogonal factor rotation that is often called as varimax rotation. This is based on the assumption that the interpretability of factor j can be measured by the variance of the square of its factor loadings, i.e., the variance of $a_{1j}^2, a_{2j}^2, \dots, a_{pj}^2$. If this variance is large then the a_{ij}^2 values tend to be either close to zero or close to unity. Varimax rotation therefore maximizes the sum of these variances for all the factors.

Friel (2010) described the interpretation of the KMO as characterized by Kaiser, Meyer and Olkin as follows:

- KMO value was 0.90-1.00 that degree of common variance is “Marvelous (excellent)”
- KMO value was 0.80-0.89 that degree of common variance is “Meritorious (good)”
- KMO value was 0.70-0.79 that degree of common variance is “Middling (intermediate)”
- KMO value was 0.60-0.69 that degree of common variance is “Mediocre (average)”
- KMO value was 0.50-0.59 that degree of common variance is “Miserable (Despondent)”

- KMO value was 0.00-0.49 that degree of common variance is “Don’t Factor”

Secondly, communality of variables was reiterately computed by taking the sum of the squared loadings for all variables. In fact, communality value varies between 0 and 1 and appropriate variables should have communality value more than 0.5 (Field, Online, 2005).

3.2.2 Component extraction of factor analysis

The number of the selected component depends on the percentage of variance explained by each component. There are different component extraction methods. The principal component analysis (PCA) that is one of favorite method of factor analysis (Li and Weng, 2007) was applied in this study. Components which has eigenvalues greater than 1 were here firstly extracted, then rotation of initial solution factors was applied using Varimax to clarify the component pattern in order to better interpret the nature of the components. Each component is explained by percentage of variance and factor loading values.

3.2.3 Development of local influential factor on temperature

In principle, each component that consists of number of significant variables can be viewed as one aspect on temperature pattern such as biophysical, demographic or environmental component. In practice, influential factor map on temperature pattern from each principal component was firstly constructed based on factor scores, which are derived from factor analysis. Then, pattern of each influential factor map was spatially compared with LST pattern of MODIS for identifying correlation coefficient using spatial linear regression analysis. The top three variables

from n component, which provide the highest correlation value, were identified as top three dominant factors on temperature pattern for mean temperature interpolation under multivariate geostatistic method in the next component.

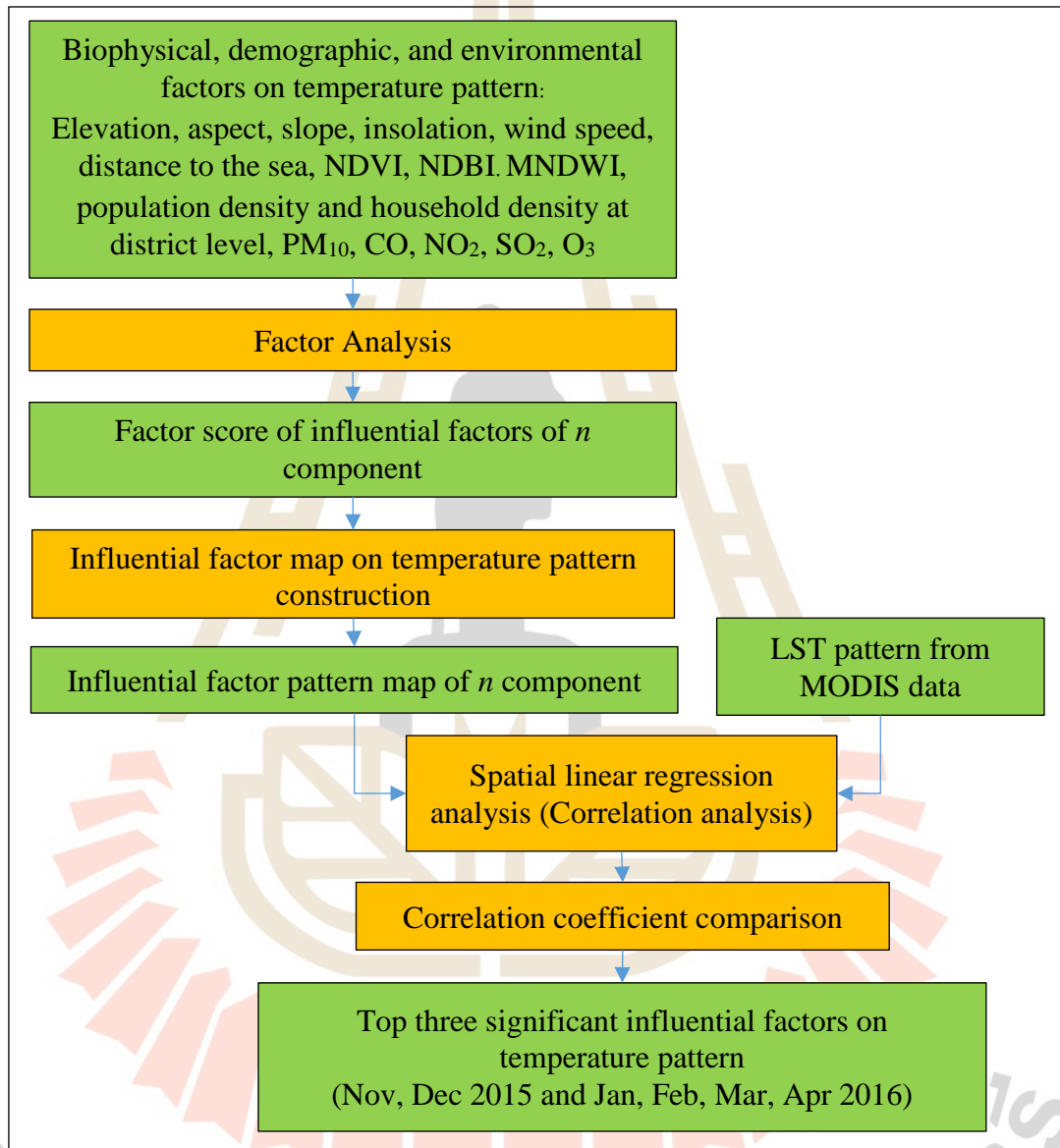


Figure 3.2 Workflow of influential factors on temperature pattern identification.

Details of influential factors on temperature pattern are summarized as follows.

(1) Elevation

The Digital Elevation Model (DEM), which is downloaded from USGS web site (www.earthexplorer.usgs.gov) is applied to represent elevation of terrain.

The DEM is created from Shuttle Radar Topographic Mission (SRTM) with resolution of 30 m.

(2) Aspect

Aspect that identifies the slope direction in compass degrees is extracted based on a 3 x 3 grid neighborhood from the DEM. Aspect is measured clockwise in degrees from zero (due north) to 360. The value of each cell in an aspect dataset indicates the direction the cell's slope faces. Flat areas having no downslope direction are given a value of -1.

(3) Slope

The slope function calculates the maximum rate of change from every cell to its neighbors. The function is calculated over a 3 x 3 set of cells and can yield slope in angular degrees (0-90) or in percent, which is a measure of vertical rise over horizontal run and it is created from the DEM.

(4) Insolation

Insolation or incoming solar radiation is the primary driving force for temperature change. The insolation is derived using DEM based on Area Solar Radiation function in ESRI ArcGIS as shown in Figure 3.3. The derived monthly insolation in raster format has measurement unit in WH/m^2 .

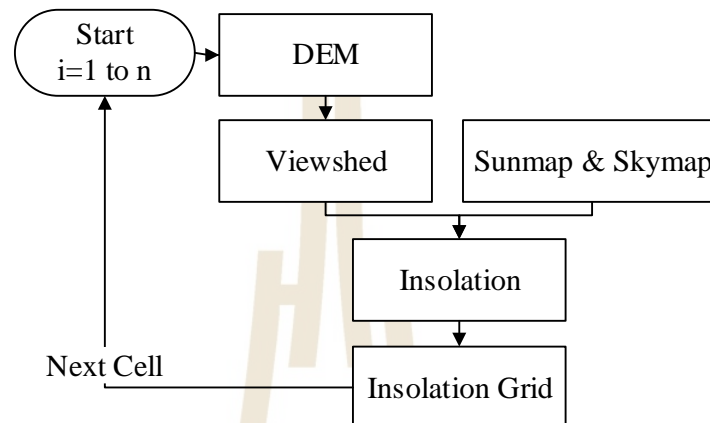


Figure 3.3 Flow diagram for insolation extraction under function of Area Solar Radiation.

(5) Wind speed

In general, wind station of TMD records observation values of wind speed and direction. In this study, wind speed is interpolated using the Ordinary Kriging under ESRI ArcGIS software.

(6) Distance to the sea

The sea affects the climate of a place. Coastal areas are cooler and wetter than inland areas. Clouds form when warm air from inland areas meets cool air from the sea. Herein, distance to the sea is calculated using Euclidean Distance from the coastal area of Thailand and neighboring country, namely, Myanmar, Laos, Cambodia and Vietnam.

(7) Derivation of NDVI

The normalized difference vegetation index (NDVI) is used to identify vegetation in the study area. The NDVI is a measure of the amount of vegetation at the

surface. The value of NDVI varied between -1 and +1. NDVI that were obtained as equation:

$$NDVI = \frac{NIR - RED}{NIR + RED} \quad (3.2)$$

Where RED is red color bands and NIR is Near Infrared Reflectance.

(8) Derivation of NDBI

The normalized difference built-up index (NDBI) is used to identify built-up areas. The NDBI is sensitive to the built-up area and it is calculated as:

$$NDBI = \frac{MIR - NIR}{MIR + NIR} \quad (3.3)$$

Where NIR is Near Infrared Reflectance and MIR is Mid Infrared Reflectance.

(9) Derivation of MNDWI

The modified normalized difference water index (MNDWI) is used to enhance open water features while efficiently suppressing and even removing built up area noise. The MNDWI is more suitable for enhancing and extracting water information for a water region with a background dominated by built-up areas because of its advantage in reducing and even removing built-up land noise over the NDWI (Hanqiu Xu, 2006) and it is determined as equation:

$$MNDWI = \frac{GREEN - MIR}{GREEN + MIR} \quad (3.4)$$

Where MIR is mid infrared reflectance and GREEN is green color bands.

(10) Population density

The monthly population density (people/sq. km) at district level of Thailand are extracted from the official report of the DOPA.

(11) Number of household

The monthly household density (household/sq. km) at district level of Thailand are extracted from the official report of the DOPA.

(12) Air pollutants

The monthly air pollutants data from the PCD ground station, which include PM₁₀, CO, NO₂, SO₂, and O₃ are interpolated using the Ordinary Kriging under ESRI ArcGIS software.

3.3 Optimum geostatistical method for mean temperature interpolation

Workflow of optimum geostatistical method for mean temperature interpolation is schematically displayed in Figure 3.4. Under this component, standard geostatistical methods of univariate (OK, SK, and UK) and multivariate (SCK, OCK, and UCK) were here examined to identify an optimum method for in situ mean temperature interpolation from ground stations of the TMD.

In this study, average monthly temperature data in November, December 2015 and January, February, March, and April 2016 were firstly interpolated using univariate geostatistic methods (OK, SK, and UK) with cell size of 1 km. At the same time, those average mean temperature data were also interpolated using multivariate geostatistic methods (SCK, OCK, and UCK) with the derived top three influential factors on temperature pattern from the previous component. Then, accuracy assessment based on model-based inference method, which is automatically reported with standard measurement: Root Mean Squared Error (RMSE), Mean Relative Error (MRE) and

Mean Absolute Error (MAE) were applied to identify an optimum method of univariate and multivariate geostatistic method. Basic characteristic and its equation of standard measurement of accuracy are summarized as below:

(1) Root Mean Square Error (RMSE). RMSE provides a measure that is sensitive to outliers as:

$$RMSE = \sqrt{\frac{1}{n} \sum_{i=1}^n (y_{predicted} - y_{measured})^2} \quad (3.5)$$

Where n is the number of observations, i is the observation number and y is the concerned factor (air temperature in this study)

(2) Mean Relative Error (MRE). MRE provides a measure of how far the estimate can be in error relative to the measured mean as:

$$MRE = \frac{\sum_{i=1}^n \left[\sum_{j=1}^t |(x_{i,j} - y_{i,j}) / x_{i,j}| \right]}{n} \quad (3.6)$$

Where $x_{i,j}$ denotes the experimental time series data for the i -th at time point j , $y_{i,j}$ is the simulation data for the i -th given by the model at time point j , n is the total number of genes, and t is the number of samples in the time series data.

(3) Mean Absolute Error (MAE). MAE measures of accuracy between predicted and observed temperature for a particular dataset by ignoring its sign as:

$$MAE = \frac{1}{M_{total}} \sum_{i=1}^{M_{total}} |P_i - P_i^*| \quad (3.7)$$

Where P_i , P_i^* and M_{total} are exact values, predicted values and total number of the test data respectively.

Moreover, the best method of kriging and cokriging were here again considered by Akaike Information Criterion (AIC). It is a measure of the relative goodness of fit of a statistical model (Akaike, 1974) and is calculated using the following equation:

$$AIC = -2\log L(\hat{\theta}) + 2k \quad (3.8)$$

Where $L(\hat{\theta})$ is the maximized likelihood function and k is the number of free parameters in the model. The geostatistical method with minimum AIC value is chosen as the best method to interpolate mean temperature.

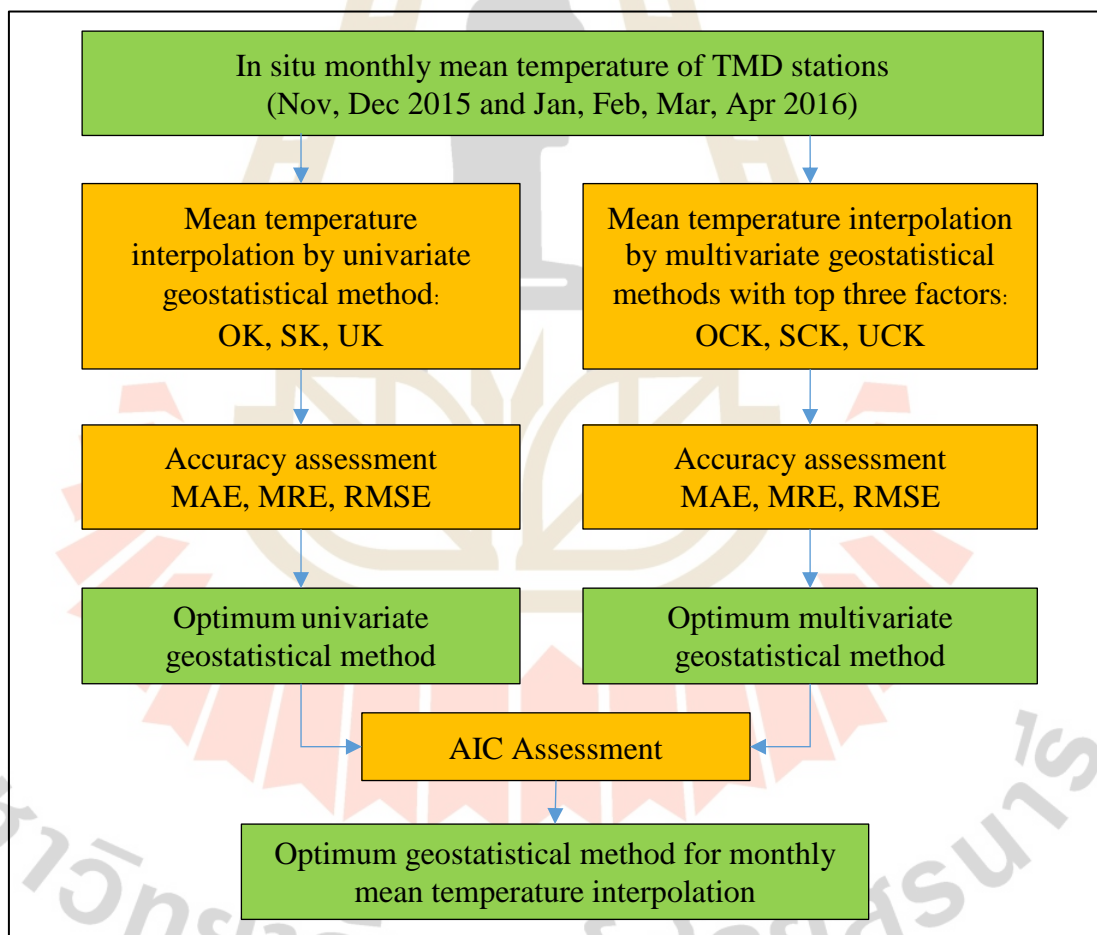


Figure 3.4 Workflow of optimum geostatistical method for mean temperature interpolation.

3.4 Satellite-based LST extraction and prediction

Workflow of satellite-based LST extraction for UHI phenomena study is schematically presented in Figure 3.5. Herein, series of Landsat LST data during November, December, January, February, March, and April between 2006 and 2016 were extracted using standard conversion method: Equations 2.4, 2.5, and 2.6 that were mentioned in Section 2.3 in Chapter II. After that, the derived LST data were refined using simple linear regression analysis between in situ mean temperature data of the TMD stations in Bangkok Metropolitan and its vicinity as independent variable and the derived LST data as dependent variable. The refinement of monthly satellite-based LST data between 2006 and 2016 were further used to predict LST between 2018 and 2026 using Trend analysis function of MS-Excel and Image conversion function of ERDAS Imagine software for UHI phenomena study in the next component.

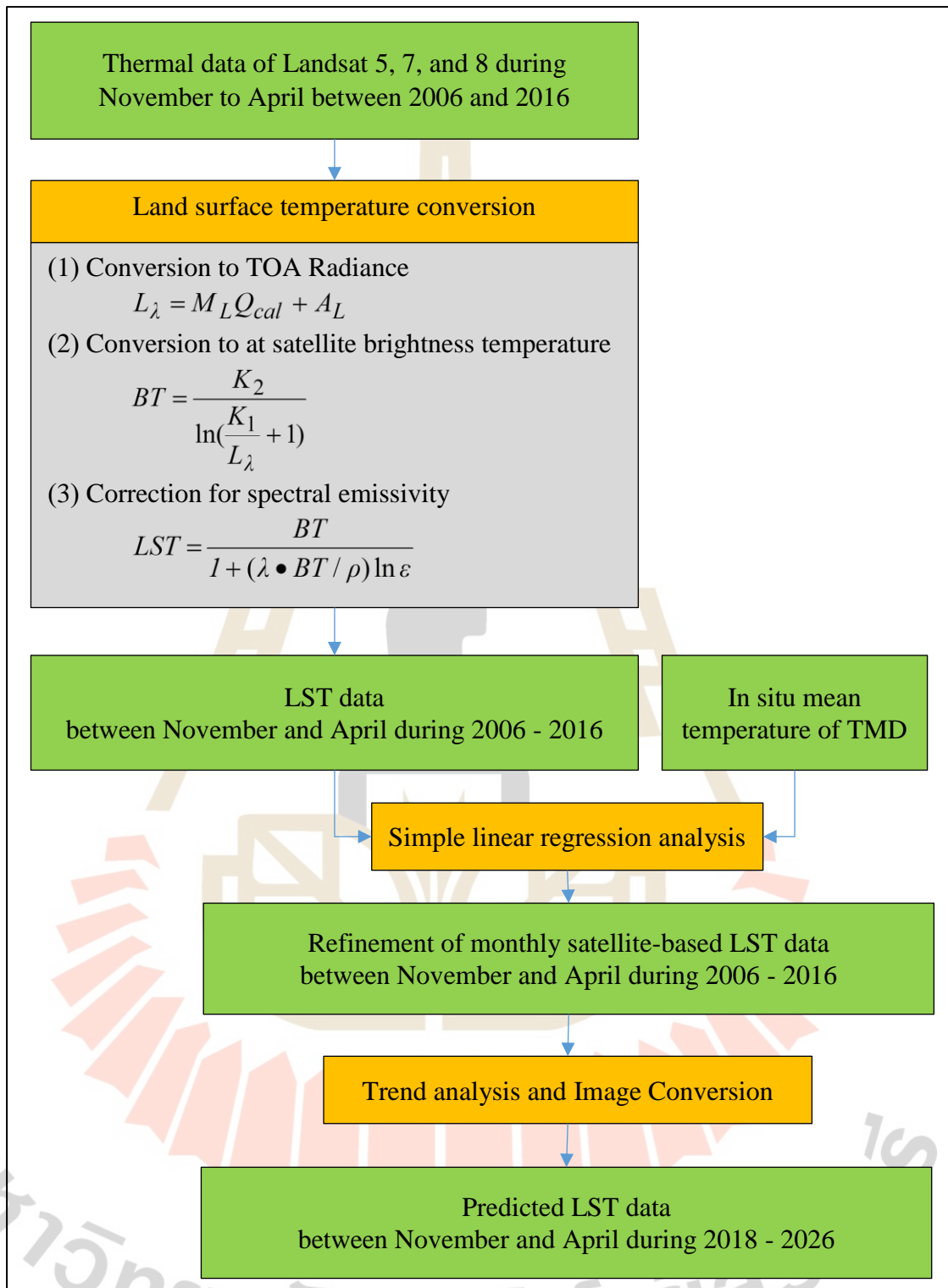


Figure 3.5 Workflow satellite-based LST extraction and LST prediction.

3.5 UHI phenomena evaluation and prediction

Workflow of UHI phenomena evaluation and prediction is schematically displayed in Figure 3.6. Under this component, urban and non-urban area between 2006 and 2016 were firstly extracted using BUI based on NDBI and NDVI, then the derived results were accessed accuracy using Google Earth data. Afterthat the extracted urban and non-urban areas area between 2006 and 2016 were further used to predict urban and non-urban areas between 2018 and 2026. Finally, the derived LST between 2006 and 2026 from the previous component and the extracted urban and non-urban areas in the same period were applied to evaluate UHI phenomena including UHI intensity extraction by WAI, degree of urban heat island development by URI and overall change in temperature by TGCI. Details of major processes are separately described in the following sections.

3.5.1 Urban and non-urban extraction

In the study, series of Landsat data during November to April between 2006 and 2016 were applied to calculate NDBI and NDVI to extract urban area based on a built-up index (BUI) as suggested by Zha, Gao, and Ni (2003) by using following equation:

$$\text{Built-Up Index}(BUI) = NDBI - NDVI \quad (3.9)$$

Zha, Gao, and Ni (2003) reported that the accuracy of extracting urban areas based on the difference between NDBI and NDVI was approximately 92.6%. In this study, urban areas consists of city, town, commercial, village, institutional, transportation, communication and utilities, industrial land, and bare land while non-urban areas include agricultural land, forest land and parks.

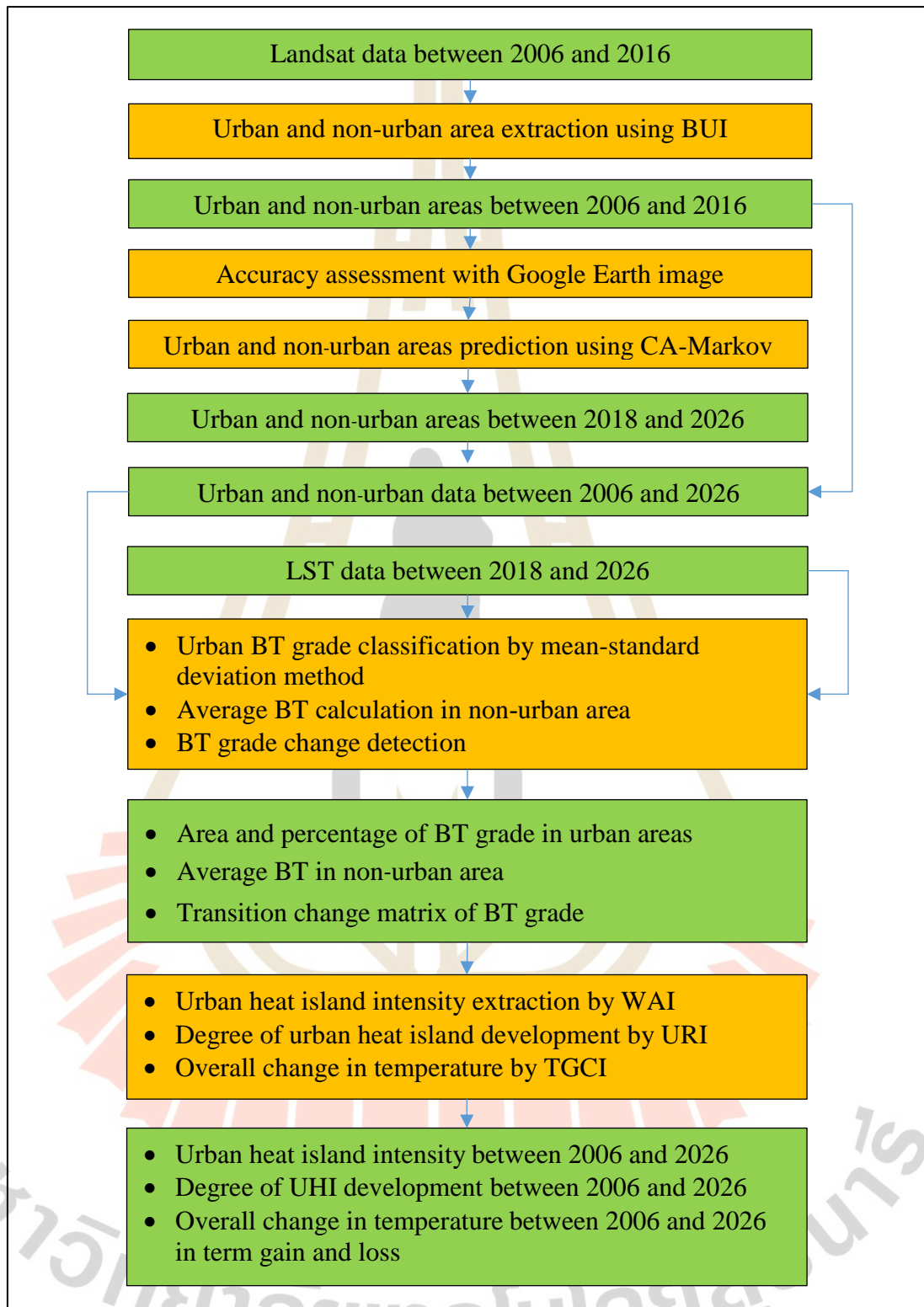


Figure 3.6 Workflow of UHI phenomena evaluation and prediction.

The extracted urban and non-urban data between 2006 and 2016 were assessed accuracy using stratified random sampling scheme with very high spatial resolution image of Google Earth.

3.5.2 Urban and non-urban prediction

The derived urban and non-urban areas between 2006 and 2016 were applied to predict urban and non-urban areas between 2018 and 2026 using CA-Makov model. Herein, pairwise of input data for urban and non-urban areas prediction between 2018 and 2026 is presented in Table 3.2.

Table 3.2 Pairwise of input data for urban and non-urban areas prediction between 2018 and 2026.

No.	Pairwise of input data		Output prediction
	First date	Second date	date
1	2014	2016	2018
2	2012	2016	2020
3	2010	2016	2022
4	2008	2016	2024
5	2006	2016	2026

3.5.3 Urban BT grade classification

Urban brightness temperature (BT) series data between 2006 and 2026 that were converted from Landsat data and predicted using Trend Analysis were classified into 5 temperature grades using Mean-Standard deviation method, which is an ideal method to temperature grade classification (Xu, Chen, Dan, and Qiu, 2011). Standard deviation reflects the deviation value for average temperature. Herein, temperature grade classification of urban BT consists of (1) low temperature area, (2)

secondary low temperature area, (3) medium temperature area, (4) secondary high temperature area, and (5) high temperature area according to average (mean) temperature (μ) and its standard deviation (σ) of BT and T_s using the following conditions:

- | | |
|-------------------------------------|---|
| (1) Low temperature area | $T_s < \mu - \sigma$ |
| (2) Secondary low temperature area | $\mu - \sigma \leq T_s < \mu - 0.5\sigma$ |
| (3) Medium temperature area | $\mu - 0.5\sigma \leq T_s \leq \mu + 0.5\sigma$ |
| (4) Secondary high temperature area | $\mu + 0.5\sigma < T_s \leq \mu + \sigma$ |
| (5) High temperature area | $T_s > \mu + \sigma$ |

The derived BT grade classification were further used to extract area and percentage of BT grade in urban areas, to calculate average BT in non-urban area, and to detect change of BT grade as transition change matrix.

3.5.4 UHI phenomena evaluation and prediction

The selected UHI indices included WAI, URI, and TGCI were here applied to evaluate UHI phenomena of Bangkok and its vicinity between 2006 and 2026.

The WAI which is an index for describing heat island intensity (Dan, Xu, Xue, He, and Dan, 2010) by sum of products between the difference five grade temperature in built-up area (T_{iavg}) with average temperature in outskirt area (T_{oavg}) and percent of temperature grade area (A_i) as shown in the following equation:

$$WAI = \sum_{i=1}^5 (T_{iavg} - T_{oavg}) \times A_i \quad (3.10)$$

Where T_{iavg} represents average temperature of different temperature grade from high to low respectively, T_{oavg} is the average temperature in outskirts area and A_i represents the percentage of different temperature grade from high to low.

Meanwhile, the URI, which is used to depict development degree of heat island (Xu and Chen, 2004) was also extracted using the following equation.

$$URI = \frac{1}{100m} \sum_{i=1}^n w_i p_i \quad (3.11)$$

Where m is the number of BT grade, i represents temperature grade that in urban region is higher than in suburbs, n is the number of temperature grade that in urban region is higher than in suburbs, w is weighted value, it takes the value of temperature grade as result, and p is area percentage. The greater URI is the more severe the heat island phenomenon.

In addition, the TGCI that reflects the overall change in temperature is decreased or increased (Xu, Chen, Dan, and Qiu, 2011) was extracted based on transition matrix of BT grade between two dates using the following equation:

$$TGCI = \sum_{i=1}^n w_i \times GB_i \quad (3.12)$$

Where n is the number of BT grade change types that has twenty-five types in theory, GB is grade change series of temperature brightness. If grade change become decreasing, GB is negative, while if grade changes become increasing, GB is positive and w is the area percentage ((Xu, Chen, Dan, and Qiu, 2011). As a result, if $TGCI > 0$, it shows that increasing trend is greater than decreasing trend, and change trend performances overall increasing. If $TGCI < 0$, it shows that increasing trend is weaker than decreasing trend, and change trend performances overall decreasing.

CHAPTER IV

LOCAL PRINCIPAL INFLUENTIAL FACTORS ON TEMPERATURE PATTERN

Major results under this chapter consist of (1) local principal influential factors on temperature by factor analysis and (2) top three influential factors on temperature pattern using spatial linear regression analysis. Details of each major result are separately explained and discussed in the following sections.

4.1 Local principal influential factors on temperature by factor analysis

The local principal influential factors on temperature, which include (1) biophysical: elevation, aspect, slope, insolation, wind speed, distance to the sea, NDVI, NDBI, and MNDWI; (2) demographic: population density at district level and household density at district level; and (3) environmental: PM₁₀, CO, NO₂, SO₂, and O₃, was examined using factor analysis. The input data of biophysical factors including elevation, slope, aspect, and distance to the sea were here considered as static data which other factors including insolation, wind speed, NDVI, NDBI, and MNDWI were considered as dynamic data. Both static and dynamic factors are displayed in Figures 4.1 to 4.6, respectively. Meanwhile the input data of demographic factor as static data

is displayed in Figure 4.7 and the input data of environmental factor (PM₁₀, CO, NO₂, SO₂, and O₃) as dynamic data is displayed in Figures 4.8 to 4.12, respectively.

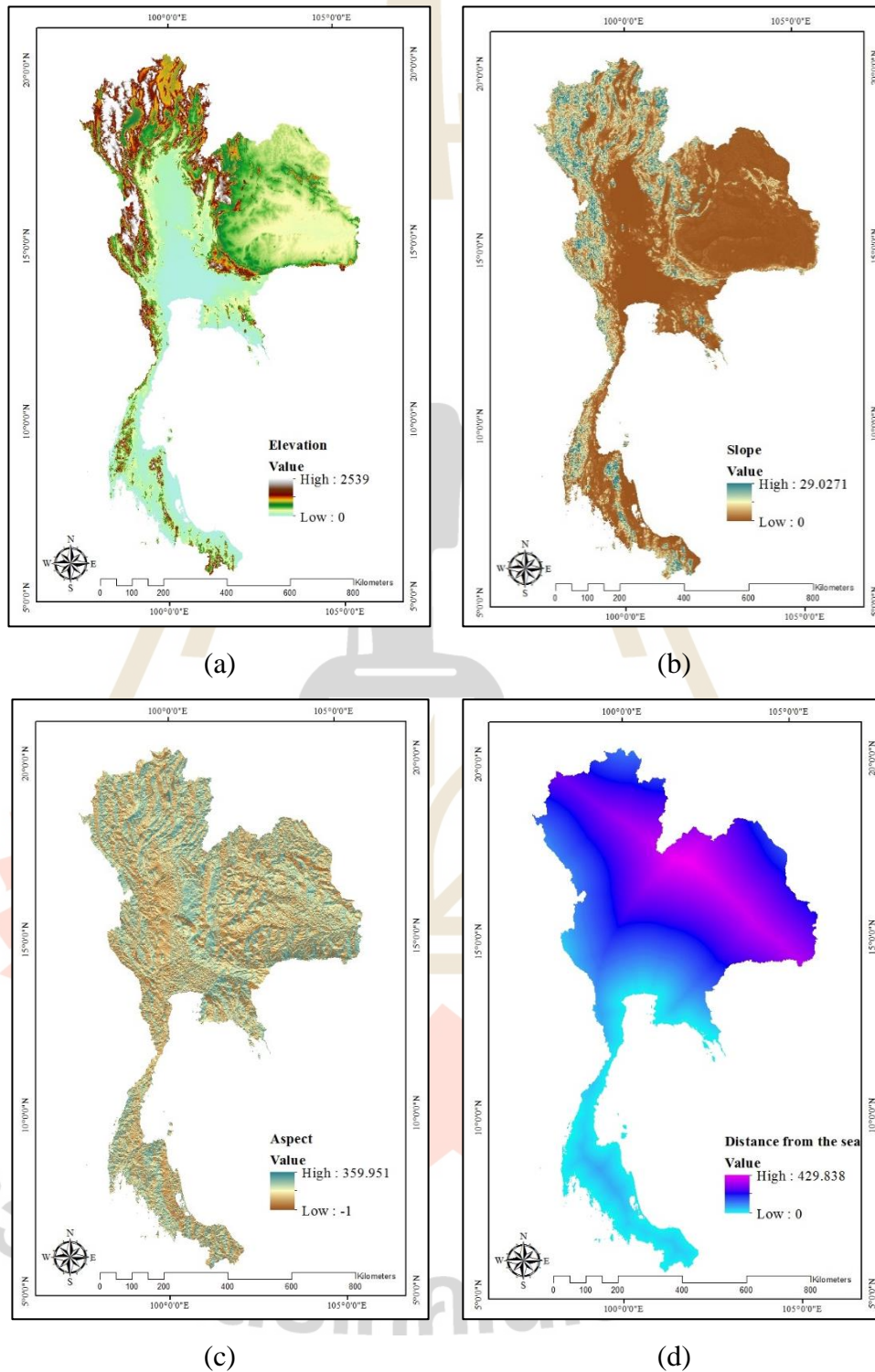


Figure 4.1 Biophysical factors as static data in 2014: (a) elevation, (b) slope, (c) aspect, and (d) Distance to the sea.

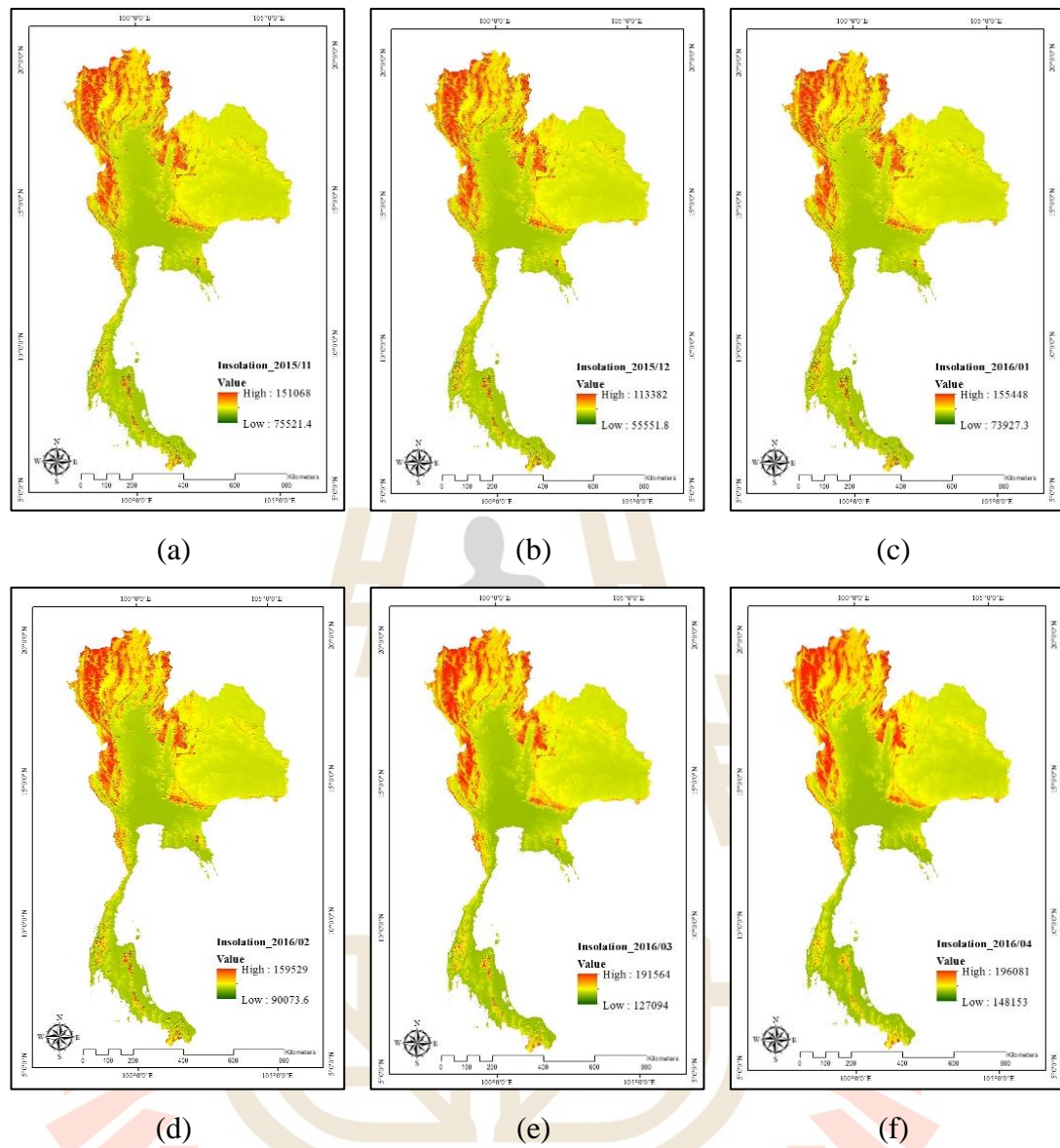


Figure 4.2 Average monthly insolation during November 2015 to April 2016:

(a) November 2015, (b) December 2015, (c) January 2016, (d) February 2016, (e)

March 2016, and (f) April 2016.

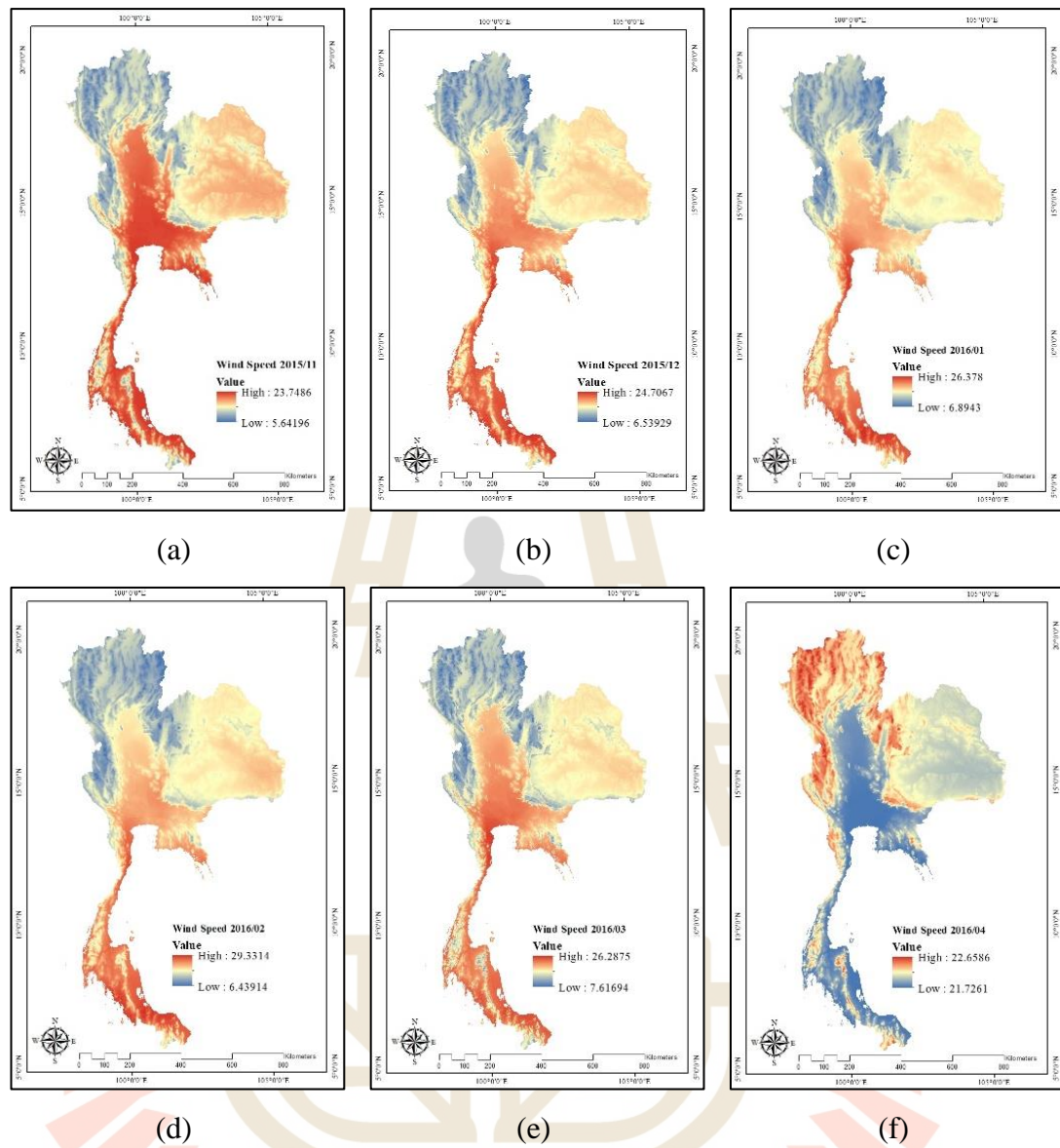


Figure 4.3 Average monthly wind speed during November 2015 to April 2016:

(a) November 2015, (b) December 2015, (c) January 2016, (d) February 2016, (e)

March 2016, and (f) April 2016.

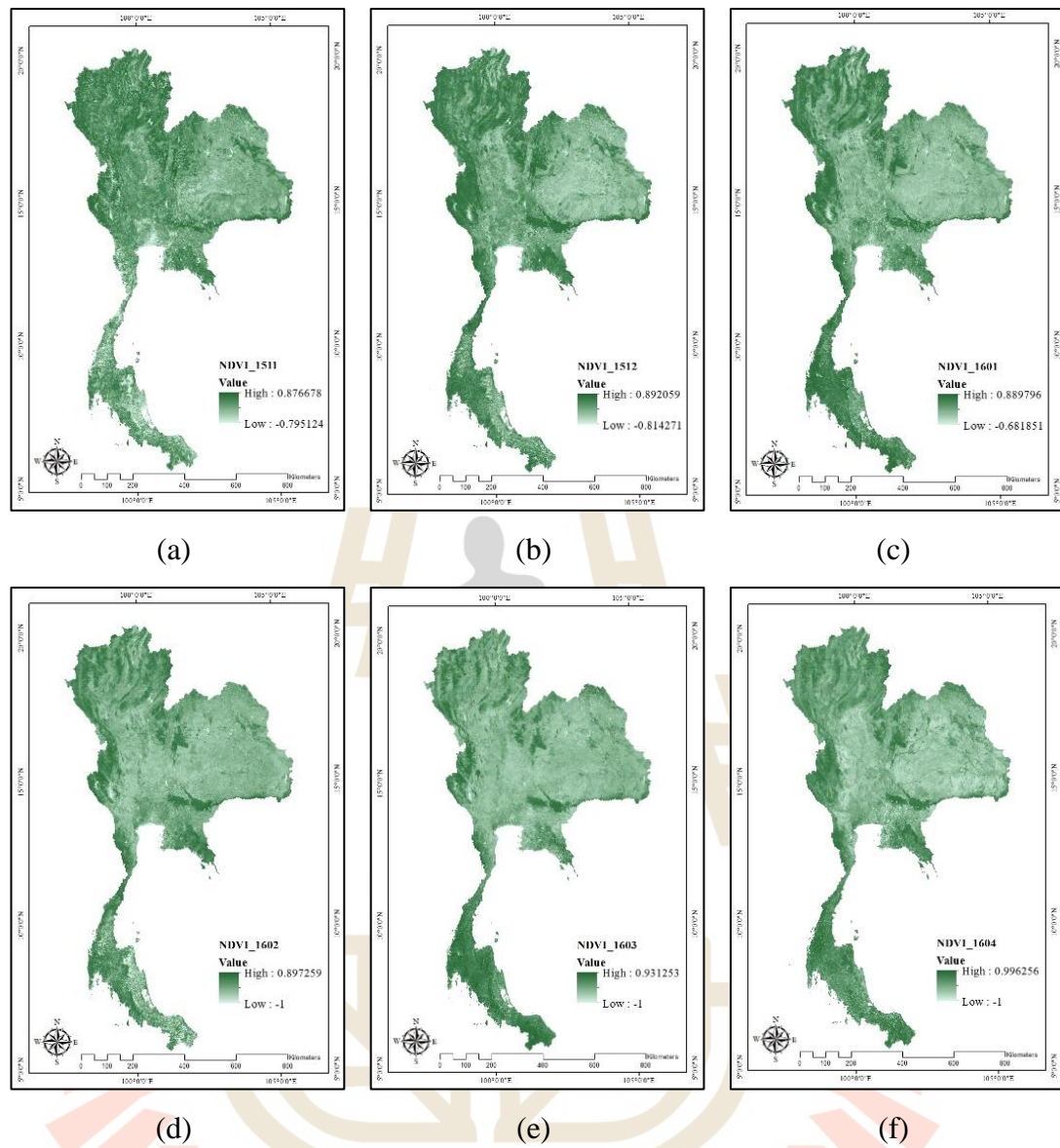


Figure 4.4 NDVI during November 2015 to April 2016: (a) November 2015, (b) December 2015, (c) January 2016, (d) February 2016, (e) March 2016, and (f) April 2016.

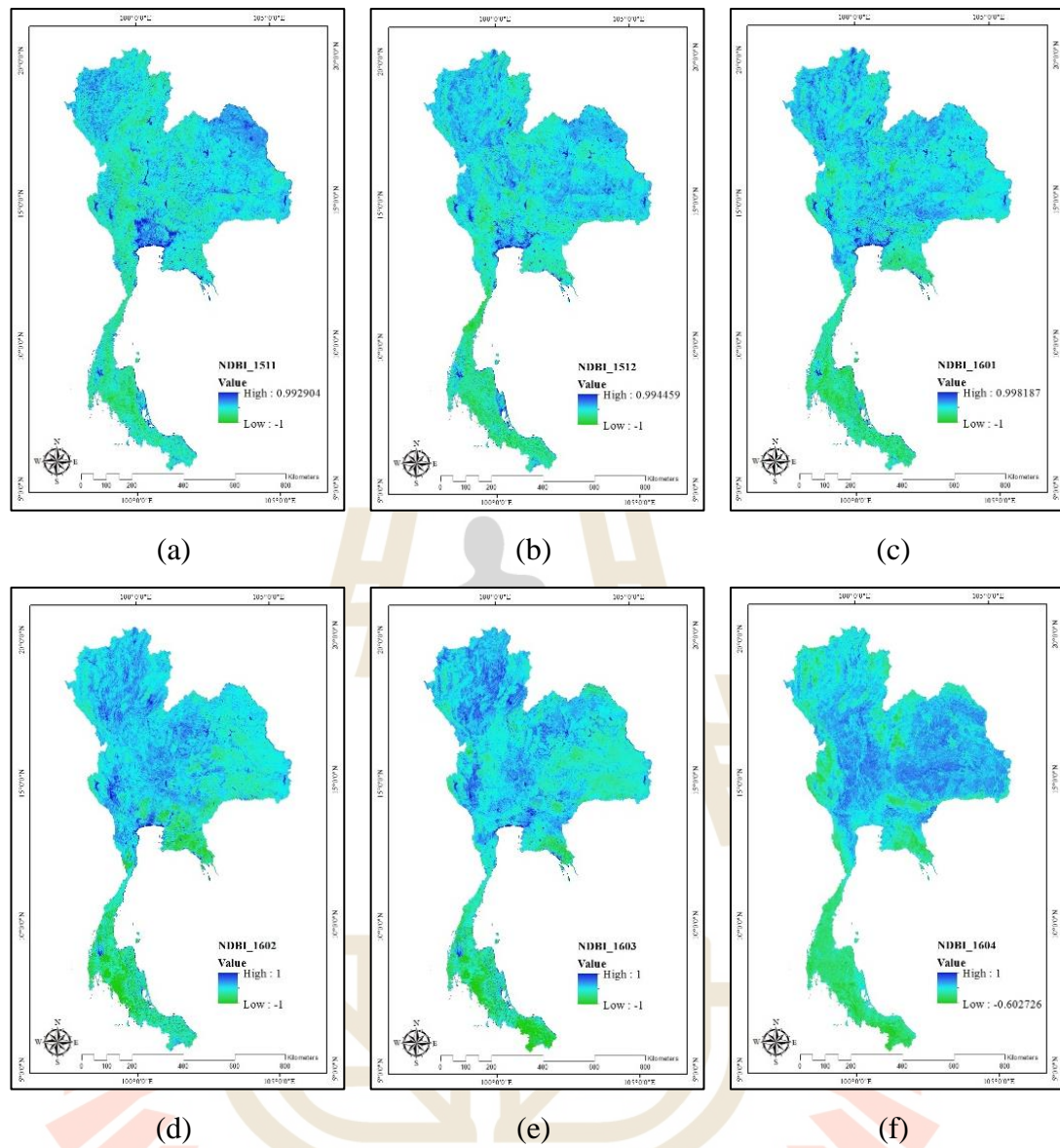


Figure 4.5 NDBI during November 2015 to April 2016: (a) November 2015, (b) December 2015, (c) January 2016, (d) February 2016, (e) March 2016, and (f) April 2016.

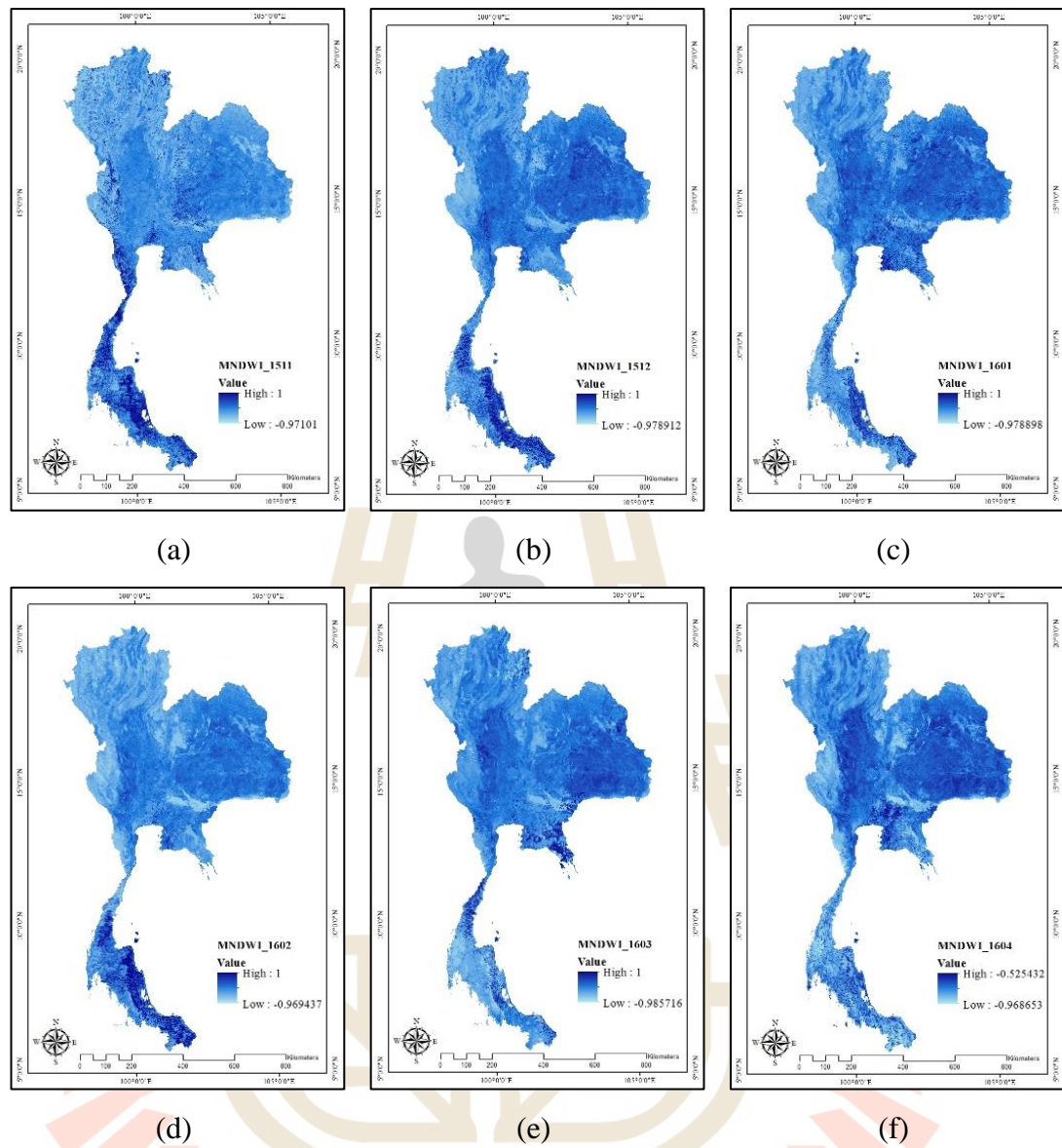


Figure 4.6 MNDWI during November 2015 to April 2016: (a) November 2015, (b) December 2015, (c) January 2016, (d) February 2016, (e) March 2016, and (f) April 2016.

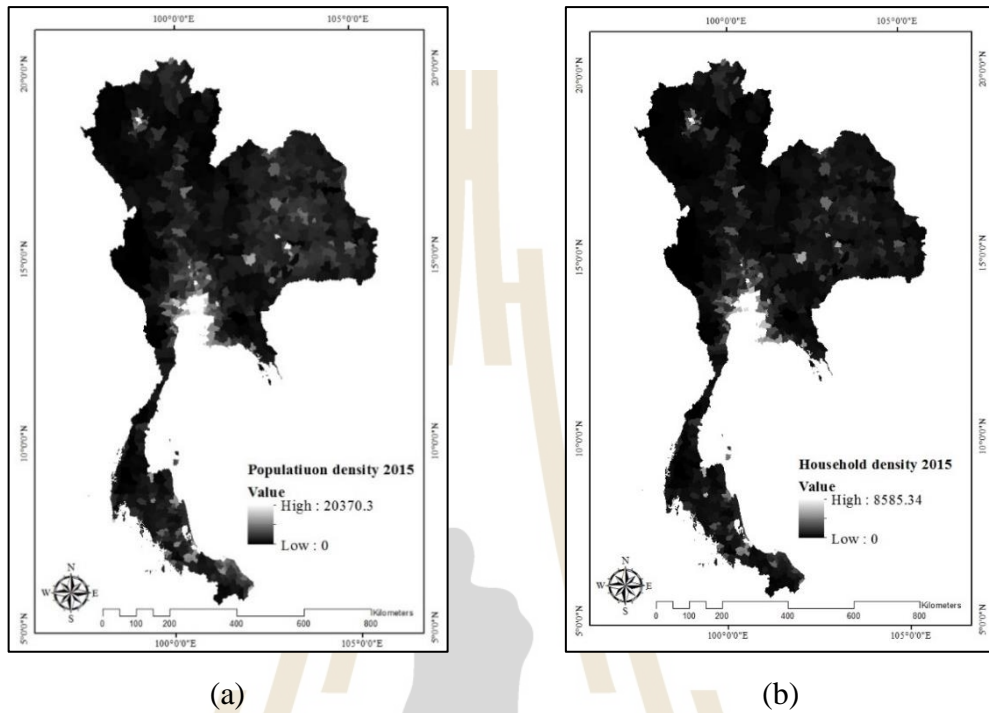


Figure 4.7 Demographic factors as static data in 2015: (a) population density, (b) household density.

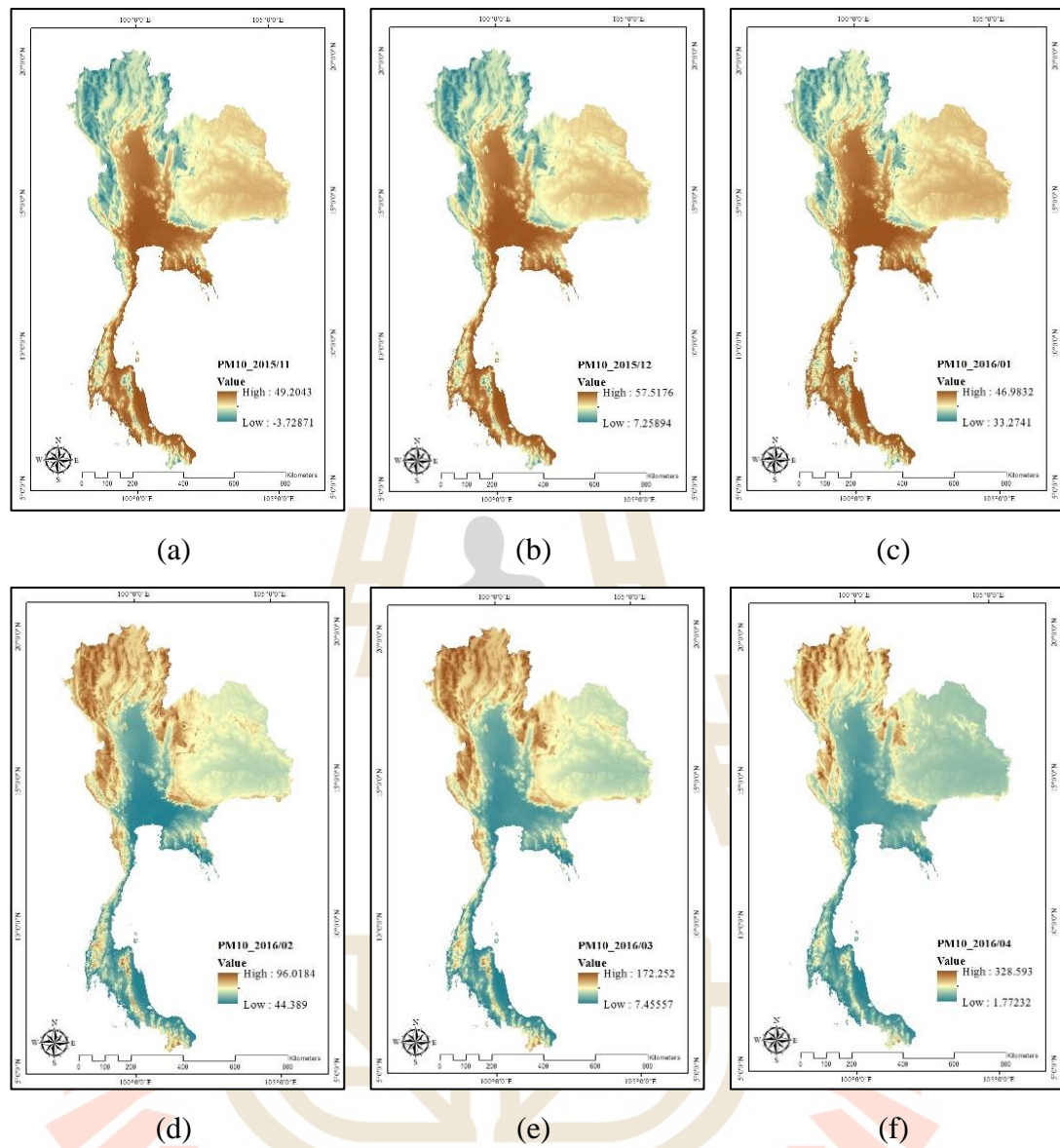


Figure 4.8 Average monthly particulate matter (PM₁₀) during November 2015 to April 2016: (a) November 2015, (b) December 2015, (c) January 2016, (d) February 2016, (e) March 2016, and (f) April 2016.

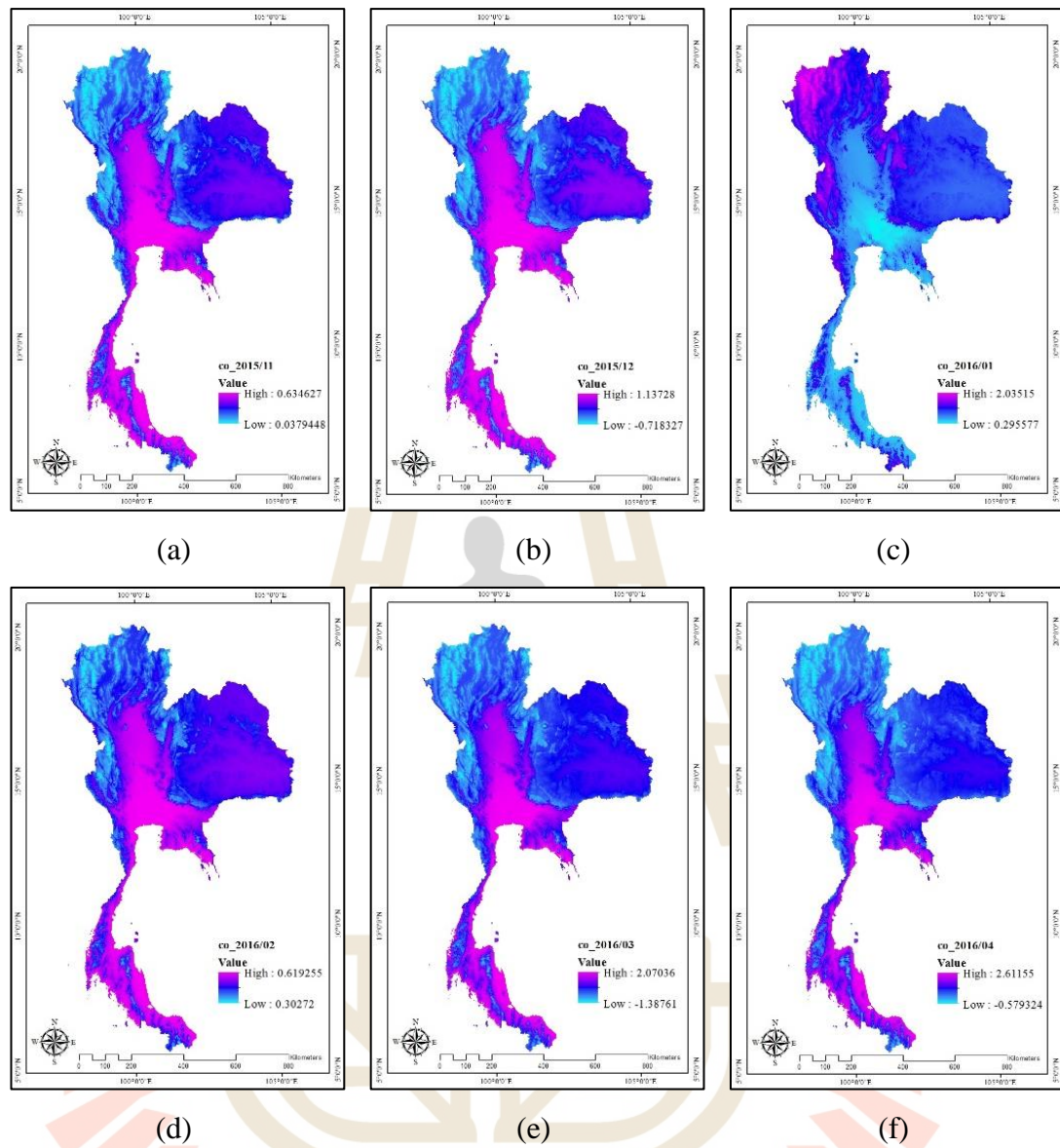


Figure 4.9 Average monthly carbon monoxide (CO) during November 2015 to April 2016: (a) November 2015, (b) December 2015, (c) January 2016, (d) February 2016, (e) March 2016, and (f) April 2016.

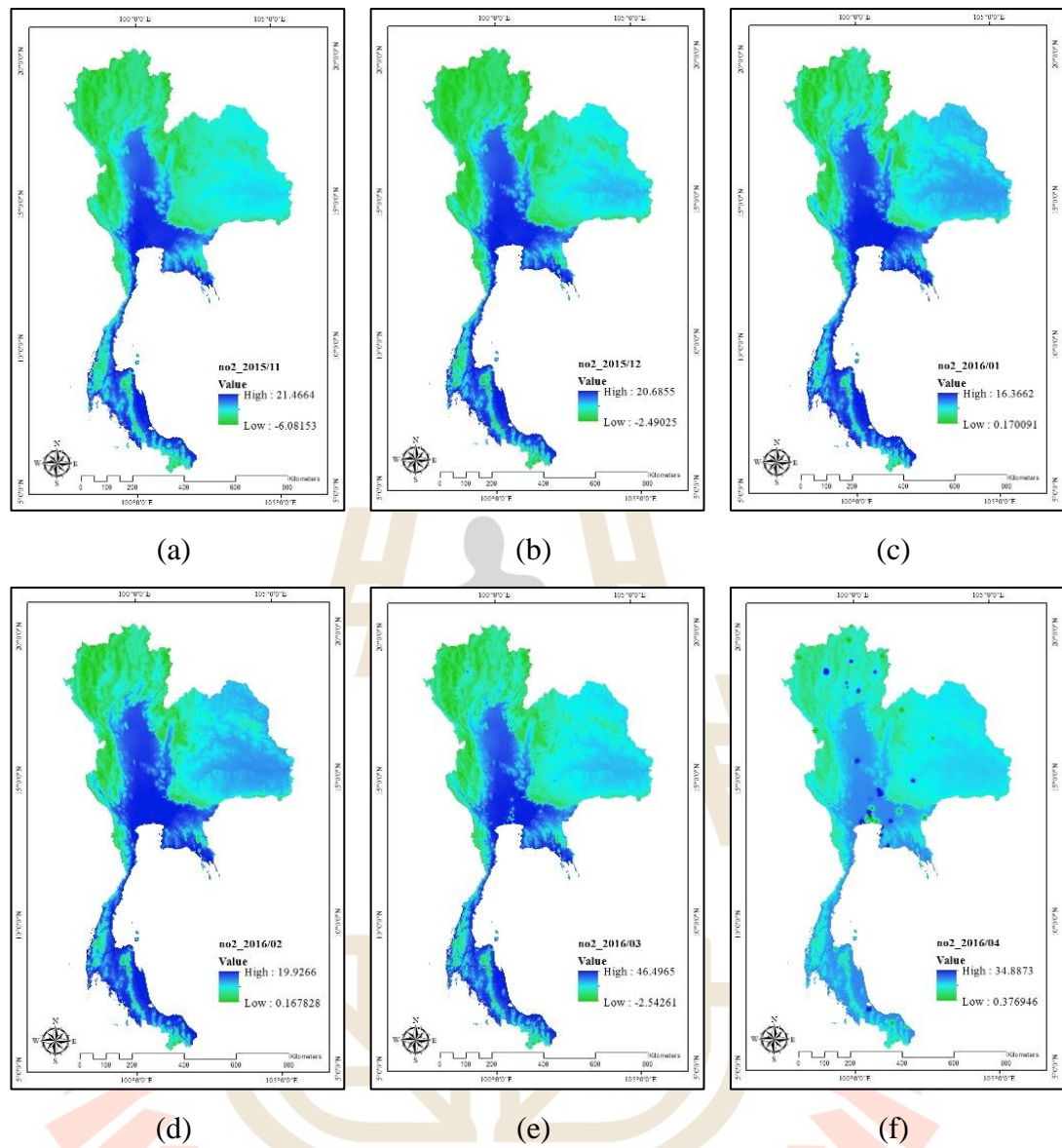


Figure 4.10 Average monthly nitrogen dioxide (NO₂) during November 2015 to April 2016: (a) November 2015, (b) December 2015, (c) January 2016, (d) February 2016, (e) March 2016, and (f) April 2016.

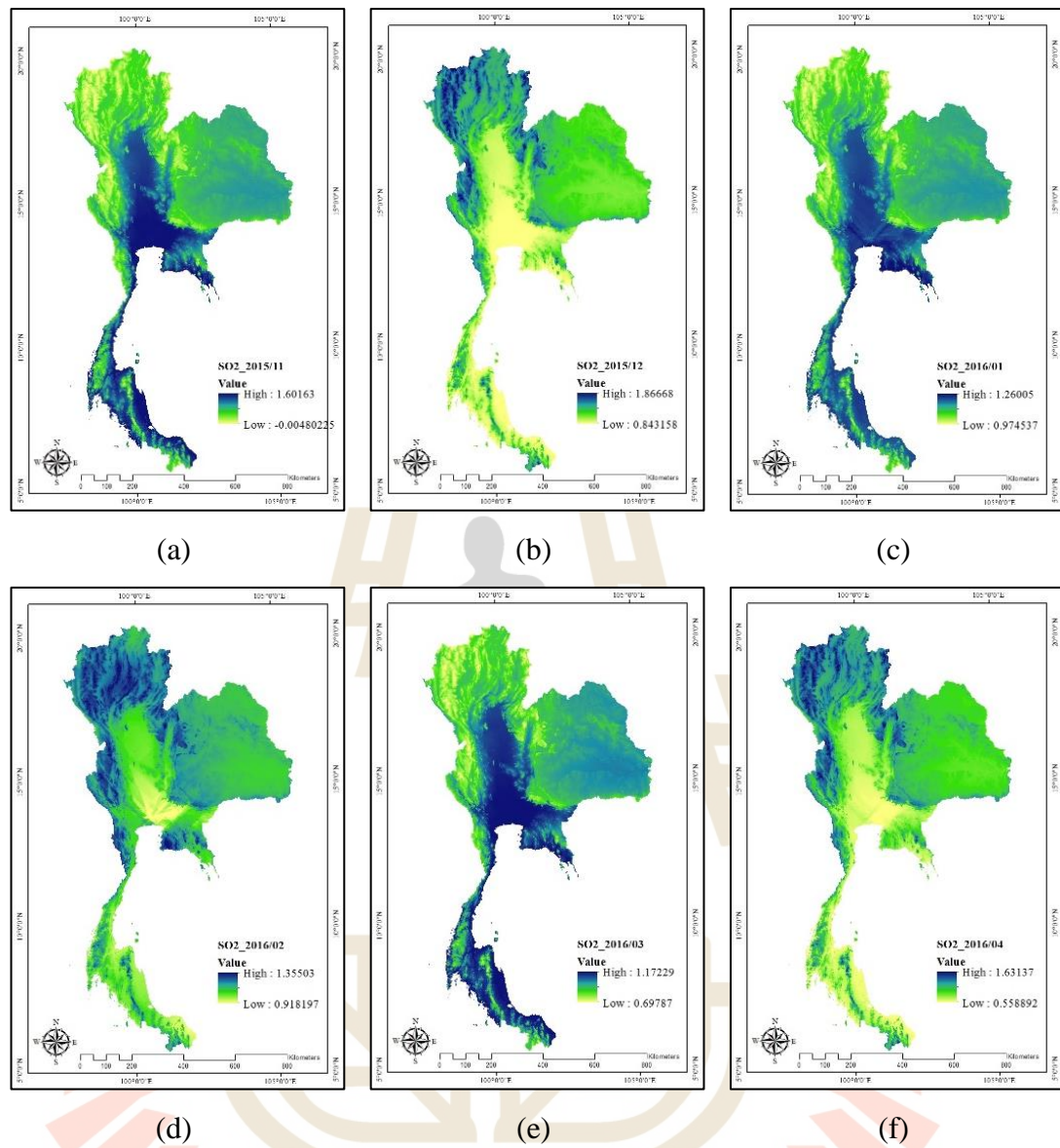


Figure 4.11 Average monthly sulfur dioxide (SO₂) during November 2015 to April 2016: (a) November 2015, (b) December 2015, (c) January 2016, (d) February 2016, (e) March 2016, and (f) April 2016.

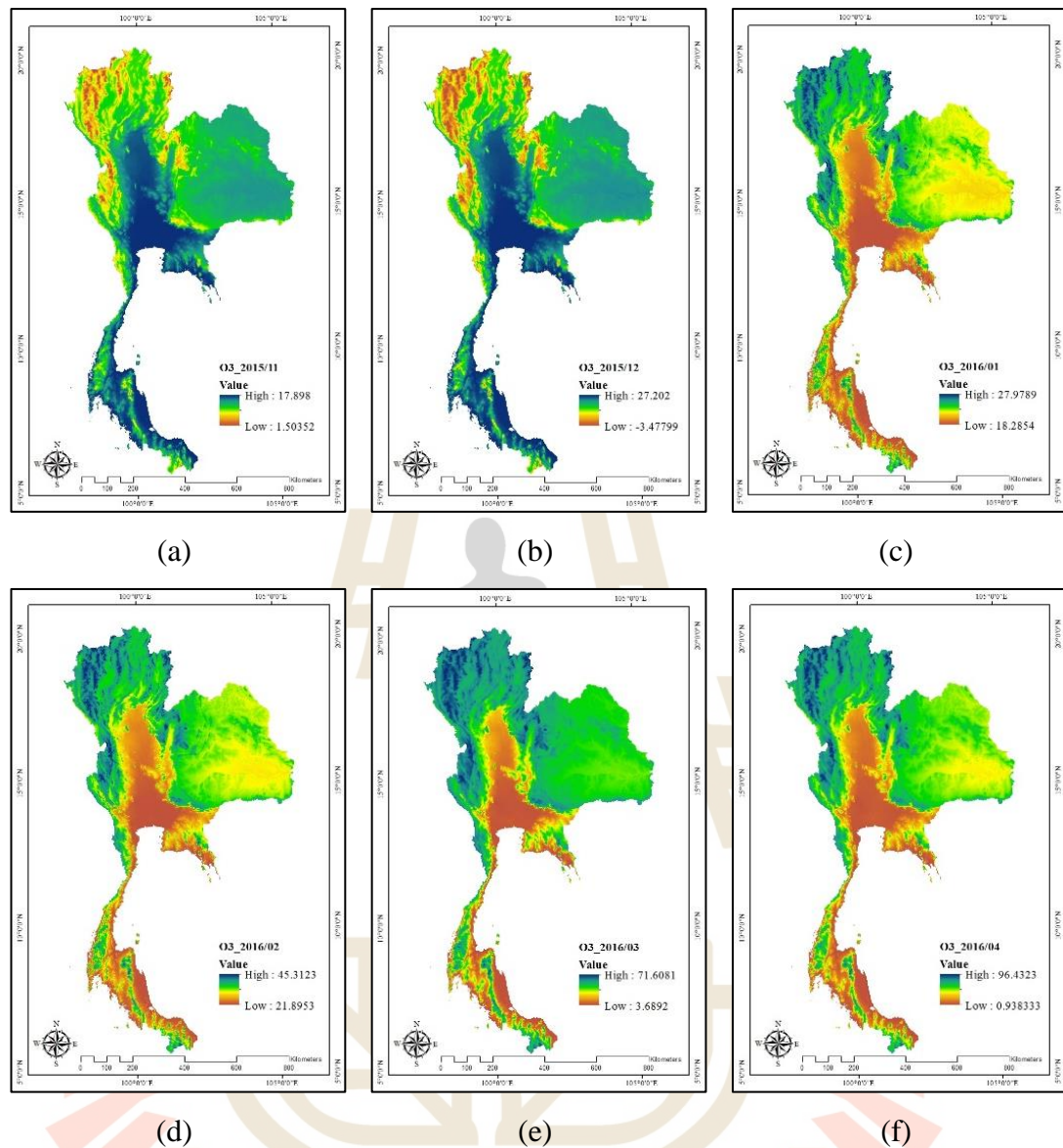


Figure 4.12 Average monthly ozone (O_3) during November 2015 to April 2016: (a) November 2015, (b) December 2015, (c) January 2016, (d) February 2016, (e) March 2016, and (f) April 2016.

The main results of local principal influential factors on temperature by factor analysis are summarized according to major steps of factor analysis in the following section.

4.1.1 Standardization of variable values for factor analysis

As the values of the selected 16 variables for factor analysis on monthly temperature have different ranges and units among them (Table 4.1). Consequently, it is necessary to normalize these values before variable selection for factor analysis. So the original value of each variable was normalized using a standardized normal distribution with Z-score based on Mean (μ) and Standard deviation (σ) using Equation 3.1 as mentioned in Section 3.2 in Chapter III. The descriptive statistical data of 16 factors after normalization is summarized in Table 4.2.

As results, it can be observed that the interpolated environmental variables including CO, NO₂, O₃, and PM₁₀ using simple cokriging with elevation generates unexpected minus value in some months (see Table 4.1). However, number of unexpected value are very low when they compared with corrected value. This finding shows the effect of interpolation technique.

Table 4.1 Descriptive statistical data of 16 variables before normalization.

Variables	Minimum	Maximum	Mean	Std. Deviation	Unit
Elevation	0.00	2539.00	289.35	288.63	Meter
Slope	0.00	29.03	1.86	2.65	Degree
Aspect	-1.00	359.95	171.18	101.84	Degree
Distance to the sea	0.00	429.84	194.16	119.41	Meter
Population	0.00	20370.31	128.37	302.28	Person/sq.km
Number of household	0.00	8585.34	48.24	149.53	Household/sq.km
Insolation					
2015_11	75521.42	151067.67	110985.07	4224.35	WH/m ²
2015_12	55551.77	113382.05	82309.95	3216.24	
2016_01	73927.31	155448.13	112219.14	4430.26	
2016_02	90073.61	159529.39	122273.76	4194.88	
2016_03	127094.24	191563.81	152062.75	4469.96	
2016_04	148153.23	196081.45	159458.46	4358.67	
CO					
2015_11	0.04	0.63	0.41	0.13	parts per million (ppm)
2015_12	-0.72	1.14	0.50	0.41	
2016_01	0.30	2.04	0.59	0.10	
2016_02	0.30	0.62	0.53	0.05	
2016_03	-1.39	2.07	0.56	0.55	
2016_04	-0.58	2.61	0.49	0.36	
NO ₂					
2015_11	-6.08	21.47	9.63	5.76	Parts per Billion (ppb)
2015_12	-2.49	20.69	10.13	5.74	
2016_01	0.17	16.37	10.40	3.57	
2016_02	0.17	19.93	12.64	4.52	
2016_03	-2.54	46.50	11.51	4.76	
2016_04	0.38	34.89	7.74	0.39	
O ₃					
2015_11	1.50	17.90	14.74	2.14	Parts per Billion (ppb)
2015_12	-3.48	27.20	20.02	5.49	
2016_01	18.29	27.98	21.53	1.73	
2016_02	21.90	45.31	30.25	4.17	
2016_03	3.69	71.61	29.62	12.13	
2016_04	0.94	96.43	27.16	13.74	
SO ₂					
2015_11	0.00	1.60	0.99	0.32	Parts per Billion (ppb)
2015_12	0.84	1.87	1.07	0.15	
2016_01	0.97	1.26	1.14	0.04	
2016_02	0.92	1.36	1.16	0.05	
2016_03	0.70	1.17	1.03	0.08	
2016_04	0.56	1.63	0.86	0.15	

Table 4.1 (Continued).

Variables	Minimum	Maximum	Mean	Std. Deviation	Unit
PM ₁₀					
2015_11	-3.73	49.20	32.58	9.67	Microgram/cubic meter
2015_12	7.26	57.52	41.99	9.20	
2016_01	33.27	46.98	43.46	2.14	
2016_02	44.39	96.02	60.10	8.47	
2016_03	7.46	172.25	62.21	30.65	
2016_04	1.77	328.59	52.63	30.19	
Wind speed					
2015_11	5.64	23.75	17.46	3.65	km/h
2015_12	6.54	24.71	17.54	3.26	
2016_01	6.89	26.38	17.48	3.39	
2016_02	6.44	29.33	19.26	4.10	
2016_03	7.62	26.29	19.29	3.01	
2016_04	21.73	22.66	22.01	0.17	
NDVI					
2015_11	-0.80	0.88	0.61	0.14	Unit less
2015_12	-0.81	0.89	0.58	0.16	
2016_01	-0.68	0.89	0.55	0.16	
2016_02	-1.00	0.90	0.48	0.17	
2016_03	-1.00	0.93	0.47	0.17	
2016_04	-1.00	0.99	0.88	0.04	
NDBI					
2015_11	-1.00	0.99	0.67	0.05	Unit less
2015_12	-1.00	0.99	0.70	0.04	
2016_01	-1.00	1.00	0.70	0.04	
2016_02	-1.00	1.00	0.72	0.06	
2016_03	-1.00	1.00	0.71	0.06	
2016_04	-0.60	1.00	-0.01	0.02	
MNDWI					
2015_11	-0.97	1.00	-0.90	0.04	Unit less
2015_12	-0.98	1.00	-0.91	0.03	
2016_01	-0.98	1.00	-0.90	0.03	
2016_02	-0.97	1.00	-0.89	0.03	
2016_03	-0.99	1.00	-0.88	0.04	
2016_04	-0.97	-0.53	-0.88	0.03	

Table 4.2 Descriptive statistical data of 16 variables after normalization.

Variables	Minimum	Maximum	Mean	Standard Deviation
Elevation	-1.00	7.79	0.00	1.00
Slope	-0.70	10.25	0.00	1.00
Aspect	-1.69	1.85	0.00	1.00
Distance to the sea	-1.63	1.97	0.00	1.00
Population	-0.42	66.96	0.00	1.00
Number of household	-0.32	57.09	0.00	1.00
Insolation				
2015_11	-8.40	9.49	0.00	1.00
2015_12	-8.32	9.66	0.00	1.00
2016_01	-8.64	9.76	0.00	1.00
2016_02	-7.68	8.88	0.00	1.00
2016_03	-5.59	8.84	0.00	1.00
2016_04	-2.59	8.40	0.00	1.00
CO				
2015_11	-2.77	1.65	0.00	1.00
2015_12	-2.95	1.56	0.00	1.00
2016_01	-3.11	15.02	0.00	1.00
2016_02	-4.14	1.68	0.00	1.00
2016_03	-3.54	2.74	0.00	1.00
2016_04	-2.94	5.87	0.00	1.00
NO ₂				
2015_11	-2.73	2.05	0.00	1.00
2015_12	-2.20	1.84	0.00	1.00
2016_01	-2.86	1.67	0.00	1.00
2016_02	-2.76	1.61	0.00	1.00
2016_03	-2.95	7.36	0.00	1.00
2016_04	0.39	69.91	0.00	1.00
O ₃				
2015_11	-6.20	1.48	0.00	1.00
2015_12	-4.28	1.31	0.00	1.00
2016_01	-1.88	3.73	0.00	1.00
2016_02	-2.00	3.61	0.00	1.00
2016_03	-2.14	3.46	0.00	1.00
2016_04	-1.91	5.04	0.00	1.00
SO ₂				
2015_11	-3.14	1.95	0.00	1.00
2015_12	-1.51	5.27	0.00	1.00
2016_01	-3.96	3.00	0.00	1.00
2016_02	-4.56	3.82	0.00	1.00
2016_03	-3.99	1.72	0.00	1.00
2016_04	-1.95	4.98	0.00	1.00

Table 4.2 (Continued).

Variables	Minimum	Maximum	Mean	Standard Deviation
PM₁₀				
2015_11	-3.75	1.72	0.00	1.00
2015_12	-3.77	1.69	0.00	1.00
2016_01	-4.77	1.65	0.00	1.00
2016_02	-1.85	4.24	0.00	1.00
2016_03	-1.79	3.59	0.00	1.00
2016_04	-1.68	9.14	0.00	1.00
Wind speed				
2015_11	-3.24	1.72	0.00	1.00
2015_12	-3.37	2.20	0.00	1.00
2016_01	-3.12	2.62	0.00	1.00
2016_02	-3.13	2.46	0.00	1.00
2016_03	-3.88	2.32	0.00	1.00
2016_04	-1.69	3.87	0.00	1.00
NDVI				
2015_11	-10.27	1.96	0.00	1.00
2015_12	-8.76	1.94	0.00	1.00
2016_01	-7.63	2.12	0.00	1.00
2016_02	-8.78	2.50	0.00	1.00
2016_03	-8.61	2.72	0.00	1.00
2016_04	-42.14	2.60	0.00	1.00
NDBI				
2015_11	-33.88	6.57	0.00	1.00
2015_12	-38.65	6.75	0.00	1.00
2016_01	-38.77	6.68	0.00	1.00
2016_02	-30.90	5.02	0.00	1.00
2016_03	-30.21	5.17	0.00	1.00
2016_04	-32.49	55.92	0.00	1.00
MNDWI				
2015_11	-2.03	51.33	0.00	1.00
2015_12	-2.50	65.39	0.00	1.00
2016_01	-2.52	63.14	0.00	1.00
2016_02	-2.16	54.23	0.00	1.00
2016_03	-2.78	51.07	0.00	1.00
2016_04	-3.07	12.09	0.00	1.00

4.1.2 Variables selection for factor analysis

For variable selection of factor analysis, two statistic methods: Kaiser-Meyer-Olkin (KMO) of sampling adequacy and Bartlett's test of sphericity were firstly applied for testing of data appropriation based on correlation coefficient among variables. Then, communality of variables was computed to identify the suitable variables for factor analysis (see detail in Section 3.2.1 in Chapter III). In this study, sixteen variables of each month: November 2015, December 2015, January 2016, February 2016, March 2016, and April 2016 were used to select suitable variables for each month under factor analysis.

It reveals that five variables, except February 2016 are dropped one or two variables for factor analysis after applying Kaiser-Meyer-Olkin (KMO) of sampling adequacy and Bartlett's test of sphericity and communality of variables extraction on correlation matrix among 16 variables. Summary of suitable variable selection of six months datasets for factor analysis with statistical test data is displayed in Table 4.3. As results, it can be observed that aspect variables from biophysical factor is least suitable for factor analysis and all variables of demographic and environmental factors are selected for factor analysis. Details of variables selection of six months are systematically reported in Appendix A.

Table 4.3 Summary of suitable variable selection of six months datasets for factor analysis.

	Statistical test	November	December	January	February	March	April
Influential factor	KMO	0.677	0.724	0.789	0.738	0.742	0.744
	Baelette's test	0.000	0.000	0.000	0.000	0.000	0.000
	Communality	14**	14**	15**	16*	14***	15**
Biophysical	Elevation	✓	✓	✓	✓	✓	✓
	Slope	✓	✓	✓	✓	✓	✓
	Aspect	X	X	X	✓	X	✓
	Distance to the sea	X	X	✓	✓	✓	X
	Insolation	✓	✓	✓	✓	✓	✓
	Wind speed	✓	✓	✓	✓	✓	✓
	NDVI	✓	✓	✓	✓	✓	✓
	NDBI	✓	✓	✓	✓	✓	✓
	MNDWI	✓	✓	✓	✓	X	✓
Demographic	Population Density	✓	✓	✓	✓	✓	✓
	Household Density	✓	✓	✓	✓	✓	✓
Enviromental	PM₁₀	✓	✓	✓	✓	✓	✓
	CO	✓	✓	✓	✓	✓	✓
	NO₂	✓	✓	✓	✓	✓	✓
	SO₂	✓	✓	✓	✓	✓	✓
	O₃	✓	✓	✓	✓	✓	✓

Note * One iteration for Communality value extraction
 ** Two iterations for Communality value extraction
 *** Three iterations for Communality value extraction

4.1.3 Component extraction by factor analysis

To extract an initial solution for factor loading, principal component analysis was firstly applied. Herein, component whose has eigenvalues greater than 1 is extracted. Then, rotation of initial solution component was applied using Varimax to clarify the component pattern in order to better interpret the nature of the components. Major results of component extraction by factor analysis of suitable variable datasets from six months datasets for temperature pattern and its interpretation are here separately describes in the following sections.

4.1.3.1 Component extraction of November 2015 dataset

The result of factor analysis of November 2015 dataset in form of factor loading matrix is presented in Table 4.4. In principle, each component is explained by percentage of variance with factor loading of each variable. Herein, the first component can explain the variance of dataset about 50.519% and five components can explain the variance of dataset as cumulative variance about 94.112%. The derived component with its score is further used to construct factor map for representation dominant variables on temperature. Each factor map is further used in spatial regression analysis for identifying top three influential factors on temperature pattern with MODIS LST data.

Table 4.4 Factor loading matrix by factor analysis of November 2015 dataset.

Variables	Component				
	1	2	3	4	5
Elevation	-0.377	.870	-0.040	-0.058	.035
Slope	-0.128	.791	-0.039	-0.090	-0.109
Population	.138	-0.054	.982	.023	.032
Household	.115	-0.034	.986	.011	.025
NDVI_1511	-0.150	.167	-0.029	-.915	-0.307
NDBI_1511	-0.074	-0.052	.050	-0.012	.988
MNDWI_1511	.198	-0.003	.009	.896	-0.373
SO ₂ _1511	.965	-0.194	.097	.093	-0.029
PM ₁₀ _1511	.964	-0.219	.081	.102	-0.032
O ₃ _1511	.946	-0.231	.072	.106	-0.026
CO_1511	.963	-0.207	.081	.097	-0.024
NO ₂ _1511	.959	-0.182	.101	.088	-0.043
Inso_1511	-0.309	.827	-0.029	-0.023	.020
Wind_1511	.958	-0.226	.080	.121	-0.032
Initial eigenvalues	7.073	1.883	1.623	1.507	1.089
% of variance	50.519	13.453	11.594	10.764	7.782
Cumulative %	50.519	63.973	75.566	86.330	94.112

Based on Comrey and Lee (1992), a range of values to interpret the strength of the relationships between variables and components using factor loading are as follows:

Factor loading of 0.71 and higher are considered as excellent relationship;

Factor loading between 0.63-0.70 is considered as very good relationship;

Factor loading of 0.55-0.62 is considered as good relationship;

Factor loading of 0.45-0.54 is considered as fair relationship and;

Factor loading of 0.32-0.44 is considered as poor relationship.

The result of factor analysis in Table 4.4 can explain the influence of variables on temperature in term of strengthen of relationship between variables and component as following.

Component 1: This component represents the influence of environmental factor on temperature. They are five significant environmental variables including SO_2 , PM_{10} , CO , NO_2 , and O_3 that have excellent relationship with temperature. One biophysical factor, wind speed, has excellent relationship with temperature. The representation map of this component based on the derived factor scored with regression method is displayed in Figure 4.13(a). This map is here assumed as the representation of SO_2 because it provides the highest factor loading in Component 1.

Component 2: This component represents the influence of biophysical factor on temperature. They are elevation, slope, and insolation that have excellent relationship with temperature. The representation map of this component based on the derived factor scored with regression method is displayed in Figure

4.13(b). This map is here assumed as the representation of elevation because it provides the highest factor loading in Component 2.

Component 3: This component represents the influence of demographic factor on temperature. They are population and household densities that have excellent relationship with temperature. The representation map of this component based on the derived factor scored with regression method is displayed in Figure 4.13(c). This map is here assumed as the representation of household density because it provides the highest factor loading in Component 3.

Component 4: This component represents the influence of biophysical factor on temperature. They are two significant biophysical variables including NDVI and MNDWI that have excellent relationship with temperature. The representation map of this component based on the derived factor scored with regression method is displayed in Figure 4.13(d). This map is here assumed as the representation of NDVI because it provides the highest factor loading in Component 4.

Component 5: This component represents the influence of biophysical factor on temperature. The most significant biophysical variable is NDBI that has excellent relationship with temperature. The representation map of this component based on the derived factor scored with regression method is displayed in Figure 4.13(e). This map is here assumed as the representation of NDBI because it provides the highest factor loading in Component 5.

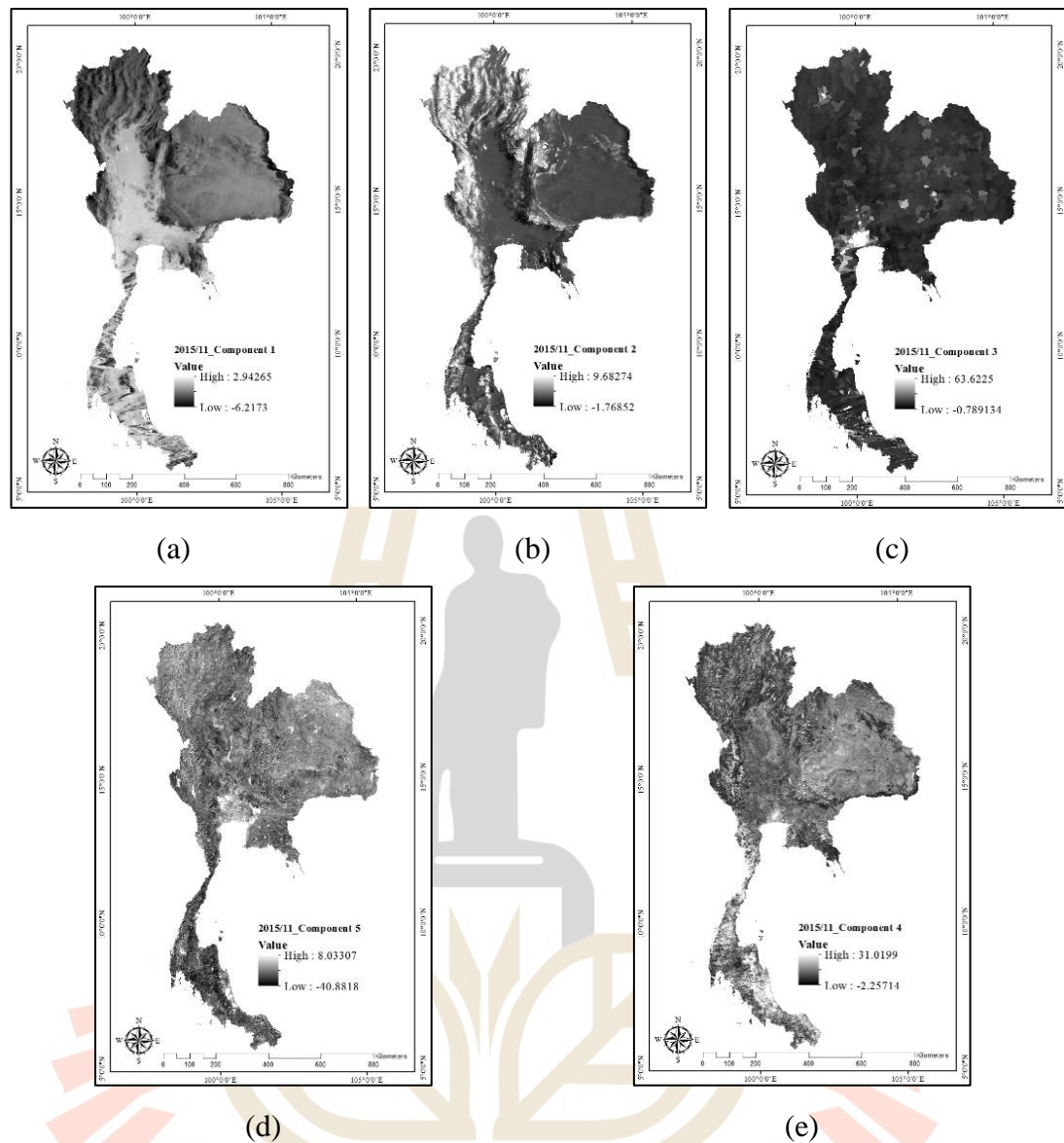


Figure 4.13 Factor map of November 2015 dataset by factor analysis (a) Component 1, (b) Component 2, (c) Component 3, (d) Component 4, and (e) Component 5.

4.1.3.2 Component extraction of December 2015 dataset

The result of factor analysis of December 2015 dataset in form of factor loading matrix is presented in Table 4.5. Herein, the first component can explain the variance of dataset about 50.307% and five components can explain the variance of dataset as cumulative variance about 93.351%. The derived component

with its score is further used to construct factor map for representation dominant variables on temperature.

Table 4.5 Factor loading matrix by factor analysis of December 2015 dataset.

Variables	Component				
	Factor 1	Factor 2	Factor 3	Factor 4	Factor 5
Elevation	-.385	.857	-.041	-.157	.031
Slope	-.140	.750	-.040	-.220	-.124
Population	.133	-.049	.983	.035	.024
Household	.108	-.034	.987	.004	.018
NDVI_1512	-.100	.305	-.026	-.821	-.444
NDBI_1512	-.104	-.051	.036	.009	.985
MNDWI_1512	.180	-.182	.022	.932	-.213
SO ₂ _1512	-.965	.210	-.080	-.086	.017
PM ₁₀ _1512	.969	-.203	.090	.078	-.027
O ₃ _1512	.943	-.223	.066	.098	-.007
CO_1512	.957	-.191	.081	.081	-.011
NO ₂ _1512	.958	-.185	.099	.064	-.035
Inso_1512	-.311	.836	-.030	-.075	.007
Wind_1512	.920	-.219	.069	.109	-.109
Initial eigenvalues	7.043	2.061	1.874	1.087	1.005
% of variance	50.307	14.718	13.386	7.764	7.177
Cumulative %	50.307	65.025	78.411	86.174	93.351

The result of factor analysis in Table 4.5 can explain the influence of variables on temperature in term of strengthen of relationship between variables and component as following.

Component 1: This component represents the influence of environmental factor on temperature. There are five significant environmental variables including PM₁₀, NO₂, CO, O₃, and SO₂ that have excellent relationship with temperature. One biophysical factor, wind speed, has excellent relationship with

temperature. The representation map of this component based on the derived factor scored with regression method is displayed in Figure 4.14(a). This map is here assumed as the representation of PM_{10} because it provides the highest factor loading in Component 1.

Component 2: This component represents the influence of biophysical factor on temperature. They are elevation, slope, and insolation that have excellent relationship with temperature. The representation map of this component based on the derived factor scored with regression method is displayed in Figure 4.14(b). This map is here assumed as the representation of elevation because it provides the highest factor loading in Component 2.

Component 3: This component represents the influence of demographic factor on temperature. They are household and population densities that have excellent relationship with temperature. The representation map of this component based on the derived factor scored with regression method is displayed in Figure 4.14(c). This map is here assumed as the representation of household density because it provides the highest factor loading in Component 3.

Component 4: This component represents the influence of biophysical factor on temperature including MNDWI and NDVI that have excellent relationship with temperature. The representation map of this component based on the derived factor scored with regression method is displayed in Figure 4.14(d). This map is assumed as the representation of MNDWI because it provides the highest factor loading in Component 4.

Component 5: This component represents the influence of biophysical factor on temperature. The most significant biophysical variables is NDBI

that has excellent relationship with temperature. The representation map of this component based on the derived factor scored with regression method is displayed in Figure 4.14(e). This map is here assumed as the representation of NDBI because it provides the highest factor loading in Component 5.



Figure 4.14 Factor map of December 2015 dataset by factor analysis (a) Component 1, (b) Component 2, (c) Component 3, (d) Component 4, and (e) Component 5.

4.1.3.3 Component extraction of January 2016 dataset

The result of factor analysis of January 2016 dataset in form of factor loading matrix is presented in Table 4.6. Herein, the first component can explain the variance of dataset about 46.010% and five components can explain the variance of dataset as cumulative variance about 89.649%. The derived component with its score is further used to construct factor map for representation dominant variables on temperature.

Table 4.6 Factor loading matrix by factor analysis of January 2016 dataset.

Variables	Component				
	Factor 1	Factor 2	Factor 3	Factor 4	Factor 5
Elevation	-.346	.873	-.037	-.140	.015
Slope	-.142	.671	-.039	-.344	-.098
Distance	-.301	.277	-.077	.645	.289
Population	.129	-.058	.983	.014	.025
Household	.105	-.045	.987	-.020	.022
NDVI_1601	-.099	.364	-.032	-.820	-.285
NDBI_1601	-.073	-.052	.050	.120	.956
MNDWI_1601	.154	-.320	.021	.792	-.395
SO ₂ _1601	.961	-.226	.073	.021	-.026
PM ₁₀ _1601	.963	-.239	.087	.017	-.042
O ₃ _1601	-.962	.238	-.098	.008	.048
CO_1601	-.941	.270	-.067	-.019	.045
NO ₂ _1601	.952	-.258	.094	.008	-.049
Inso_1601	-.265	.828	-.021	-.059	-.043
Wind_1601	.467	-.779	.099	-.108	-.160
Initial eigenvalues	6.902	2.363	1.876	1.243	1.063
% of variance	46.101	15.755	12.508	8.289	7.087
Cumulative %	46.010	61.765	74.273	82.562	89.649

The result of factor analysis in Table 4.6 can explain the influence of variables on temperature in term of strengthen of relationship between variables and component as following.

Component 1: This component represents the influence of environmental factor on temperature including PM₁₀, SO₂, NO₂, CO, and O₃ that have excellent relationship with temperature. The representation map of this component based on the derived factor scored with regression method is displayed in Figure 4.15(a). This map is here assumed as the representation of PM₁₀ because it provides the highest factor loading in Component 1.

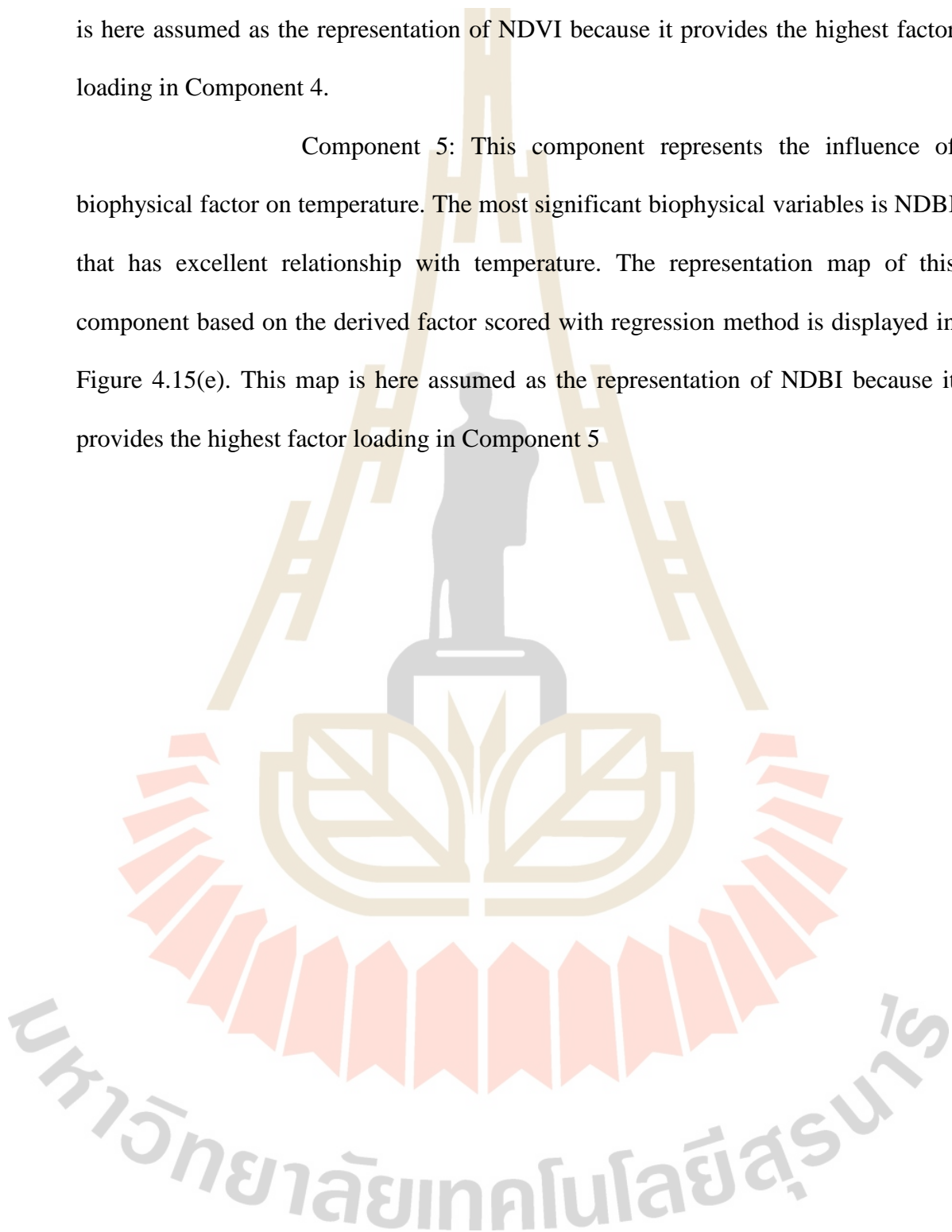
Component 2: This component represents the influence of biophysical factor on temperature. They are elevation, insolation, and wind speed that have excellent relationship with temperature. The representation map of this component based on the derived factor scored with regression method is displayed in Figure 4.15(b). This map is here assumed as the representation of elevation because it provides the highest factor loading in Component 2.

Component 3: This component represents the influence of demographic factor on temperature. They are household and population densities that have excellent relationship with temperature. The representation map of this component based on the derived factor scored with regression method is displayed in Figure 4.15(c). This map is here assumed as the representation of household density because it provides the highest factor loading in Component 3.

Component 4: This component represents the influence of biophysical factor on temperature including NDVI and MNDWI that have excellent relationship with temperature. The representation map of this component based on the

derived factor scored with regression method is displayed in Figure 4.15(d). This map is here assumed as the representation of NDVI because it provides the highest factor loading in Component 4.

Component 5: This component represents the influence of biophysical factor on temperature. The most significant biophysical variables is NDBI that has excellent relationship with temperature. The representation map of this component based on the derived factor scored with regression method is displayed in Figure 4.15(e). This map is here assumed as the representation of NDBI because it provides the highest factor loading in Component 5



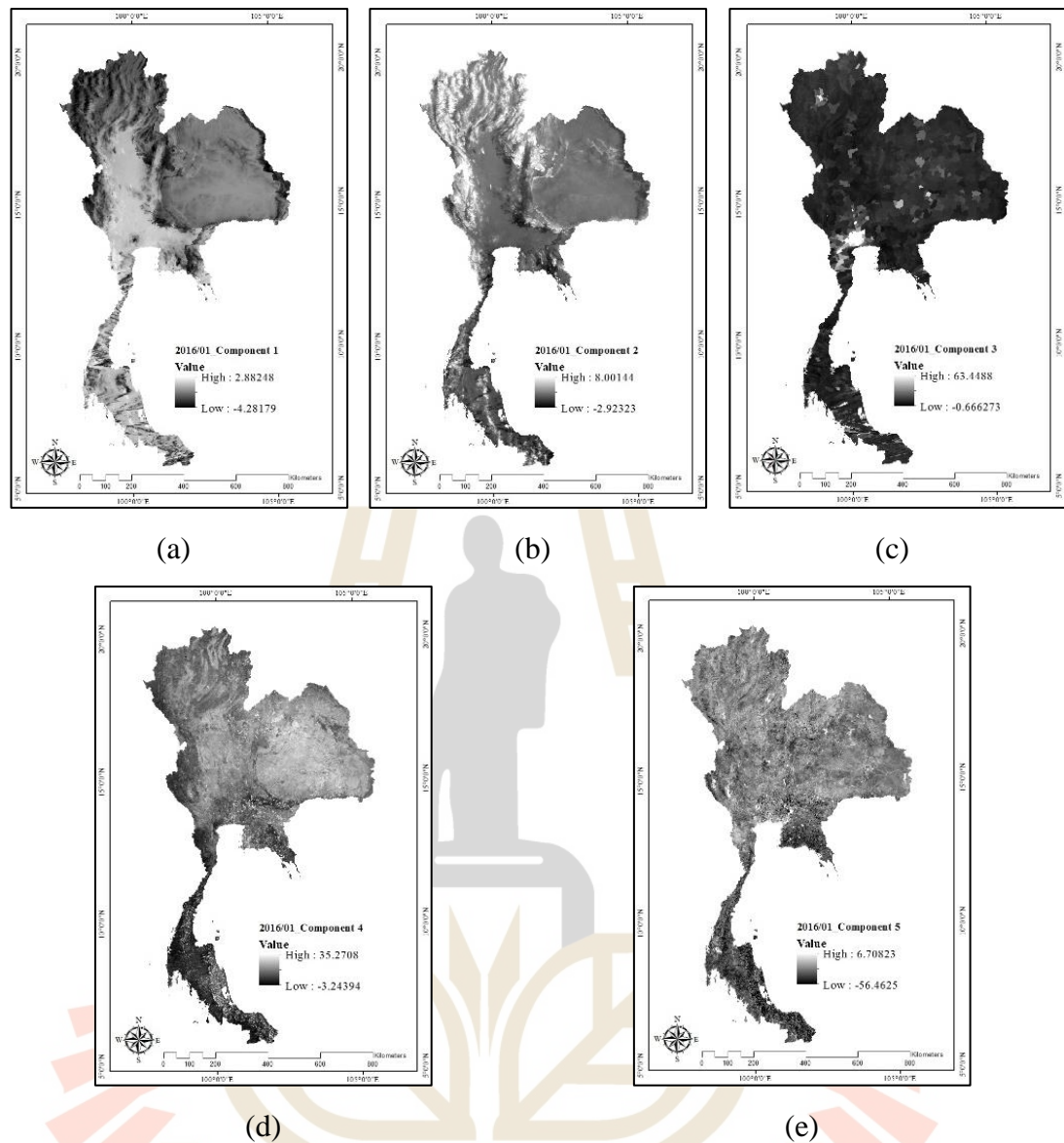


Figure 4.15 Factor map of January 2016 dataset by factor analysis (a) Component 1, (b) Component 2, (c) Component 3, (d) Component 4, and (e) Component 5.

4.1.3.4 Component extraction of February 2016 dataset

The result of factor analysis of February 2016 dataset in form of factor loading matrix is presented in Table 4.7. Herein, the first component can explain the variance of dataset about 43.783% and five components can explain the variance of dataset as cumulative variance about 83.508%. The derived component with its score

is further used to construct factor map for representation dominant variables on temperature.

Table 4.7 Factor loading matrix by factor analysis of February 2016 dataset.

Variables	Component				
	Factor 1	Factor 2	Factor 3	Factor 4	Factor 5
Elevation	.347	.863	-.047	.078	-.058
Slope	.139	.724	-.051	-.115	-.080
Aspect	.068	-.063	-.028	.011	.855
Distance	.323	.038	-.073	.652	.031
Population	-.139	-.061	.981	-.003	-.018
Household	-.114	-.035	.986	-.020	-.008
NDVI_1602	.108	.624	.001	-.580	.330
NDBI_1602	.049	.103	.044	.868	.066
MNDWI_1602	-.144	-.631	-.036	-.133	-.462
SO ₂ _1602	.880	.236	-.102	.087	.065
PM ₁₀ _1602	.955	.237	-.088	.106	.043
O ₃ _1602	.955	.231	-.093	.115	.043
CO_1602	-.953	-.248	.077	-.091	-.044
NO ₂ _1602	-.941	-.266	.079	-.100	-.046
Inso_1602	.305	.800	-.040	.072	-.059
Wind_1602	-.457	-.719	.072	-.362	-.016
Initial eigenvalues	7.005	2.127	1.838	1.368	1.023
% of variance	43.783	13.294	11.489	8.547	6.395
Cumulative %	43.783	57.077	68.566	77.113	83.508

The result of factor analysis in Table 4.7 can explain the influence of variables on temperature in term of strengthen of relationship between variables and component as following.

Component 1: This component represents the influence of environmental factor on temperature including PM₁₀, O₃, SO₂, CO, and NO₂ that have excellent relationship with temperature. The representation map of this component

based on the derived factor scored with regression method is displayed in Figure 4.16(a). This map is here assumed as the representation of PM_{10} because it provides the highest factor loading in Component 1.

Component 2: This component represents the influence of biophysical factor on temperature. They are elevation, insolation, slope and wind speed that have excellent relationship with temperature. The representation map of this component based on the derived factor scored with regression method is displayed in Figure 4.16(b). This map is here assumed as the representation of elevation because it provides the highest factor loading in Component 2.

Component 3: This component represents the influence of demographic factor on temperature. They are household and population densities that have excellent relationship with temperature. The representation map of this component based on the derived factor scored with regression method is displayed in Figure 4.16(c). This map is here assumed as the representation of household density because it provides the highest factor loading in Component 3.

Component 4: This component represents the influence of biophysical factor on temperature. The most significant biophysical variable is NDBI that has excellent relationship with temperature. The representation map of this component based on the derived factor scored with regression method is displayed in Figure 4.16(d). This map is here assumed as the representation of aspect because it provides the highest factor loading in Component 4.

Component 5: This component represents the influence of biophysical factor on temperature. The most significant biophysical variables is aspect that has excellent relationship with temperature. The representation map of this

component based on the derived factor scored with regression method is displayed in Figure 4.16(e). This map is here assumed as the representation of aspect because it provides the highest factor loading in Component 5.

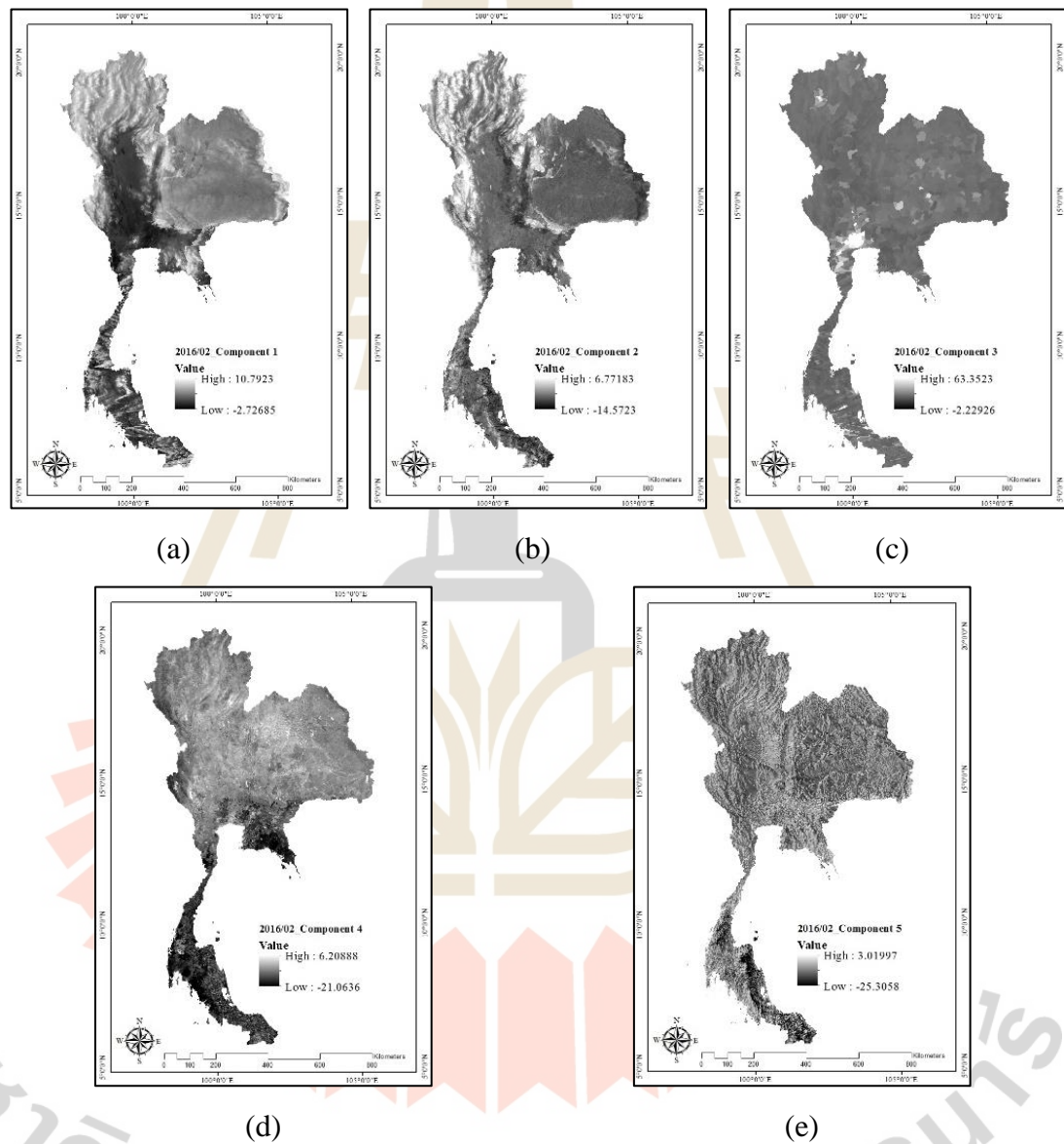


Figure 4.16 Factor map of February 2016 dataset by factor analysis (a) Component 1, (b) Component 2, (c) Component 3, (d) Component 4, and (e) Component 5.

4.1.3.5 Component extraction of March 2016 dataset

The result of factor analysis of March 2016 dataset in form of factor loading matrix is presented in Table 4.8. Herein, the first component can explain the variance of dataset about 49.233% and four components can explain the variance of dataset as cumulative variance about 87.979%. The derived component with its score is further used to construct factor map for representation dominant variables on temperature.

Table 4.8 Factor loading matrix by factor analysis of March 2016 dataset.

Variables	Component			
	Factor 1	Factor 2	Factor 3	Factor 4
Elevation	-.327	.914	-.035	-.004
Slope	-.089	.773	-.040	-.153
Distance	-.415	.037	-.071	.571
Population	.129	-.067	.982	.005
Household	.110	-.044	.987	-.007
NDVI_1603	-.042	.400	-.019	-.846
NDBI_1603	-.042	.158	.029	.844
SO ₂ _1603	.948	-.262	.085	-.046
PM ₁₀ _1603	-.933	.291	-.069	.084
O ₃ _1603	-.945	.221	-.111	.106
CO_1603	.957	-.242	.103	-.067
NO ₂ _1603	.956	-.244	.077	-.065
Inso_1603	-.323	.870	-.031	.011
Wind_1603	.483	-.793	.092	-.171
Initial eigenvalues	6.893	2.213	1.866	1.345
% of variance	49.233	15.810	13.329	9.607
Cumulative %	49.233	65.043	78.371	87.979

The result of factor analysis in Table 4.8 can explain the influence of variables on temperature in term of strengthen of relationship between variables and component as following.

Component 1: This component represents the influence of environmental factor on temperature including CO, NO₂, SO₂, O₃, and PM₁₀ that have excellent relationship with temperature. The representation map of this component based on the derived factor scored with regression method is displayed in Figure 4.17(a). This map is here assumed as the representation of CO because it provides the highest factor loading in Component 1.

Component 2: This component represents the influence of biophysical factor on temperature. They are elevation, insolation, slope, and wind speed that have excellent relationship with temperature. The representation map of this component based on the derived factor scored with regression method is displayed in Figure 4.17(b). This map is here assumed as the representation of elevation because it provides the highest factor loading in Component 2.

Component 3: This component represents the influence of demographic factor on temperature. They are household and population densities that have excellent relationship with temperature. The representation map of this component based on the derived factor scored with regression method is displayed in Figure 4.17(c). This map is here assumed as the representation of household density because it provides the highest factor loading in Component 3.

Component 4: This component represents the influence of biophysical factor on temperature including NDVI and MNDWI that have excellent relationship with temperature. The representation map of this component based on the

derived factor scored with regression method is displayed in Figure 4.17(d). This map is here assumed as the representation of NDVI because it provides the highest factor loading in Component 4.

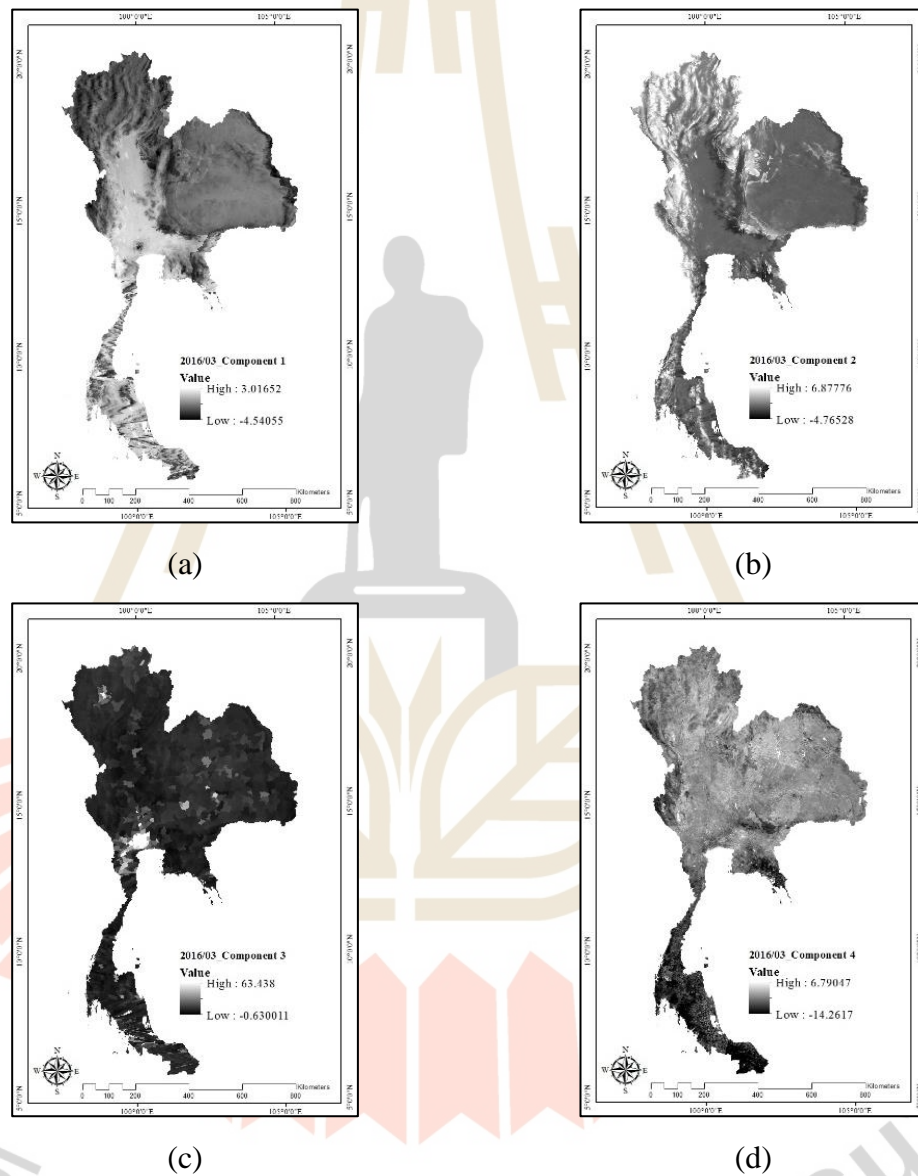


Figure 4.17 Factor map of March 2016 dataset by factor analysis (a) Component 1, (b) Component 2, (c) Component 3, (d) Component 4, and (e) Component 5.

4.1.3.6 Component extraction of April 2016 dataset

The result of factor analysis of April 2016 dataset in form of factor loading matrix is presented in Table 4.9. Herein, the first component can explain the variance of dataset about 44.878% and four components can explain the variance of dataset as cumulative variance about 86.024%. The derived component with its score is further used to construct factor map for representation dominant variables on temperature.

Table 4.9 Factor loading matrix by factor analysis of April 2016 dataset.

Variables	Component			
	Factor 1	Factor 2	Factor 3	Factor 4
Elevation	.317	.909	-.151	-.038
Slope	.110	.679	-.341	-.046
Distance	.327	.272	.686	-.063
Population	-.126	-.060	.017	.984
Household	-.105	-.047	-.013	.987
NDVI_1604	.099	.315	-.898	-.014
NDBI_1604	.024	-.130	.867	.028
MNDWI_1604	-.178	-.377	.769	.008
SO ₂ _1604	.937	.274	-.008	-.084
PM ₁₀ _1604	.914	.301	-.026	-.060
O ₃ _1604	.932	.285	.051	-.097
CO_1604	-.938	-.262	-.040	.100
NO ₂ _1604	-.787	-.100	.049	.058
Inso_1604	.325	.885	-.119	-.035
Wind_1604	.434	.858	-.028	-.071
Initial eigenvalues	6.732	3.040	1.853	1.279
% of variance	44.878	20.266	12.352	8.528
Cumulative %	44.878	65.144	77.497	86.024

The result of factor analysis in Table 4.9 can explain the influence of variables on temperature in term of strengthen of relationship between variables and component as following.

Component 1: This component represents the influence of environmental factor on temperature including SO₂, O₃, PM₁₀, CO, and NO₂ that have excellent relationship with temperature. The representation map of this component based on the derived factor scored with regression method is displayed in Figure 4.18(a). This map is here assumed as the representation of CO because it provides the highest factor loading in Component 1.

Component 2: This component represents the influence of biophysical factor on temperature. They are elevation, insolation, and wind speed that have excellent relationship with temperature. The representation map of this component based on the derived factor scored with regression method is displayed in Figure 4.18(b). This map is here assumed as the representation of elevation because it provides the highest factor loading in Component 2.

Component 3: This component represents the influence of biophysical factor on temperature including NDVI, NDBI, and MNDWI that have excellent relationship with temperature. The representation map of this component based on the derived factor scored with regression method is displayed in Figure 4.18 (c). This map is here assumed as the representation of NDVI because it provides the highest factor loading in Component 3.

Component 4: This component represents the influence of demographic factor on temperature. They are household and population densities that have excellent relationship with temperature. The representation map of this component

based on the derived factor scored with regression method is displayed in Figure 4.18(d). This map is here assumed as the representation of household density because it provides the highest factor loading in Component 4.

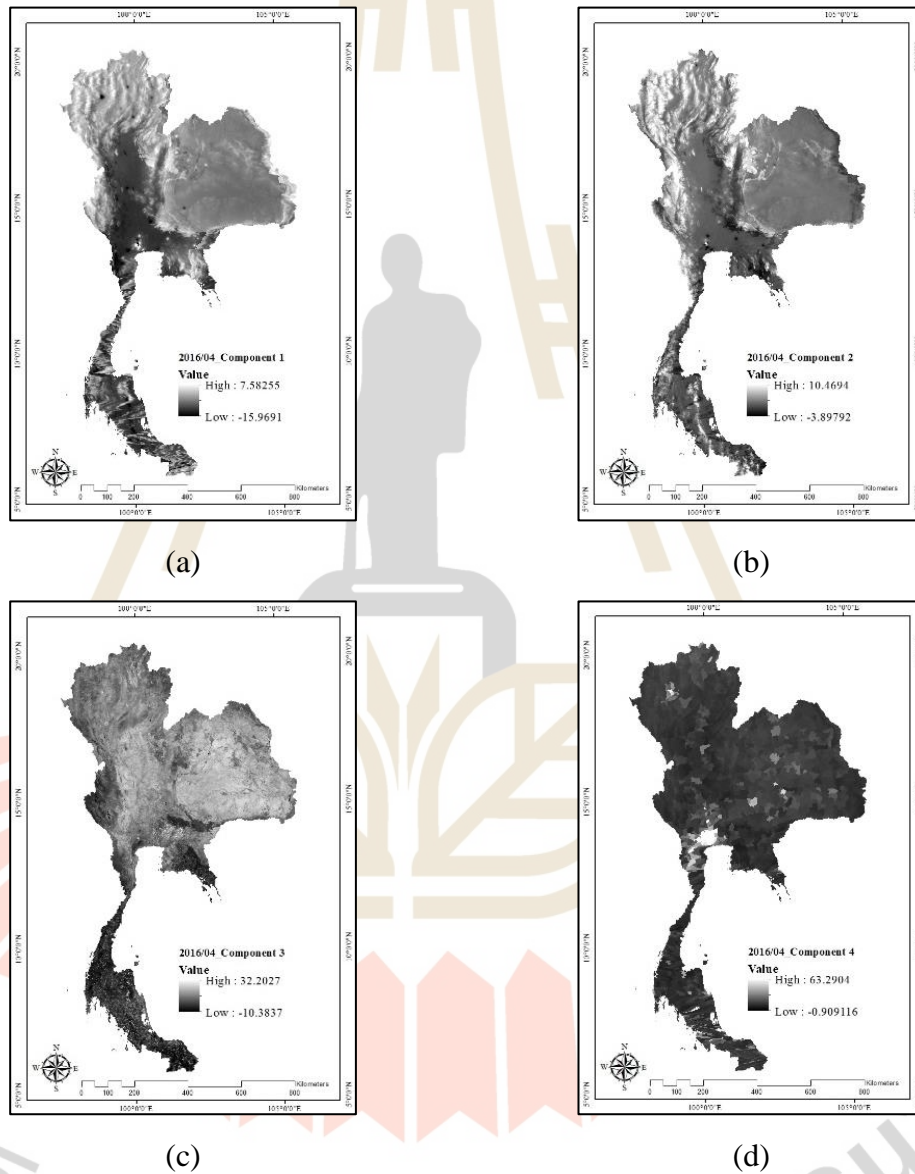


Figure 4.18 Factor map of April 2016 dataset by factor analysis (a) Component 1, (b) Component 2, (c) Component 3, (d) Component 4, and (e) Component 5.

In summary, local influential factors (environmental, biophysical, demographic) on temperature can be overall interpreted based on factor loading values and percent of variance of six months as summary in Table 4.10.

Table 4.10 Highest significant variable in each component with percent of variance and cumulative percent of variance in each month (November to April).

Month/ Statistic data	Components				
	1	2	3	4	5
November	Environmental	Biophysical	Demographic	Biophysical	Biophysical
Dominant variable	SO ₂	Elevation	Household	NDVI	NDBI
Factor loading	0.965	0.870	0.986	-0.915	0.988
% of variance	50.519	13.453	11.594	10.764	7.782
December	Environmental	Biophysical	Demographic	Biophysical	Biophysical
Dominant variable	PM ₁₀	Elevation	Household	MNDWI	NDBI
Factor loading	0.969	0.857	0.987	0.932	0.985
% of variance	50.307	14.718	13.386	7.764	7.177
January	Environmental	Biophysical	Demographic	Biophysical	Biophysical
Dominant variable	PM ₁₀	Elevation	Household	NDVI	NDBI
Factor loading	0.963	0.873	0.987	-0.820	0.956
% of variance	46.101	15.755	12.508	8.289	7.087
February	Environmental	Biophysical	Demographic	Biophysical	Biophysical
Dominant variable	PM ₁₀	Elevation	Household	NDBI	Aspect
Factor loading	0.955	0.863	0.986	0.868	0.855
% of variance	43.783	13.294	11.489	8.547	6.395
March	Environmental	Biophysical	Demographic	Biophysical	n.a.
Dominant variable	CO	Elevation	Household	NDVI	n.a.
Factor loading	0.957	0.914	0.987	-0.846	n.a.
% of variance	49.233	15.810	13.329	9.607	n.a.
April	Environmental	Biophysical	Biophysical	Demographic	n.a.
Dominant variable	CO	Elevation	NDVI	Household	n.a.
Factor loading	-0.938	0.909	-0.898	0.987	n.a.
% of variance	44.878	20.266	12.352	8.528	n.a.

As a result, it reveals that the most significant local influential factor on temperature in the study area (Thailand) according percent of variance of the derived components is environmental factor including SO₂, PM₁₀, CO, NO₂, and O₃. The derived percent of variance, which shows relative important among components in each

month, varies between 43.783% in February and 50.519% in November. The most dominant variable of environmental factor according to factor loading value is PM₁₀ that provides the highest value in December, January, and February. Likewise, CO provides the highest factor loading value in March and April while SO₂ is dominate in November. The major causes of air pollutants during winter season in Thailand are burning of agricultural debris, forest fire, mining, and transporation.

Meanwhile the secondary dominant factor on temperature in this study is (bio)physical factor including elevation, slope, insolation, and wind speed. The derived percent of variance of the component varies between 13.294% in February and 20.266% in April. Elevation and insolation show excellent relationship with temperature in all six months.

Likewise, the third important factor on temperature is demographic factor including household density and population density at sub-district level. The derived percent of variance of the component varies between 8.528% in April and 13.386% in December. Both variables show excellent relationship with temperature in all six months.

The fourth important factor on temperature is biophysical factor including NDVI, NDBI, and MNDWI. The derived percent of variance of the component varies between 6.395% in February and 13.329% in March. Herein, NDBI variable shows excellent relationship with temperature in all six months. This is true, because NDBI characterizes urban and built-up areas that are directly relate with temperature. Meanwhile NDVI variable shows excellent relationship with temperature in five months, except Februry. Because most deciduous forest and rubber trees in Thailand is

shed-off and rainfed paddy fields is off-farm activities. Likewise, MNDWI only provides excellent relationship in four months, except February and March.

4.2 Top three influential factors on temperature pattern using spatial simple linear regression analysis

The selected representative of factor map of each component in each month (November and April) were further analyzed spatial linear relationship with MODIS LST pattern (Figure 4.19) under IDRISI software. Results of spatial simple relationship analysis include correlation coefficient (R) and coefficient of determination (R^2) from each month is first separately considered to identify top three influential factors. Then they are considered together to finally justify top three influential factors on temperature pattern in the study area (Thailand). Results and discussion are firstly separately described by month and then summarized for all six months in the following sections.

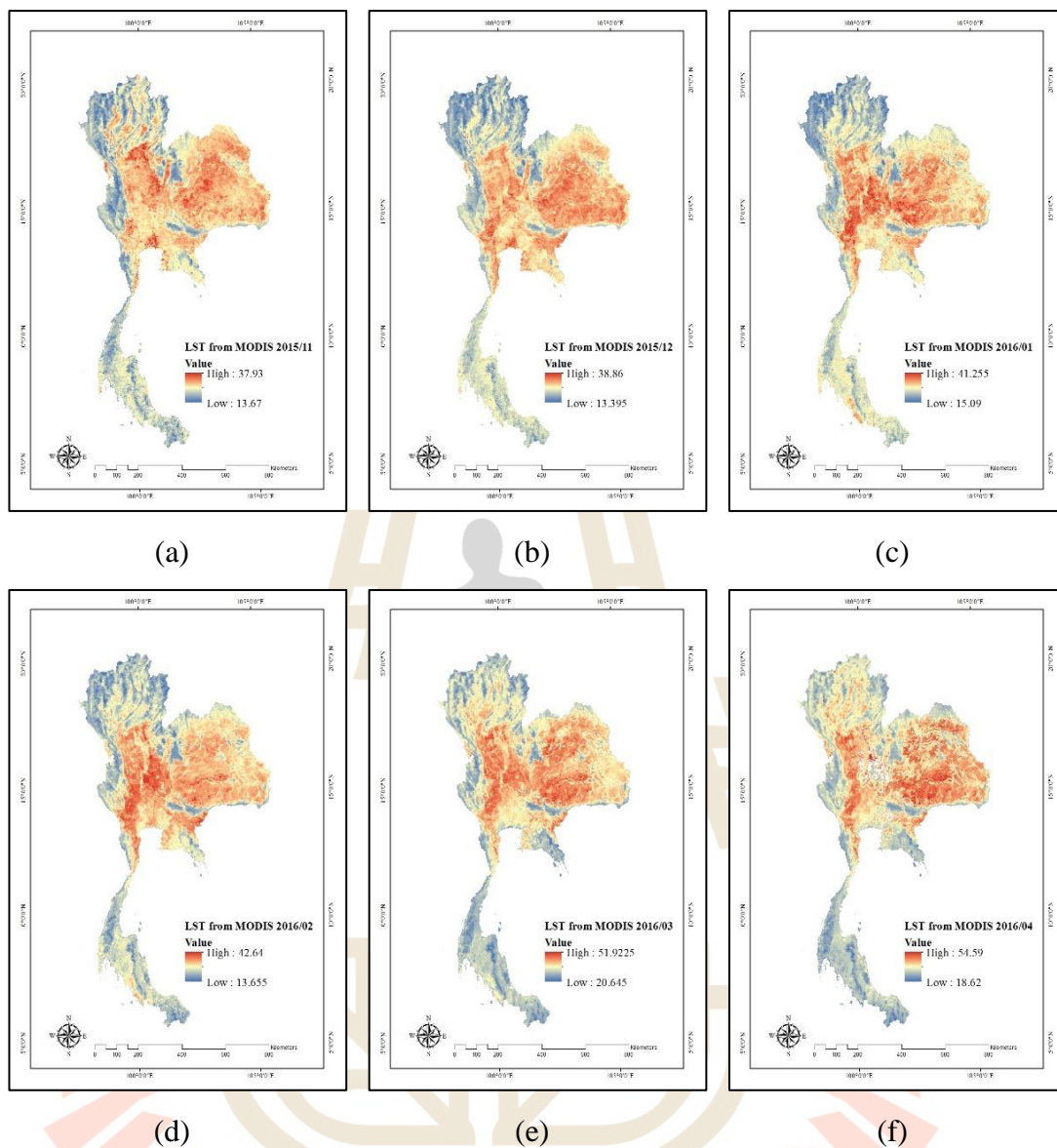


Figure 4.19 Monthly MODIS LST during November 2015 to April 2016: (a) November 2015, (b) December 2015, (c) January 2016, (d) February 2016, (e) March 2016, and (f) April 2016.

4.2.1 Top three influential factors on temperature pattern in November

According to spatial simple linear analysis between the factor map of each component from factor analysis and MODIS LST data, it reveals that top three influential factors on temperature pattern in November are NDBI, SO₂, and NDVI. They provide the correlation coefficient (R) and coefficient of determination (R²) values of 0.971, 0.955, and 0.858, and 94.18%, 91.17%, and 73.68%, respectively. Details of spatial linear regression analysis and its equation is displayed in Table 4.11.

As a result, top three influential factors have highly correlation with MODIS LST pattern. Simple linear equations of SO₂, household density, and NDBI provide positive correlation with LST data. This finding infers that when air pollutant, household density and urban and built-up area increase, LST increase. However, simple linear equation of NDVI and elevation show an unexpected result. In principal, NDVI and elevation should have negatively correlation with LST. In other words, when NDVI and elevation increase, LST should decrease. The possible reason could be here mentioned because both variables do not have perfectly relationship with the LST as linear form as suggested by Wu, Lord, and Zou (2015).

Table 4.11 Spatial regression analysis between factor map from November 2015 and MODIS LST data.

Component	R	R ²	Simple linear equation	Representative variable	Ranking
1	0.955	91.17	$Y = 1.817735 + 0.834161X$	SO ₂	2
2	0.697	48.54	$Y = 21.605912 + 2.231662X$	Elevation	4
3	0.528	27.90	$Y = 37.089022 + 13.993639X$	Household	5
4	0.858	73.68	$Y = 11.744174 + 6.722074X$	NDVI	3
5	0.971	94.18	$Y = -0.004057 + 0.701614X$	NDBI	1

Note X is factor map of each component as independent variable
Y is temperature pattern from MODIS LST as dependent variable

4.2.2 Top three influential factors on temperature pattern in December

According to spatial linear analysis between the factor map from each component and MODIS LST data, it shows that top three influential factors on temperature pattern in December are NDBI, PM₁₀, and MNDWI. They provide R and R² values of 0.960, 0.952, and 0.905, and 92.24%, 90.57%, and 81.92%, respectively. Details of spatial linear regression analysis and its equation is displayed in Table 4.12.

As a result, top three influential factors have highly correlation with MODIS LST pattern. Simple linear equations of PM₁₀, household density, and NDBI provide positive correlation with LST data. This finding implies that when air pollutant, household density, and urban and built-up area increase, LST increase. However, simple linear equation of MNDWI and elevation show an unexpected result again as mentioned reason earlier.

Table 4.12 Spatial regression analysis between factor map from December 2015 and MODIS LST data.

Component	R	R ²	Simple linear equation	Representative variable	Ranking
1	0.952	90.57	$Y = 1.635523 + 0.849440X$	PM ₁₀	2
2	0.731	53.49	$Y = 17.829869 + 2.308643X$	Elevation	4
3	0.489	23.91	$Y = 38.407127 + 13.078967X$	Household	5
4	0.905	81.92	$Y = 7.792990 + 10.112169X$	MNDWI	3
5	0.960	92.24	$Y = -0.030131 + 0.668788X$	NDBI	1

Note X is factor map of each component as independent variable
Y is temperature pattern from MODIS LST as dependent variable

4.2.3 Top three influential factors on temperature pattern in January

According to spatial linear analysis between the factor map from each component and MODIS LST data, it reveals that top three influential factors on temperature pattern in December are NDBI, PM₁₀, and MNDWI. They provide R and R² values of 0.960, 0.952, and 0.905, and 92.24%, 90.57%, and 81.92%, respectively. Details of spatial linear regression analysis and its equation is displayed in Table 4.13.

As a result, top three influential factors have highly positively correlation with MODIS LST pattern. Simple linear equations of PM₁₀, household density and NDBI provide positive correlation with LST data. This finding infers that when air pollutant, household density and urban and built-up area increase, LST increase. However, simple linear equation of NDVI and elevation show an unexpected result as same as the previous result of November.

Table 4.13 Spatial regression analysis between factor map from January 2016 and MODIS LST data.

Component	R	R ²	Simple linear equation	Representative variable	Ranking
1	0.941	88.51	$Y = 2.394700 + 0.817305X$	PM ₁₀	2
2	0.805	64.79	$Y = 10.622481 + 1.546708X$	Elevation	4
3	0.456	20.75	$Y = 35.826481 + 11.179417X$	Household	5
4	0.941	88.51	$Y = 3.709378 + 5.682263X$	NDVI	3
5	0.955	91.75	$Y = 0.013411 + 0.574897X$	NDBI	1

Note X is factor map of each component as independent variable
Y is temperature pattern from MODIS LST as dependent variable

4.2.4 Top three influential factors on temperature pattern in February

According to spatial linear analysis between the factor map from each component and MODIS LST data, it reveals that top three influential factors on temperature pattern in February are NDBI, aspect, and elevation. They provide R and R² values of 0.963, 0.958, and 0.940, and 92.67%, 91.81%, and 88.33%, respectively. Details of spatial linear regression analysis and its equation is displayed in Table 4.14.

As a result, top three influential factors have highly positively correlation with MODIS LST pattern. Simple linear equations of PM₁₀, household density and NDBI provide positive correlation with LST data. This find suggests that when air pollutant, household density, and urban and built-up area increase, LST increase. However, simple linear equation of elevation and aspect show an unexpected result like November.

Table 4.14 Spatial regression analysis between factor map from February 2016 and MODIS LST data.

Component	R	R ²	Simple linear equation	Representative variable	Ranking
1	0.849	72.04	$Y = 9.7980115 + 2.249889X$	PM ₁₀	4
2	0.940	88.33	$Y = 1.225340 + 0.831356X$	Elevation	3
3	0.842	10.86	$Y = 11.923806 + 12.825096X$	Household	5
4	0.963	92.67	$Y = -0.101158 + 0.737434X$	NDBI	1
5	0.958	91.81	$Y = 0.102959 + 0.632142X$	Aspect	2

Note X is factor map of each component as independent variable
Y is temperature pattern from MODIS LST as dependent variable

4.2.5 Top three influential factors on temperature pattern in March

According to spatial linear analysis between the factor map from each component and MODIS LST data, top three influential factors on temperature pattern in March are NDVI, CO and elevation. They provide R and R² values of 0.945, 0.906, and 0.856, and 89.34%, 82.03%, and 73.32%, respectively. Details of spatial linear regression analysis and its equation is displayed in Table 4.15.

As a result, top three influential factors have highly positively correlation with MODIS LST pattern. Simple linear equations of CO and household density provide positive correlation with LST data. This finding deduces that when air pollutant, household density and urban and built-up area increase, LST increase. However, simple linear equation of NDVI and elevation show an unexpected result like November.

Table 4.15 Spatial regression analysis between factor map from March 2016 and MODIS LST data.

Component	R	R ²	Simple linear equation	Representative variable	Ranking
1	0.906	82.03	$Y = 2.692976 + 0.759534X$	CO	2
2	0.856	73.32	$Y = 4.823312 + 1.047704X$	Elevation	3
3	0.420	17.67	$Y = 34.889460 + 10.134904X$	Household	4
4	0.945	89.34	$Y = -.0477975 + 0.730667X$	NDVI	1

Note X is factor map of each component as independent variable

Y is temperature pattern from MODIS LST as dependent variable

4.2.6 Top three influential factors on temperature pattern in April

According to spatial linear analysis between the factor map from each component and MODIS LST data, it reveals that top three influential factors on temperature pattern in April are NDVI, CO and elevation. They provide R and R² values of 0.960, 0.930, and 0.867, and 92.22%, 86.55%, and 75.13%, respectively. Details of spatial linear regression analysis and its equation is displayed in Table 4.16.

As a result, top three influential factors have highly positively correlation with MODIS LST pattern. Simple linear equations of CO and household density provide positive correlation with LST data. This finding deduces that when air pollutant, household density and urban and built-up area increase, LST increase. However, simple linear equation of NDVI and elevation show an unexpected result like November.

Table 4.16 Spatial regression analysis between factor map from April 2016 and MODIS LST data.

Component	R	R ²	Linear regression equation	Representative variable	Ranking
1	0.930	86.55	$Y = 0.323175 + 0.762009X$	CO	2
2	0.867	75.13	$Y = 5.173589 + 1.725510X$	Elevation	3
3	0.960	92.22	$Y = -0.941957 + 2.186806X$	NDVI	1
4	0.558	30.61	$Y = 30.058627 + 12.879790X$	Household	4

Note X is factor map of each component as independent variable

Y is temperature pattern from MODIS LST as dependent variable

In summary, top three significant influential factors on temperature pattern of MODIS LST data form six month is comparatively displayed in Table 4.17 again.

As a result, it can be here concluded that significant influential factors in the study area (Thailand) consists NDVI, NDBI, elevation, and MNDWI as of biophysical factor and PM₁₀, CO, and SO₂ as environmental factor. In addition, it can be here observed that all significant influential factors show positively correlate with LST. Herewith, NDVI, MNDWI, and elevation provide an unexpected result while NDBI, PM₁₀, CO, and SO₂ show an expected result as mentioned in the literature reviews.

These findings show similar and dissimilar results with the previous work of Liu and Zhang (2011), El-Magd, Ismail, and Zanaty (2016) and Peng, Zhou, Wen, Xue, and Dong (2016) who suggested that LST had medium to very high negative correlation with NDVI and MNDWI while NDBI was a medium to highly significant positive correlation with LST.

The identified top three influential factors from each month are further applied to identify an optimum multivariate geostatistical method for monthly mean temperature interpolation in the next Chapter.

Table 4.17 Monthly top three significant influential factors on temperature pattern of MODIS data.

Influential factor	Nov	Dec	Jan	Feb	Mar	Apr
1	NDBI	NDBI	NDBI	NDBI	NDVI	NDVI
2	SO ₂	PM ₁₀	PM ₁₀	Aspect	CO	CO
3	NDVI	MNDWI	NDVI	Elevation	Elevation	Elevation

CHAPTER V

OPTIMUM GEOSTATISTICAL METHOD FOR IN SITU MEAN TEMPERATURE INTERPOLATION

Under this chapter, there are two standard geostatistical methods for monthly mean temperature interpolation include univariate (OK, SK, and UK) and multivariate (SCK, OCK, and UCK) are here examined to identify an optimum geostatistical method for mean temperature of TMD interpolation.

In practice, monthly mean temperature data of TMD were directly applied to interpolate surface monthly mean temperature with univariate geostatistical methods (OK, SK, and UK) and then their results were assessed accuracy using RMSE, MRE and MAE for identifying an optimum univariate method. Meanwhile, top three influential factors on temperature pattern of MODIS LST data in each month (November to April) from the previous chapter were here applied with monthly mean temperature data of TMD under multivariate geostatistical methods (SCK, OCK, and UCK) to interpolate surface monthly mean temperature. Then their results were also assessed accuracy using RMSE, MRE, and MAE to identify an optimum multivariate method. Finally, results of univariate and multivariate geostatistical method were simultaneously considered to identify an optimum method for monthly mean temperature interpolation using Akaike Information Criterion (AIC).

5.1 Optimum univariate geostatistical method for monthly mean temperature interpolation

Results of monthly mean temperature interpolation using OK, SK, and UK are displayed in Figures 5.1 to 5.3, respectively. The basic statistical data of the interpolated monthly mean temperature of three methods are compared in Table 5.1.

According to basic statistical data of three methods, it can be observed that the interpolated mean temperature of three methods are not so much different. However, the minimum and maximum values of SK method are significantly different from OK and UK methods. The minimum and maximum values of OK and UK are equal.

Table 5.1 Basic statistical data of the interpolated monthly mean temperature of univariate methods.

Method	OK			SK			UK		
	Min.	Max.	Mean	Min.	Max.	Mean	Min.	Max.	Mean
November	25.44	29.63	27.85	22.43	30.44	27.92	25.44	29.63	27.85
December	22.13	28.73	26.19	20.47	30.96	26.31	22.13	28.73	26.19
January	18.66	30.26	25.30	20.66	28.94	25.24	18.66	30.26	25.30
February	21.66	29.52	25.44	22.23	29.17	25.54	21.66	29.52	25.44
March	21.07	31.29	29.30	28.29	30.96	29.74	21.07	31.29	29.30
April	22.14	34.30	32.05	29.68	34.00	32.50	22.14	34.30	32.05

In addition, the pattern of monthly mean temperature of SK method is also different from OK and UK methods while the pattern of monthly mean temperature of OK and UK are similar. The correlation coefficient of monthly mean temperature among three methods based on interpolated values at selected thirty-six TMD station is reported in Table 5.2.

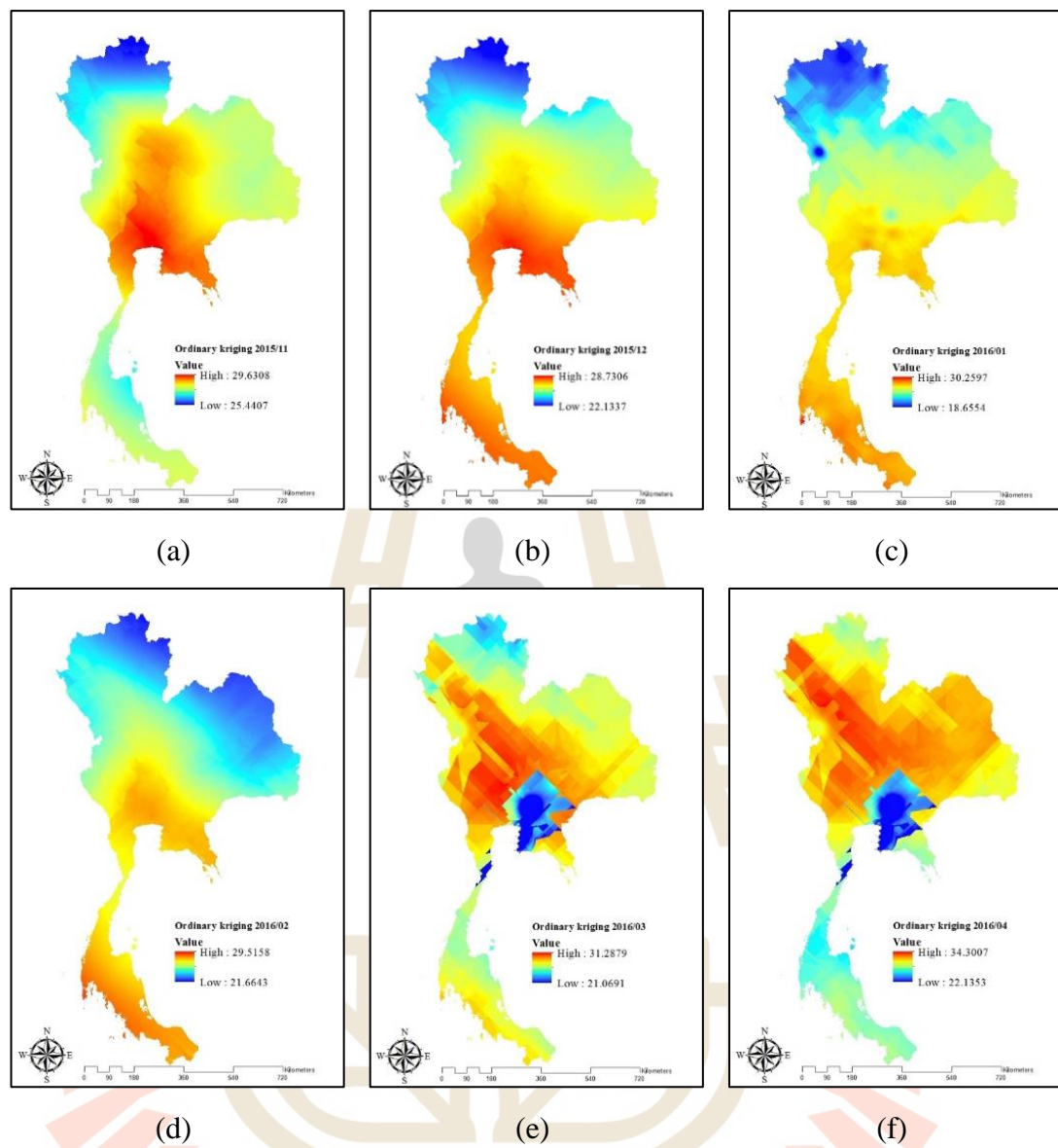


Figure 5.1 Monthly mean temperature interpolation using OK: (a) November, (b) December, (c) January, (d) February, (e) March, and (f) April.

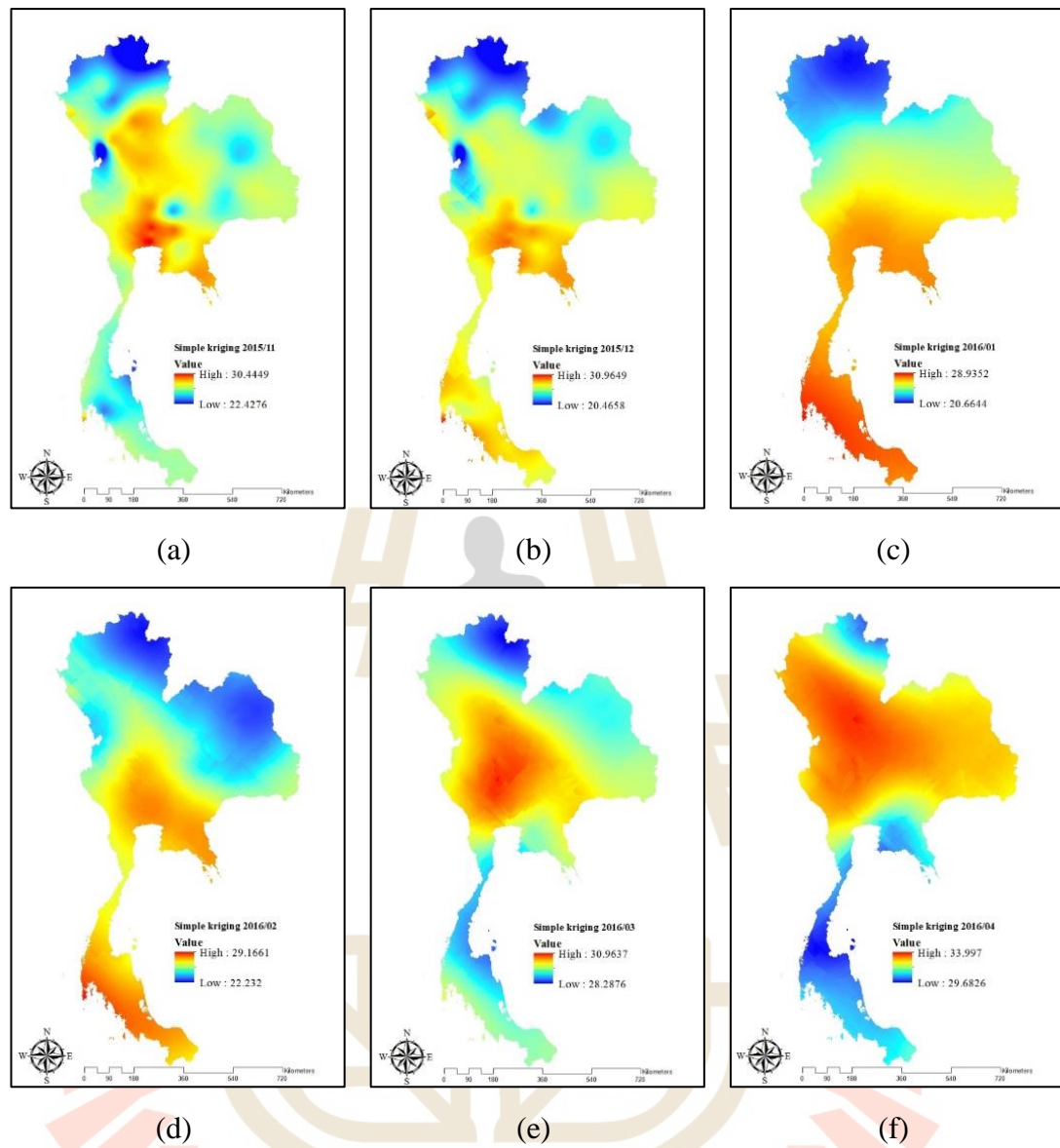


Figure 5.2 Monthly mean temperature interpolation using SK: (a) November, (b) December, (c) January, (d) February, (e) March, and (f) April.

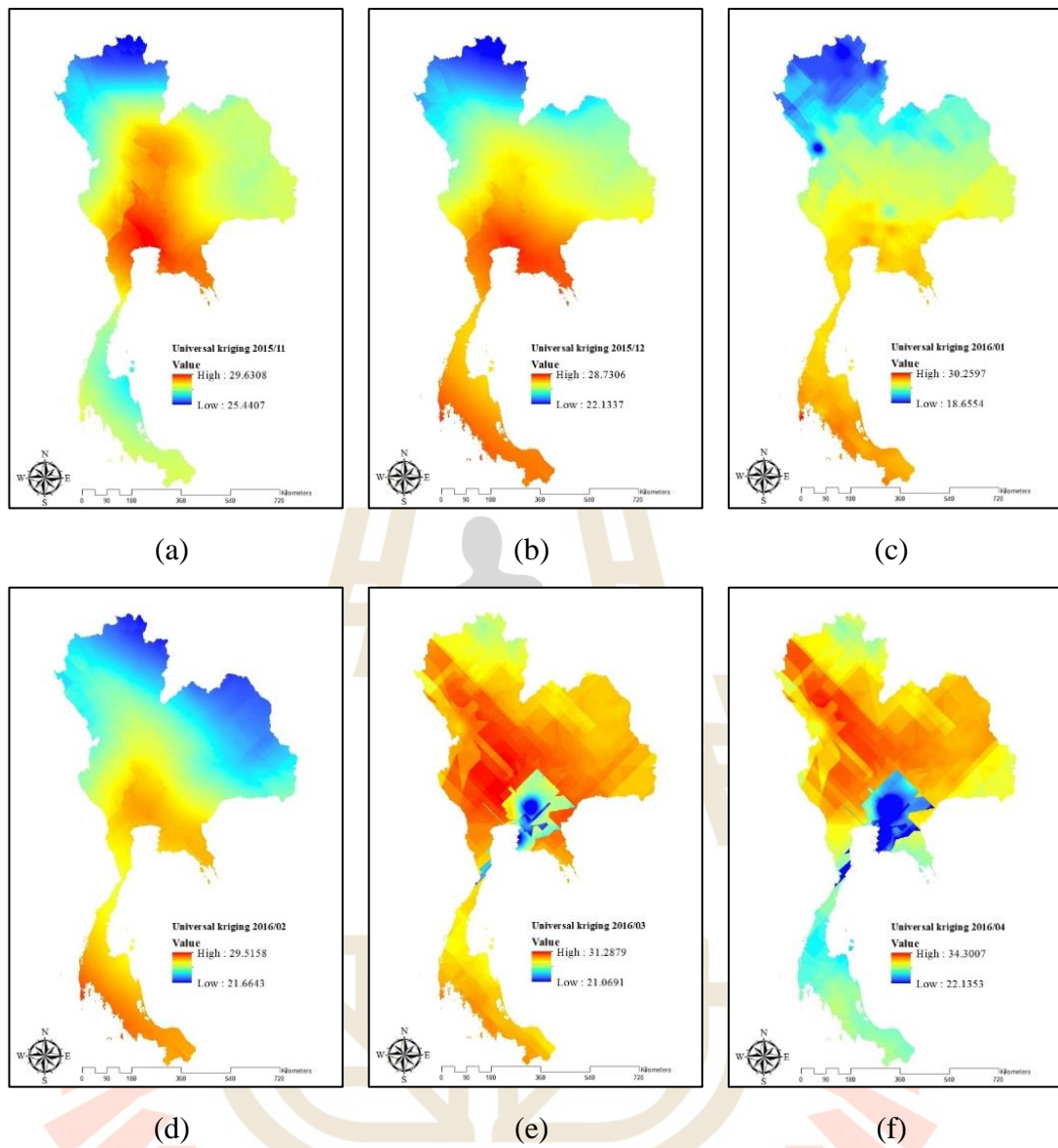


Figure 5.3 Monthly mean temperature interpolation using UK: (a) November, (b) December, (c) January, (d) February, (e) March, and (f) April.

Table 5.2 Correlation coefficient (R) of monthly mean temperature among three univariate methods.

Month	OK and SK	SK and UK	UK and OK
November	0.916	0.916	1.00
December	0.939	0.939	1.00
January	0.979	0.979	1.00
February	0.986	0.986	1.00
March	0.543	0.543	1.00
April	0.710	0.710	1.00

As a result, it reveals that the R values between the interpolated monthly mean temperature data of OK and UK method equals 1.00. This implies that pattern of the interpolated monthly mean temperature data of OK and UK method is the same. Meanwhile, the interpolated monthly mean temperature data in November, December, January, and February of SK method have highly correlation with the interpolated data of OK and UK method. The R values range between 0.916 in November and 0.986 in February. Meanwhile, the interpolated monthly mean temperature data in March and April of SK method have low correlation with the interpolated data of OK and UK method. The R values range between 0.543 in March and 0.710 in April. This finding implies that pattern of the interpolated monthly mean temperature data between November and February of SK method is quite similar with the pattern of the OK and UK methods. In contrast, pattern of the interpolated monthly mean temperature data in March and April is dissimilar with the pattern of the OK and UK methods. However, the interpolated monthly mean temperature data of SK method appears more smoothness than OK and UK methods.

Meanwhile, results of accuracy assessment among univariate geostatistical methods for monthly mean temperature interpolation based on the reference data from thirty-six TMD ground stations data is summarized in Table 5.3.

Table 5.3 Accuracy assessment of monthly mean temperature interpolation by univariate geostatistical method using MAE, MRE, and RMSE.

Month	Methods	MAE (°C)	MRE (°C)	RMSE (°C)	Optimum method
November	OK	0.79981	0.03145	1.314963	OK or UK
	SK	0.82957	0.03278	1.35811	
	UK	0.79981	0.03145	1.314963	
December	OK	0.81257	0.0345	1.263644	OK or UK
	SK	0.75003	0.03241	1.303698	
	UK	0.81257	0.0345	1.263644	
January	OK	0.77461	0.03493	1.274243	OK or UK
	SK	0.8791	0.03894	1.3267	
	UK	0.77461	0.03493	1.274243	
February	OK	0.8674	0.03643	1.257532	OK or UK
	SK	0.80442	0.03418	1.27582	
	UK	0.8674	0.03643	1.257532	
March	OK	0.4219462	0.0149782	0.5486517	OK or UK
	SK	0.8941896	0.0323609	1.3238691	
	UK	0.4219462	0.0149782	0.5486517	
April	OK	0.3550634	0.011481	0.4762094	OK or UK
	SK	0.523358	0.017056	0.7019973	
	UK	0.3550634	0.011481	0.4762094	

As results, it reveals that optimum method of univariate geostatistics for mean temperature interpolation is OK or UK method. Both methods provide MAE, MRE,

and RMSE with same value in each month. However, Detail of input data and its comparison is show in Appendix B.

5.2 Optimum multivariate geostatistical method for monthly mean temperature interpolation

Results of monthly mean temperature interpolation using Ordinary CoKriging (OCK), Simple CoKriging (SCK) and Universal CoKriging (UCK) with top three influential factors on temperature pattern from each month are displayed in Figures 5.4 to 5.6, respectively. The basic statistical data of the interpolated monthly mean temperature of three methods are compared in Table 5.4.

According to basic statistical data of three methods, it can be observed that the interpolated mean temperature of three methods are not so much different. However, the minimum and maximum values of SCK method are significantly different from OCK and UCK methods. The minimum and maximum values of OCK and UCK are equal.

Table 5.4 Basic statistical data of the interpolated monthly mean temperature of multivariate methods.

Method	OCK			SCK			UCK		
	Min.	Max.	Mean	Min.	Max.	Mean	Min.	Max.	Mean
November	25.42	29.63	27.85	9.71	31.24	27.76	25.42	29.63	27.85
December	20.70	29.82	26.24	13.10	29.89	26.44	20.70	29.82	26.24
January	19.03	29.65	25.14	12.08	29.37	25.55	19.03	29.65	25.14
February	20.32	30.47	25.50	20.11	29.33	25.63	20.32	30.47	25.50
March	25.43	30.99	29.20	21.80	33.55	29.70	25.43	30.99	29.20
April	26.78	33.62	31.92	-0.17	34.67	31.69	26.78	33.62	31.92

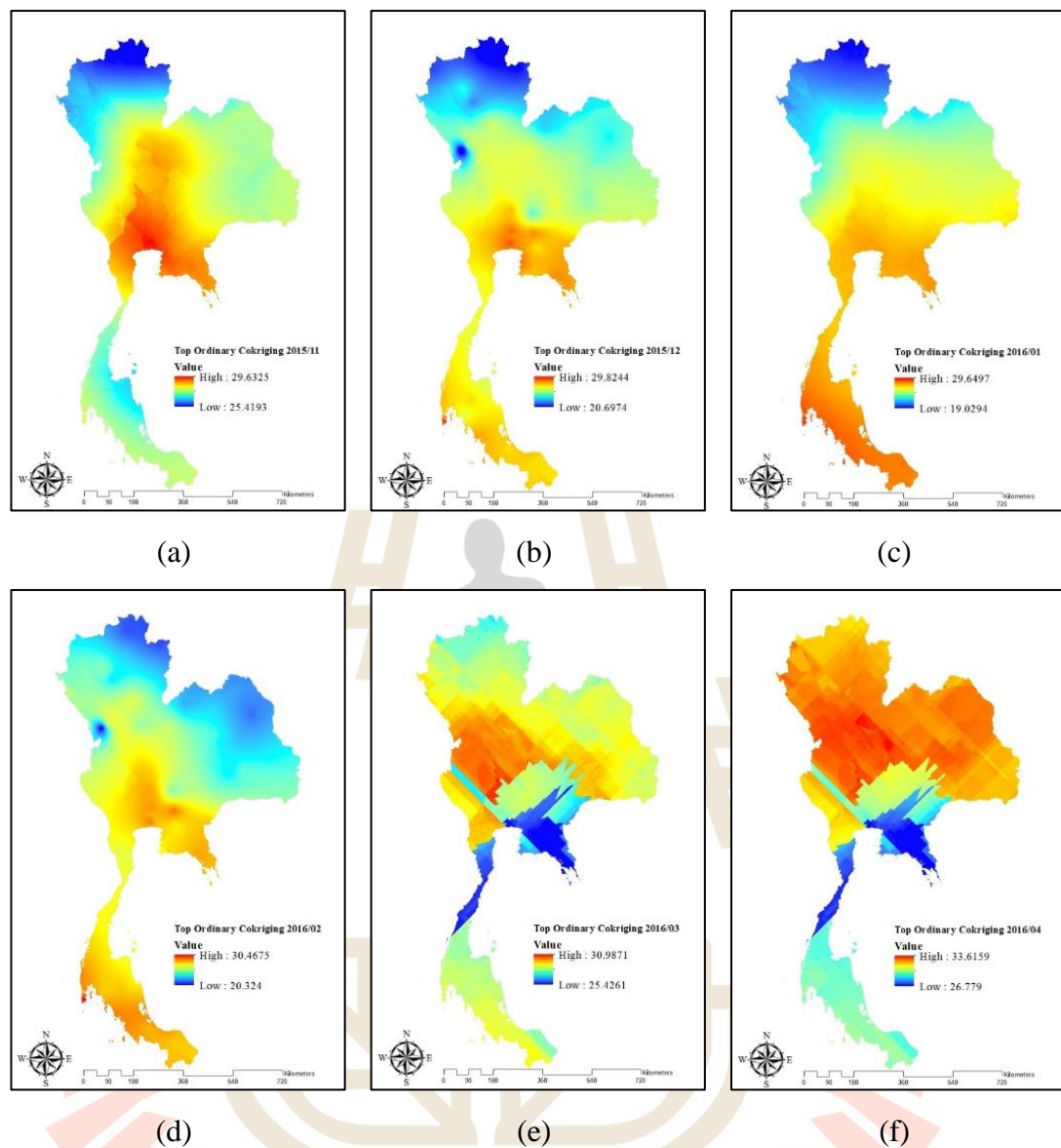


Figure 5.4 Monthly mean temperature interpolation using OCK: (a) November, (b) December, (c) January, (d) February, (e) March, and (f) April.

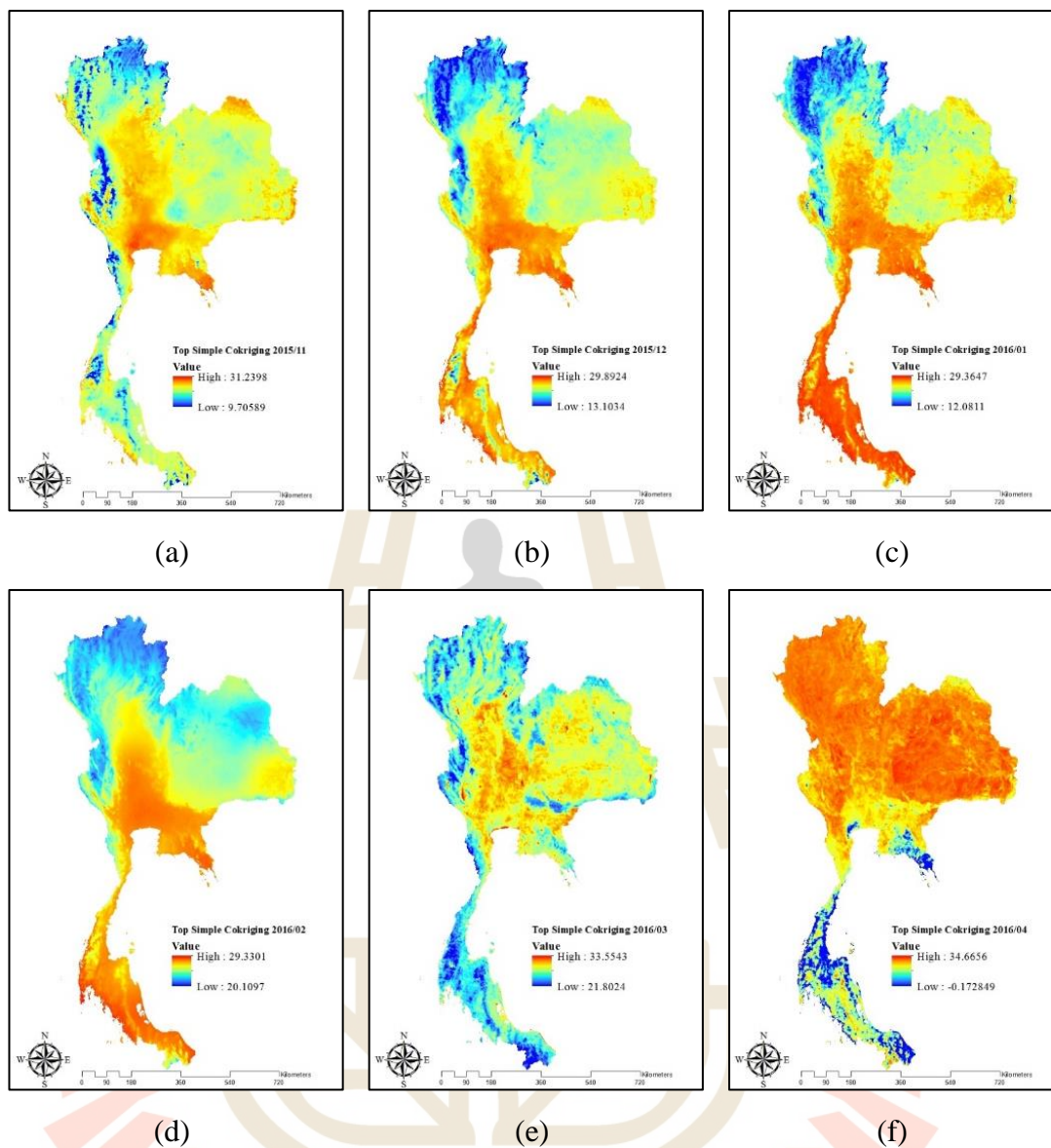


Figure 5.5 Monthly mean temperature interpolation using SCK: (a) November, (b) December, (c) January, (d) February, (e) March, and (f) April.

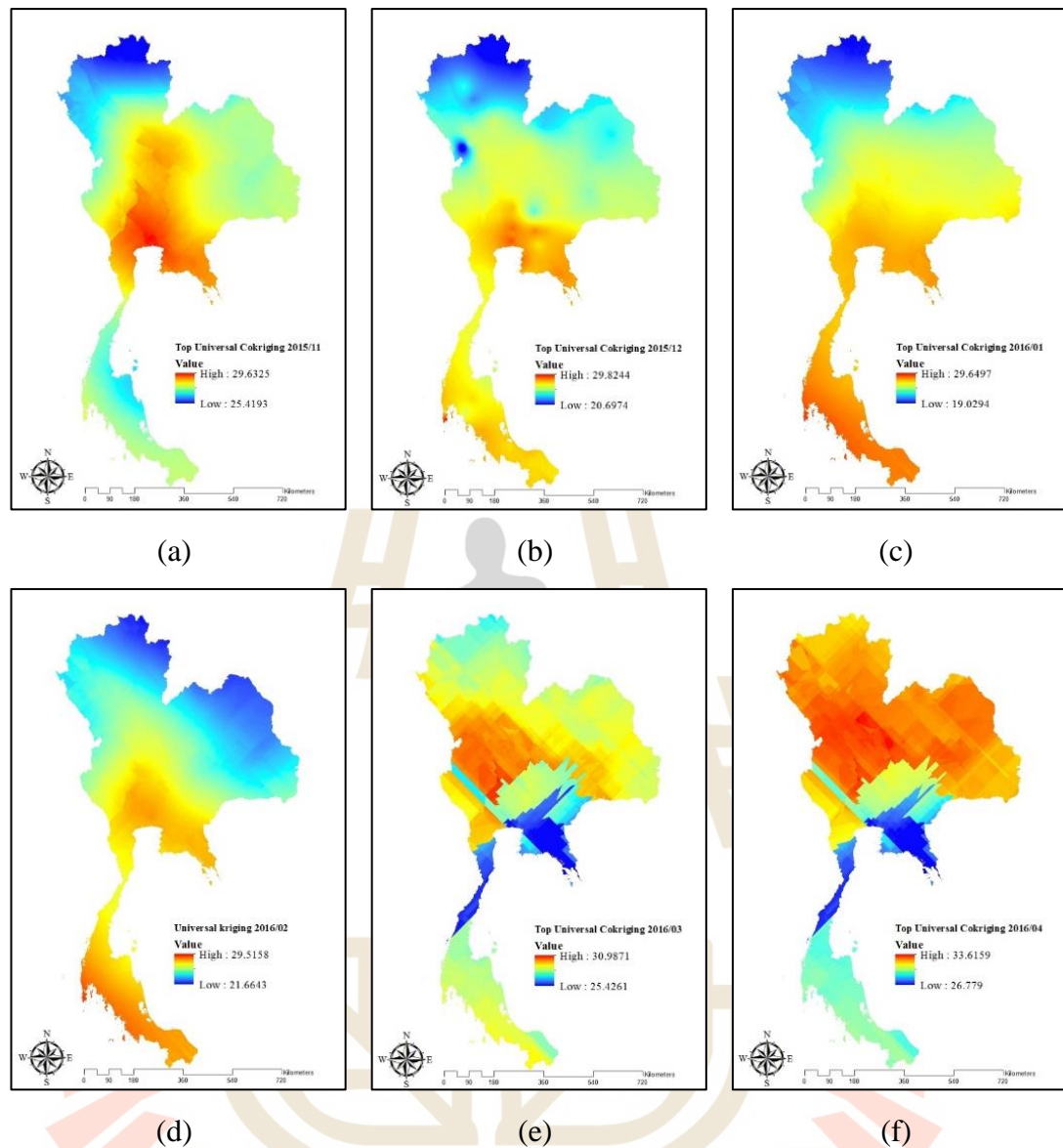


Figure 5.6 Monthly mean temperature interpolation using UCK: (a) November, (b) December, (c) January, (d) February, (e) March, and (f) April.

In addition, pattern of monthly mean temperature of SCK method is also different from OCK and UCK methods while pattern of monthly mean temperature of OCK and UCK are similar. The correlation coefficient of monthly mean temperature among three methods based on interpolated values at selected thirty-six TMD station is reported in Table 5.5.

Table 5.5 Correlation coefficient (R) of monthly mean temperature among three multivariate methods.

Month	OCK and SCK	SCK and UCK	UCK and OCK
November	0.833	0.833	1.00
December	0.869	0.869	1.00
January	0.923	0.923	1.00
February	0.869	0.869	1.00
March	0.112	0.112	1.00
April	0.626	0.626	1.00

As a result, it reveals that the R value between the interpolated monthly mean temperature data of OCK and UCK method equal 1.00. This implies that pattern of the interpolated monthly mean temperature data of OCK and UCK method is the same. Meanwhile the interpolated monthly mean temperature data in November, December, January, and February of SCK method have high correlation with the interpolated data of OCK and UCK method. The R values range between 0.833 in November and 0.923 in January. Meanwhile, the interpolated monthly mean temperature data in March of SCK method shows relatively low correlation with the interpolated data of OCK and UCK method with the R value of 0.112. While, the interpolated monthly mean temperature data in April of SCK method shows moderate correlation with the interpolated data of OCK and UCK method with the R value of 0.626. This finding implies that pattern of the interpolated monthly mean temperature data between November and February of SCK method is quite similar with the pattern of the OCK and UCK methods. On contrary, pattern of the interpolated monthly mean temperature data in March and April is dissimilar with the pattern of the OCK and UCK methods.

However, the interpolated monthly mean temperature data of SCK method appears more smoothness than OCK and UCK methods.

Furthermore, results of accuracy assessment among multivariate geostatistical methods for monthly mean temperature interpolation using thirth-six TMD ground station data is summarized in Table 5.6.

As results, it was found that an optimum multivariate geostatistical method for mean temperature interpolation is different among six months. SCK method is optimum method for mean temperature interpolation in four months: November, December, February, and March. Meanwhile OCK method is an optimum method for mean temperature interpolation in three months include November, December and March while OCK or UCK method is an optimum method for mean temperature interpolation in January and April. Detail of input data and its comparison is shown in Appendix B.

Table 5.6 Accuracy assessment of monthly mean temperature interpolation by multivariate geostatistical method using MAE, MRE, and RMSE.

Month	Methods	MAE (°C)	MRE (°C)	RMSE (°C)	Optimum method
November	OCK	0.79916	0.03142	1.31235	SCK
	SCK	0.77825	0.02904	0.984834	
	UCK	0.79916	0.03142	1.31235	
December	OCK	0.74548	0.03207	1.24431	SCK
	SCK	0.80899	0.03145	1.011759	
	UCK	0.74548	0.03207	1.24431	
January	OCK	0.77126	0.03376	1.111951	OCK and UCK
	SCK	0.94349	0.04034	1.19473	
	UCK	0.77126	0.03376	1.111951	
February	OCK	0.85718	0.036	1.233957	SCK
	SCK	0.87359	0.03615	1.146758	
	UCK	0.85718	0.036	1.233957	
March	OCK	1.57683	0.05595	2.12639	SCK
	SCK	1.10119	0.0394	1.453363	
	UCK	1.57683	0.05595	2.12639	
April	OCK	1.63154	0.05266	2.182241	OCK or UCK
	SCK	2.30285	0.07525	3.3511	
	UCK	1.63154	0.05266	2.182241	

5.3 Optimum geostatistical method for monthly mean temperature interpolation

Results of monthly mean temperature interpolation data from optimum univariate and multivariate geostatistical method as conclusion in two previous Sections: 5.1 and 5.2 were here calculated AIC to justify an optimum geostatistical method for monthly mean temperature interpolation. The result of AIC calculation is summarized in Table 5.7.

According to AIC values, it reveals that an optimum geostatistical method for mean temperature interpolation is different among six months. Univariate geostatistical method (OK or UK), is optimum method for mean temperature interpolation in four months: November, December, January, and April. Meanwhile multivariate geostatistical method, SCK is an optimum method for mean temperature interpolation in two months include February and March. Herein, it can be observed that AIC value of SCK method and OCK or UCK is very slightly different for mean temperature interpolation in March.

As results, it can be here suggested that OK and UK methods are suitable for monthly mean temperature interpolation from TMD data. This finding is consistent with the previous work of Eldrandaly and Abu-Zaid (2011) who suggested that the OK and UK were the most optimal methods for interpolating mean monthly air temperature in western Saudi Arabia. In addition, Goovaerts (1997) stated that the OK and UK methods yield similar interpolating estimates. In practice, the OK method with local search neighbourhoods is preferred in interpolations because it provides results similar to UK estimate and it is easier to implement. In addition, the UK method may yield aberrant extrapolation estimates (Li and Heap, 2008). However, Attorre, Alfo, Sanctis,

Francesconia and Bruno (2007) and Sluiter (2009) suggested that UK is a very common method in meteorology.

In conclusion, it can be here concluded that UK method is the most suitable method for monthly mean temperature interpolation from TMD data since it fits with UHI phenomena studies in this research.

Table 5.7 Accuracy assessment of monthly mean temperature interpolation based on geostatistical method using AIC.

Month	Geostatistical method	Optimum method	AIC	Choose method
November	Univariate	OK	0.927951274	OK or UK
		UK	0.927951274	
	Multivariate	SCK	37.23661628	
December	Univariate	OK	42.50793936	OK or UK
		UK	42.50793936	
	Multivariate	SCK	61.1314764	
January	Univariate	OK	66.02799422	OK or UK
		UK	66.02799422	
	Multivariate	OCK	71.24537358	
		UCK	71.24537358	
February	Univariate	OK	53.80055395	SCK
		UK	53.80055395	
	Multivariate	SCK	53.10870971	
March	Univariate	OK	32.03681717	SCK
		UK	32.03681717	
	Multivariate	SCK	5.230276734	
April	Univariate	OK	33.32462093	OK or UK
		UK	33.32462093	
	Multivariate	OCK	38.00534536	
		UCK	38.00534536	

CHAPTER VI

LAND SURFACE TEMPERATURE EXTRACTION AND PREDICTION

Results of the third objective which consist of (1) satellite-based LST extraction and (2) land surface temperature prediction of Bangkok Metropolitan and its vicinity are presented under this chapter. Details of each major result are separately explained and discussed in the following sections.

6.1 Satellite-based LST extraction

The selected Landsat data during November to April between 2006 and 2016 covering Bangkok and its vicinity were used to extract LST based on standard method (Equations 2.4 - 2.6) that was mentioned in Section 2.3 Conversion of LST from satellite data. After that, the derived LST data were refined based on their relationships with in situ mean temperature data of eight TMD stations of Bangkok Metropolitan and its vicinity using simple linear regression analysis.

6.1.1 Conversion of LST

Representative of Landsat LST data during November to April between 2006 and 2016 covering Bangkok and its vicinity were selected based on percent of cloud cover as summary in Table 6.1.

Table 6.1 List of selected Landsat data for LST extraction over Bangkok and its vicinity.

Satellite	Path/row	Year	Month	Date	Scene Cloud Cover
Landsat 5	12950	2006	January	27	2.62
	12951				0.00
	12950	2008	January	9	0.06
	12951				0.02
Landsat 7	12950	2010	November	14	25.04
	12951				0.71
	12950	2012	February	21	0.00
	12951				0.00
	12950	2014	November	17	3.14
	12951				9.67
Landsat 8	12950	2016	April	12	4.49
	12951				1.33

Results of satellite-based LST extraction for UHI phenomena in 2006, 2008, 2010, 2012, 2014, and 2016 are displayed in Figures 6.1 to 6.6, respectively. Meanwhile, basic statistic of LST data is summarized in Table 6.2.

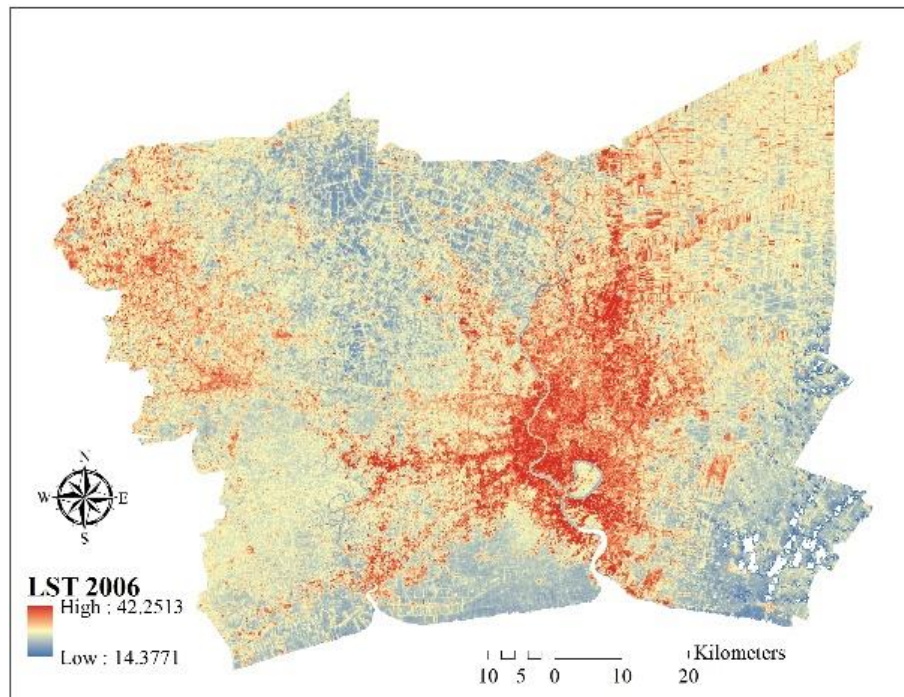


Figure 6.1 Land surface temperature from Landsat-5 in January 2006.

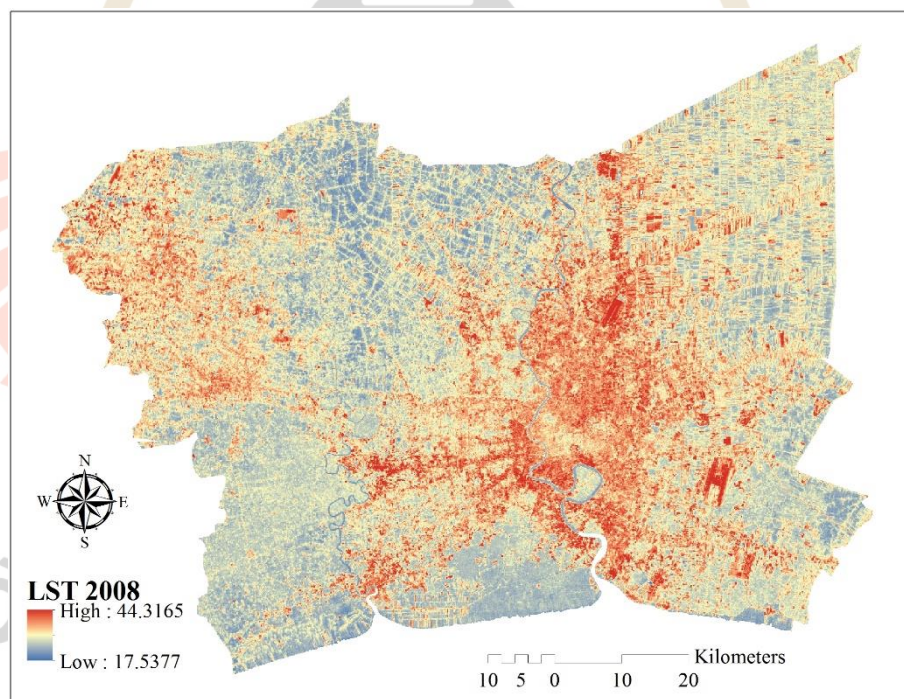


Figure 6.2 Land surface temperature from Landsat-7 in January 2008.

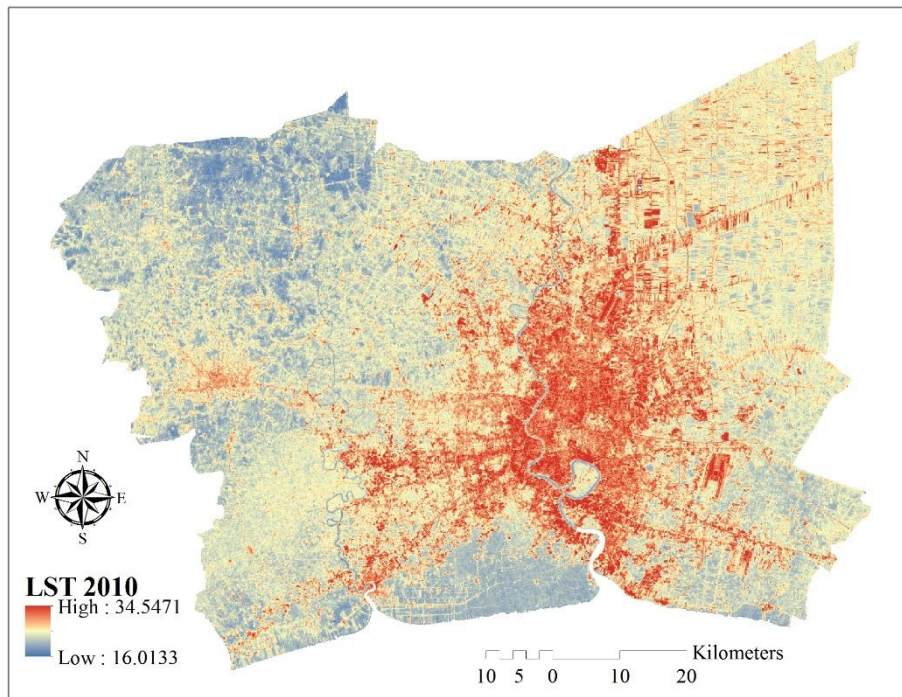


Figure 6.3 Land surface temperature from Landsat-7 in November 2010.

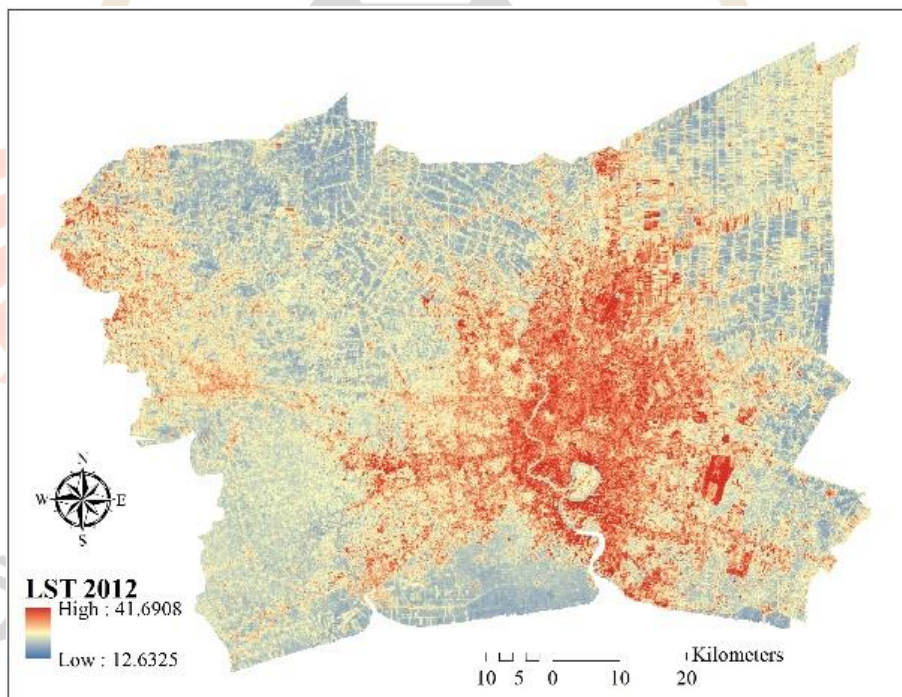


Figure 6.4 Land surface temperature from Landsat-7 in February 2012.

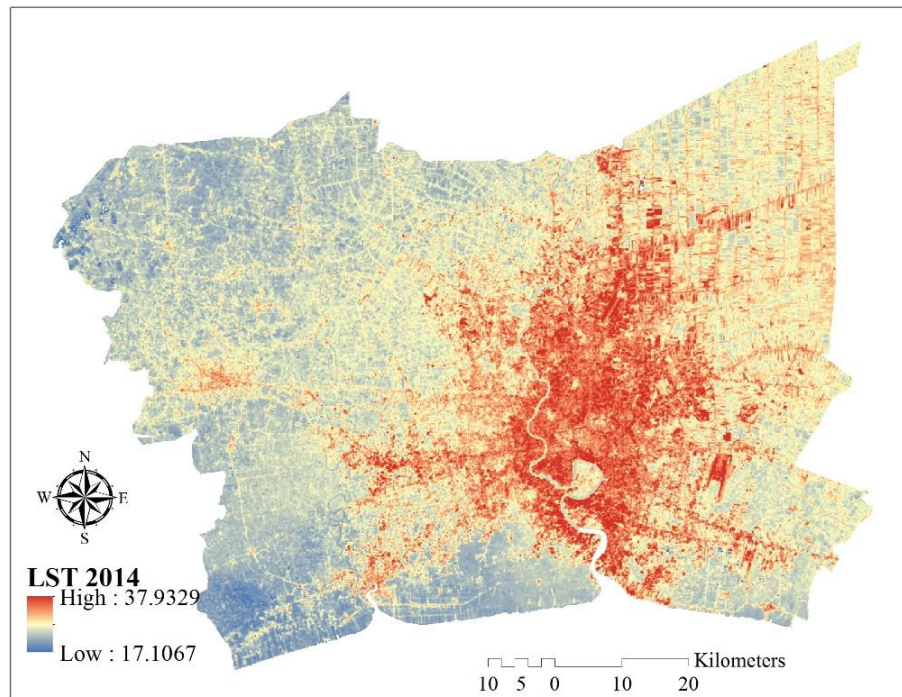


Figure 6.5 Land surface temperature from Landsat-8 in November 2014.

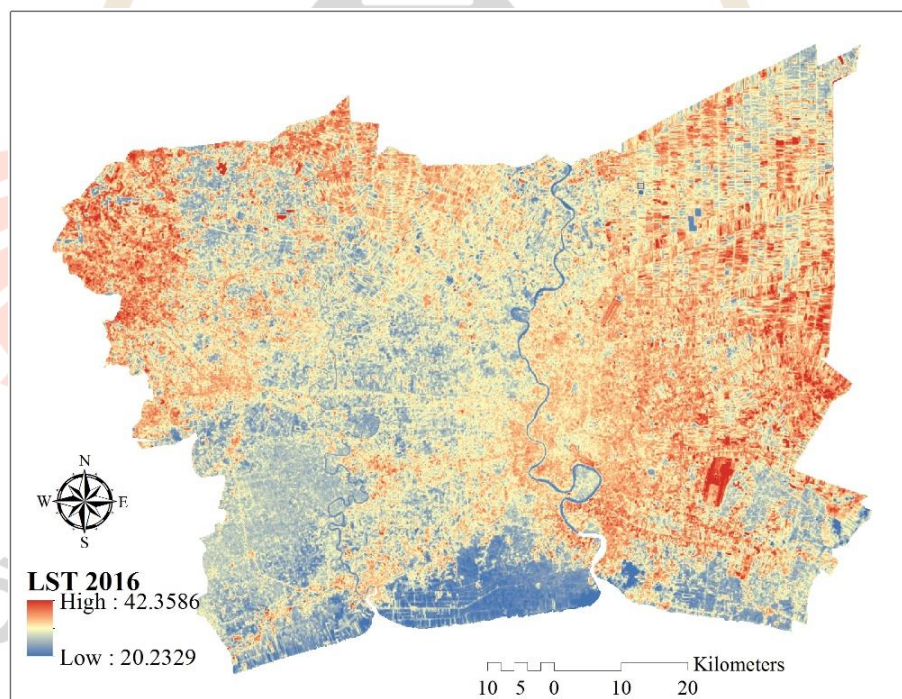


Figure 6.6 Land surface temperature from Landsat-8 in April 2016.

Table 6.2 Basic statistical data of LST.

Month	Year	LST (°C)			
		Minimum	Maximum	Mean	Standard Deviation
January	2006	14.38	42.25	27.56	2.58
January	2008	17.54	44.32	26.51	1.75
November	2010	16.01	34.55	23.24	1.61
February	2012	12.63	41.69	27.16	2.15
November	2014	17.10	37.93	27.08	1.84
April	2016	20.23	42.36	32.35	2.08

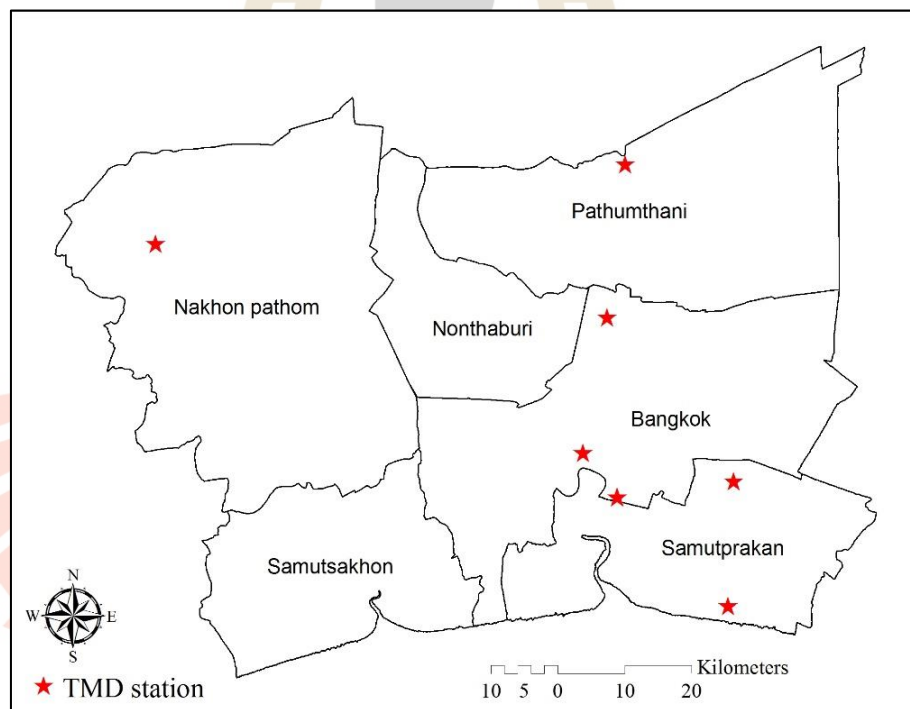
As results, it can be observed that the representative LST data in 2016, acquired date 12 April 2016 shows the highest average LST while the representative LST data in 2010, acquired date 14 November 2010 shows the lowest average LST. This information presents variation of the representative LST in between 2006 and 2016 due to seasonal change. Ideally, the representative LST data between 2006 and 2016 should be extracted from Landsat data acquired from the same month. However, due to variation of percentage cloud covering during November to April over Bangkok and its vicinity between 2006 and 2016, Landsat data between 2006 and 2016 for LST extraction could not be selected from the same month.

6.1.2 Refinement of LST using simple regression analysis.

The extracted LST data between 2006 and 2016 from thermal band of Landsat data as dependent variable were simple linear regressed with the mean temperature data of 8 TMD stations (Table 6.3 and Figure 6.7). Independent and dependent variables for simple linear regression analysis is summarized in Table 6.4.

Table 6.3 Temperature station in the study area from TMD.

No.	Name	Province
1	Pathumthani meteorological station	Pathumthani
2	Nakhon Pathom meteorological station	Nakhon Pathom
3	Bangkok meteorological station	Bangkok
4	Chaloemprakiet meteorological station	
5	Bang na agrometeorological station	
6	Don muang (airport) meteorological station	
7	Suvarnabhumi airport meteorological station	Samutprakan
8	Samutprakan meteorological station	

**Figure 6.7** Distribution of TMD location over Bangkok and its vicinity.

Results of simple linear regression between the extracted satellite-based LST data and in situ mean temperature of TMD data is presented in Table 6.5 and Figure 6.8.

Table 6.4 Independent and dependent variables for simple linear regression analysis.

Month Year	Station ID (°C)								Source
	1	2.	3.	4.	5.	6.	7.	8.	
January 2006	27.60	25.25	28.25	28.35	27.10	28.05	-	-	TMD Landsat 5
January 2008	27.30	28.25	27.50	27.85	27.10	27.85	25.50	28.50	TMD Landsat 7
November 2010	27.73	28.75	27.77	27.75	27.77	27.70	25.26	28.22	TMD Landsat 7
February 2012	28.00	26.15	28.60	28.90	28.45	27.90	-	27.85	TMD Landsat 7
February 2012	27.37	25.85	28.37	27.88	28.36	27.88	-	27.38	TMD Landsat 7
November 2014	28.75	29.24	28.73	28.22	28.73	-	27.22	29.14	TMD Landsat 7
November 2014	28.75	29.24	28.73	29.22	28.73	-	28.22	29.14	TMD Landsat 7
April 2016	29.50	29.85	29.55	28.95	29.25	29.30	27.45	30.15	TMD Landsat 7
April 2016	29.06	29.72	28.98	28.10	28.66	29.79	27.05	30.68	TMD Landsat 8
April 2016	33.35	32.75	32.65	32.45	32.90	33.00	30.95	32.25	TMD Landsat 8
April 2016	33.07	32.64	32.57	32.52	32.31	33.52	30.10	32.47	TMD Landsat 8

Table 6.5 List of linear equations and its R and R² coefficients values of simple linear regression analysis.

No	Date	Equation	R	R ²
1	January 2006	$Y = 0.9022X + 3.1222$	0.9357	0.8756
2	January 2008	$Y = 0.8454X + 4.1313$	0.9308	0.8663
3	November 2010	$Y = 0.9567X + 1.5897$	0.9230	0.852
4	February 2012	$Y = 0.4383X + 16.74$	0.8424	0.7096
5	November 2014	$Y = 0.6643X + 9.9818$	0.9078	0.8241
6	April 2016	$Y = 0.6643X + 11.017$	0.9239	0.8535

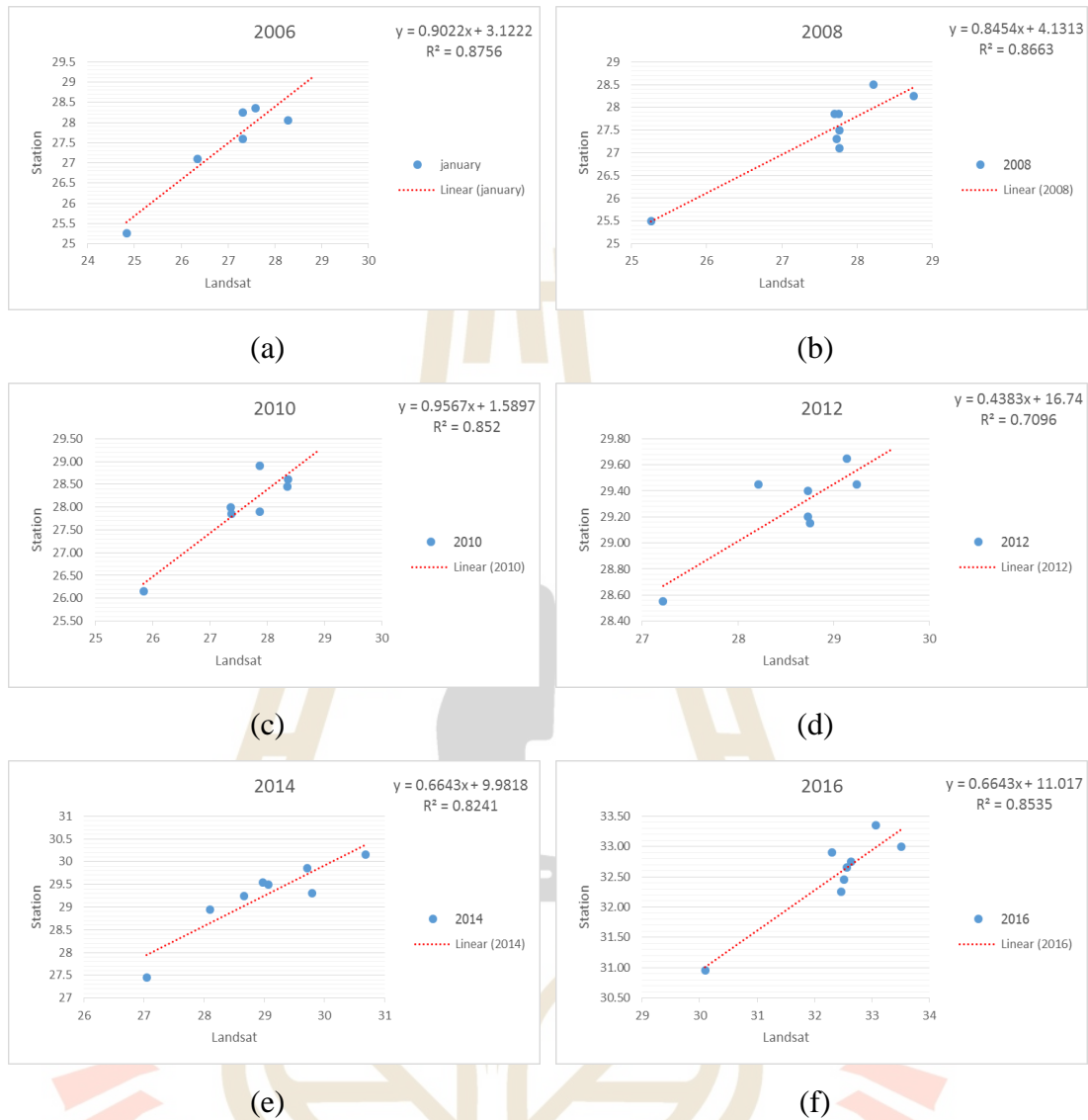


Figure 6.8 Simple linear regression analysis between LST extraction from Landsat data and TMD station during 2006 to 2016: (a) January 2006, (b) January 2008, (c) November 2010, (d) February 2012, (e) November 2014, and (f) April 2016.

As results, it was found that satellite LST temperature data show positive highly correlation with in situ mean temperature of TMD data. The R values vary between 0.8424 and 0.9357 and the R^2 values vary between 0.7096 and 0.8756.

The derived equations were applied to correct satellite-based LST data as result shown in Figures 6.9 to 6.14. Basic statistic of refinement LST data is summarized in Table 6.6. These information are further applied to evaluate and predict UHI phenomena in the following sections.

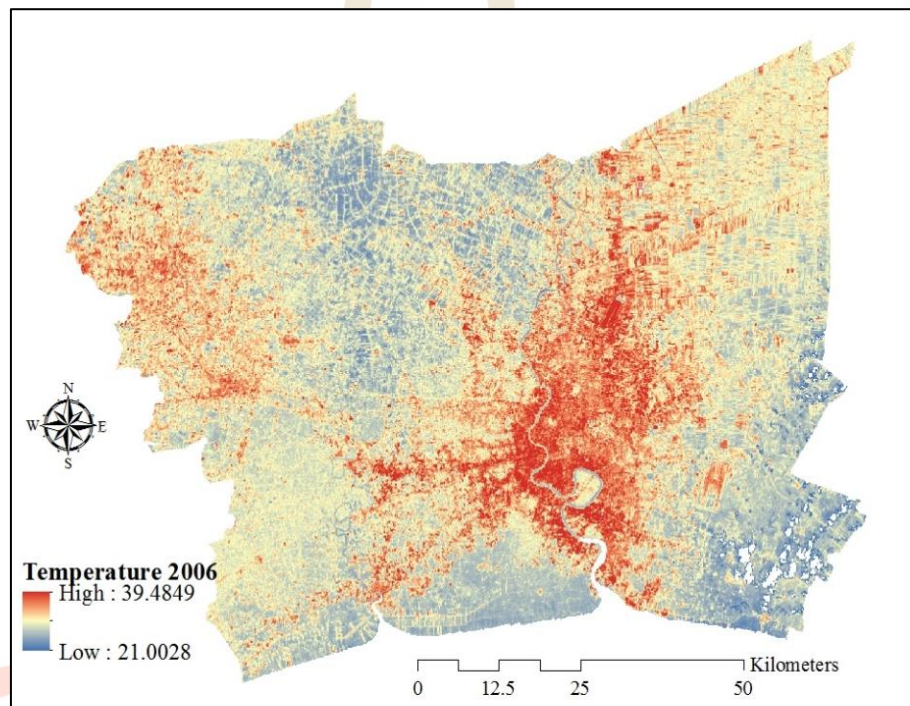


Figure 6.9 Refinement of land surface temperature in January 2006.

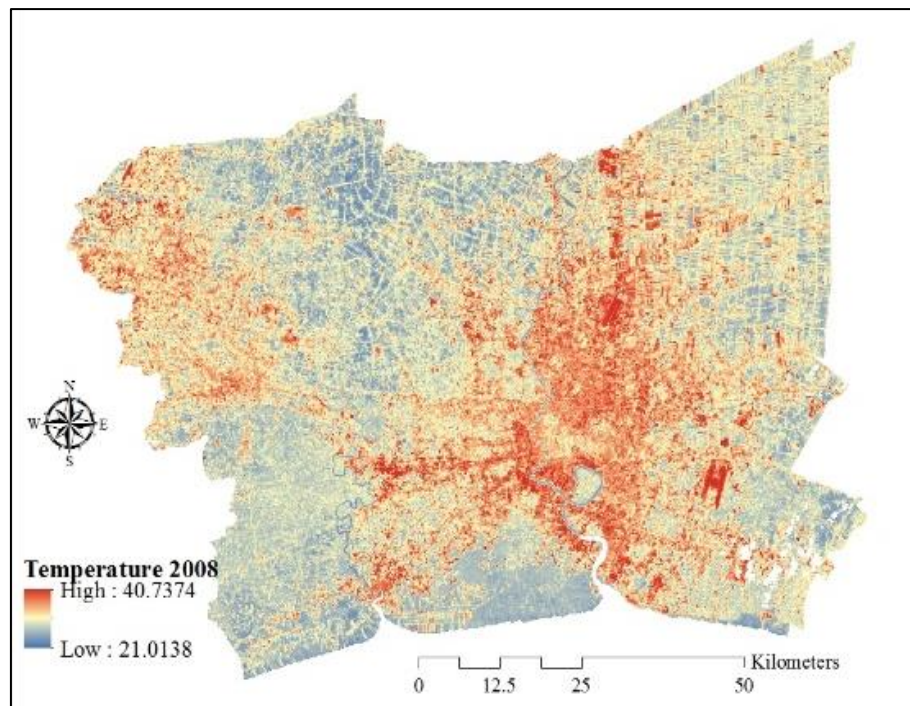


Figure 6.10 Refinement of land surface temperature in January 2008.

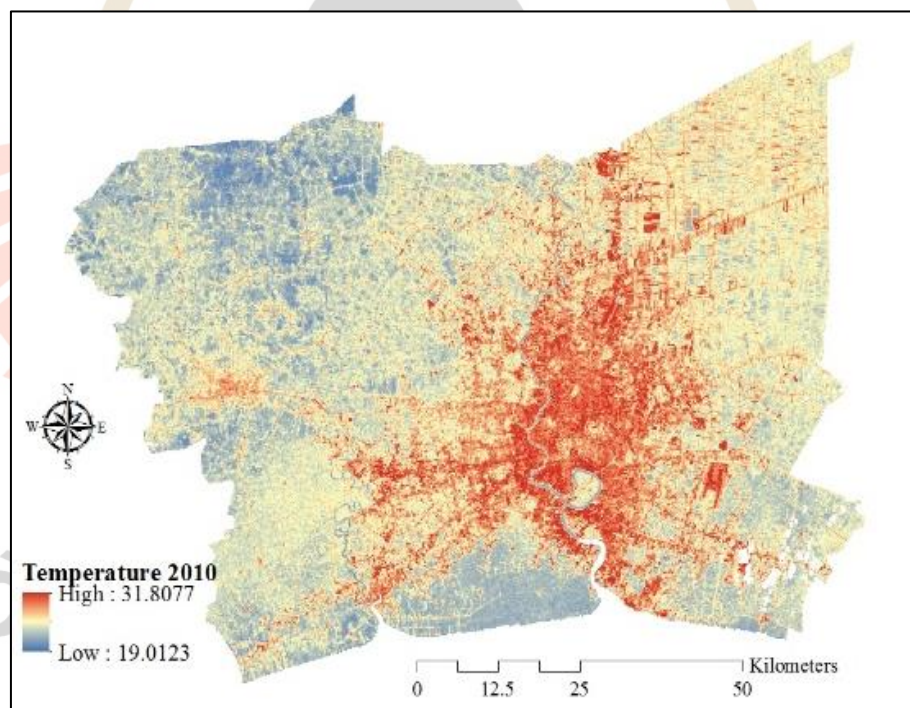


Figure 6.11 Refinement of land surface temperature in November 2010.

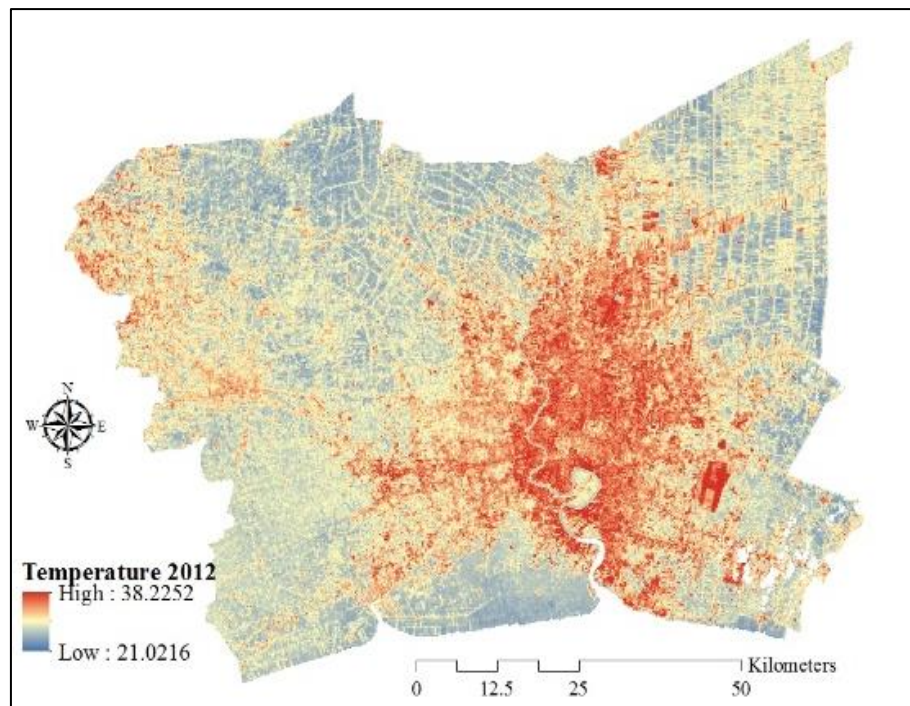


Figure 6.12 Refinement of land surface temperature in February 2012.

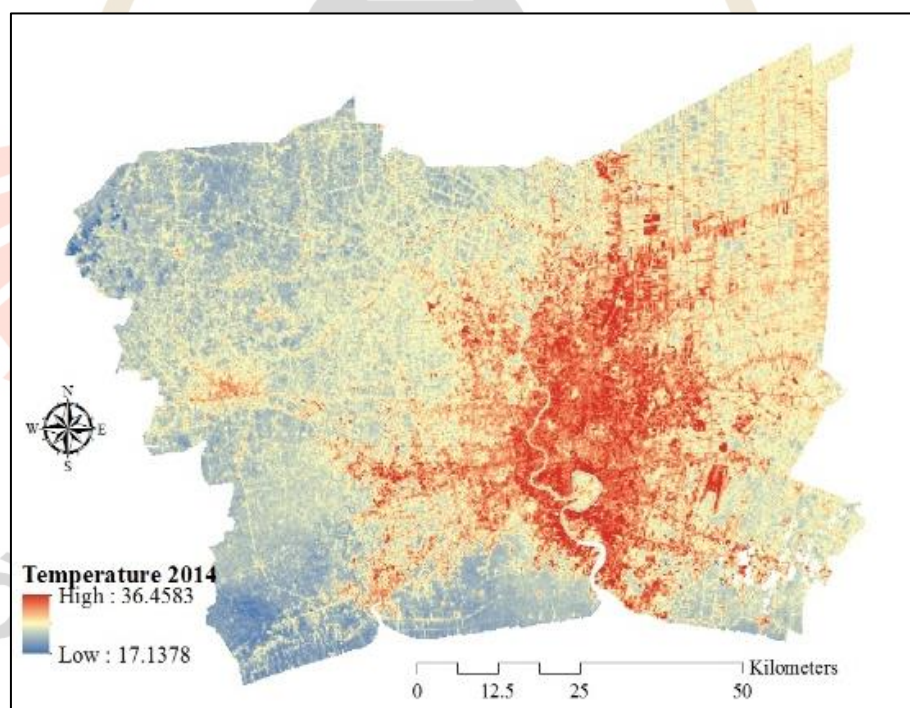


Figure 6.13 Refinement of land surface temperature in November 2014.

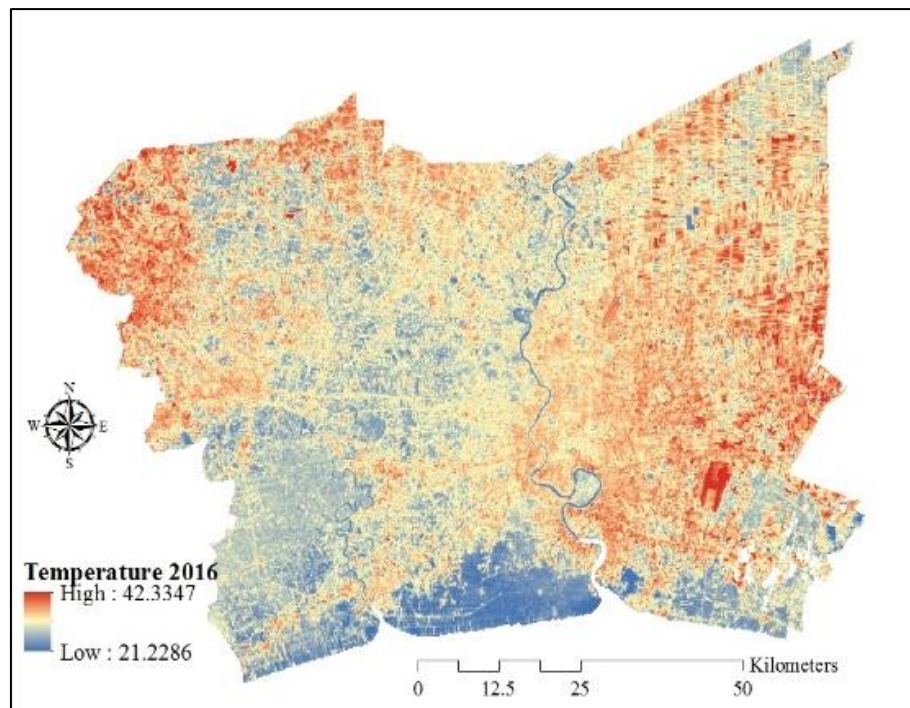


Figure 6.14 Refinement of land surface temperature in April 2016.

Table 6.6 Basic statistical data of LST refinement with masking cloud.

Year	LST (°C)			
	Minimum	Maximum	Mean	Standard Deviation
2006	21.00	39.48	27.56	2.12
2008	21.01	40.74	26.51	1.70
2010	19.01	31.81	23.24	1.57
2012	21.02	38.23	27.16	2.09
2014	17.14	36.46	27.08	1.83
2016	21.23	42.33	32.35	2.06

6.2 LST prediction

The refined LST data between 2018 and 2026 were here extrapolated using Trend Analysis function of MS Excel spreadsheet software and Image conversion function of ERDAS Imagine software. Distribution of predicted LST between 2018 and 2026 are displayed in Figures 6.15 to 6.19. The basic statistic data of predicted LST between 2018 and 2026 is presented in Table 6.7

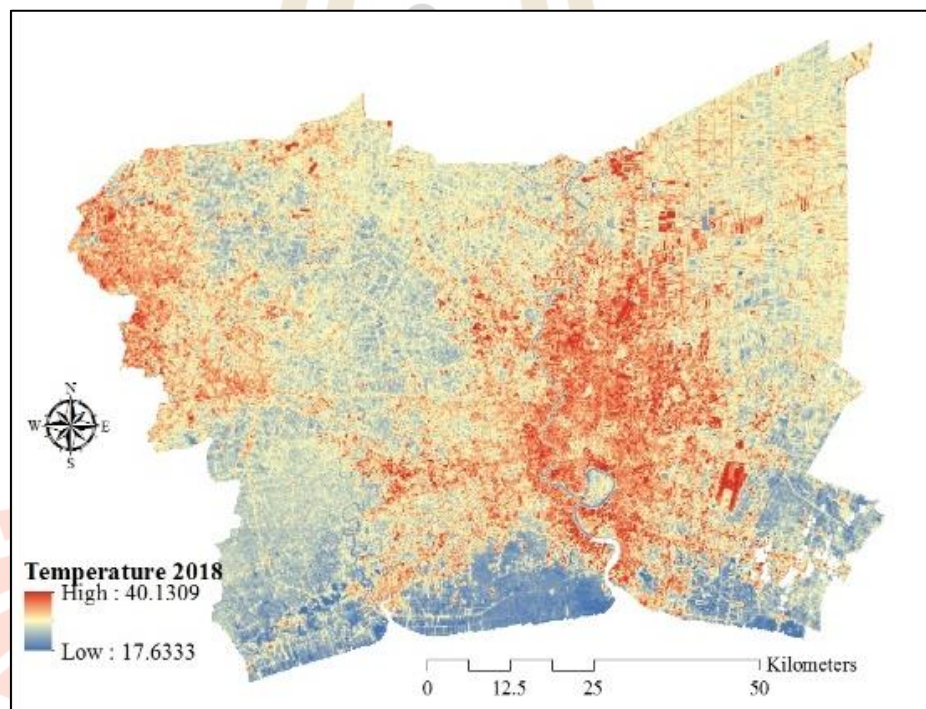


Figure 6.15 Distribution of predicted LST in 2018.

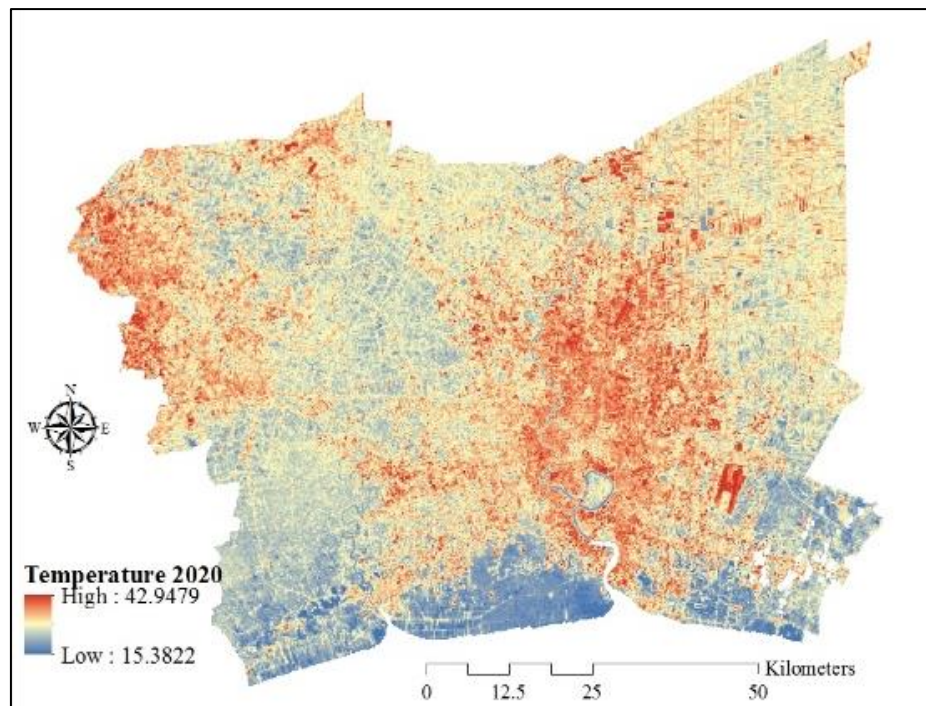


Figure 6.16 Distribution of predicted LST in 2020.

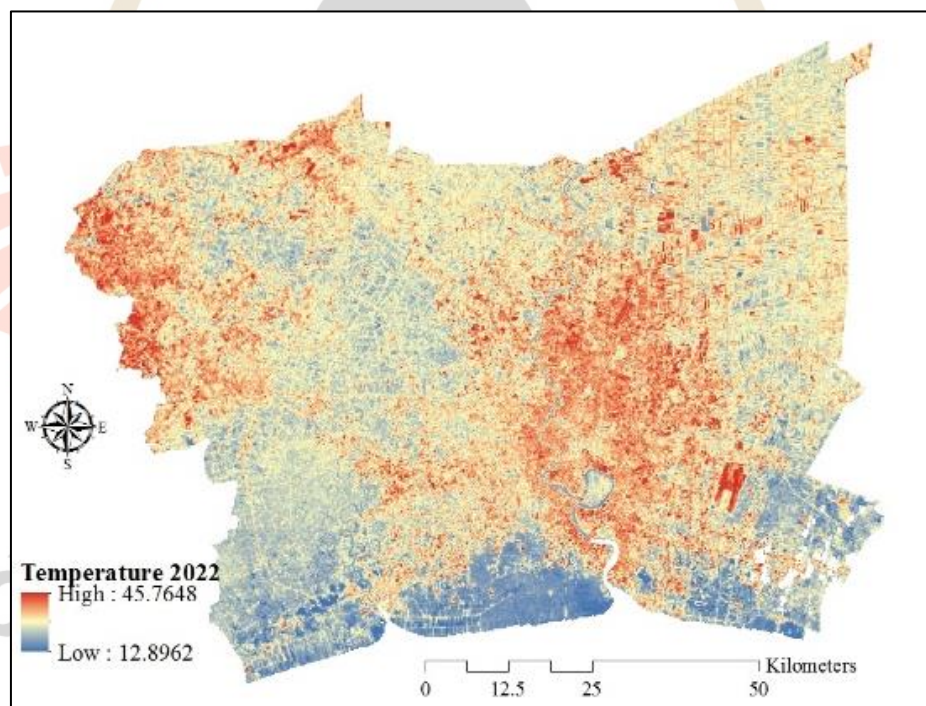


Figure 6.17 Distribution of predicted LST in 2022.

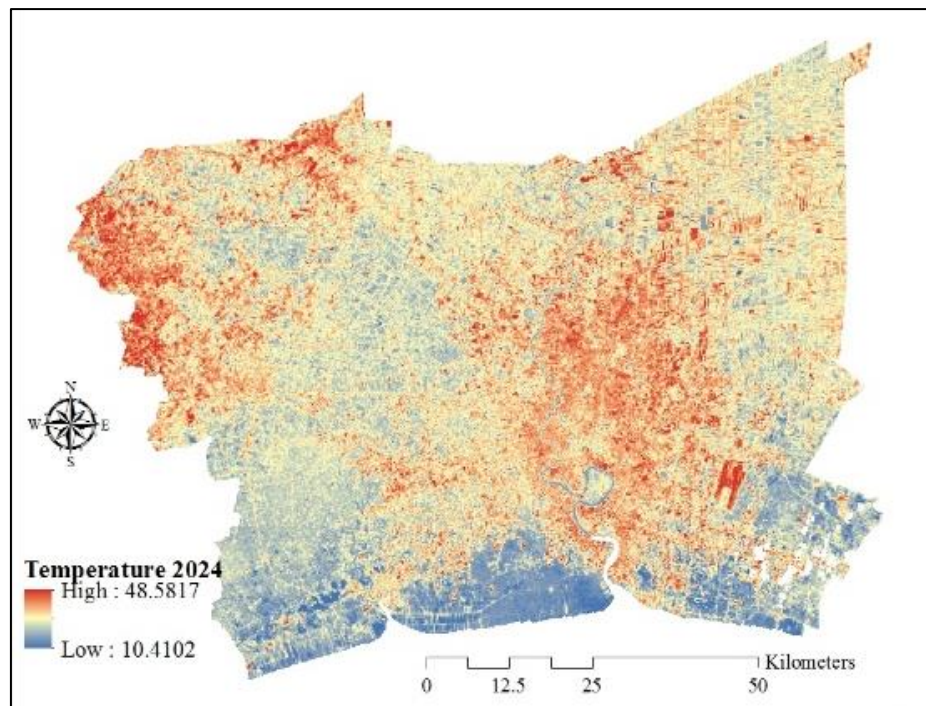


Figure 6.18 Distribution of predicted LST in 2024.

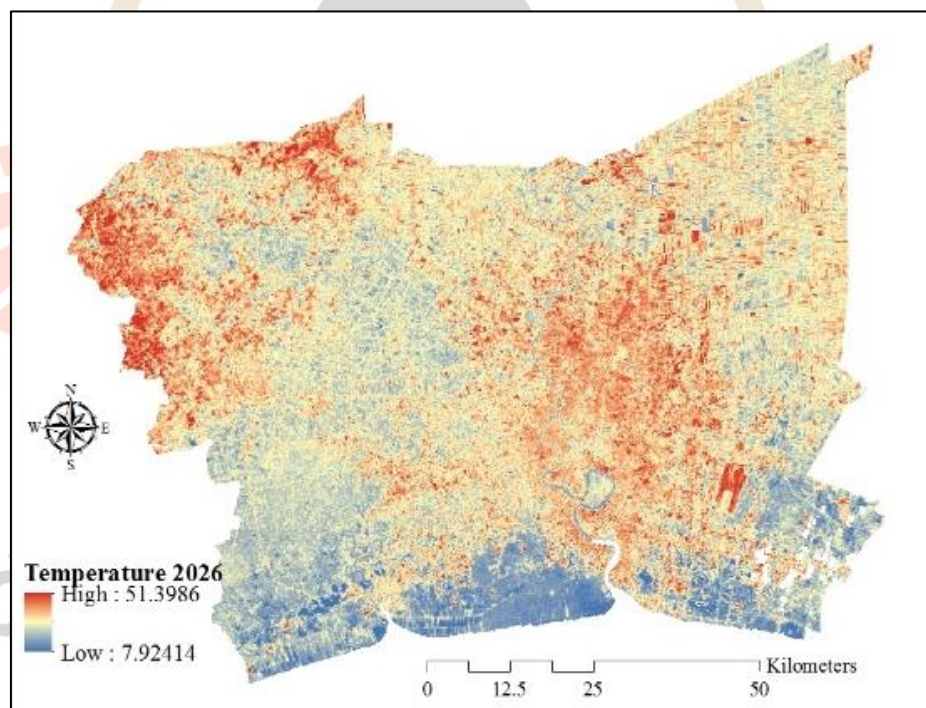


Figure 6.19 Distribution of predicted LST in 2026.

Table 6.7 Basic statistical data of predicted LST between 2018 and 2026 with masking cloud.

Year	Minimum	Maximum	Mean	Standard Deviation
2018	17.63	40.13	27.81	1.79
2020	15.38	42.95	28.35	1.94
2022	12.90	45.77	28.88	2.11
2024	10.41	48.58	29.42	2.30
2026	7.92	51.40	29.96	2.50

In summary variation of basic statistical data include minimum, mean, and maximum data of temperature between 2006 and 2016 as historical data and between 2016 and 2026 as extrapolate data can be compared as shown in Figure 6.20.



Figure 6.20 Comparison of basic statistical data of LST between 2006 and 2026.

CHAPTER VII

UHI PHENOMENA EVALUATION AND PREDICTION

Results of the fourth objective which consist of (1) urban and non-urban area extraction, (2) urban and non-urban area prediction, (3) temperature grade classification, (4) urban heat island intensity and its severity, (5) quantitative analysis of UHI, are presented under this chapter. Details of each major result are separately explained and discussed in the following sections.

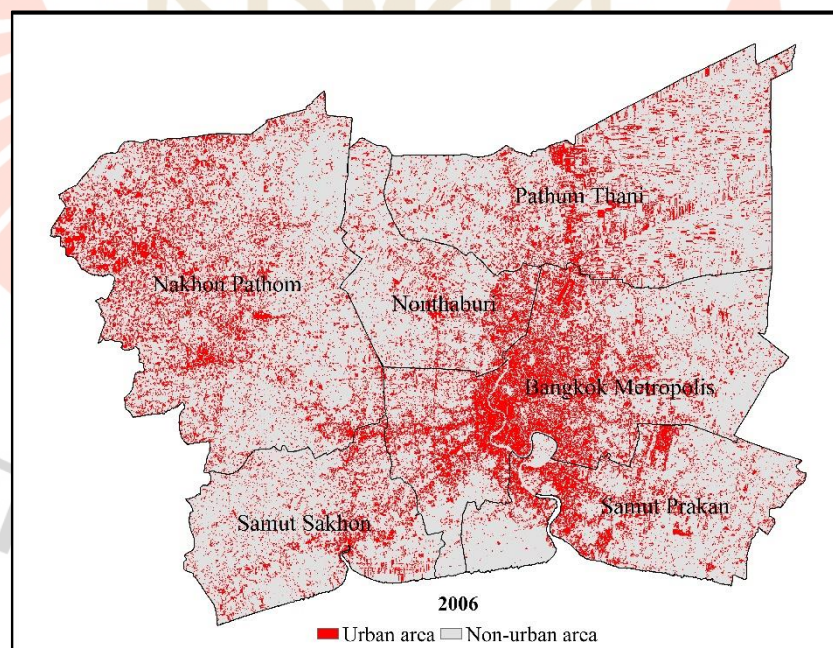
7.1 Urban and non-urban area extraction

Urban and non-urban areas were here extracted using BUI equation (Equation 3.9) based on NDBI and NDVI that was mentioned in Section 3.5 UHI phenomena evaluation and prediction in Chapter III. In practice, NDVI and NDBI data were firstly calculated from Landsat data using Equation 3.2 and 3.3, respectively and the derived NDVI and NDBI were recoded with 254 for all pixel having positive indices and 0 for all remaining pixels of negative indices to extract urban and built-up area as summary in Table 7.1 and displaying in Figures 7.1 to 7.6. Herein, urban areas consisted of city, town, commercial, village, institutional, transportation, communication and utilities, industrial land, and bare land while non-urban areas are comprised of agricultural land, forest land and parks and water bodies.

Table 7.1 Pixel value of representative land covers.

Indices	Urban and built-up	Bare land	Forest land and parks	Agriculture land	Rivers	Lakes
NDVI	0	0	254	254	0	0
NDBI	254	254	254 or 0	254 or 0	0	0
NDBI-NDVI	254	254	0 or -254	0 or -254	0	0

The derived urban and non-urban areas were assessed accuracy with sampling points of 426 points based on binomial probability theory. Herein, the expected accuracy is 80% and the allowable error of sampling is 5%. The overall accuracy of the extracted urban and non-urban areas from 2006, 2008, 2010, 2012, 2014, and 2016 based on Google Earth data are 81.46%, 85.21%, 87.56%, 87.79%, 88.97%, and 91.08%, respectively. Details of accuracy assessment are summarized in Tables 7.2 to 7.7. Distribution of sampling points for accuracy assessment of urban and non-urban areas between 2006 and 2016 is displayed in Figure 7.7

**Figure 7.1** Distribution of urban and non-urban areas in 2006.

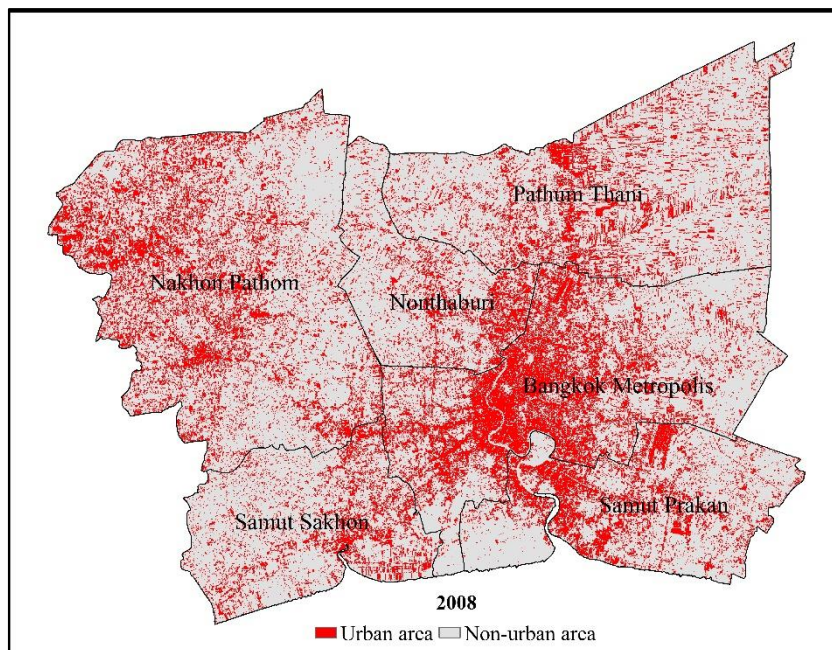


Figure 7.2 Distribution of urban and non-urban areas in 2008.

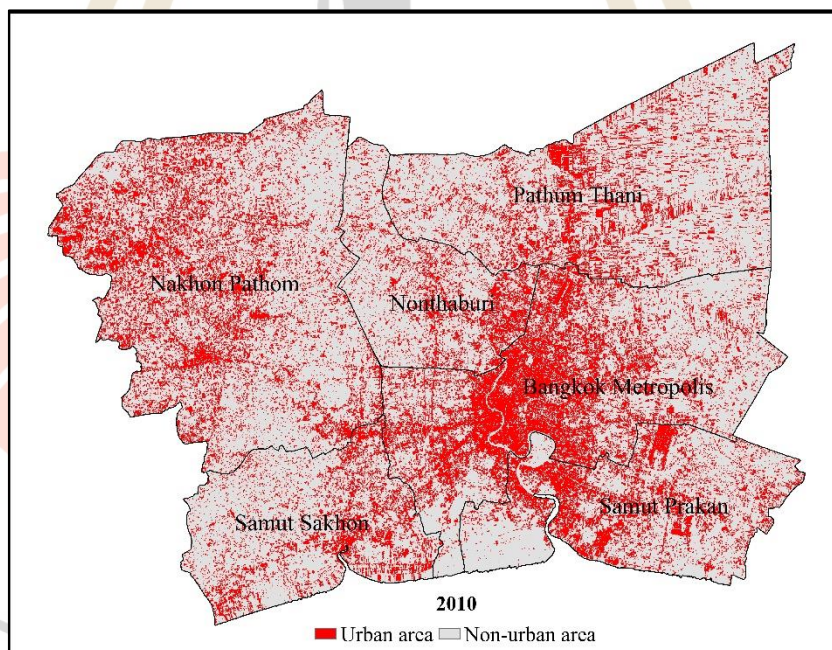


Figure 7.3 Distribution of urban and non-urban areas in 2010.

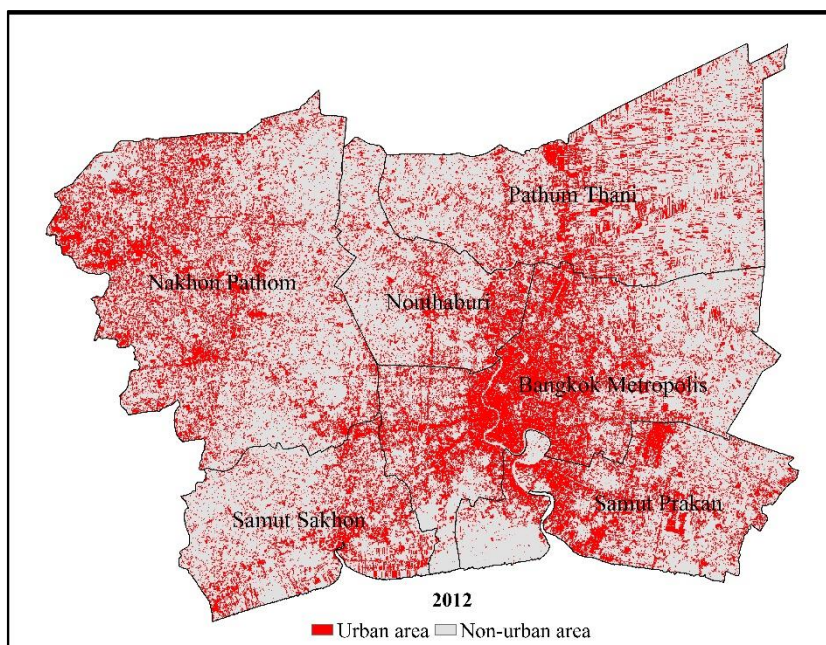


Figure 7.4 Distribution of urban and non-urban areas in 2012.

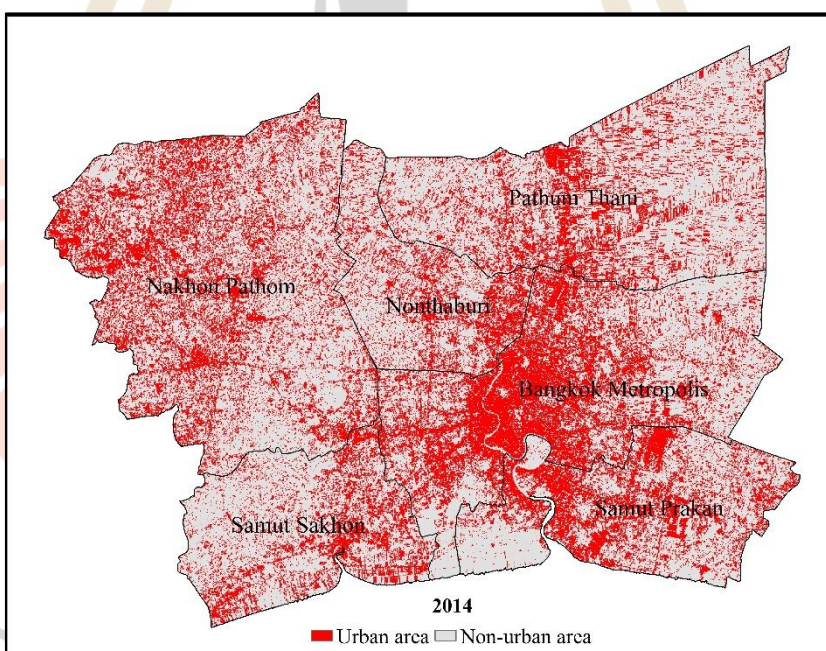


Figure 7.5 Distribution of urban and non-urban areas in 2014.

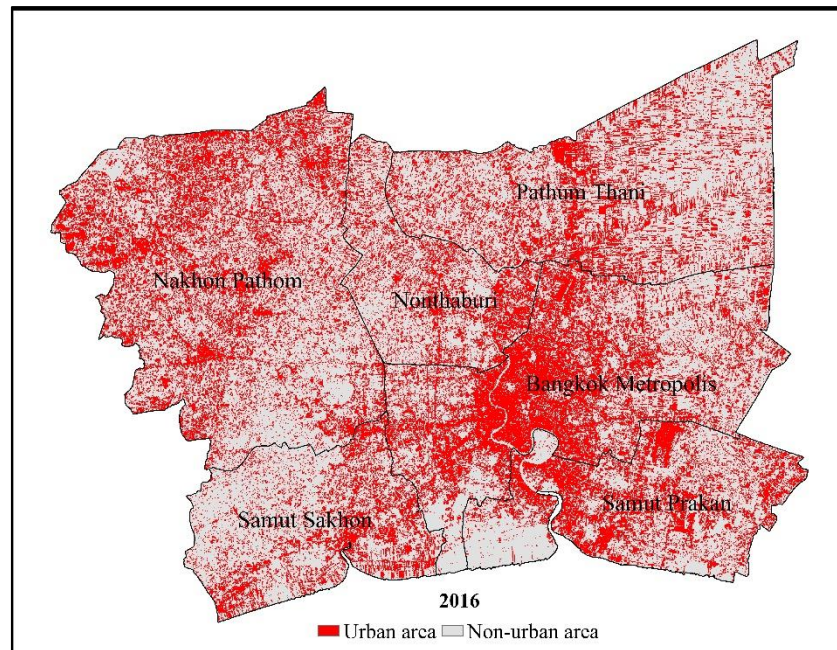


Figure 7.6 Distribution of urban and non-urban areas in 2016.

Table 7.2 Accuracy assessment of urban and non-urban areas in 2006.

BUI Extraction	Reference		
	Urban	Non-urban	Total
Urban	93	68	161
Non-urban	11	254	265
Total	104	322	426
Overall accuracy	81.46%		

Table 7.3 Accuracy assessment of urban and non-urban areas in 2008.

BUI Extraction	Reference		
	Urban	Non-urban	Total
Urban	258	55	313
Non-urban	8	105	113
Total	266	160	426
Overall accuracy	85.21%		

Table 7.4 Accuracy assessment of urban and non-urban areas in 2010.

BUI Extraction	Reference		
	Urban	Non-urban	Total
Urban	258	45	303
Non-urban	8	115	123
Total	266	160	426
Overall accuracy	87.56%		

Table 7.5 Accuracy assessment of urban and non-urban areas in 2012.

BUI Extraction	Reference		
	Urban	Non-urban	Total
Urban	248	46	294
Non-urban	6	126	132
Total	254	172	426
Overall accuracy	87.79%		

Table 7.6 Accuracy assessment of urban and non-urban areas in 2014.

BUI Extraction	Reference		
	Urban	Non-urban	Total
Urban	263	40	303
Non-urban	7	116	123
Total	270	156	426
Overall accuracy	88.97%		

Table 7.7 Accuracy assessment of urban and non-urban areas in 2016.

BUI Extraction	Reference		
	Urban	Non-urban	Total
Urban	236	29	265
Non-urban	9	152	161
Total	245	181	426
Overall accuracy	91.08%		

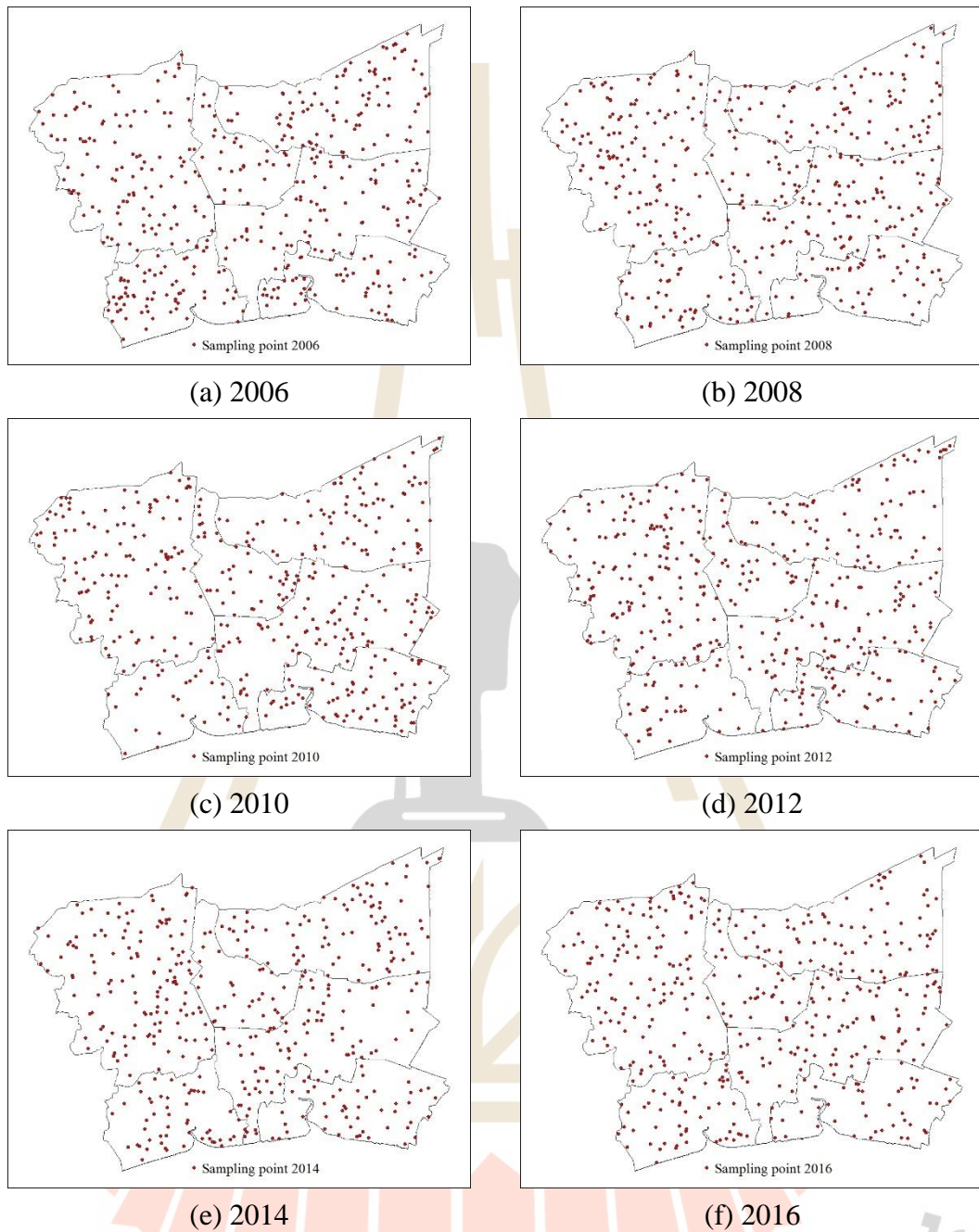


Figure 7.7 Distribution of sampling points for accuracy assessment of urban and non-urban area in: (a) 2006, (b) 2008, (c) 2010, (d) 2012, (e) 2014, and (f) 2016,

7.2 Urban and non-urban area prediction

The extracted urban and non-urban areas between 2006 and 2016 were here applied to predict urban and non-urban areas between 2018 and 2026 using CA-Markov model as results shown in Figures 7.8 to 7.12.

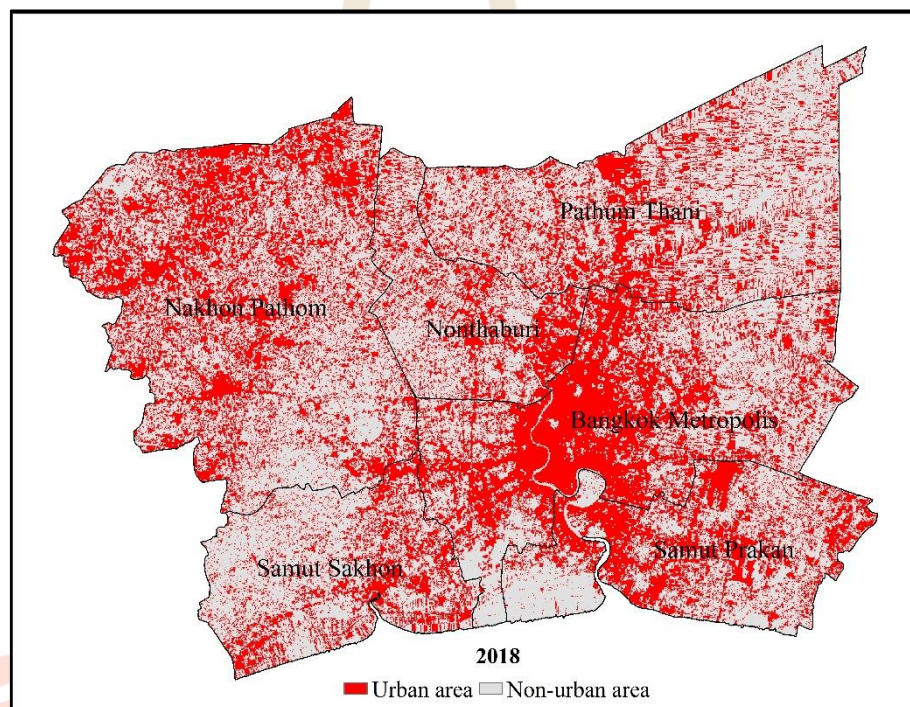


Figure 7.8 Distribution of predicted urban and non-urban areas in 2018.

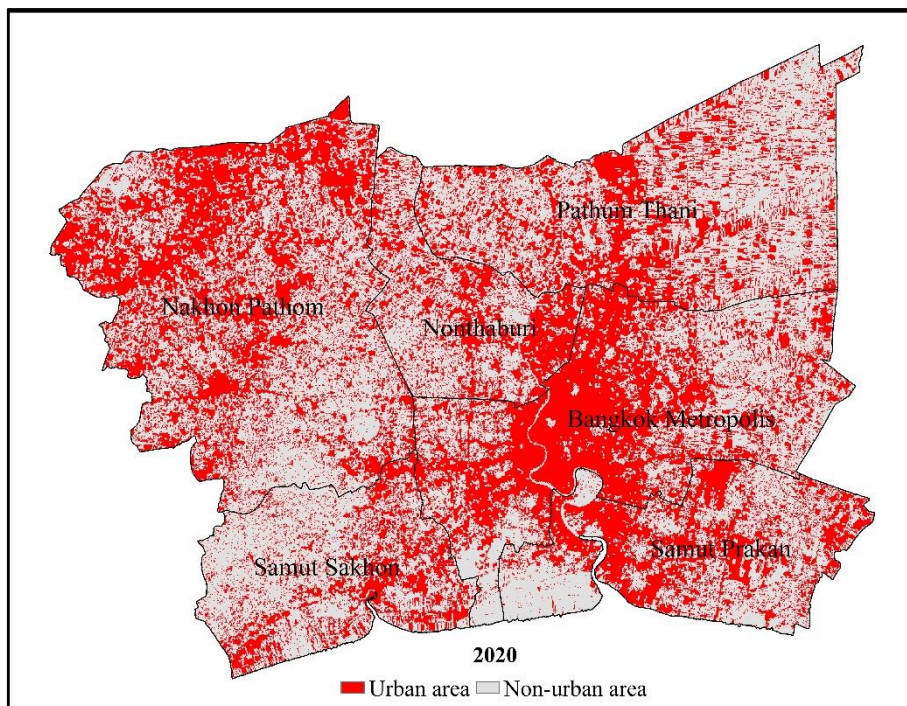


Figure 7.9 Distribution of predicted urban and non-urban areas in 2020.

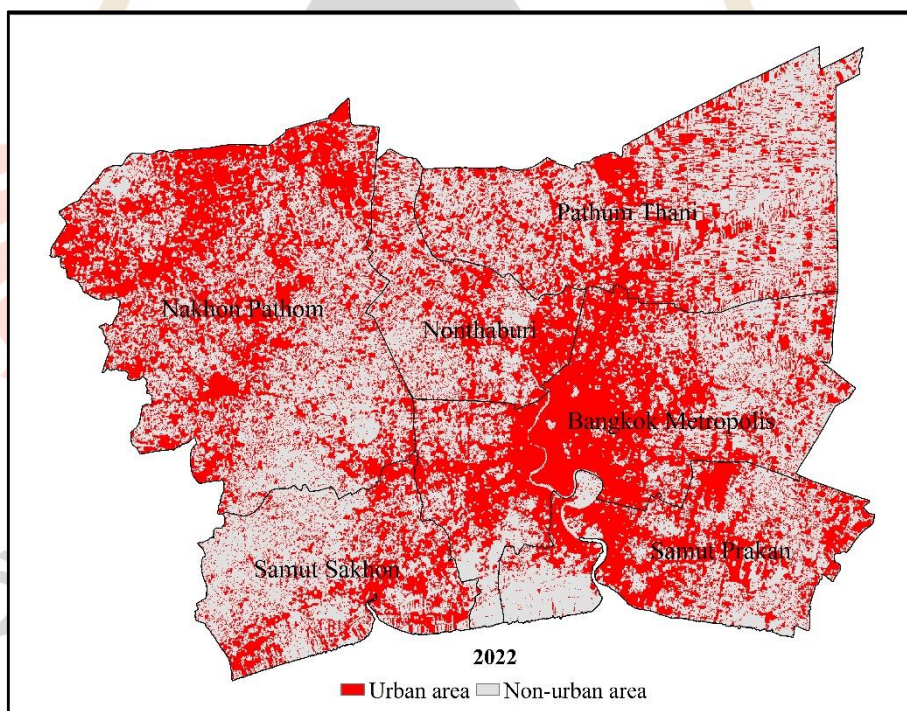


Figure 7.10 Distribution of predicted urban and non-urban areas in 2022.

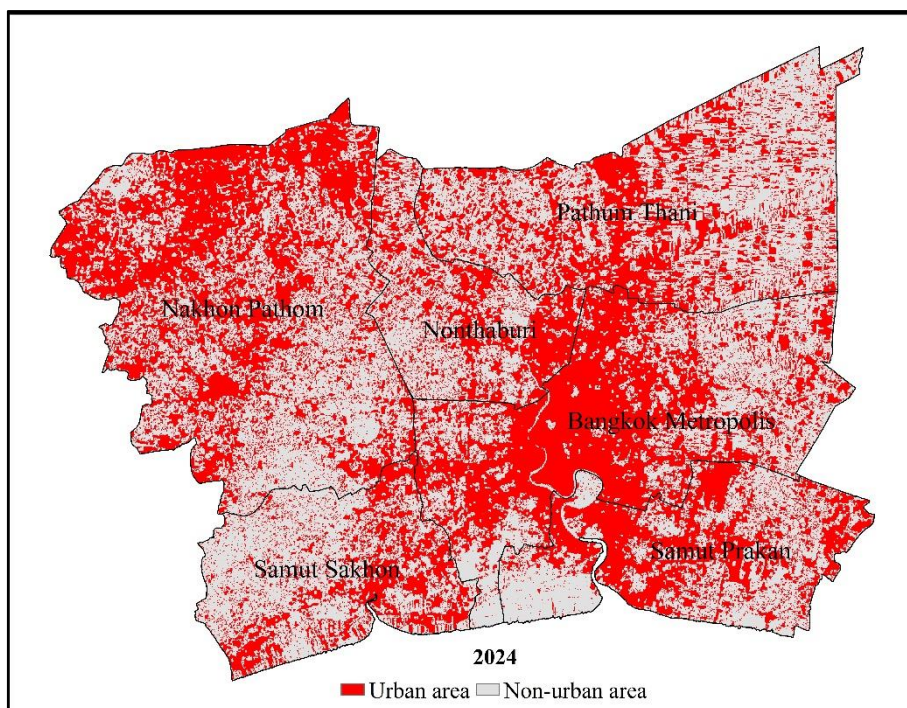


Figure 7.11 Distribution of predicted urban and non-urban areas in 2024.

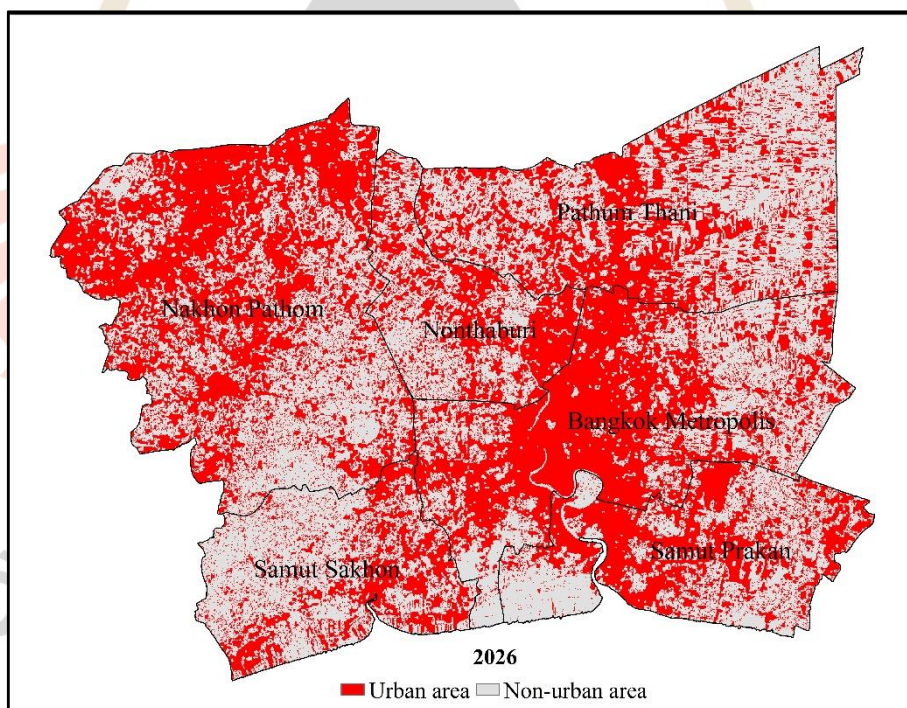


Figure 7.12 Distribution of predicted urban and non-urban areas in 2026.

As results of urban and non-urban areas extraction and prediction between 2006 and 2026, it was found that urban areas had been continuously increased while non-urban areas had been continuously decreased as summarized in Table 7.8 and as shown in Figure 7.13.

In addition, it was found reveals that urban growth areas of Bangkok Metropolitan and its vicinity during 2006 and 2016 as historical period increase about 1,160 sq.km with annual growth rate of 116 sq. km. Meanwhile, urban growth areas of Bangkok Metropolitan and its vicinity during 2016 and 2026 as future trend will increase about 932.64 sq.km with annual growth rate of 93.26 sq. km. This finding shows the limitation of land for urban expansion. In addition, pattern of urban distribution is more allocated in vertical direction due to land price.

Table 7.8 Area and percentage of urban and non-urban area between 2006 and 2026.

Year	Area (square kilometer)			Area (Percent)		
	Urban	Non-urban	Total	Urban	Non-urban	Total
2006	1735.64	5918.65	7654.29	22.68	77.32	100.00
2008	2038.75	5615.54	7654.29	26.64	73.36	100.00
2010	2209.45	5444.84	7654.29	28.87	71.13	100.00
2012	2379.52	5274.77	7654.29	31.09	68.91	100.00
2014	2638.47	5015.82	7654.29	34.47	65.53	100.00
2016	2895.61	4758.68	7654.29	37.83	62.17	100.00
2018	3139.58	4514.71	7654.29	41.02	58.98	100.00
2020	3361.20	4293.09	7654.29	43.91	56.09	100.00
2022	3495.29	4159.00	7654.29	45.66	54.34	100.00
2024	3621.76	4032.53	7654.29	47.32	52.68	100.00
2026	3828.25	3826.04	7654.29	50.01	49.99	100.00

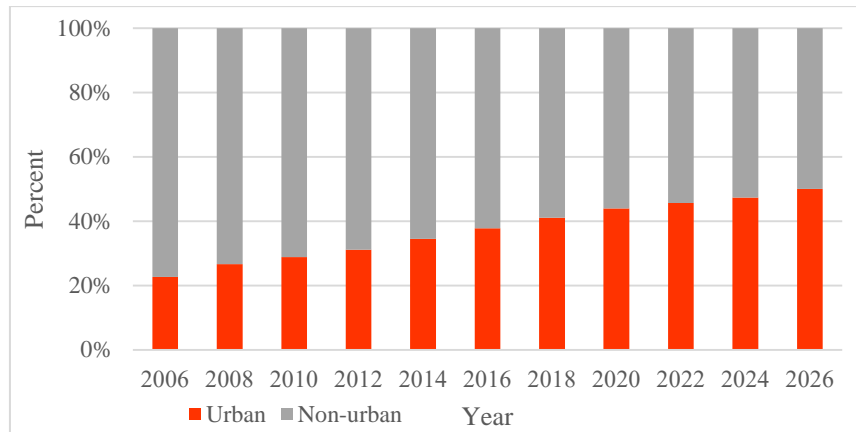


Figure 7.13 Urban and non-urban areas change between 2006 and 2026.

7.3 Temperature grade classification

The extracted and predicted LST data between 2006 and 2026 as reported in Chapter 6 were here firstly normalized with value between 0 and 1 to eliminate the impact of the imaging time and make the UHI effect more comparable before temperature grade classification. The normalization result of the extracted and predicted LST data between 2006 and 2026 is summarized in Table 7.9 and displaying in Figure 7.14. Later, the normalized data of LST in urban areas were extracted as summary in Table 7.10. This data were further used to classify brightness temperature grade of urban areas using Mean-Standard deviation method into 5 classes as suggested by Xu, Chen, Dan, and Qiu (2011) as follows:

(1) Low temperature area $T_s < \mu - \sigma$

(2) Secondary low temperature area $\mu - \sigma \leq T_s < \mu - 0.5\sigma$

(3) Medium temperature area $\mu - 0.5\sigma \leq T_s \leq \mu + 0.5\sigma$

(4) Secondary high temperature area $\mu + 0.5\sigma < T_s \leq \mu + \sigma$

(5) High temperature area $T_s > \mu + \sigma$

Distribution of brightness temperature grade classification of urban areas in Bangkok and its vicinity between 2006 and 2026 are displayed in Figures 7.15 to 7.25. Area and percentage of brightness temperature grade of urban areas between 2006 and 2026 is summarized in Table 7.11 and Table 7.12, respectively while dynamic change of proportional area of brightness temperature grade is displayed in Figure 7.26.

Table 7.9 Basic statistics of normalized LST data in Bangkok Metropolitan and its vicinity between 2006 and 2026.

Year	Normalized LST data		
	Minimum	Maximum	Mean
2006	0.45	1.00	0.64
2008	0.28	1.00	0.48
2010	0.22	0.90	0.44
2012	0.49	1.00	0.67
2014	0.18	1.00	0.58
2016	0.00	1.00	0.53
2018	0.20	0.86	0.50
2020	0.17	0.86	0.49
2022	0.15	0.85	0.49
2024	0.13	0.85	0.49
2026	0.12	0.84	0.48

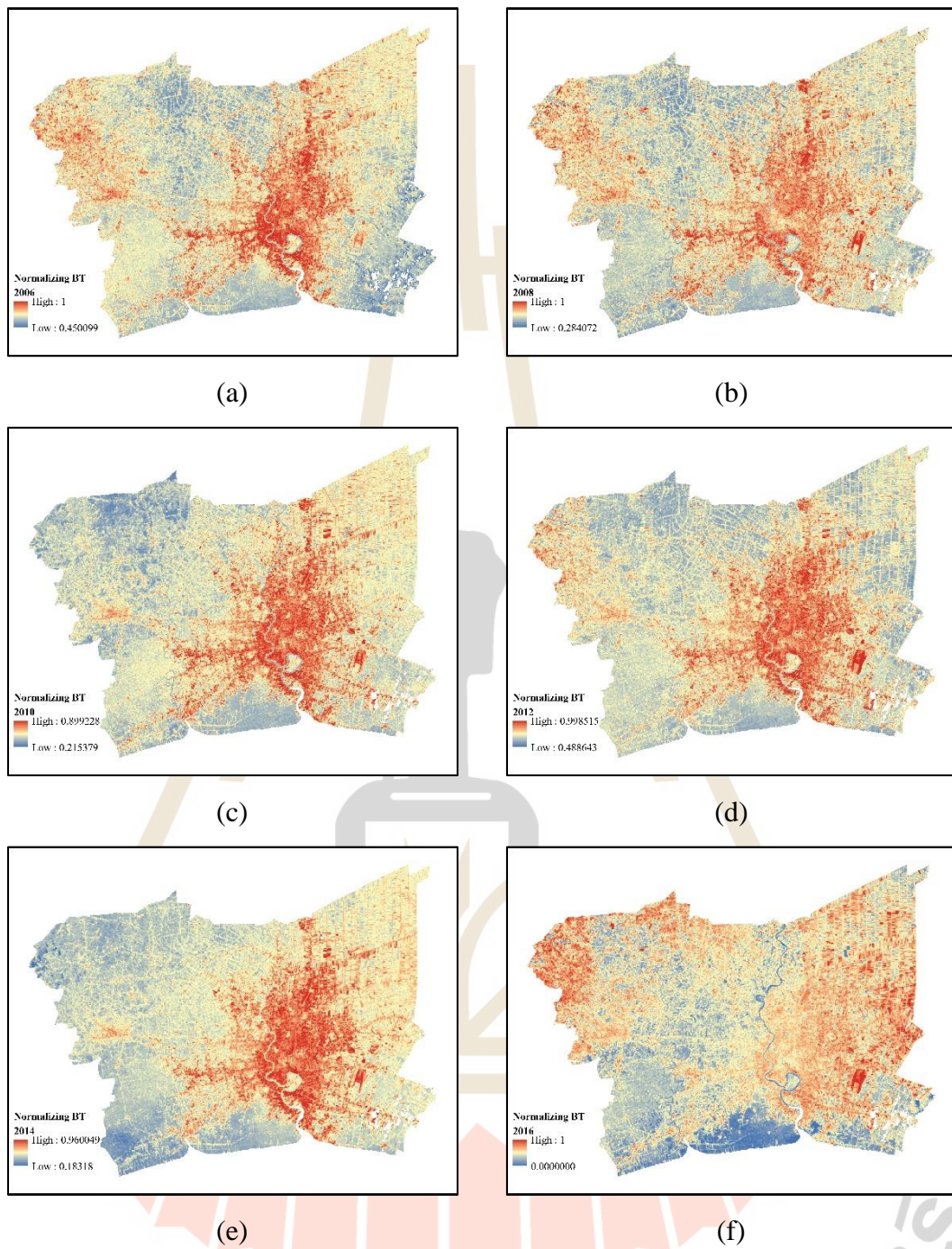


Figure 7.14 Normalized LST data: (a) 2006, (b) 2008, (c) 2010, (d) 2012, (e) 2014, and (f) 2016.

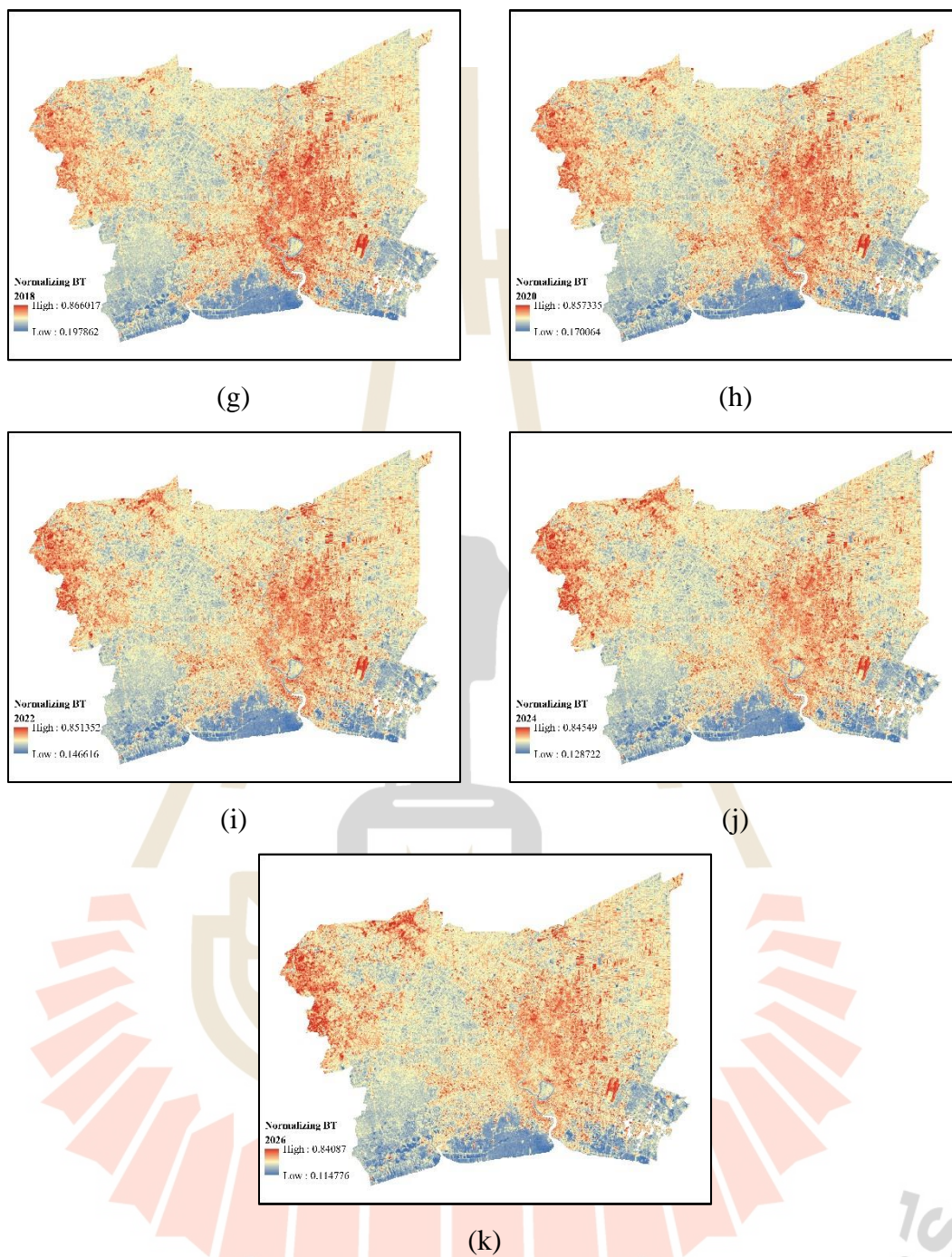


Figure 7.14 (Continued) (g) 2018, (h) 2020, (i) 2022, (j) 2024, and (k) 2026.

Table 7.10 Basic statistics of normalized LST data in urban areas of Bangkok Metropolitan and its vicinity between 2006 and 2026.

Year	Normalized LST data			
	Minimum	Maximum	Mean	SD
2006	0.45	1	0.71	0.07
2008	0.28	0.85	0.53	0.06
2010	0.22	0.90	0.49	0.10
2012	0.49	1	0.71	0.07
2014	0.13	0.96	0.62	0.09
2016	0.08	1	0.56	0.09
2018	0.20	0.87	0.52	0.06
2020	0.17	0.86	0.51	0.05
2022	0.15	0.85	0.51	0.45
2024	0.13	0.85	0.50	0.04
2026	0.11	0.84	0.50	0.04

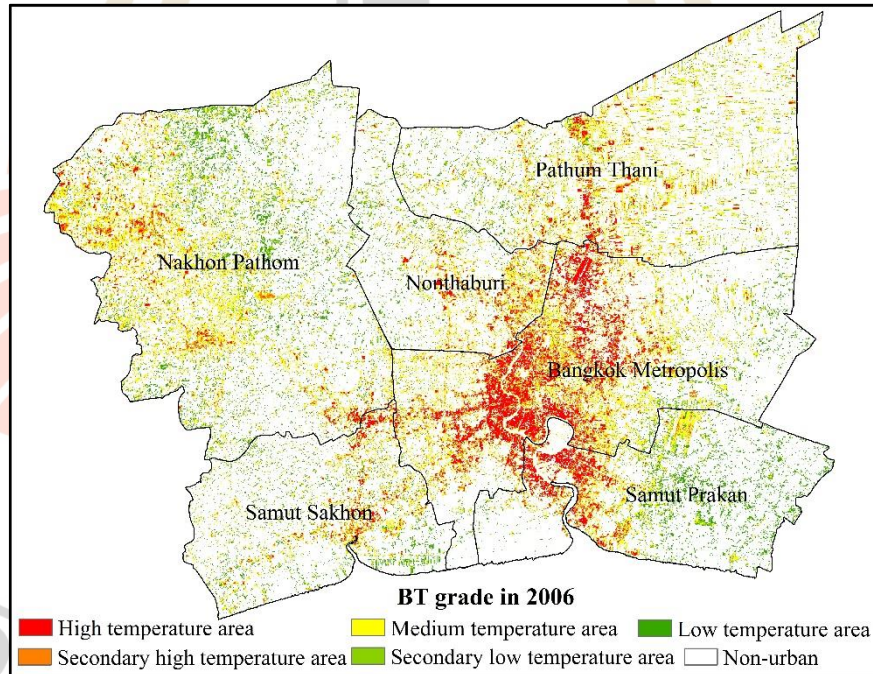


Figure 7.15 Distribution brightness temperature grade classification of Bangkok and its vicinity in 2006.

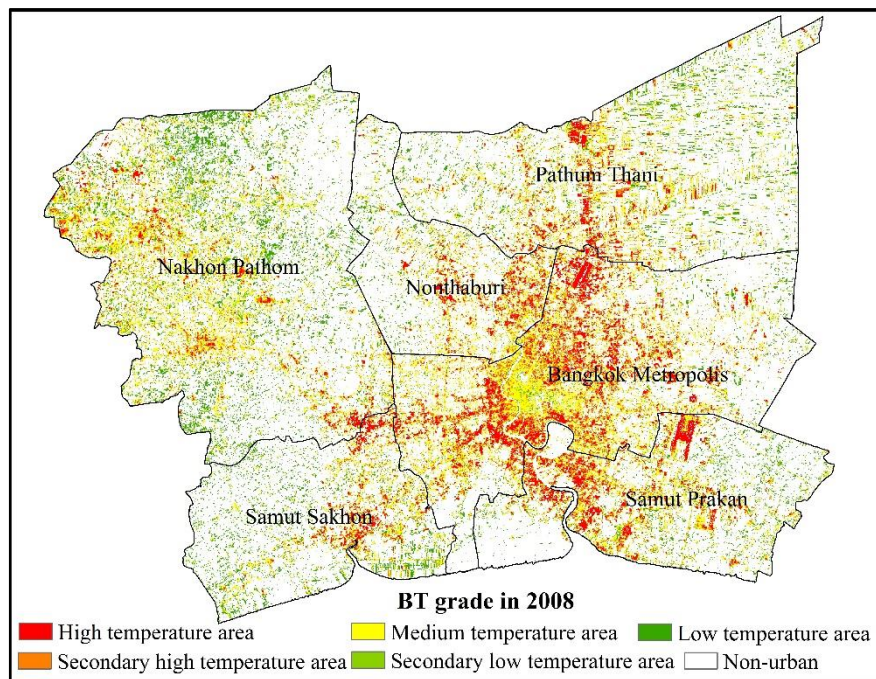


Figure 7.16 Distribution brightness temperature grade classification of Bangkok and its vicinity in 2008.

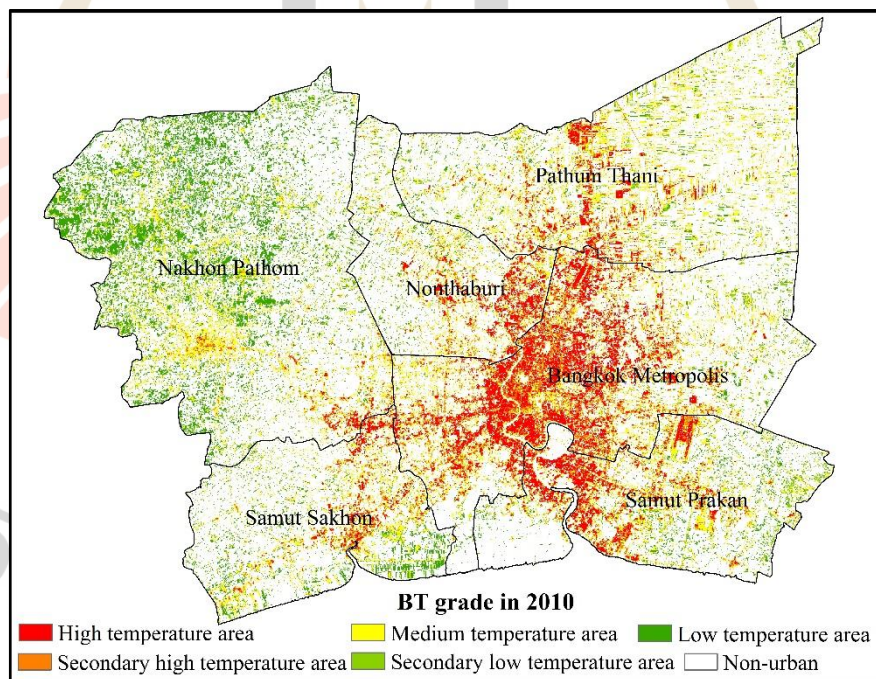


Figure 7.17 Distribution brightness temperature grade classification of Bangkok and its vicinity in 2010.

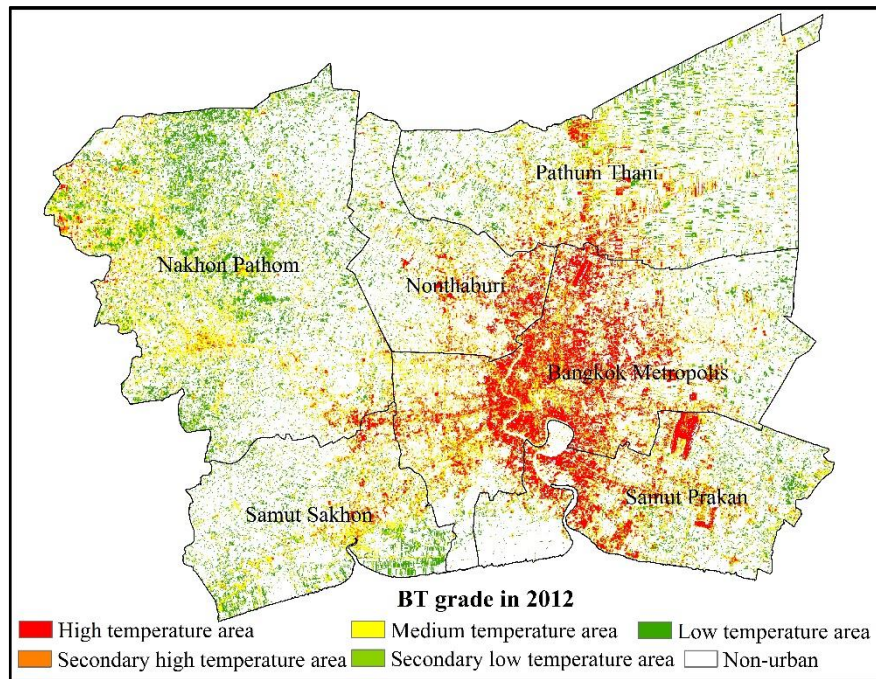


Figure 7.18 Distribution brightness temperature grade classification of Bangkok and its vicinity in 2012.

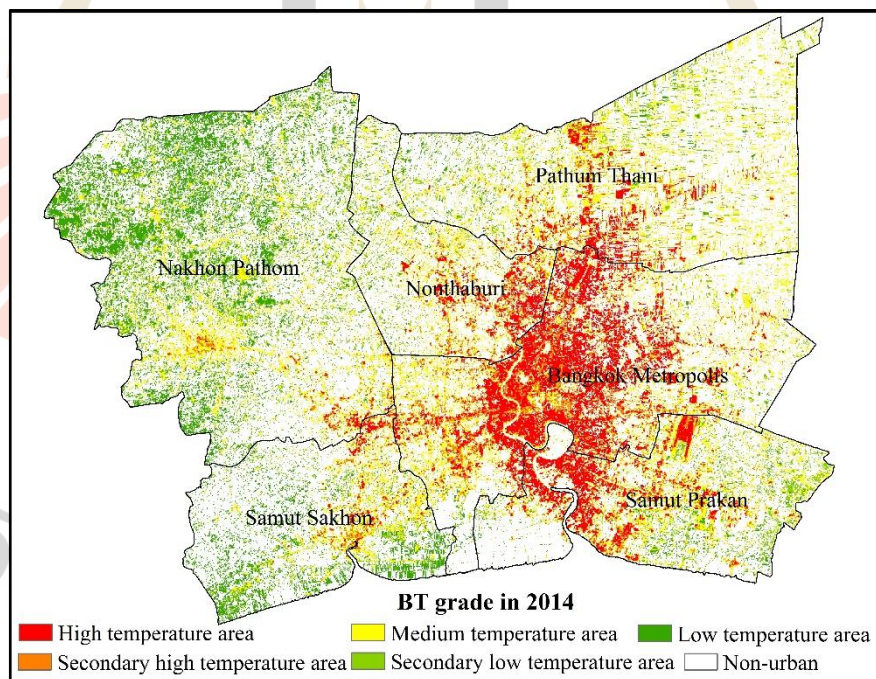


Figure 7.19 Distribution brightness temperature grade classification of Bangkok and its vicinity in 2014.

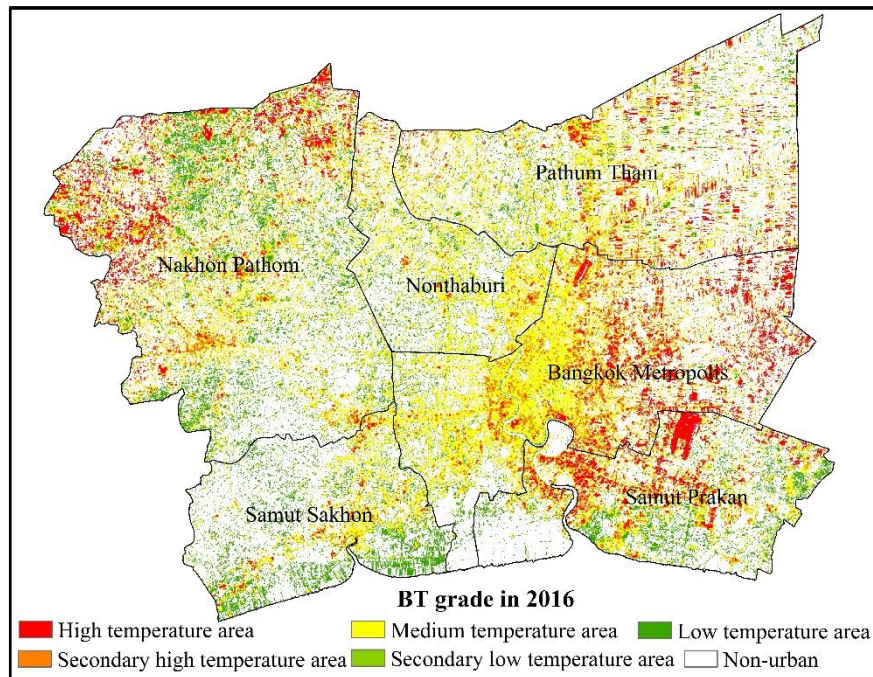


Figure 7.20 Distribution brightness temperature grade classification of Bangkok and its vicinity in 2016.

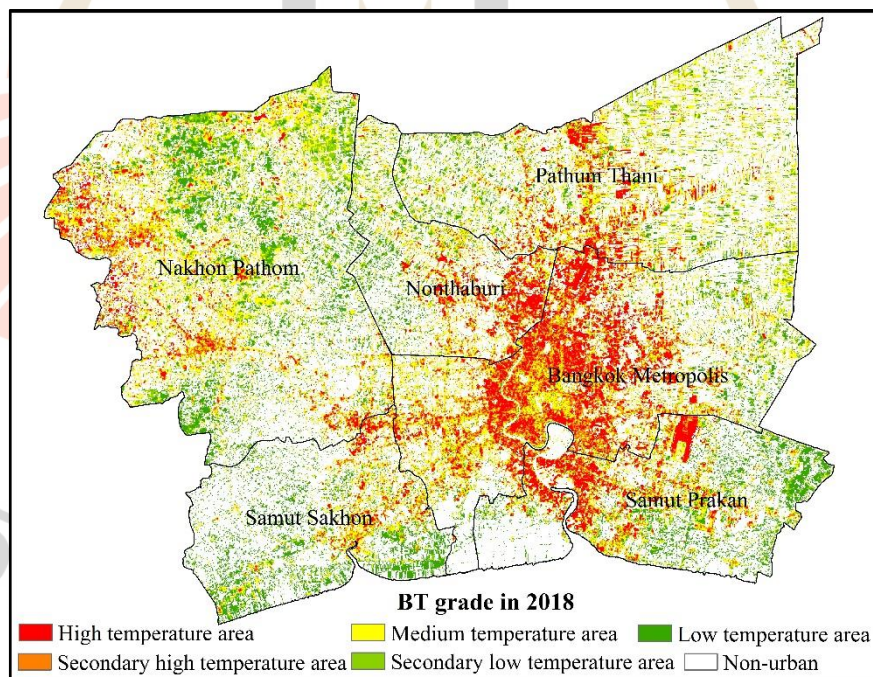


Figure 7.21 Distribution brightness temperature grade classification of Bangkok and its vicinity in 2018.

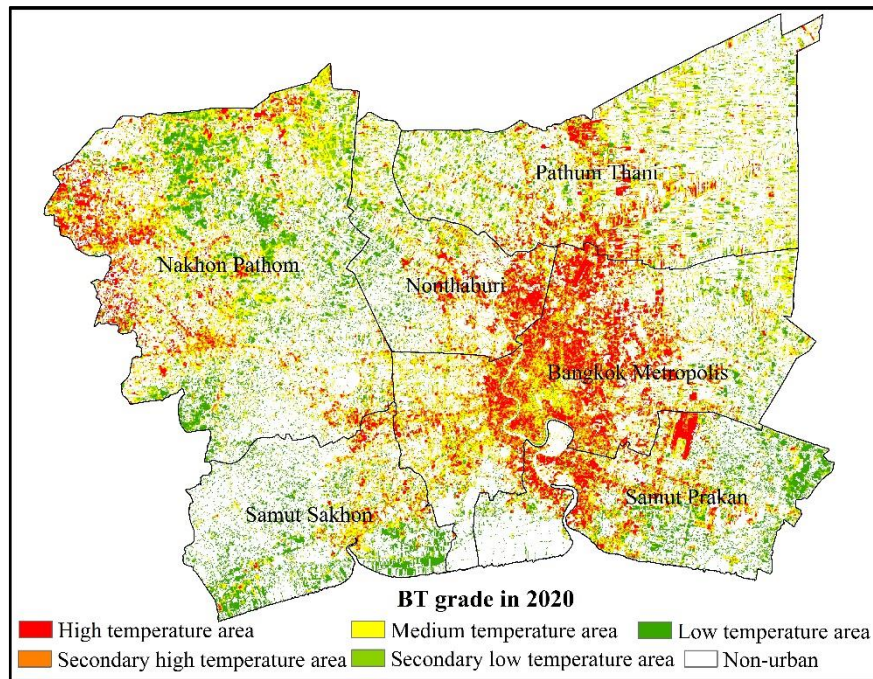


Figure 7.22 Distribution brightness temperature grade classification of Bangkok and its vicinity in 2020.

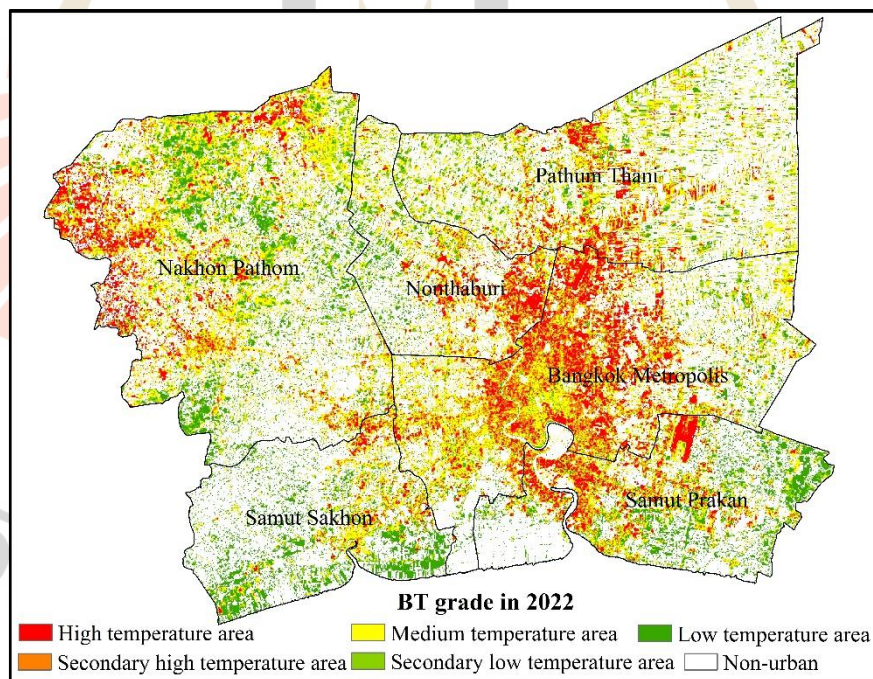


Figure 7.23 Distribution brightness temperature grade classification of Bangkok and its vicinity in 2022.

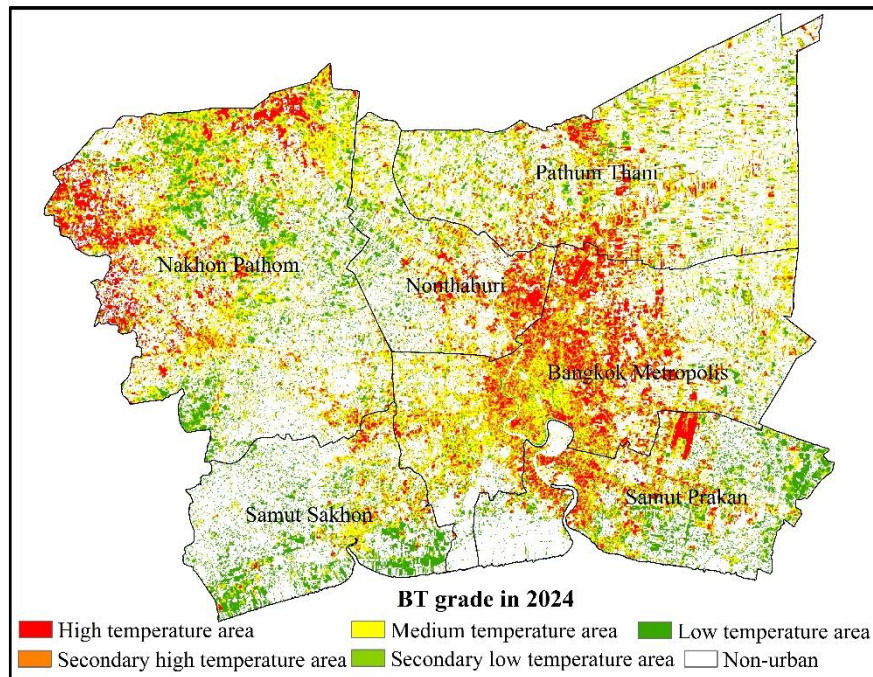


Figure 7.24 Distribution brightness temperature grade classification of Bangkok and its vicinity in 2024.

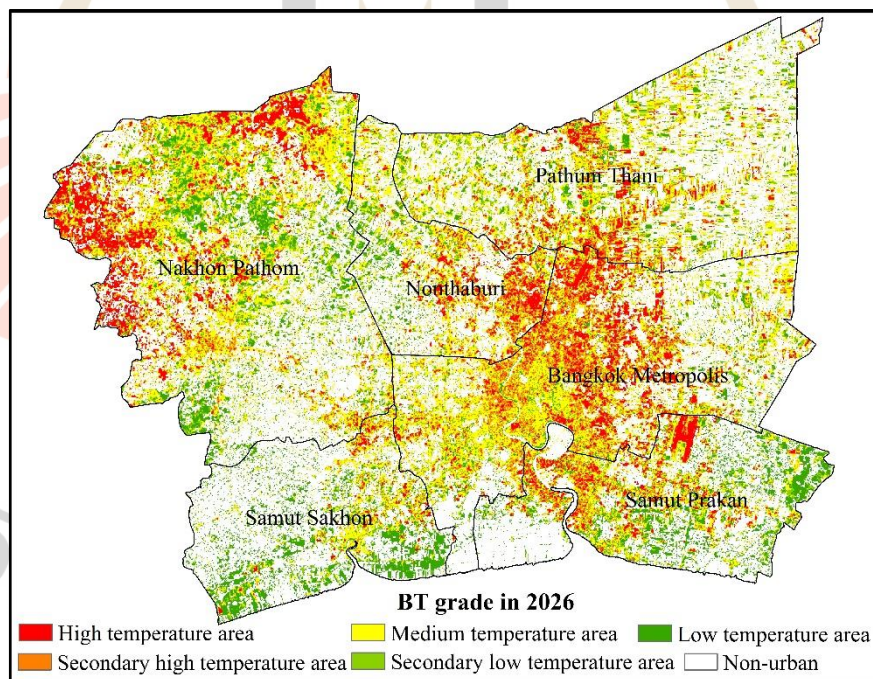


Figure 7.25 Distribution brightness temperature grade classification of Bangkok and its vicinity in 2026.

Table 7.11 Area of brightness temperature grade in Bangkok and its vicinity between 2006 and 2026.

Year	Low	2 nd Low	Medium	2 nd High	High	Total
2006	268.09	279.88	645.91	270.79	270.97	1,735.64
2008	356.76	274.85	747.70	344.55	314.89	2,038.75
2010	420.85	348.16	667.13	368.10	405.20	2,209.45
2012	454.06	357.65	763.62	385.27	418.92	2,379.52
2014	487.64	465.35	798.67	378.86	507.95	2,638.47
2016	474.81	329.15	1,169.11	518.81	403.73	2,895.61
2018	537.36	494.23	1,067.94	517.93	522.12	3,139.58
2020	548.14	510.83	1,209.65	553.45	539.13	3,361.20
2022	547.87	518.34	1,316.78	571.92	540.38	3,495.29
2024	549.14	529.47	1,416.86	585.52	540.76	3,621.75
2026	562.88	559.59	1,547.47	603.85	554.46	3,828.25

Table 7.12 Percent of brightness temperature grade in Bangkok and its vicinity between 2006 and 2026.

Year	Low	2 nd Low	Medium	2 nd High	High	Total
2006	15.6121	15.6018	37.2146	16.1255	15.4460	100
2008	15.4451	16.9000	36.6745	13.4812	17.4991	100
2010	18.3395	16.6604	30.1944	15.7578	19.0478	100
2012	17.6054	16.1910	32.0913	15.0302	19.0821	100
2014	19.2517	14.3591	30.2701	17.6372	18.4818	100
2016	13.9428	17.9169	40.3753	11.3673	16.3977	100
2018	16.6302	16.4968	34.0155	15.7419	17.1157	100
2020	16.0397	16.4658	35.9888	15.1980	16.3077	100
2022	15.4601	16.3627	37.6731	14.8295	15.6745	100
2024	14.9310	16.1669	39.1207	14.6192	15.1622	100
2026	14.4834	15.7735	40.4225	14.6174	14.7033	100

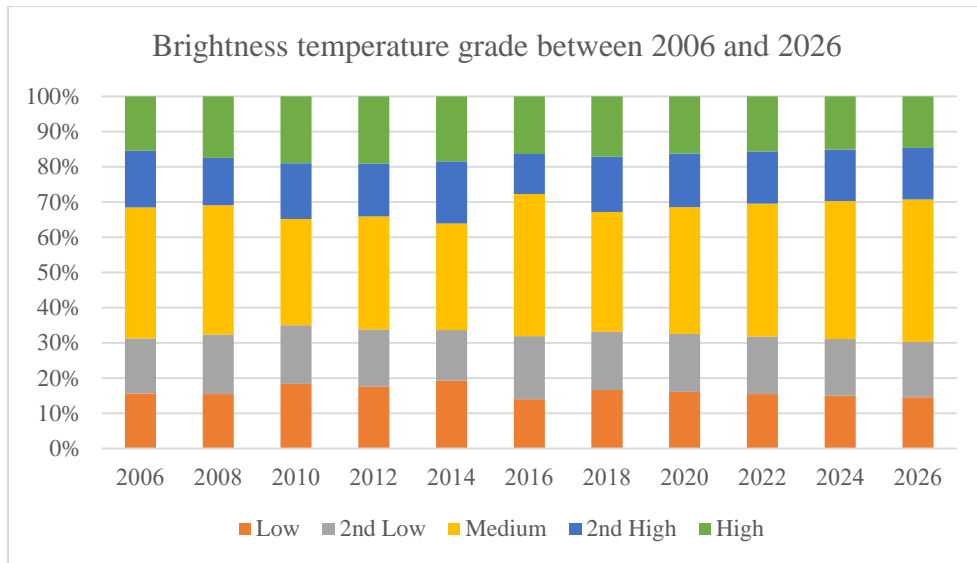


Figure 7.26 Dynamic change of proportional area of brightness temperature grade in Bangkok and its vicinity between 2006 and 2026.

As results, it reveals that pattern of BT grade classification between 2006 and 2026 cannot be compared together because BT grade class in each year depends on average and standard deviation values of LST (Table 7.10). For example, BT grade class of central business district (CBD) of Bangkok Metropolitan in 2014 was high temperature area but this area became medium temperature area in 2016. On contrary, pattern of BT grade class is consistent with pattern of LST (Figure 7.27)

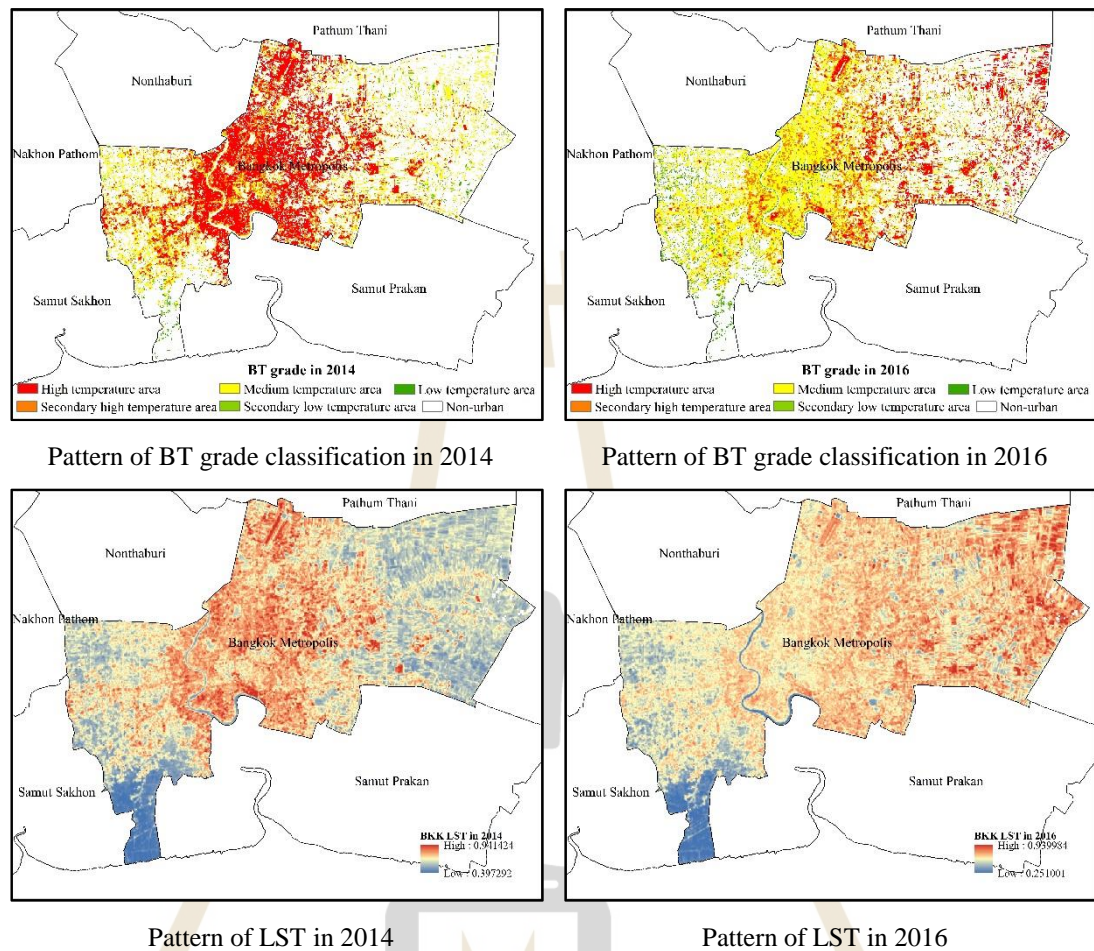


Figure 7.27 Comparison of BT grade classification pattern and LST pattern in 2014 and 2016.

In addition, it should be here mentioned that the limitation of Landsat data due to cloud cover directly effects on LST data which are related with BT grade classification. In this study, LST data between 2006 and 2016 were converted from different months (See Table 6.1). Therefore, comparison of BT grade classification between 2006 and 2026 is not appropriate. Ideally, Landsat data should be acquired based on anniversary dates to ensure seasonal agreement of temperature conditions among multi-dates data.

7.4 Urban heat island intensity and its severity

The WAI, which is an index for describing UHI intensity by sum of products between the difference five grade temperature in built-up area (T_{iavg}) with average temperature in outskirts area (T_{oavg}) and percent of temperature grade area (A_i), was here calculated using Equation 3.10. Meanwhile, URI, which is used to depict development degree of UHI was also extracted over Bangkok and its vicinity between 2006 and 2026 using Equation 3.11. Result of WAI and URI are represented in Table 7.13.

As results, it was found that WAI as UHI intensity continuously decreases from historical to present record (between 2006 and 2016) except in 2010 and 2016 and it gradually continuously decreases in the future (between 2018 and 2026) as shown in Figure 7.28. Furthermore, according to standard classification of WAI as UHI intensity of Dan et al. (2010) as shown in Table 7.14, the UHI intensity between 2006 and 2016 as historical record shows very strong intensity while UHI intensity in the future shows very strong intensity between 2018 and 2022 and it will decline to strong intensity between 2024 and 2026.

Meanwhile, URI for describing degree of UHI development reveals that degree of UHI development increases in 2010 and 2016 during 2006 to 2016 as historical record and it will suddenly decrease in 2018 and continuously increases between 2020 and 2026 in the future as shown in Figure 7.29. Based on this finding, it should be here mentioned that UHI phenomena of Bangkok Metropolitan and its vicinity should be seriously considered to mitigate its effect in near future.

Table 7.13 WAI and URI calculation of Bangkok and its vicinity between 2006 and 2026.

Year	Average Temp. (T_{iavg})					Average Temp. outskirt (T_{oavg})	% Area (A_i)					WAI	URI
	High	2 nd High	Medium	2 nd Low	Low		High	2 nd High	Medium	2 nd Low	Low		
2006	0.8065	0.7554	0.7078	0.6594	0.6099	0.6267	15.6121	15.6018	37.2146	16.1255	15.4460	8.1009	0.5996
2008	0.6282	0.5798	0.5352	0.4862	0.4377	0.4651	15.4451	16.9000	36.6745	13.4812	17.4991	6.8334	0.5986
2010	0.6396	0.5700	0.4932	0.4188	0.3534	0.4196	18.3395	16.6604	30.1944	15.7578	19.0478	7.4892	0.5990
2012	0.8120	0.7620	0.7107	0.6576	0.6119	0.6525	17.6054	16.1910	32.0913	15.0302	19.0821	5.7506	0.5964
2014	0.7458	0.6842	0.6173	0.5530	0.5002	0.5640	19.2517	14.3591	30.2701	17.6372	18.4818	5.4662	0.5965
2016	0.6945	0.6280	0.5660	0.4961	0.4150	0.5054	13.9428	17.9169	40.3753	11.3673	16.3977	5.6919	0.6033
2018	0.6048	0.5643	0.5240	0.4818	0.4412	0.4836	16.6302	16.4968	34.0155	15.7419	17.1157	3.9671	0.5996
2020	0.5851	0.5489	0.5129	0.4759	0.4373	0.4780	16.0397	16.4658	35.9888	15.1980	16.3077	3.4456	0.6015
2022	0.5735	0.5393	0.5062	0.4720	0.4345	0.4755	15.4601	16.3627	37.6731	14.8295	15.6745	3.0210	0.6022
2024	0.5652	0.5318	0.5005	0.4683	0.4317	0.4726	14.9310	16.1669	39.1207	14.6192	15.1622	2.7482	0.6022
2026	0.5597	0.5262	0.4961	0.4652	0.4295	0.4696	14.4834	15.7735	40.4225	14.6174	14.7033	2.6150	0.6014

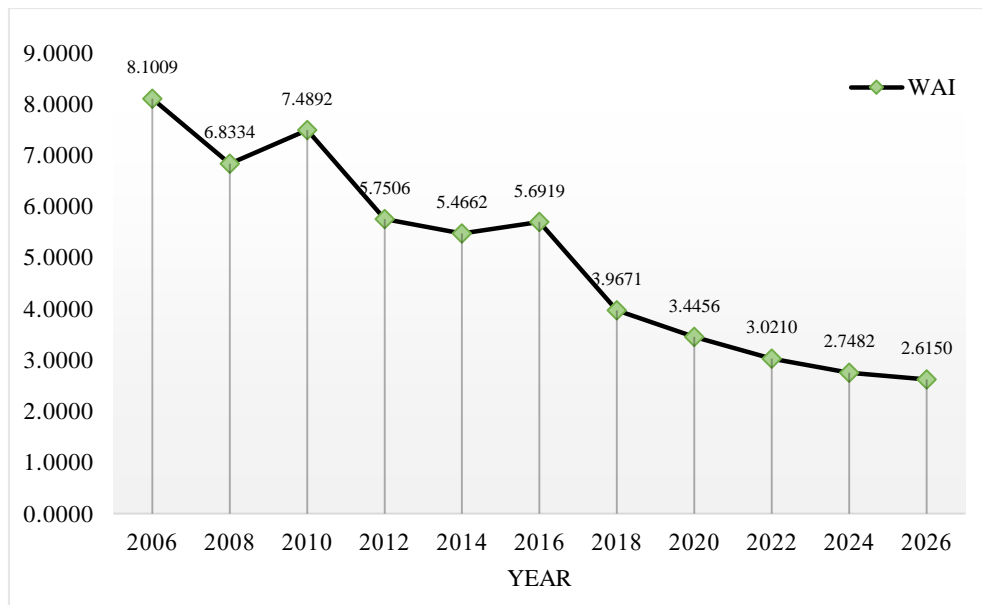


Figure 7.28 Dynamic change of WAI between 2006 and 2026.

Table 7.14 Classification of heat island intensity based on WAI.

Temperature range (WAI)	Intensity Definition
≤ 0.5 °C	very weak
0.5 °C - 0.1 °C	weak
1.0 °C - 2.0 °C	medium
2.0 °C - 3.0 °C	strong
> 3.0 °C	very strong

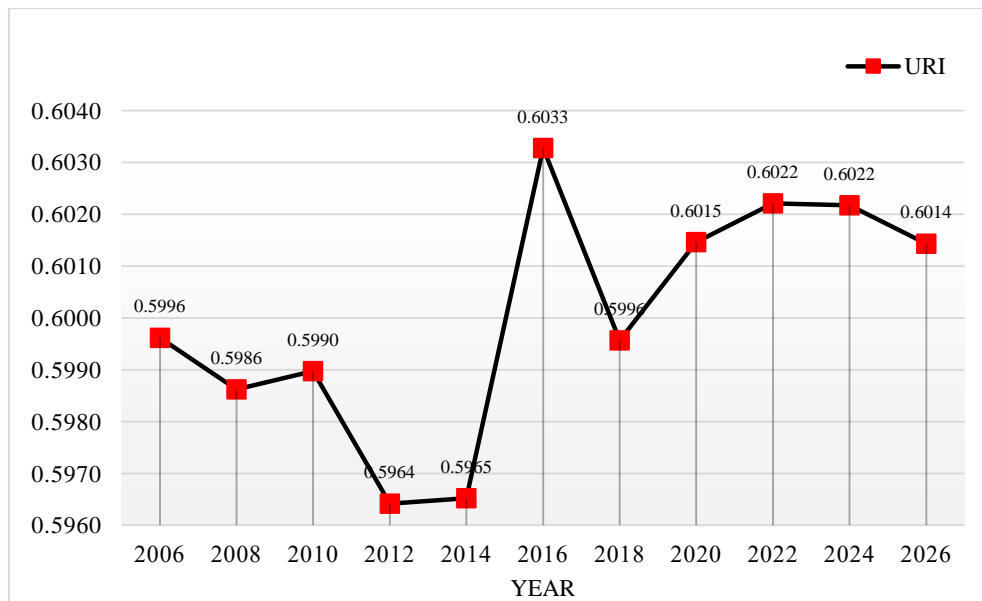


Figure 7.29 Dynamic change of URI between 2006 and 2026.

In addition, it should be here mentioned that the dynamic change of URI directly relate with the results of extraction and prediction urban and non-urban area using BUI and CA-Markov model. At the same time, LST data, that was converted from Landsat data and predicted by Trend Analysis, also plays an important role on dynamic change of URI in this study.

7.5 Quantitative analysis of UHI

Two methods for quantitative analysis are here reported and discussed include (1) quantitative analysis of UHI in different urban regions and (2) overall analysis of UHI change.

7.5.1 Quantitative analysis of UHI in different urban regions

Transitional area change of brightness temperature grade in old urban area and urban expansion in each period are here extracted to describe quantitative

change in three aspects: unchanged, increase and decrease of brightness temperature grades. Results of transitional area change of brightness temperature grade in old urban area and urban expansion in 2006-2008, 2008-2010, 2010-2012, 2012-2014, 2014-2016, 2016-2018, 2018-2020, 2022-2024, and 2024-2026 periods in details are describe as matrix form in Tables 7.15 to 7.34, respectively. The summary area and percentage of unchanged, increase and decrease of BT temperature grades in old urban in each period is presented in Table 7.35 and Figure 7.30 while the summary area and percentage of unchanged, increase and decrease of BT temperature grades in urban expansion in each period is presented in Table 7.36 and Figure 7.31. Distribution of unchanged, increase and decrease areas of BT temperature grades in old urban and urban expansion in each period are displayed in Figures 7.32 to 7.41.

Table 7.15 Transition matrix of difference BT grade in old urban areas in 2006-2008.

Old urban in 2006-2008 period	Area of brightness temperature grade in sq. km				
	High	2 nd High	Medium	2 nd Low	Low
High	670.87	115.05	63.92	9.23	5.95
2 nd High	90.74	96.78	95.92	16.73	7.33
Medium	49.31	62.22	222.03	85.33	46.00
2 nd Low	4.33	4.60	22.21	18.30	13.30
Low	4.68	3.16	13.98	8.25	5.40

Table 7.16 Transition matrix of difference BT grade in urban expansion region in 2006-2008.

Urban expansion in 2006-2008 period	Area of brightness temperature grade in sq. km				
	High	2 nd High	Medium	2 nd Low	Low
High	50.61	12.79	3.87	0.11	0.07
2 nd High	16.43	16.36	10.41	0.33	0.19
Medium	22.76	23.68	57.64	7.84	1.01
2 nd Low	8.80	6.90	23.75	8.08	2.11
Low	7.71	4.92	11.83	3.35	1.55

Table 7.17 Transition matrix of difference BT grade in old urban region in 2008-2010.

Old urban in 2008-2010 period	Area of brightness temperature grade in sq. km				
	High	2 nd High	Medium	2 nd Low	Low
High	697.09	80.94	90.42	32.23	25.58
2 nd High	114.96	84.53	102.03	28.83	16.12
Medium	32.29	66.86	256.43	108.30	61.68
2 nd Low	2.06	4.63	55.66	51.21	44.00
Low	1.12	1.81	20.24	22.44	37.29

Table 7.18 Transition matrix of difference BT grade in urban expansion region in 2008-2010.

Urban expansion in 2008-2010 period	Area of brightness temperature grade in sq. km				
	High	2 nd High	Medium	2 nd Low	Low
High	24.20	3.09	2.28	0.80	0.74
2 nd High	9.23	4.65	3.99	0.95	0.79
Medium	9.19	10.08	22.10	5.61	3.43
2 nd Low	3.92	4.54	15.41	5.61	3.30
Low	2.79	3.43	19.49	6.33	4.75

Table 7.19 Transition matrix of difference BT grade in old urban region in 2010-2012.

Old urban in 2010-2012 period	Area of brightness temperature grade in sq. km				
	High	2 nd High	Medium	2 nd Low	Low
High	772.07	92.23	24.31	3.89	4.35
2 nd High	64.16	114.53	69.93	8.46	7.49
Medium	33.15	90.12	329.35	83.41	52.03
2 nd Low	14.73	14.72	104.15	85.89	42.80
Low	6.84	5.33	46.13	69.99	69.40

Table 7.20 Transition matrix of difference BT grade in urban expansion region in 2010-2012.

Urban expansion in 2010-2012 period	Area of brightness temperature grade in sq. km				
	High	2 nd High	Medium	2 nd Low	Low
High	26.19	4.02	0.76	0.10	0.08
2 nd High	7.93	9.40	4.09	0.23	0.11
Medium	8.67	13.90	32.40	3.46	0.68
2 nd Low	4.54	4.16	16.78	5.66	0.90
Low	2.33	2.35	13.10	6.40	1.83

Table 7.21 Transition matrix of difference BT grade in old urban region in 2012-2014.

Old urban in 2012-2014 period	Area of brightness temperature grade in sq. km				
	High	2 nd High	Medium	2 nd Low	Low
High	771.23	86.90	49.43	17.67	15.37
2 nd High	88.91	114.69	112.66	21.38	13.11
Medium	23.71	69.39	333.57	138.39	75.93
2 nd Low	1.95	7.76	82.01	94.34	81.43
Low	1.50	5.59	53.01	52.82	66.75

Table 7.22 Transition matrix of difference BT grade in urban expansion region in 2012-2014.

Urban expansion in 2012-2014 period	Area of brightness temperature grade in sq. km				
	High	2 nd High	Medium	2 nd Low	Low
High	26.86	3.48	1.48	0.27	0.18
2 nd High	9.28	8.97	5.15	0.61	0.36
Medium	7.85	13.39	39.62	9.39	3.24
2 nd Low	2.45	5.05	28.93	16.15	6.66
Low	1.49	5.90	30.01	22.56	9.63

Table 7.23 Transition matrix of difference BT grade in old urban region in 2014-2016.

Old urban in 2014-2016 period	Area of brightness temperature grade in sq. km				
	High	2 nd High	Medium	2 nd Low	Low
High	314.38	358.22	255.23	4.69	2.71
2 nd High	46.79	74.97	182.44	12.57	4.37
Medium	113.20	125.58	320.36	116.03	60.72
2 nd Low	67.23	48.63	111.04	71.06	75.60
Low	48.15	25.98	52.19	43.56	102.78

Table 7.24 Transition matrix of difference BT grade in urban expansion region in 2014-2016.

Urban expansion in 2014-2016 period	Area of brightness temperature grade in sq. km				
	High	2 nd High	Medium	2 nd Low	Low
High	2.75	1.81	1.79	0.13	0.06
2 nd High	8.79	3.08	2.96	0.21	0.15
Medium	43.50	22.94	28.93	4.16	1.67
2 nd Low	27.38	21.08	25.15	4.70	1.97
Low	22.11	11.93	13.86	3.50	2.54

Table 7.25 Transition matrix of difference BT grade in old urban region in 2016-2018.

Old urban in 2016-2018 period	Area of brightness temperature grade in sq. km				
	High	2 nd High	Medium	2 nd Low	Low
High	406.06	99.73	154.47	28.82	5.19
2 nd High	350.56	138.02	165.62	33.19	6.83
Medium	156.39	239.45	447.90	118.26	31.93
2 nd Low	1.00	4.76	108.56	98.80	47.49
Low	0.11	0.56	23.18	72.35	156.36

Table 7.26 Transition matrix of difference BT grade in urban expansion region in 2016-2018.

Urban expansion in 2016-2018 period	Area of brightness temperature grade in sq. km				
	High	2 nd High	Medium	2 nd Low	Low
High	26.58	8.72	11.75	1.56	0.28
2 nd High	34.09	15.21	13.49	1.86	0.40
Medium	18.74	29.52	41.18	8.18	1.47
2 nd Low	0.05	0.32	7.33	6.27	2.27
Low	0.01	0.06	1.56	4.80	6.98

Table 7.27 Transition matrix of difference BT grade in old urban region in 2018-2020.

Old urban in 2018-2020 period	Area of brightness temperature grade in sq. km				
	High	2 nd High	Medium	2 nd Low	Low
High	898.98	94.59	0.02	0.00	0.00
2 nd High	39.09	422.68	74.57	0.00	0.00
Medium	0.00	50.59	893.37	31.01	0.06
2 nd Low	0.00	0.00	46.25	305.48	22.36
Low	0.00	0.00	0.00	13.27	245.93

Table 7.28 Transition matrix of difference BT grade in urban expansion region in 2018-2020.

Urban expansion in 2018-2020 period	Area of brightness temperature grade in sq. km				
	High	2 nd High	Medium	2 nd Low	Low
High	38.37	3.20	0.00	0.00	0.00
2 nd High	4.52	34.34	3.56	0.00	0.00
Medium	0.00	5.80	82.63	1.67	0.00
2 nd Low	0.00	0.00	5.75	23.99	1.13
Low	0.00	0.00	0.00	1.79	13.78

Table 7.29 Transition matrix of difference BT grade in old urban region in 2020-2022.

Old urban in 2020-2022 period	Area of brightness temperature grade in sq. km				
	High	2 nd High	Medium	2 nd Low	Low
High	886.26	94.14	0.00	0.00	0.00
2 nd High	37.14	493.96	79.65	0.00	0.00
Medium	0.00	46.30	1028.70	29.70	0.01
2 nd Low	0.00	0.00	37.01	321.55	18.14
Low	0.00	0.00	0.00	11.31	271.78

Table 7.30 Transition matrix of difference BT grade in urban expansion region in 2020-2022.

Urban expansion in 2020-2022 period	Area of brightness temperature grade in sq. km				
	High	2 nd High	Medium	2 nd Low	Low
High	17.80	1.96	0.00	0.00	0.00
2 nd High	1.50	22.32	3.42	0.00	0.00
Medium	0.00	2.12	53.99	1.58	0.00
2 nd Low	0.00	0.00	1.63	15.28	0.84
Low	0.00	0.00	0.00	0.44	13.46

Table 7.31 Transition matrix of difference BT grade in old urban region in 2022-2024.

Old urban in 2022-2024 period	Area of brightness temperature grade in sq. km				
	High	2 nd High	Medium	2 nd Low	Low
High	855.23	87.46	0.00	0.00	0.00
2 nd High	31.54	548.78	80.48	0.00	0.00
Medium	0.00	39.96	1135.43	29.00	0.00
2 nd Low	0.00	0.00	28.96	334.34	16.56
Low	0.00	0.00	0.00	9.24	294.99

Table 7.32 Transition matrix of difference BT grade in urban expansion region in 2022-2024.

Urban expansion in 2022-2024 period	Area of brightness temperature grade in sq. km				
	High	2 nd High	Medium	2 nd Low	Low
High	20.35	0.80	0.00	0.00	0.00
2 nd High	1.83	20.10	1.51	0.00	0.00
Medium	0.00	2.41	54.93	0.70	0.00
2 nd Low	0.00	0.00	1.52	13.49	0.35
Low	0.00	0.00	0.00	0.46	7.49

Table 7.33 Transition matrix of difference BT grade in old urban region in 2024-2026.

Old urban in 2024-2026 period	Area of brightness temperature grade in sq. km				
	High	2 nd High	Medium	2 nd Low	Low
High	908.95	0.00	0.00	0.00	0.00
2 nd High	0.00	699.51	0.00	0.00	0.00
Medium	0.00	0.00	1302.83	0.00	0.00
2 nd Low	0.00	0.00	0.00	387.24	0.00
Low	0.00	0.00	0.00	0.00	319.31

Table 7.34 Transition matrix of difference BT grade in urban expansion region in 2024-2026.

Urban expansion in 2024-2026 period	Area of brightness temperature grade in sq. km				
	High	2 nd High	Medium	2 nd Low	Low
High	37.34	0.95	0.00	0.00	0.00
2 nd High	2.19	32.89	1.78	0.00	0.00
Medium	0.00	2.62	89.85	1.09	0.00
2 nd Low	0.00	0.00	1.85	22.66	0.57
Low	0.00	0.00	0.00	0.78	11.46

Table 7.35 Area and percentage of unchanged, increase and decrease of BT temperature grades in old urban in each period.

No	Period	Area in sq. km				Area in percent			
		Unchanged	Increase	Decrease	Total	Unchanged	Increase	Decrease	Total
1	2006-2008	1,013.38	263.48	458.76	1,735.62	58.39	15.18	26.43	100
2	2008-2010	1,126.55	322.07	590.13	2,038.75	55.26	15.80	28.95	100
3	2010-2012	1,371.24	449.32	388.90	2,209.46	62.06	20.34	17.60	100
4	2012-2014	1,380.58	386.65	612.27	2,379.50	58.02	16.25	25.73	100
5	2014-2016	883.55	682.35	1,072.58	2,638.48	33.49	25.86	40.65	100
6	2016-2018	1,247.14	956.92	691.53	2,895.59	43.07	33.05	23.88	100
7	2018-2020	2,766.44	149.20	222.61	3,138.25	88.15	4.75	7.09	100
8	2020-2022	3,002.25	131.76	221.64	3,355.65	89.47	3.93	6.60	100
9	2022-2024	3,168.77	109.70	213.50	3,491.97	90.74	3.14	6.11	100
10	2024-2026	3,617.84	0.00	0.00	3,617.84	100.00	0.00	0.00	100

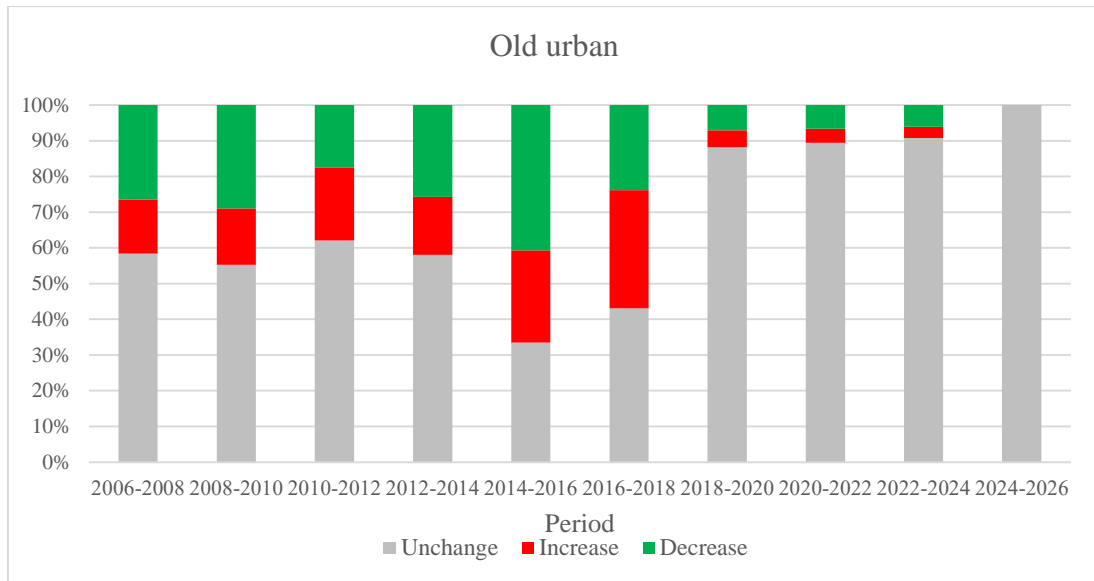


Figure 7.30 Comparison of percentage of unchanged, increase and decrease of BT temperature grades in old urban in each period.

Table 7.36 Area and percentage of unchanged, increase and decrease of BT temperature grades in urban expansion in each period.

No	Period	Area in sq. km				Area in percent			
		Unchanged	Increase	Decrease	Total	Unchanged	Increase	Decrease	Total
1	2006-2008	134.24	130.13	38.73	303.10	44.29	42.93	12.78	100
2	2008-2010	61.31	84.41	24.98	170.70	35.92	49.45	14.63	100
3	2010-2012	75.48	80.16	14.43	170.07	44.38	47.13	8.48	100
4	2012-2014	101.23	126.91	30.82	258.96	39.09	49.01	11.90	100
5	2014-2016	42.00	200.24	14.91	257.15	16.33	77.87	5.80	100
6	2016-2018	96.22	96.48	49.98	242.68	39.65	39.76	20.60	100
7	2018-2020	193.11	17.86	9.56	220.53	87.57	8.10	4.34	100
8	2020-2022	122.85	5.69	7.80	136.34	90.11	4.17	5.72	100
9	2022-2024	116.36	6.22	3.36	125.94	92.39	4.94	2.67	100
10	2024-2026	194.20	7.44	4.39	206.03	94.26	3.61	2.13	100

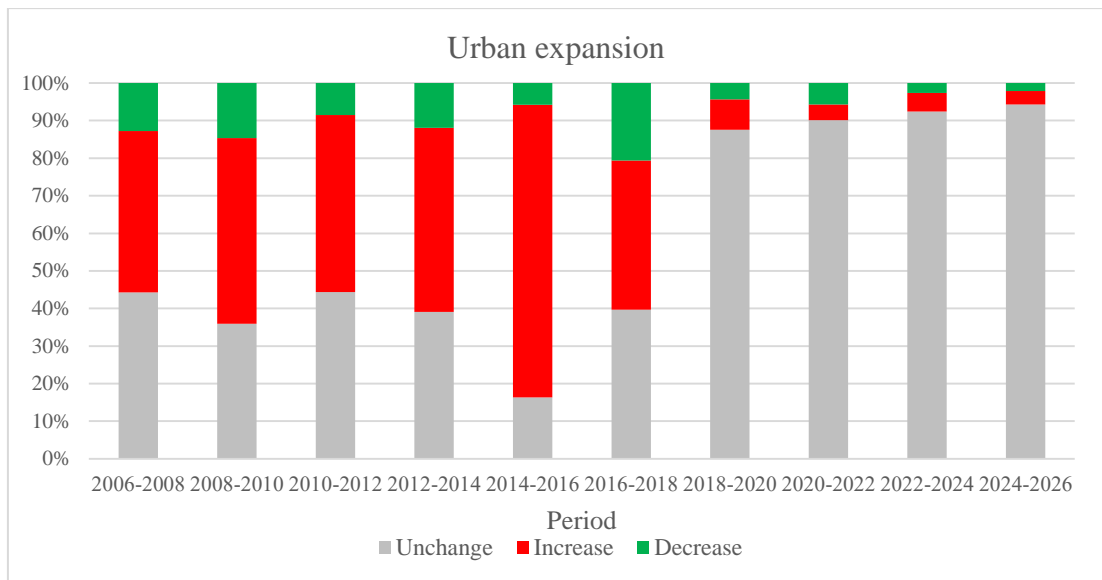
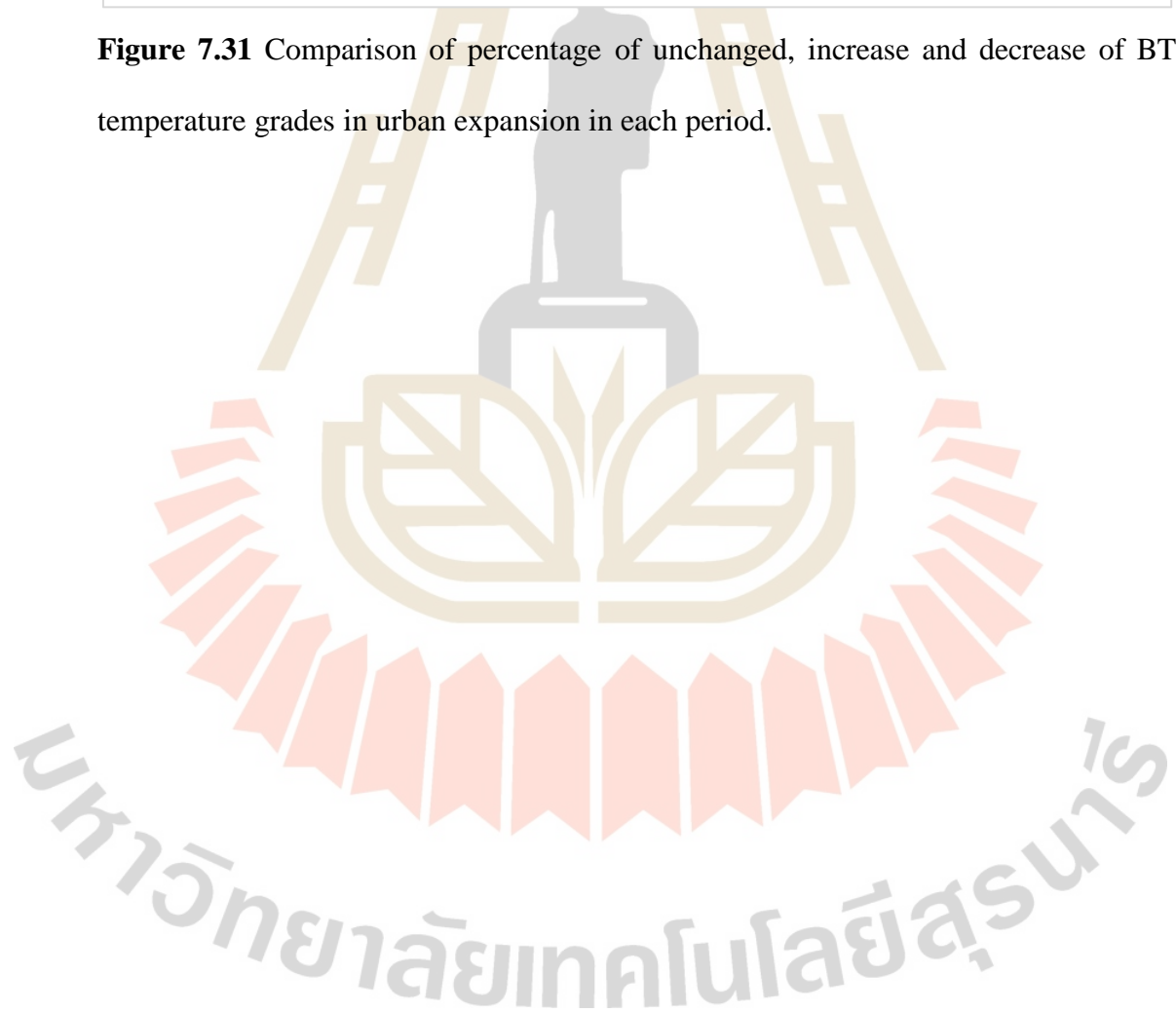


Figure 7.31 Comparison of percentage of unchanged, increase and decrease of BT temperature grades in urban expansion in each period.



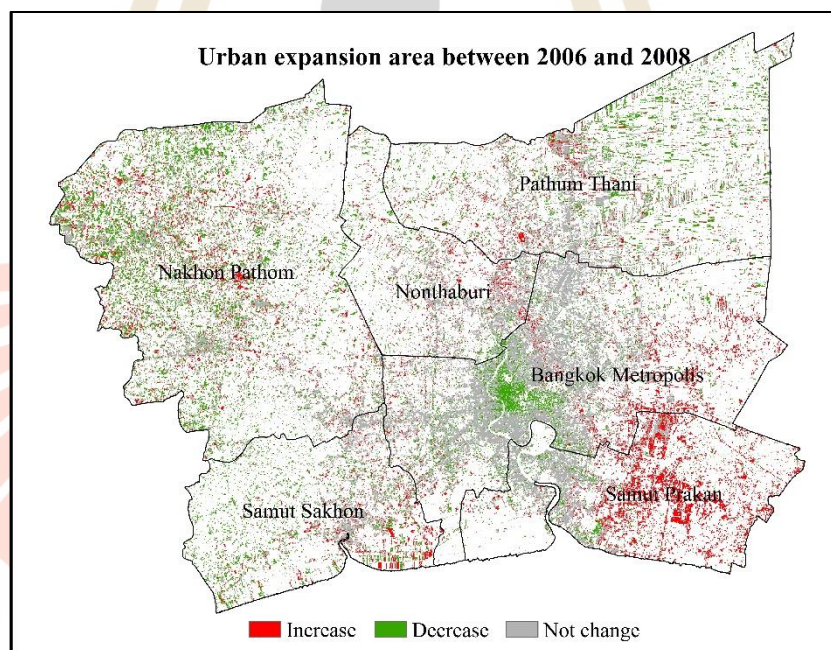
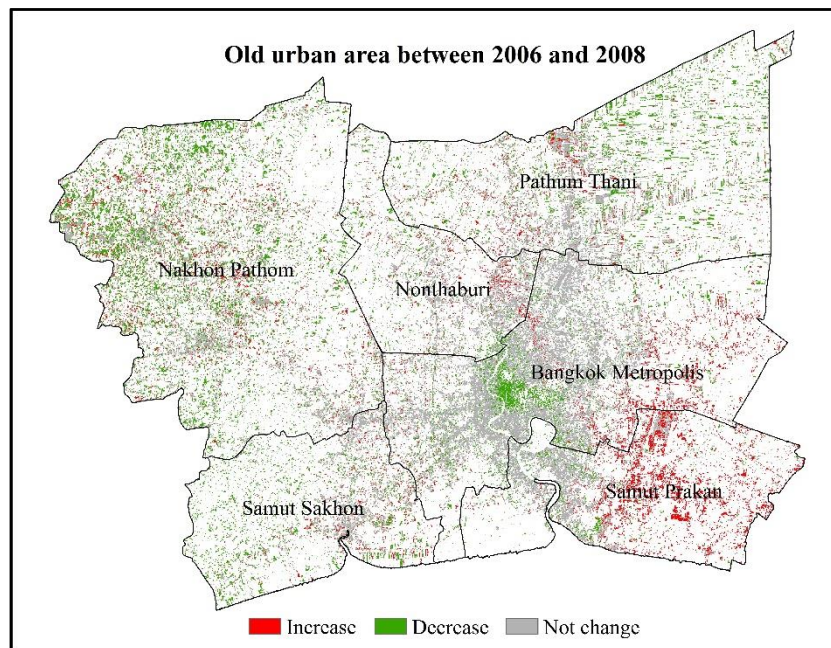
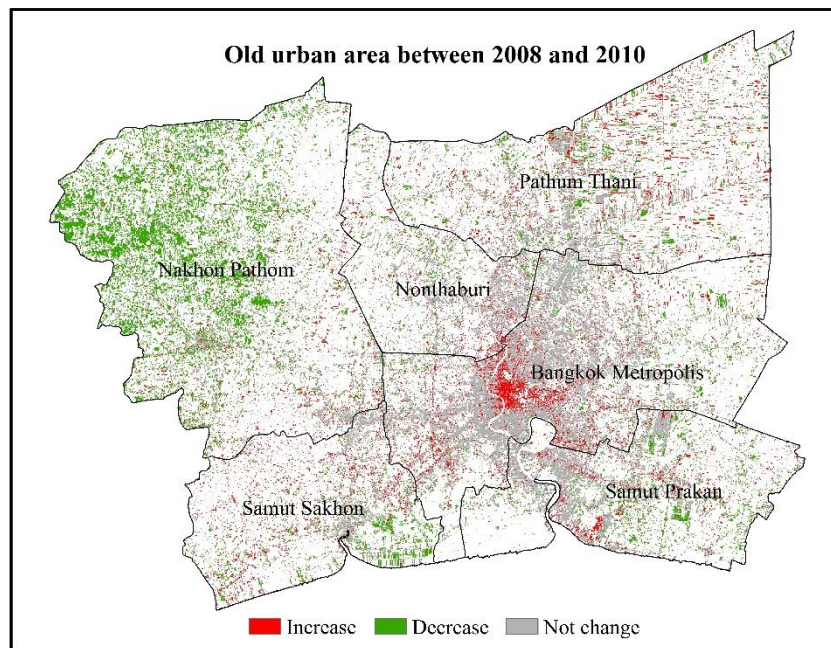
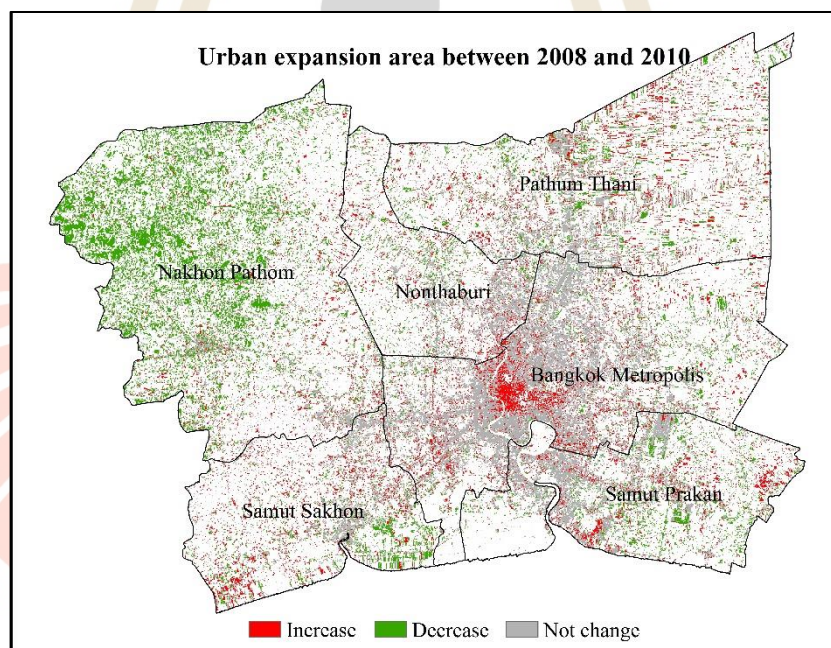


Figure 7.32 Distribution of unchanged, increase and decrease areas of BT temperature grades in old urban and urban expansion between 2006 and 2008: (a) Old urban and (b) Urban expansion.

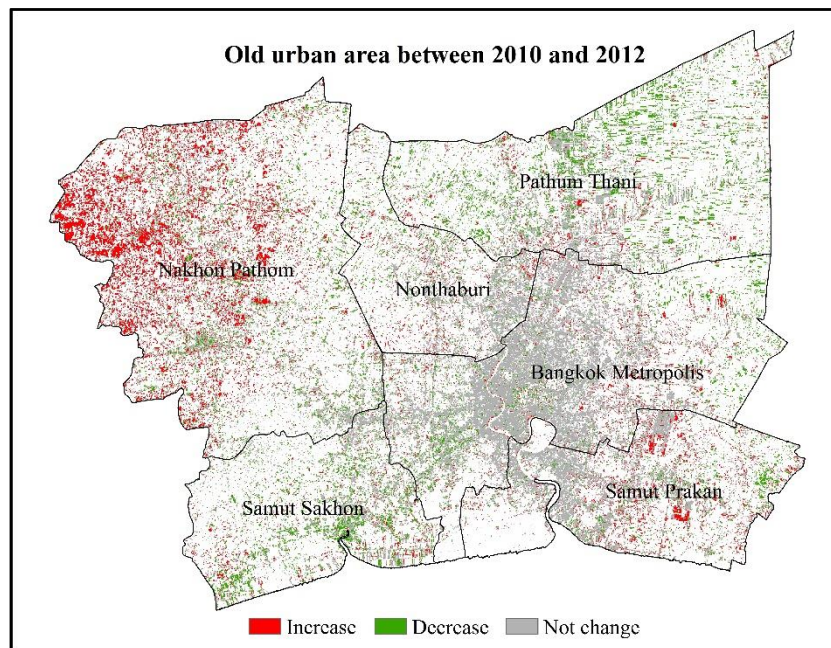


(a)

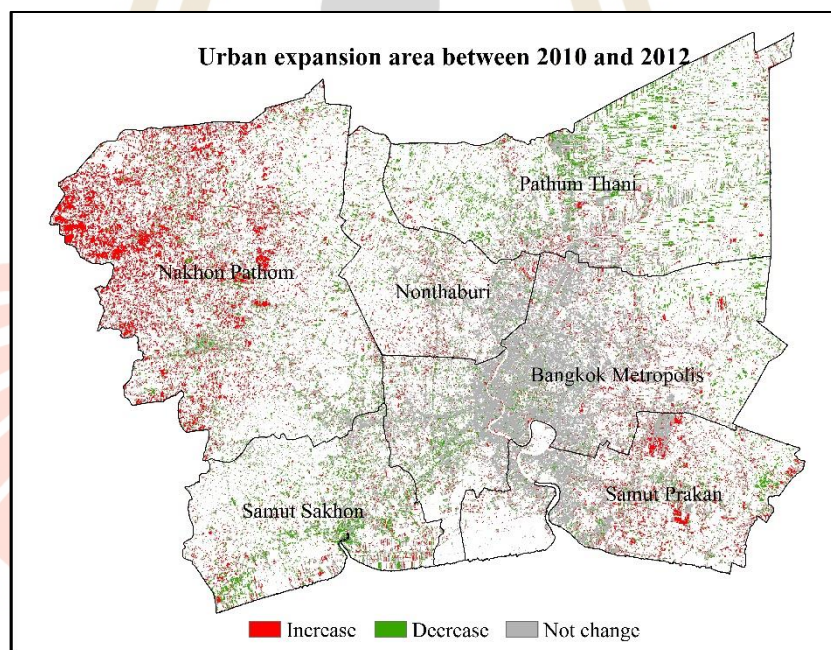


(b)

Figure 7.33 Distribution of unchanged, increase and decrease areas of BT temperature grades in old urban and urban expansion between 2008 and 2010: (a) Old urban and (b) Urban expansion.



(a)



(b)

Figure 7.34 Distribution of unchanged, increase and decrease areas of BT temperature grades in old urban and urban expansion between 2010 and 2012: (a) Old urban and (b) Urban expansion.

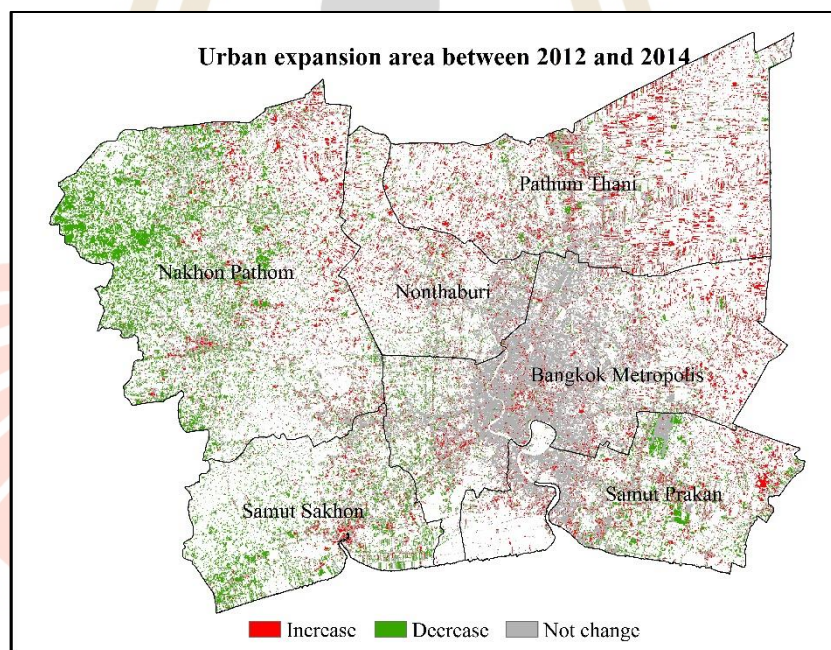
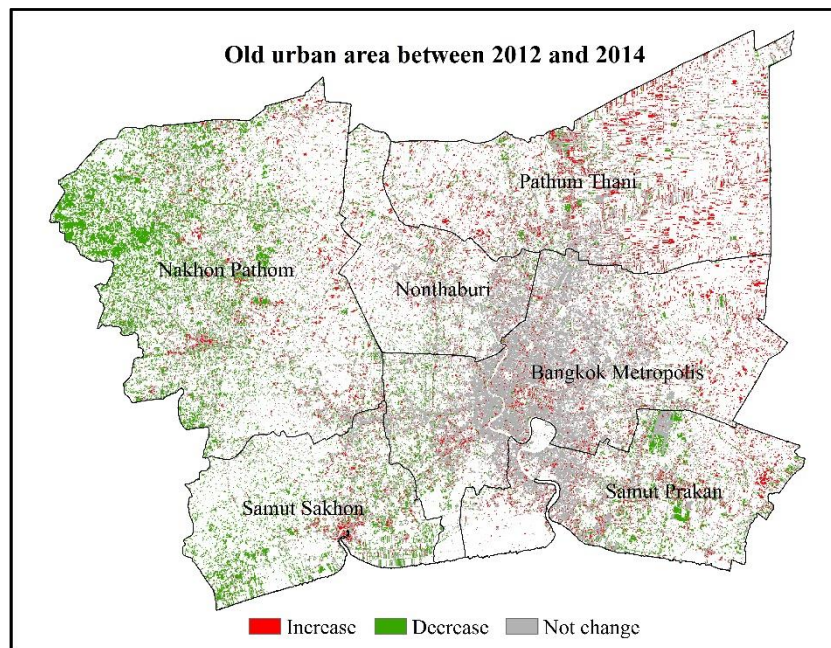
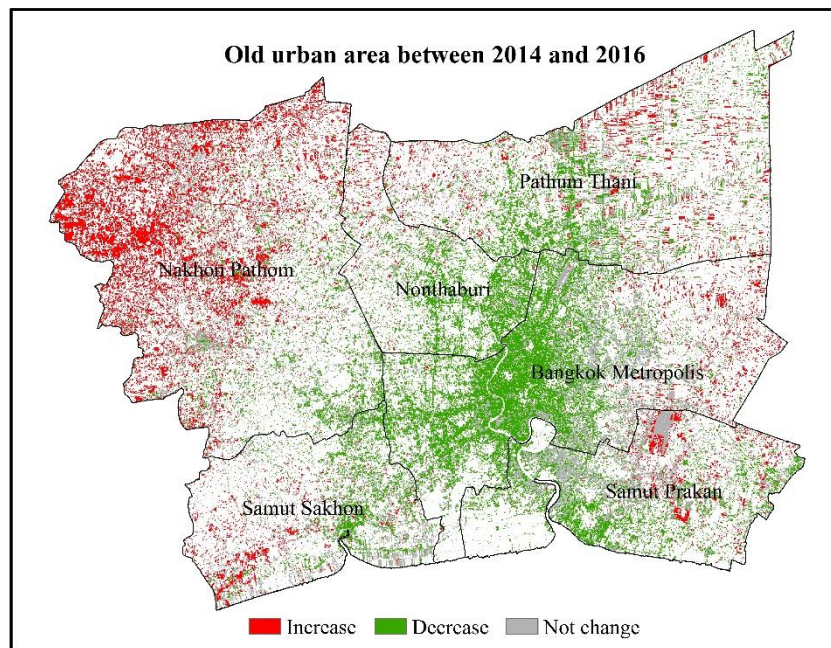
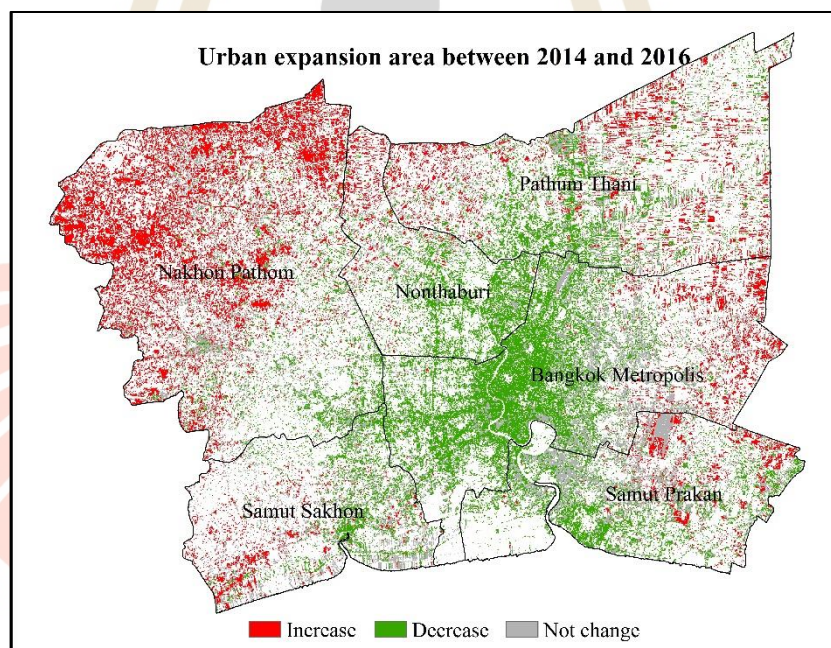


Figure 7.35 Distribution of unchanged, increase and decrease areas of BT temperature grades in old urban and urban expansion between 2012 and 2014: (a) Old urban and (b) Urban expansion.

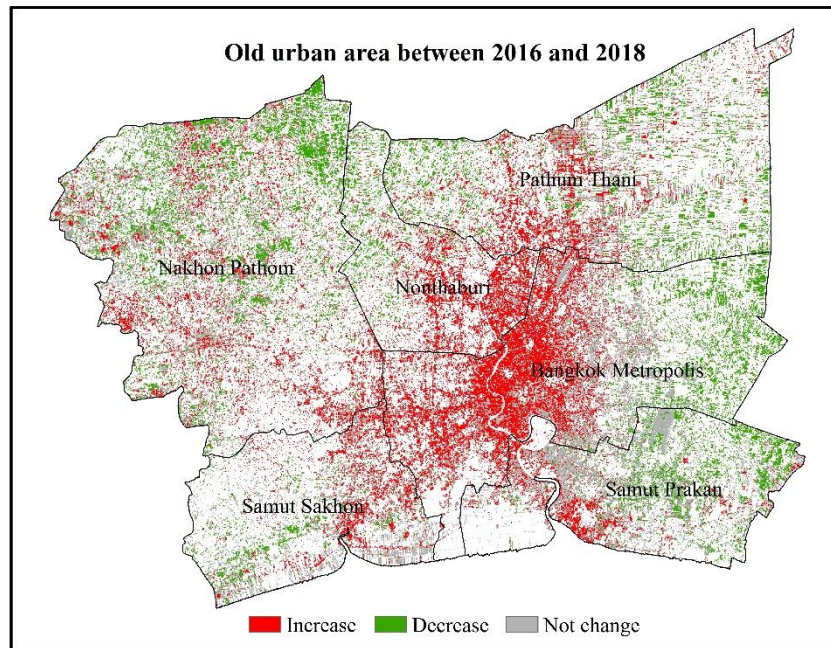


(a)

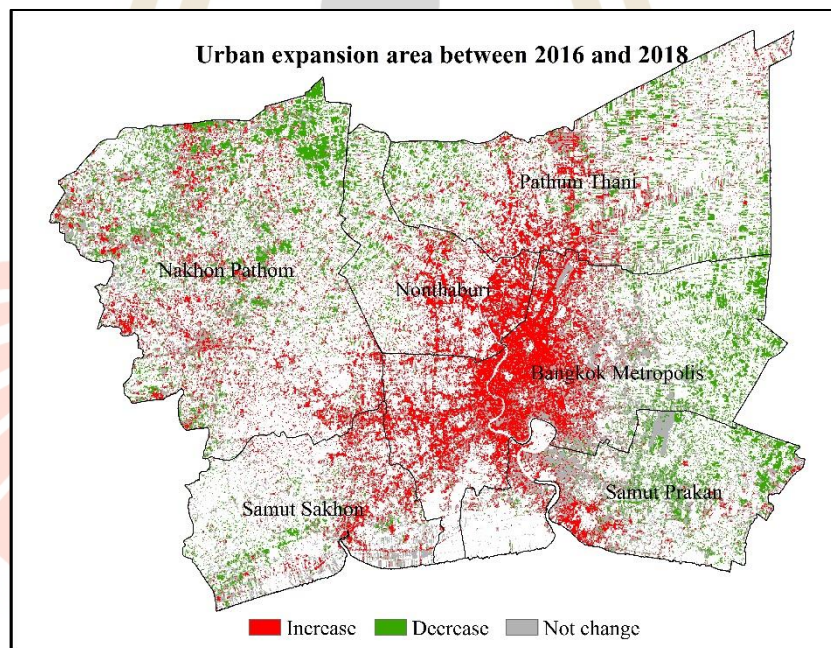


(b)

Figure 7.36 Distribution of unchanged, increase and decrease areas of BT temperature grades in old urban and urban expansion between 2014 and 2016: (a) Old urban and (b) Urban expansion

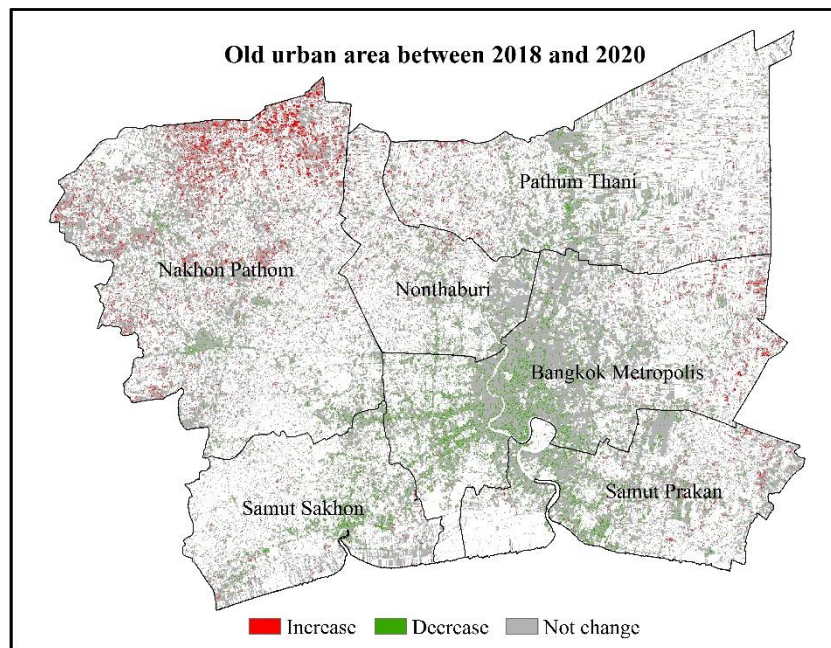


(a)

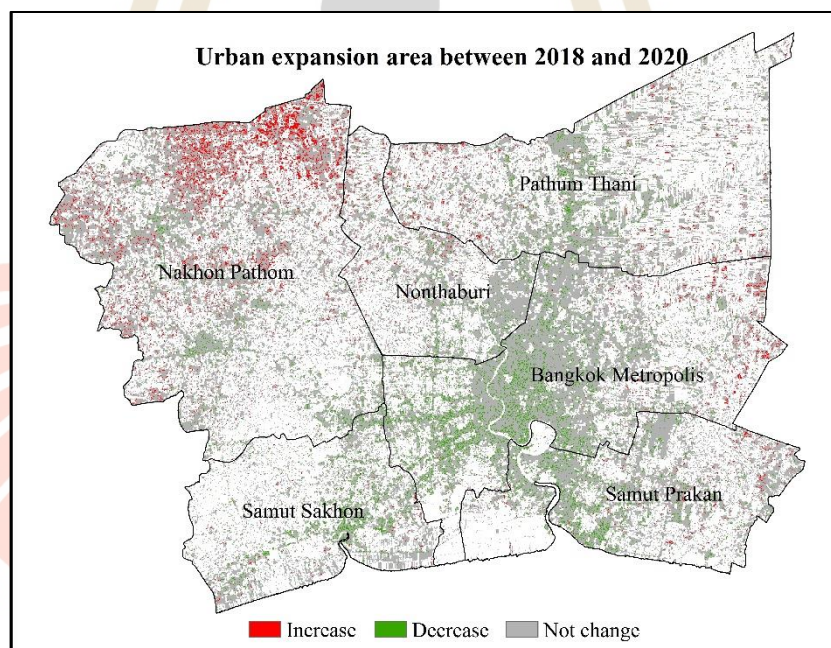


(b)

Figure 7.37 Distribution of unchanged, increase and decrease areas of BT temperature grades in old urban and urban expansion between 2016 and 2018: (a) Old urban and (b) Urban expansion.



(a)



(b)

Figure 7.38 Distribution of unchanged, increase and decrease areas of BT temperature grades in old urban and urban expansion between 2018 and 2020: (a) Old urban and (b) Urban expansion.

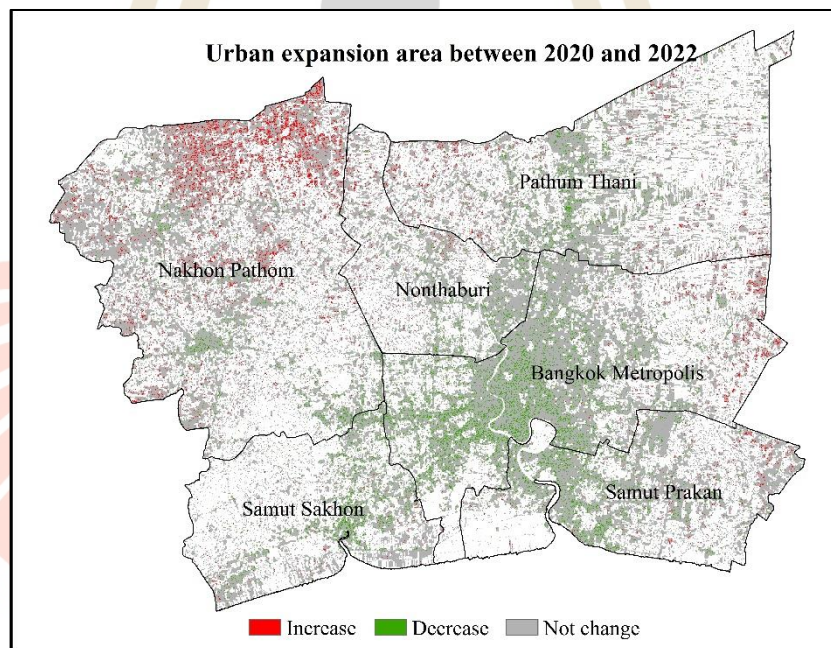
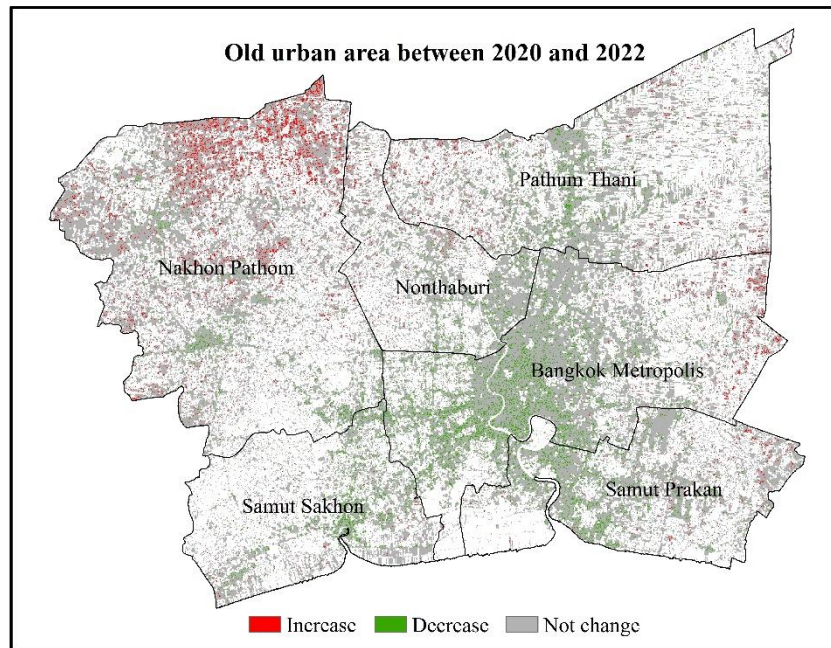
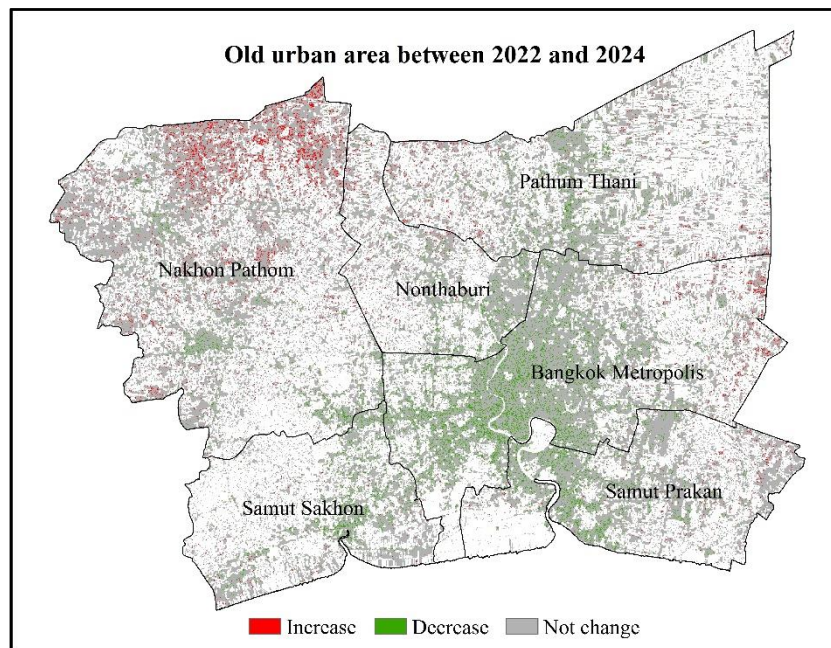
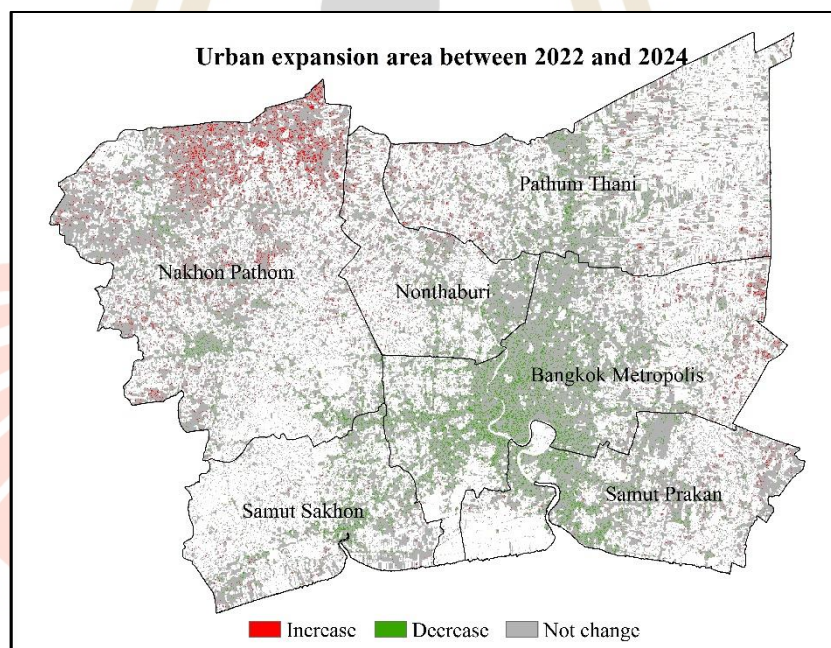


Figure 7.39 Distribution of unchanged, increase and decrease areas of BT temperature grades in old urban and urban expansion between 2020 and 2022: (a) Old urban and (b) Urban expansion.

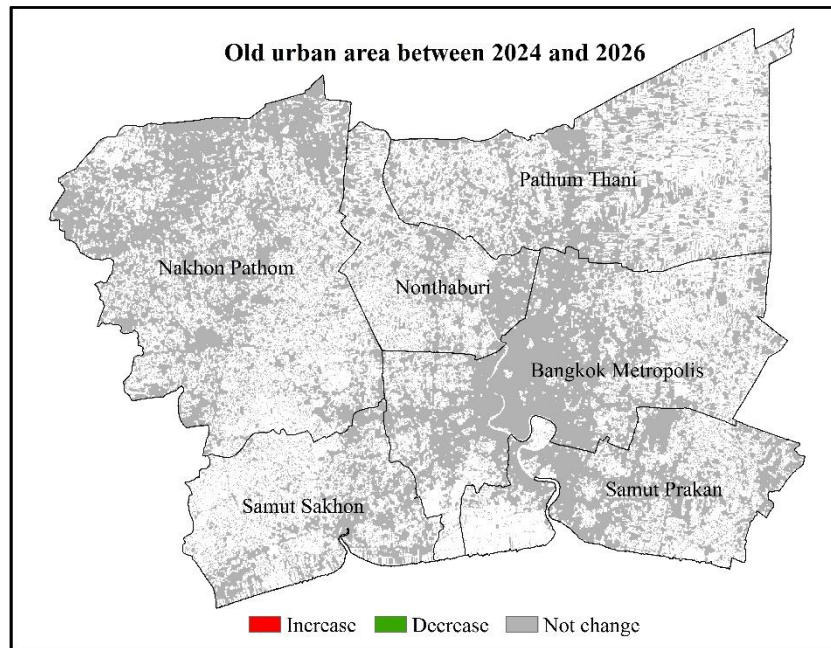


(a)

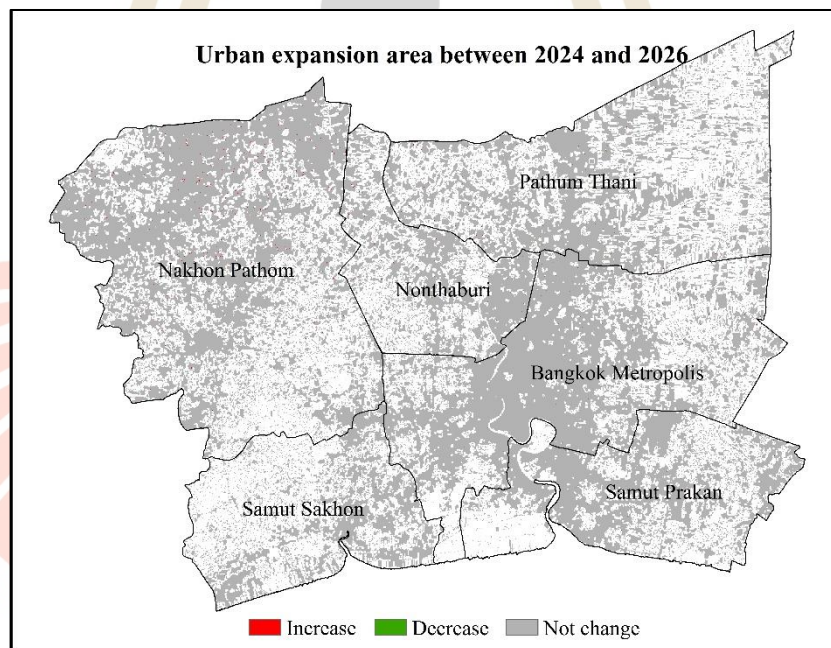


(b)

Figure 7.40 Distribution of unchanged, increase and decrease areas of BT temperature grades in old urban and urban expansion between 2022 and 2024: (a) Old urban and (b) Urban expansion



(a)



(b)

Figure 7.41 Distribution of unchanged, increase and decrease areas of BT temperature grades in old urban and urban expansion between 2024 and 2026: (a) Old urban and (b) Urban expansion.

As results, a systematic summary of quantitative analysis can be separately reported in each period in the following sections.

During 2006 and 2008, the area of the old urban in 2006 that BT grade did not change was 1,013.38 km² or 58.39% of old urban area. Meanwhile, the area of the old urban in 2006 that BT grade increase was 263.48 km² or 15.18% of old urban area and BT grade decrease was 458.76 km² or 26.43% of old urban area. In the same period, the area of the urban expansion that BT grade did not change was 134.24 km² or 44.29% of urban expansion. Meanwhile, the area of the urban expansion that BT grade increase was 130.13 km² or 42.93% of urban expansion and BT grade decrease was 38.73 km² or 12.78% of urban expansion. In this period, the area of the urban expansion that BT grade increase was taken place in Samut Prakarn province.

During 2008 and 2010, the area of the old urban in 2008 that BT grade did not change was 1,126.55 km² or 55.26% of old urban area. Meanwhile, the area of the old urban in 2008 that BT grade increase was 322.07 km² or 15.80% of old urban area and BT grade decrease was 590.13 km² or 28.95% of old urban area. In the same period, the area of the urban expansion that BT grade did not change was 61.31 km² or 35.92% of urban expansion. Meanwhile, the area of the urban expansion that BT grade increase was 84.41 km² or 49.45% of urban expansion and BT grade decrease was 24.98 km² or 14.63% of urban expansion. In this period, the area of the urban expansion that BT grade increase was taken place in Bangkok province.

During 2010 and 2012, the area of the old urban in 2010 that BT grade did not change was 1,371.24 km² or 62.06% of old urban area. Meanwhile, the area of the old urban in 2010 that BT grade increase was 449.32 km² or 20.34% of old urban

area and BT grade decrease was 388.90 km² or 17.60% of old urban area. In the same period, the area of the urban expansion that BT grade did not change was 75.48 km² or 44.38% of urban expansion. Meanwhile, the area of the urban expansion that BT grade increase was 80.16 km² or 43.13% of urban expansion and BT grade decrease was 14.43 km² or 8.48% of urban expansion. In this period, the area of the urban expansion that BT grade increase was taken place in Nakhon Pathom province.

During 2012 and 2014, the area of the old urban in 2012 that BT grade did not change was 1,380.58 km² or 58.02% of old urban area. Meanwhile, the area of the old urban in 2012 that BT grade increase was 386.65 km² or 16.25% of old urban area and BT grade decrease was 612.27 km² or 25.73% of old urban area. In the same period, the area of the urban expansion that BT grade did not change was 101.23 km² or 39.09% of urban expansion. Meanwhile, the area of the urban expansion that BT grade increase was 126.91 km² or 49.01% of urban expansion and BT grade decrease was 30.82 km² or 11.90% of urban expansion. In this period, the area of the urban expansion that BT grade increase was taken place in Pathumthani province.

During 2014 and 2016, the area of the old urban in 2014 that BT grade did not change was 883.55 km² or 33.49% of old urban area. Meanwhile, the area of the old urban in 2014 that BT grade increase was 682.35 km² or 35.86% of old urban area and BT grade decreased was 1,072.58 km² or 40.65% of old urban area. In the same period, the area of the urban expansion that BT grade did not change was 42.00 km² or 16.33% of urban expansion. Meanwhile, the area of the urban expansion that BT grade increase was 200.24 km² or 77.87% of urban expansion and BT grade

decrease was 14.91 km² or 5.80% of urban expansion. In this period, the area of the urban expansion that BT grade increase was taken place in Nakhon Pathom province.

During 2016 and 2018, the area of the old urban in 2016 that BT grade did not change was 1,247.14 km² or 43.07% of old urban area. Meanwhile, the area of the old urban in 2016 that BT grade increase was 956.92 km² or 33.05% of old urban area and BT grade decrease was 691.53 km² or 23.88% of old urban area. In the same period, the area of the urban expansion that BT grade did not change was 96.22 km² or 36.65% of urban expansion. Meanwhile, the area of the urban expansion that BT grade increase was 96.48 km² or 39.76% of urban expansion and BT grade decrease was 49.98 km² or 20.60% of urban expansion. In this period, the area of the urban expansion that BT grade increase was taken place in Bangkok province.

During 2018 and 2020, the area of the old urban in 2018 that BT grade did not change was 2,766.44 km² or 88.15% of old urban area. Meanwhile, the area of the old urban in 2018 that BT grade increase was 149.20 km² or 4.75% of old urban area and BT grade decrease was 222.61 km² or 7.09% of old urban area. In the same period, the area of the urban expansion that BT grade did not change was 193.11 km² or 87.57% of urban expansion. Meanwhile, the area of the urban expansion that BT grade increase was 17.86 km² or 8.10% of urban expansion and BT grade decrease was 9.56 km² or 4.34% of urban expansion. In this period, the area of the urban expansion that BT grade increase was taken place in Nakhon Pathom province.

During 2020 and 2022, the area of the old urban in 2020 that BT grade did not change was 3,002.25 km² or 89.47% of old urban area. Meanwhile, the area of the old urban in 2020 that BT grade increase was 131.76 km² or 3.93% of old urban

area and BT grade decrease was 221.64 km² or 6.60% of old urban area. In the same period, the area of the urban expansion that BT grade did not change was 122.85 km² or 90.11% of urban expansion. Meanwhile, the area of the urban expansion that BT grade increase was 5.69 km² or 4.17% of urban expansion and BT grade decrease was 7.80 km² or 5.72% of urban expansion. In this period, the area of the urban expansion that BT grade increase was taken place in Nakhon Pathom province.

During 2022 and 2024, the area of the old urban in 2022 that BT grade did not change was 3,168.77 km² or 90.74% of old urban area. Meanwhile, the area of the old urban in 2022 that BT grade increase was 109.70 km² or 3.14% of old urban area and BT grade decreased was 213.50 km² or 6.11% of old urban area. In the same period, the area of the urban expansion that the BT grade did not change was 116.36 km² or 92.39% of urban expansion. Meanwhile, the area of the urban expansion that BT grade increase was 6.22 km² or 4.94% of urban expansion and BT grade decrease was 3.36 km² or 2.67% of urban expansion. In this period, the area of the urban expansion that BT grade increase was taken place in Nakhon Pathom province.

During 2024 and 2026, the area of the old urban in 2024 that BT grade did not change was 3,617.84 km² or 100% of old urban area. In the same period, the area of the urban expansion that BT grade did not change was 194.20 km² or 94.26% of urban expansion. Meanwhile, the area of the urban expansion that BT grade increase was 7.44 km² or 3.61% of urban expansion and BT grade decrease was 4.39 km² or 2.13% of urban expansion.

In summary, between 2006 and 2016 as historical and recent periods, the area of the increased change of BT grade in old urban was higher than the area of the

decreased change of BT grade occurs only one period during 2010 to 2012. Likewise, in the future between 2016 and 2026, the area of the increased change of BT grade in old urban was higher than the area of the decreased change of BT grade occurs only one period during 2016 to 2018.

In contrast, in urban expansion the area of the increased change of BT grade of all periods between 2006 and 2016 were higher than the area of the decreased change of BT grade. Similarly, most of all periods in the future between 2016 and 2026, the area of the increased change of BT grade in urban expansion were higher than the area of the decreased change of BT grade, except during 2020-2024.

7.5.2 Overall analysis of UHI change

According to Tables 7.15 to 7.34 whether in old urban region or urban expansion region, the brightness temperature grades in both areas change among the classes. In order to reflect the overall change in temperature is increased or decreased, the Temperature Grade Change-Index (TGCI) as suggested by Xu, Chen, Dan, and Qiu (2011) is here calculated using Equation 3.12.

The TGCI values of overall change in temperature in old urban and urban expansion in each period is presented in Table 7.37 and Figure 7.42.

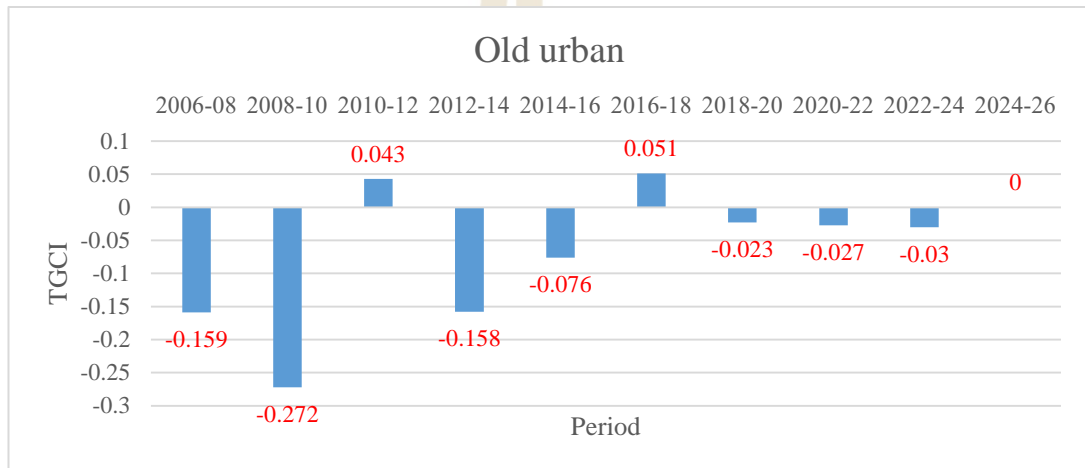
Table 7.37 TGCI value of overall change in temperature in old urban and urban expansion in each period.

Year	Old urban	Expansion urban
2006-2008	-0.159	0.586
2008-2010	-0.272	0.607
2010-2012	0.043	0.648
2012-2014	-0.158	0.591
2014-2016	-0.076	1.572
2016-2018	0.051	0.196
2018-2020	-0.023	0.038
2020-2022	-0.027	-0.016
2022-2024	-0.030	0.023
2024-2026	0.000	0.015

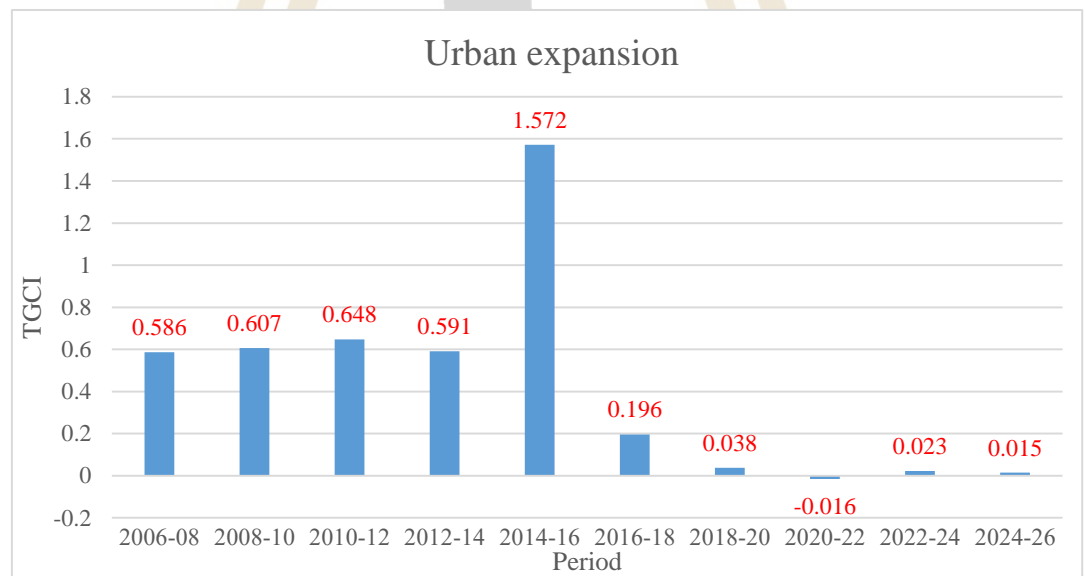
As results, most of all periods between 2006 and 2016 as historical and recent periods for old urban it shows that increasing trend of temperature grade change is weaker than decreasing trend, except during 2010 to 2012 and change trend of temperature grade change performances overall decreasing. Likewise, most of periods between 2016 and 2026 as future periods for old urban it reveals that increasing trend of temperature grade change is also weaker than decreasing trend, except during 2016 to 2018 and change trend of temperature grade change performances overall decreasing.

On contrary, all periods between 2006 and 2016 for urban expansion it shows that increasing trend of temperature grade change is stronger than decreasing trend, and change trend of temperature grade change performances overall increasing. Likewise, most of all periods between 2016 and 2026 for urban expansion it reveals that increasing trend of temperature grade change is also greater than decreasing trend,

except during 2020 to 2022 and change trend of temperature grade change performances overall increasing.



(a)



(b)

Figure 7.42 Dynamic TGCI value of overall change in temperature in old urban (a) and urban expansion (b) in each period.

CHAPTER VIII

CONCLUSION AND RECOMMENDATION

Under this chapter, major results according to objectives of the study, which were reported in Chapters IV to VII, are here separately concluded and recommendations for future research and development are suggested.

8.1 Conclusion

8.1.1 Local principal influential factors on temperature pattern

According to factor analysis and spatial linear analysis, top three significant influential factors on temperature pattern Thailand consisted of biophysical factor (NDVI, NDBI, elevation, and MNDWI) and environmental factor (PM₁₀, CO, and SO₂).

8.1.2 Optimum geostatistical method for in situ mean temperature interpolation

An optimum univariate geostatistics method for mean temperature interpolation from in situ data of TMD over Thailand was OK or UK. Both methods provided MAE, MRE and RMSE with same value in each month. Meanwhile, an optimum multivariate geostatistical method for mean temperature interpolation from in situ data of TMD was SCK method. In addition, according to AIC evaluation, an optimum geostatistics method for mean temperature interpolation from in situ data of

TMD over Thailand was OK or UK. Finally, it can be further concluded that UK method is the most suitable method for monthly mean temperature interpolation from TMD data since it fits with UHI phenomena studies in this research.

8.1.3 Land surface temperature extraction and prediction

LST data between 2006 and 2016 of Bangkok Metropolitan and its vicinity were successfully extracted using single channel method and the extracted LST were refined using simple linear regression analysis based on in situ mean temperature of TMD. Herewith, satellite-based LST data in this period showed positively correlation with in situ mean temperature data with R values between 0.8424 and 0.9357 and R^2 values between 0.7096 and 0.8756. This refined LST data were further applied to predict LST data between 2018 and 2026 using Trend Analysis function of MS Excel spreadsheet software and Image conversion function of ERDAS Imagine software.

8.1.4 UHI phenomena evaluation and prediction

Urban and non-urban areas between 2006 and 2016 of Bangkok Metropolitan and its vicinity were successfully extracted based on BUI value with overall accuracy between 81.46% and 91.08%. The extracted data were further applied to predict urban and non-urban areas between 2018 and 2026 using CA-Markov model. As a result, urban areas in both periods had been continuously increased. Based on urban and non-urban areas and LST data between 2006 and 2026 of Bangkok Metropolitan and its vicinity, quantitative analysis of UHI phenomena were successfully implemented using WAI, URI, and TGCI.

As results, the WAI as UHI intensity were very strong between 2006 and 2022 and became strong between 2024 and 2026. Meanwhile, URI as degree of UHI

development increased in 2010 and 2016 and suddenly decreased in 2018 and continuously increased between 2020 and 2026. In addition, TGCI values of overall change in temperature in old urban and urban expansion of 2 years period between 2006 and 2026 showed that increasing trend of temperature grade change was weaker than decreasing trend in old urban in almost period, except during 2010 - 2012 and 2016 - 2018. On contrary, increasing trend of temperature grade change was stronger than decreasing trend in urban expansion in almost period, except during 2020 - 2022.

In conclusion, it appears that factor analysis can be used as an efficiently tools to extract significant local influential factors on mean temperature pattern of Thailand. In addition, WAI, URI, and TGCI can be used as UHI indices to evaluate and predict UHI phenomena of Bangkok Metropolitan and its vicinity based on extracted and predicted satellite-based LST data and urban an non-urban areas.

8.2 Recommendation

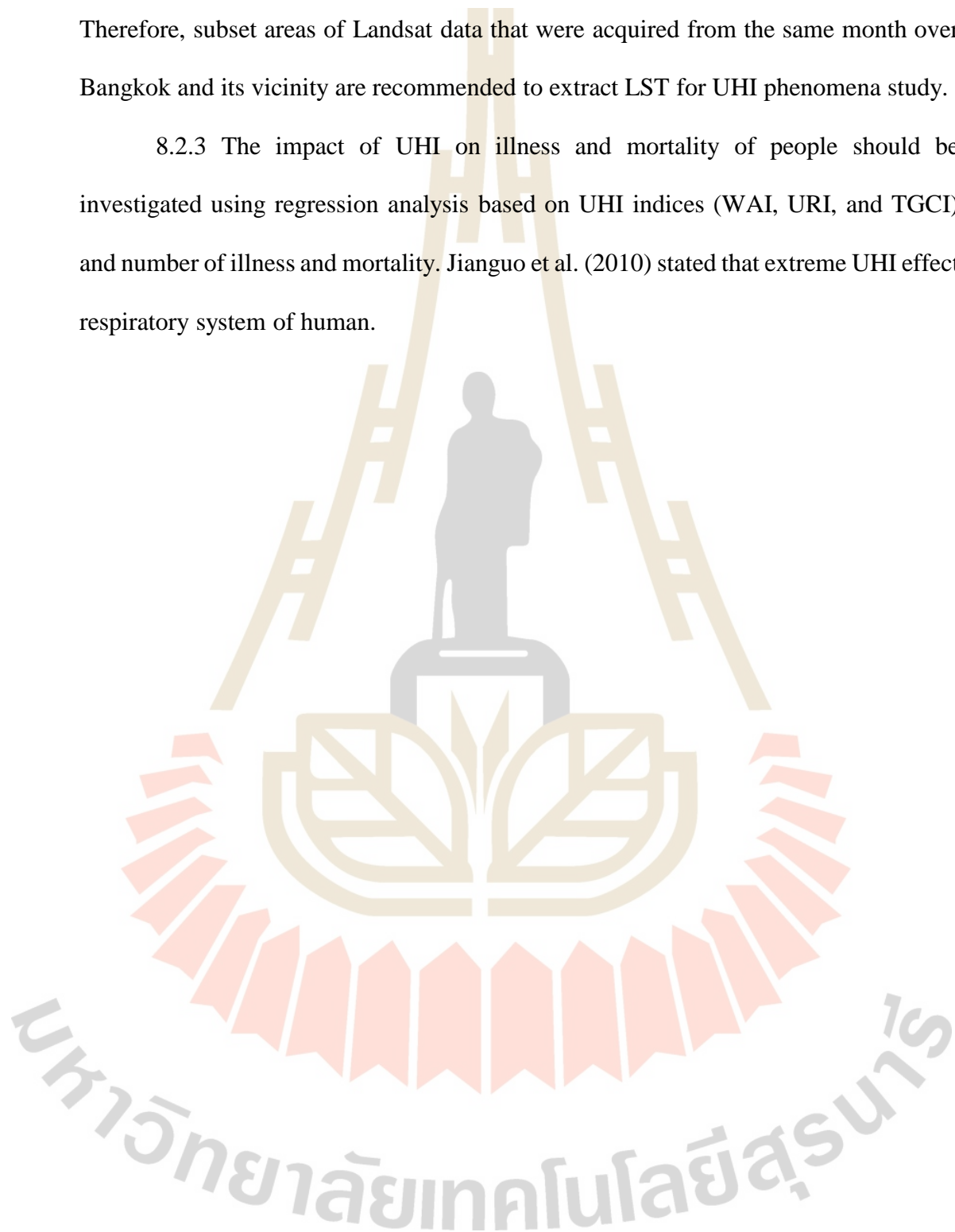
Many objectives were here investigated and implemented, the possibly expected recommendations could be made for further studies as following.

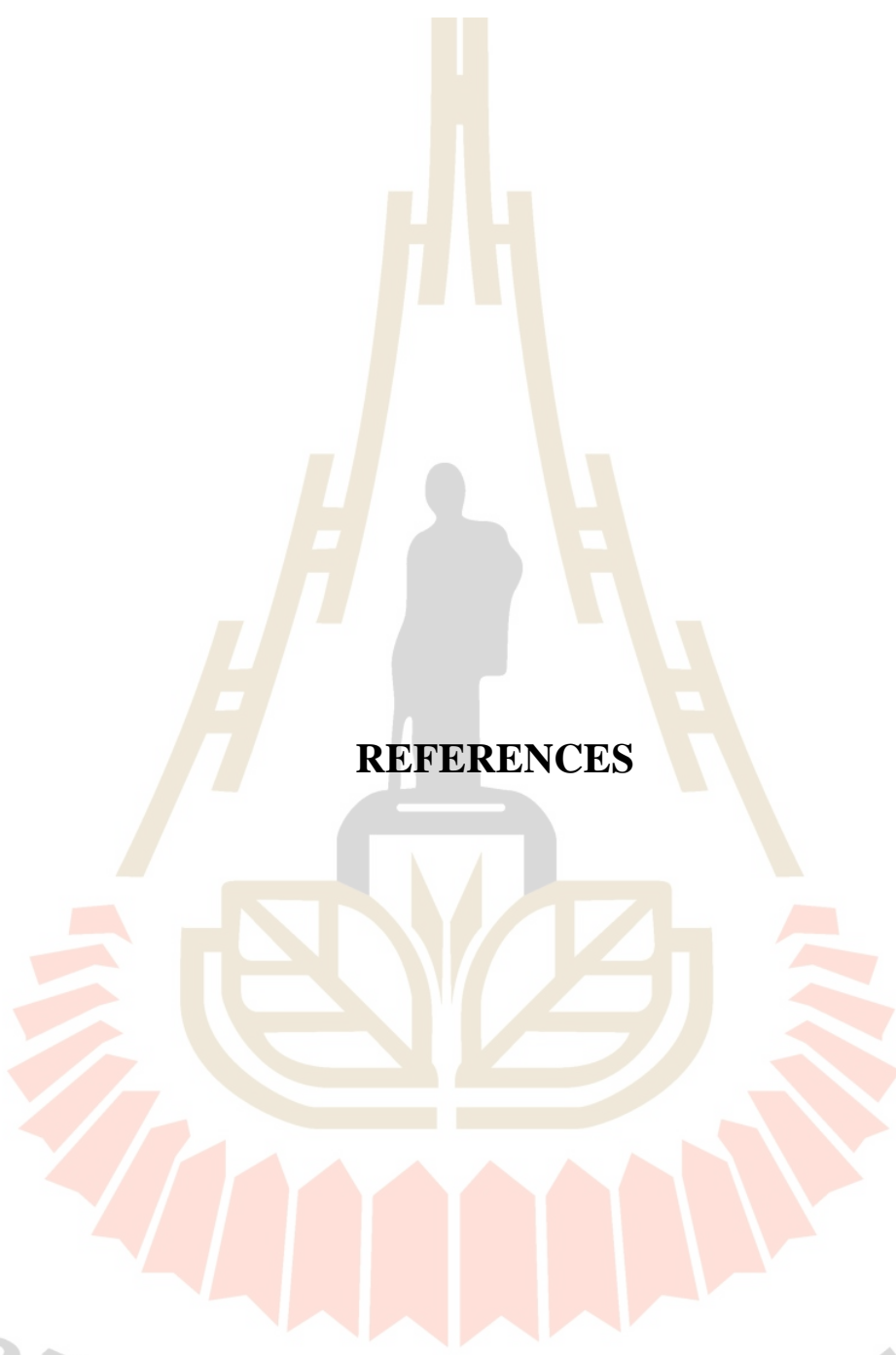
8.2.1 Influential factors on mean temperature pattern should be tested in another area for verification and validation of the influential factors. Particularly, MNDWI, NDVI, elevation, and aspect that showed positively correlation with LST in simple linear equations should be examined in form of multiple linear equation or simple non-linear equation. Because the relationship between these factors with LST should be negatively correlation.

8.2.2 Due to variation of percentage cloud covering during November to April over Bangkok and its vicinity between 2006 and 2016, representative Landsat data

between 2006 and 2016 for LST extraction could not be selected from the same month. Therefore, subset areas of Landsat data that were acquired from the same month over Bangkok and its vicinity are recommended to extract LST for UHI phenomena study.

8.2.3 The impact of UHI on illness and mortality of people should be investigated using regression analysis based on UHI indices (WAI, URI, and TGCI) and number of illness and mortality. Jianguo et al. (2010) stated that extreme UHI effect respiratory system of human.





REFERENCES

มหาวิทยาลัยเทคโนโลยีสุรนารี

REFERENCES

- Aguiar, R., Oliveira, M., and Goncalves, H. (2002). Climate change impacts on the thermal performance of Portuguese buildings: Results of the SIAM study. **Building service engineers research and technology**. 23(4): 223-231.
- Ahrens, C. D., and Henson, R. (2015) **Meteorology today: An introduction to weather, climate, and the environment** (10th ed.). United States of America: Cengage Learning.
- Akaike, H. (1974). A new look at the statistical model identification. **IEEE transactions on Automatic control**. 19: 716-723.
- Annenberg Foundation. (2017). **Atmospheric Pollution** [On-line]. Available: <https://www.learner.org/courses/envsci/unit/text.php?unit=11&secNum=2>.
- Arnfield, J. A. (2003). Two decades of urban climate research: a review of turbulence, exchanges of energy and water, and the urban heat island. **International journal of climatology**. 23: 1-26.
- Artis, D. A., and Carnahan W. H. (1982). Survey of emissivity variability in thermography of urban areas. **Remote sensing of environment**. 12(4): 313-329.
- Arvidson, T., Gasch, J., and Goward, A. N. (2001). Landsat 7's long-term acquisition plan-an innovative approach to building a global imagery archive. **Remote sensing of environment**. 78: 13-26.

- Attorre, F., Alfo, M., Sanctis, M. D., Francesconi, F., and Bruno, F. (2007). Comparison of interpolation methods for mapping climatic and bioclimatic variables at regional scale. **International journal of climatology**. 27(13): 1825-1843.
- Bain, D. J., and Brush, G. S. (2004). Placing the pieces: Reconstructing the original property mosaic in a warrant and patent watershed. **Landscape ecology**. 19: 843-856.
- Ballester, F., Corella, D., Pérez Hoyos, S., and Hervás, A. (1996). Air pollution and mortality in Valencia, Spain: a study using the APHEA methodology. **Journal of Epidemiology and Community Medicine**. 50(5): 527-533.
- Balling, R. C., Jr., Gober, P., and Jones, N. (2008). Sensitivity of residential water consumption to variations in climate: an intraurban analysis of Phoenix, Arizona. **Water resources research**. 44: W10401.
- Bhatta, B. (2010). **Analysis of urban growth and sprawl from remote sensing data**. (1 ed.). Advances in geographic information science. Springer-verlag Berlin-Heidelberg.
- Bobak, M., and Roberts, A. (1997). Heterogeneity of air pollution effects is related to average temperature. **British Medical Journal**. 315(7116): 1161-1162.
- Burrough, P. A., and McDonnell, R. A. (1998). **Principles of geographical information Systems**. United Kingdom: Oxford University Press.
- Buyantuyev, A., and Wu, J. (2010). Urban heat islands and landscape heterogeneity: linking spatiotemporal variations in surface temperatures to land-cover and socioeconomic patterns. **Landscape ecology**. 25: 17-33.

- Cao, W., Hu, J. X., and Yu, X. (2009). A study on temperature interpolation methods based on GIS. In **2009 17th international conference on geoinformatics**. Fairfax, United States.
- Castellsague, J., Sunyer, J., Saez, M., and Anto, J. M. (1995). Short-term association between air pollution and emergency room visits for asthma in Barcelona. **Thorax**. 50(10): 1051-1056.
- Chan, C. F., Lebedeva, J., Otero, J., and Richardson, G. (2007). **Urban heat island: A climate change adaptation strategy for Montreal** [On-line]. Available: <https://www.mcgill.ca/urbanplanning/files/urbanplanning/CCAPUHIFinalReport-2007.pdf>.
- Chang W-Y., Dai X-G., and Chen H-W. (2004). A case study of geostatistical interpolation in meteorological fields. **Chinese journal of geophysics**. 47(6): 1104-1112.
- Chen, X-L., Zhao, H-M., Li, P-X., and Yin, Z-Y. (2006). Remote sensing image-based analysis of the relationship between urban heat island and land use/cover changes. **Remote sensing of environment**. 104: 133-146.
- Chiras, D. D. (2014). **Human biology**. United States of America: Jones and Bartlett Learning.
- Chowdhury, E. H., and Hassan, Q. K. (2015). Operational perspective of remote sensing-based forest fire danger forecasting systems. **ISPRS journal of photogrammetry and remote sensing**. 104: 224-236
- Climate central. (2017). **Stagnant Air on the Rise, Upping Ozone Risk** [On-line]. Available: <http://www.climatecentral.org/news/stagnation-air-conditions-on-the-rise-20600>.

- Comrey, J., and Lee, H. B. (1992). *A First Course in Factor Analysis*. 2nd edition. New Jersey: Erlbaum Hillsdale. Quoted in Li, G., and Weng, Q. (2007). Measuring the quality of life in city of Indianapolis by integration of remote sensing and census data. **International Journal of Remote Sensing**. 28(2): 249-267.
- Dan, S., Xu, H., Xue, W., He, J., and Dan, B. (2010). Comparison and analysis of research methods for urban heat island effects based on Landsat TM6. In **2010 Second IITA international conference on geoscience and remote sensing** (pp. 161-164). IEEE.
- Department of Provincial Administration (DOPA). (2016). **Population in Thailand** [On-line]. Available: http://stat.dopa.go.th/stat/xstat/new/POPHSE/stat_t57.txt.
- Eldrandaly, K. A., and Abu-Zaid, M. S. (2011). Comparison of six GIS-based spatial interpolation methods for estimating air temperature in western Saudi Arabia. **Journal of environmental informatics**. 18(1): 38-45.
- El-Magd, I. A., Ismail, A., and Zanaty, N. (2016). Spatial Variability of Urban Heat Islands in Cairo City, Egypt using Time Series of Landsat Satellite Images. **International Journal of Advanced Remote Sensing and GIS**. 5(3): 1618-1638.
- Environmental Change Network (ECN). (2016). **Climate** [On-line]. Available: <http://www.ecn.ac.uk/what-we-do/education/tutorials-weather-climate/climate/factor-affecting-climate>.
- Environmental Protection Agency (EPA). (2008). **Reducing urban heat islands: compendium of strategies urban heat island basics** [On-line]. Available: <https://www.epa.gov/heat-islands/heat-island-compendium>.

- Environmental Protection Agency (EPA). (2016). **Heat island climate change and heat islands** [On-line]. Available: <https://www.epa.gov/heat-islands/climate-change-and-heat-islands>.
- Forkes, J. (2010). **Urban heat island mitigation in Canadian communities** [On-line]. Available: <http://deslibris.ca/IDFR/225369>.
- Friel, C. M. (2010). **Notes on factor analysis** [On-line]. Available: <http://www.bama.ua.edu/~jcsenkbeil/gy523/Factor%20Analysis.pdf>.
- Giguère, M. (2009). **Literature review of urban heat island mitigation strategies** [On-line]. Available: http://www.inspq.qc.ca/pdf/publications/1513_UrbanHeatIslandMitigationStrategies.pdf.
- Habing, B. (2003). **Exploratory factor analysis** [On-line]. Available: <http://www.stat.sc.edu/~habing/courses/530EFA.pdf>.
- Hajat, S., Haines, A., Goubet, S., Atkinson, R., and Anderson, H. (1999). Association of air pollution with daily GP consultations for asthma and other lower respiratory conditions in London. **Thorax**. 54(7): 597-605.
- Hale, R. C., Gallo, K. P., and Loveland, T. R. (2008). Influences of specific land use/ land cover conversions on climatological normals of near- surface temperature. **Journal of geophysical research**. 113: D14113.
- Intergovernmental Panel on Climate Change (IPCC). (2002). **Climate change and biodiversity** [On-line]. Available: <https://www.ipcc.ch/pdf/technical-papers/climate-changes-biodiversity-en.pdf>.
- Jaruwan Thongmeesang. (2011). **Parameter analysis of urban heat island in Chiang Mai**. M.S. thesis, Chiang Mai University, Thailand.

- Jianguo, T., Zheng, Y., Tang, X., Guo, C., Li, L., Song, G., Zhen, X., Yuan, D., Kalkstein, A. J., Li, F., and Chen, H. (2010). The urban heat island and its impact on heat waves and human health in Shanghai. **International Journal of Biometeorology**. 54:75-84
- Kachar, H., Vafsian, A. R., Modiri, M., Enayati, H., and Safdari Nezhad, A. R. (2015). Evaluation of spatial and temporal distribution changes of LST using Landsat images (Case study: Tehran). In **international conference on sensors and models in remote sensing and photogrammetry**. Kish Island, Iran.
- Kanokwan Komonveeraket. (2008). **Effects of land cover on urban heat island in Bangkok metropolis**. M.S. thesis, Chulalongkorn University, Thailand.
- Kovalskyy, V., and Roy, D. P. (2013). The global availability of Landsat 5 TM and Landsat 7 ETM+ land surface observations and implications for global 30 m Landsat data product generation. **Remote sensing of environment**. 130: 280-293.
- Kumar, K. S., Bhaskar, P. U., and Padmakumari, K. (2012). Estimation of land surface temperature to study urban heat island effect using landsat ETM+ image. **International journal of engineering science and technology**. 4(2): 807-814.
- Lake, I. R., Hooper, L., Abdelhamid, A., Bentham, G., Boxall, A. B. A., Draper, A., Fairweather-Tait, S., Hulme, M., Hunter, P. R., Nichols, G., and Waldron, K. W. (2012). Climate change and food security: health impacts in developed countries. **Environ health perspect**. 120(11): 1520-1526.
- Land Surface Analysis Satellite Applications Facility. (2015). **Land surface temperature** [On-line]. Available: <http://landsaf.meteo.pt/algorithms.jsp?seltab=0&starttab=0>.

- Li, G., and Weng, Q. (2007). Measuring the quality of life in city of Indianapolis by integration of remote sensing and census data. **International journal of remote sensing**. 28(2): 249-267.
- Li, J., and Heap, A. D. (2008). **A review of spatial interpolation methods for environmental scientists**. Canberra: Geoscience Australia.
- Li, J., and Heap, A. D. (2014). Spatial interpolation methods for environmental scientists: A review. **Environmental modelling and software**. 53: 173-189.
- Li, L., Tan, Y., Ying, S., Yu, Z., Li, Z., and Lan, H. (2014). Impact of land cover and population density on land surface temperature: case study in Wuhan, China. **Journal of applied remote sensing**. 8(1): 084993.
- Li, X., Cheng, G., and Lu, L. (2005). Spatial analysis of air temperature in the Qinghai-Tibet Plateau. **Arctic, Antarctic, and Alpine Research**. 37(2): 246-252.
- Li, Y-Y., Zhanga, H., and Kainz, W. (2012). Monitoring patterns of urban heat islands of the fast-growing Shanghai metropolis, China: Using time-series of Landsat TM/ETM+ data. **International journal of applied earth observation and geoinformation**. 19: 127-138.
- Li, Z-L., Tang, B-H., Wu, H., Ren, H., Yan, G., Wan, Z., Trigo, I. F., and Sobrino, J. A. (2013). Satellite-derived land surface temperature: current status and perspectives. **Remote sensing of environment**. 131: 14-37.
- Liu, L., and Zhang, Y. (2011). Urban Heat Island Analysis Using the Landsat TM Data and ASTER Data: A Case Study in Hong Kong. **Remote sensing**. 3(7):1535-1552.

- Lobell, D. B., and Bonfils, C. (2008). The effect of irrigation on regional temperatures: a spatial and temporal analysis of trends in California. **Journal of climate**. 21(10): 2063-2071.
- Luber, G., McGeehin, M. (2008). Climate change and extreme heat events. **American journal of preventive medicine**. 35(5): 429-435.
- Lutgens F. K., and Tarbuck E. J. (1998). **The atmosphere: An introduction to meteorology** (7th ed.). United States: Prentice-Hall international Inc.
- Ma, Y., Kuang, Y., and Huang, N. (2010). Coupling urbanization analyses for studying urban thermal environment and its interplay with biophysical parameters based on TM/ETM+ imagery. **International journal of applied earth observation and geoinformation**. 12: 110-118.
- Magee, N., Curtis, J., and Wendler, G. (1999). The urban heat island effect at Fairbanks, Alaska. **Theoretical and applied climatology**. 64: 39-47.
- Mendelsohn, R., Kurukulasuriya, P., Basist, A., Kogan, F., and Williams, C. (2007). Climate analysis with satellite versus weather station data. **Climatic change**. 81: 71-83.
- Michelozzi, P., Forastiere, F., Fusco, D., Tobias, A., and Anto, J. (1998). Air pollution and daily mortality in Rome, Italy. **Occupational and Environmental Medicine**. 55(9): 605-611.
- Mirzaei, P. A., and Haghghat, F. (2010). Approaches to study urban heat island-abilities and limitations. **Building and environment**. 45: 2192-2201.
- Moolgavkar, S. H., Luebeck, E. G., Hall, T. A., and Anderson, E. L. (1995). Air pollution and daily mortality in Philadelphia. **Epidemiology**. 6(5): 476-484.

- Moriyama, M., and Tanaka, T. (2012). The mitigation of UHI intensity through an improved land-use plan in the urban central area: Application to Osaka city, **Journal of heat island institute international**. 7(2): 65-71.
- Mukhopadhyay, P. (2009). **Multivariate statistical analysis**. New Jersey: World Scientific.
- Murphy, D. M. (2005). Something in the air. **Science**. 307: 1888-1890.
- Oke, T. R. (1987). **Boundary Layer Climates** (2^{ed.}). New York: Methuen and Co. Ltd.
- Panudda Tiengrod and Waranyu Wongseree. (2013). A comparison of spatial interpolation methods for surface temperature in Thailand. In **2013 international computer science and engineering conference (ICSEC)** (pp. 179-183). Nakorn Pathom, Thailand.
- Parinya Chayapong. (2010). **Spatial analysis of urban heat island phenomenon and its relationship with land use and land cover and electrical energy consumption: A case study in Bangkok metropolitan area**. Ph.D. Dissertation, Suranaree University of Technology. Thailand.
- Pathompong Sukthong. (2008) **Thermal remote sensing application on urban heat island case study: Pathumthani urban areas**. M. S. thesis, Thammasat University. Thailand.
- Peng, W., Zhou, J., Wen, L., Xue, S., and Dong, L. (2016). Land surface temperature and its impact factors in Western Sichuan Plateau, China. **Geocarto International**. 32(8): 919-934
- Pidwirny, M. (2014). **Understanding physical geography (1st Edition)** [On-line]. Available: <http://www.physicalgeography.net/understanding/contents.html>.

- Poonyanuch Ruthirako, Rotchanatch Darnsawasdi and Wichien Chatupote. (2014). Intensity and pattern of land surface temperature in Hat Yai city, Thailand. **Walailak journal of science and technology**. 12(1): 83-94.
- Potapov, P., Hansen, M. C., Stehman, S. V., Loveland, T. R., and Pittman, K. (2008). Combining MODIS and Landsat imagery to estimate and map boreal forest cover loss. **Remote sensing of environment**. 112: 3708-3719.
- Price, C., Michaelides, S., Pashiardis, S., and Alpert, P. (1999). Long term changes in diurnal temperature range in Cyprus. **Atmospheric research** 51: 85-98.
- Puangporn Puntumakoop. (2001). **Analysis of local meteorological data for an industrial source complex model: a case study of map Ta Phut Industrial Estate, Thailand**. M.S. thesis, Mahidol University, Thailand.
- Qiu, W., Xu, H., and He, Z. (2014). Study on the difference of urban heat island defined by brightness temperature and land surface temperature retrieved by RS technology. **Computer modelling and new technologies**. 18(4): 222-225.
- Roth, M. (2013). Urban Heat Islands. In H. J. S. Fernando (ed.). **Handbook of environmental fluid dynamics** Volume 2 (pp. 143-159). New York: Taylor & Francis Group.
- Roy, S. S., Mahmood, R., Niyogi, D., Lei, M., Foster, S. A., Hubbard, K. G., Douglas, E., and Pielke Sr., R. (2007). Impacts of the agricultural green revolution-induced land use changes on air temperatures in India. **Journal of geophysical research**. 112: D21108.
- Sailor, D. J. (2006). **Mitigation of urban heat islands-Recent progress and future prospects** [On-line]. Available: <http://www.coolrooftoolkit.org/wp-content/uploads/2012/04/Mitigation-of-Urban-Heat-Islands.pdf>.

- Schuermans, J. M., Bierkens, M. F. P., and Pebesma, E. J. (2007). Automatic prediction of high-resolution daily rainfall fields for multiple extents: the potential of operational radar. **Journal of hydrometeorology**. 8: 1204-1224.
- Senanayake, I. P., Welivitiya, W. D. D. P., and Nadeeka, P. M. (2013). Remote sensing based analysis of urban heat islands with vegetation cover in Colombo city, Sri Lanka using Landsat-7 ETM+ data. **Urban Climate**. 5: 19-35.
- Sluiter, R. (2009). **Interpolation methods for climate data: Literature review**. KNMI intern report: Netherlands.
- Taha, H. (1997). Urban climates and heat islands: albedo, evapotranspiration and anthropogenic heat. **Energy and buildings**. 25: 99-103.
- Tewelde, M. G., Beza, T. A., Costa, A. C., and Painho, M. (2010). Comparison of different interpolation techniques to map temperature in the southern region of Eritrea. In **13th AGILE international conference on geographic information science 2010**. Guimarães, Portugal.
- Thai Meteorological Department (TMD). (2016). **Annual Weather Summary** [On-line]. Available: <http://www.tmd.go.th/en/climate.php?FileID=5>.
- Thanakrit Teanmanee. (2002). **Urban Heat Island and Physical Environment**. M.S. thesis. Silpakorn University, Thailand.
- The Center for Innovation in Engineering and Science Education (CIESE). (2017). **Paticulate Matter Primer** [On-line]. Available: <http://ciese.org/curriculum/airproj/pmprimer>.
- Touloumi, G., Katsouyanni, K., Zmirou, D., Schwartz, J., Spix, C., Ponce de Leon, A., Tobias, A., Quennel, P., Rabczenko, D., Bacharova, L., Bisanti, L., Vonk, J. M., and Ponka, A. (1997). Short-term effects of ambient oxidant exposure on

mortality: a combined analysis with APHEA project. **American Journal of Epidemiology**. 146: 177-185.

United Nations, Department of Economic and Social Affairs, Population Division (2006). **World urbanization prospects: The 2005 Revision**. Working Paper No. ESA/P/WP/200.

USGS. (2016). **Landsat 8 (L8) data user handbook** [On-line]. Available: <http://landsat.usgs.gov/documents/Landsat8DataUsersHandbook.pdf>.

Voogt, J. A., and Oke, T. R. (1997). Complete Urban Surface Temperatures. **Journal of applied meteorology**. 36: 1117-1132.

Voogt, J. A. (2002). Urban heat island. **Encyclopedia of global environmental change**. 3: 660-666.

Weng, Q., Liu, H., and Lu, D. (2007). Assessing the effects of land use and land cover patterns on thermal conditions using landscape metrics in city of Indianapolis, United States. **Urban ecosystems**. 10: 203-219.

Wichansky, P. S., Steyaert, L. T., Walko, R. L., and Weaver, C. P. (2008). Evaluating the effects of historical land cover change on summertime weather and climate in New Jersey: Land cover and surface energy budget changes. **Journal of geophysical research**. 113: D10107.

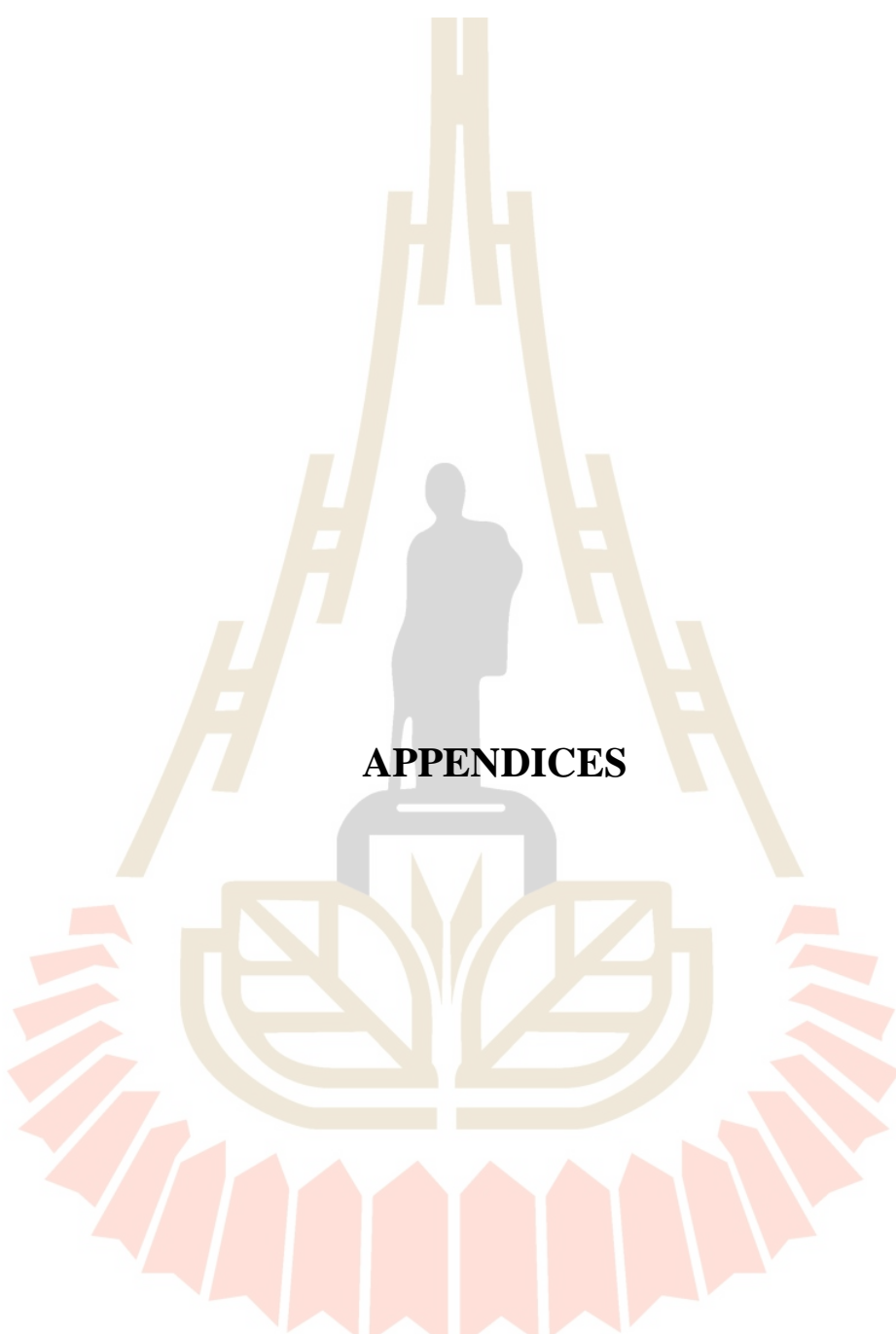
Wong, N. H., and Chen, Y. (2009). **Tropical Urban Heat Islands: Climate, Buildings and Greenery**. London; New York: Taylor & Francis.

Wu, L., Lord, D., Zou, Y. (2015). Validation of crash modification factors derived from cross-sectional studies with regression models. **Transportation Research Record: Journal of the Transportation Research Board**. 2514: 88-96.

- Xiao, R., Weng, Q., Ouyang, Z., Li, W., Schienke, E. W., and Zhang, Z. (2008). Land surface temperature variation and major factors in Beijing, China. **Photogrammetric engineering and remote sensing**. 74(4): 451-461.
- Xu, H. Q., and Chen, B. Q. (2004). Remote sensing of the urban heat island and its changes in Xiamen City of SE China. **Journal of Environmental Science**. 16: 276-281.
- Xu, H., Chen, Y., Dan, S., and Qiu, W. (2011). Dynamical monitoring and evaluation methods to urban heat island effects based on RS&GIS. **Procedia environmental sciences**. 10: 1228-1237.
- Yamamoto, Y. (2006). Measures to mitigate urban heat island. **Quarterly review**. 18: 65-83.
- Yaowaret Jantakat and Suwit Ongsomwang. (2010). Assessing the effect of incorporating topographical data with geostatistical interpolation for monthly rainfall and temperature in ping basin, Thailand. **Suranaree journal of science and technology**. 18(2): 123-139.
- Yolo-Solano Air Quality Management District (Yolo-Solano AQMD). (2016). **Temperature Inversions Impact Air Quality** [On-line]. Available: <http://www.dcn.org/go/ysaqmd/documents/TemperatureInversions.pdf>.
- Yow, D. M. (2007). Urban heat islands: observations, impacts, and adaptation. **Geography compass**. 1(6): 1227-1251.
- Yu, X., Guo, X., and Wu, Z. (2014). Land surface temperature retrieval from Landsat 8 TIRS-comparison between radiative transfer equation-based method, split window algorithm and single channel method. **Remote sensing**. 6: 9829-9852.

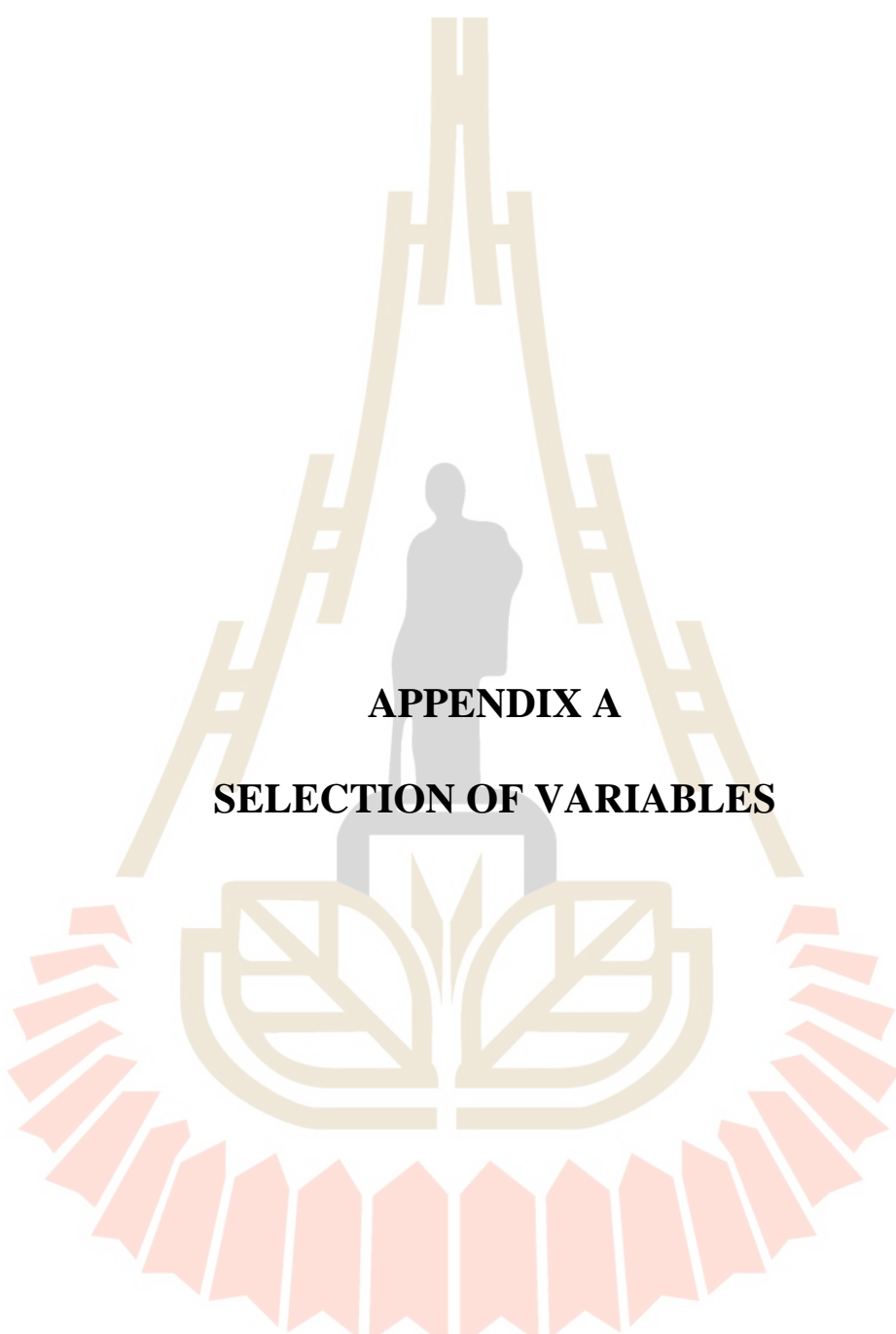
Zha, Y., Gao, J., and Ni, S. (2003). Use of normalized difference built-up index in automatically mapping urban areas from TM imagery. **International journal of remote sensing**. 24(3): 583-594.





APPENDICES

มหาวิทยาลัยเทคโนโลยีสุรนารี



APPENDIX A
SELECTION OF VARIABLES

มหาวิทยาลัยเทคโนโลยีสุรนารี

Table A1 Correlation matrix of 16 variables before variable selection of factor analysis in November, 2015.

November (2015)	Elevation	Slope	Aspect	Distance	Population	Household	NDVI	NDBI	MNDWI	SO ₂	PM ₁₀	O ₃	CO	NO ₂	Insolation	Wind
Elevation	1.00	0.636	0.037	0.182	-0.138	-0.113	0.253	0.004	-0.144	-0.537	-0.56	-0.563	-0.547	-0.527	0.842	-0.567
Slope	0.636	1.00	0.038	-0.074	-0.104	-0.078	0.25	-0.098	-0.058	-0.299	-0.318	-0.326	-0.313	-0.283	0.472	-0.32
Aspect	0.037	0.038	1.00	0.023	-0.03	-0.026	0.046	0.022	-0.043	-0.083	-0.084	-0.083	-0.082	-0.084	0.042	-0.084
Distance	0.182	-0.074	0.023	1.00	-0.095	-0.119	0.084	0.122	-0.267	-0.386	-0.36	-0.313	-0.356	-0.428	0.171	-0.385
Population	-0.138	-0.104	-0.03	-0.095	1.00	0.975	-0.091	0.072	0.044	0.239	0.226	0.216	0.225	0.241	-0.116	0.225
Household	-0.113	-0.078	-0.026	-0.119	0.975	1.00	-0.069	0.068	0.034	0.213	0.198	0.187	0.197	0.217	-0.095	0.196
NDVI	0.253	0.25	0.046	0.084	-0.091	-0.069	1.00	-0.282	-0.72	-0.255	-0.268	-0.274	-0.264	-0.24	0.209	-0.285
NDBI	0.004	-0.098	0.022	0.122	0.072	0.068	-0.282	1.00	-0.381	-0.087	-0.092	-0.086	-0.085	-0.098	-0.032	-0.09
MNDWI	-0.144	-0.058	-0.043	-0.267	0.044	0.034	-0.72	-0.381	1.00	0.288	0.295	0.289	0.287	0.29	-0.106	0.312
SO₂	-0.537	-0.299	-0.083	-0.386	0.239	0.213	-0.255	-0.087	0.288	1.00	0.986	0.967	0.995	0.984	-0.457	0.982
PM₁₀	-0.56	-0.318	-0.084	-0.36	0.226	0.198	-0.268	-0.092	0.295	0.986	1.00	0.986	0.987	0.981	-0.476	0.996
O₃	-0.563	-0.326	-0.083	-0.313	0.216	0.187	-0.274	-0.086	0.289	0.967	0.986	1.00	0.97	0.945	-0.478	0.977
CO	-0.547	-0.313	-0.082	-0.356	0.225	0.197	-0.264	-0.085	0.287	0.995	0.987	0.97	1.00	0.972	-0.464	0.986
NO₂	-0.527	-0.283	-0.084	-0.428	0.241	0.217	-0.24	-0.098	0.29	0.984	0.981	0.945	0.972	1.00	-0.449	0.978
Insolation	0.842	0.472	0.042	0.171	-0.116	-0.095	0.209	-0.032	-0.106	-0.457	-0.476	-0.478	-0.464	-0.449	1.00	-0.482
Wind	-0.567	-0.32	-0.084	-0.385	0.225	0.196	-0.285	-0.09	0.312	0.982	0.996	0.977	0.986	0.978	-0.482	1.00

Table A-2 KMO and Bartlett's Test with 16 variables in November, 2015.

Kaiser-Meyer-Olkin Measure of Sampling Adequacy.		0.682
Approximate Chi-Square		16169097.16
Bartlett's Test of Sphericity	Degree of freedom	120
Significant		0.000

Table A-3 Selection of variables based on communality values in November, 2015.

Variables	Description	First Communality 16 variables	Second Communality 14 variables
Elevation		.893	.904
Slope		.686	.664
Aspect		.012	
Distance	Distance to the sea (m)	.332	
Population	Population density (person/km ²)	.986	.988
Household	Household density (household/ km ²)	.988	.988
NDVI_1511	Normalized Difference Vegetation Index (NDVI) in November, 2015	.983	.983
NDBI_1511	Normalized Difference Built-up Index (NDBI) in November, 2015	.931	.987
MNDWI_1511	Normalized Difference Water Index (NDWI) in November, 2015	.976	.982
SO ₂ _1511	Sulfur dioxide (SO ₂) in November, 2015	.985	.989
PM ₁₀ _1511	Particulates Matter (PM10) in November, 2015	.989	.996
O ₃ _1511	Ozone (O ₃) in November, 2015	.954	.965
CO_1511	Carbon monoxide (CO) in November, 2015	.979	.987
NO ₂ _1511	Nitrogen dioxide (NO ₂) in November, 2015	.975	.972
Inso_1511	Insolation in November, 2015	.764	.782
Wind_1511	Wind speed in November, 2015	.987	.991

Table A-4 Correlation matrix of 14 Variables after variable selection of factor analysis in November, 2015.

November (2015)	Elevation	Slope	Population	Household	NDVI	NDBI	MNDWI	SO ₂	PM ₁₀	O ₃	CO	NO ₂	Insolation	Wind
Elevation	1.000	.636	-.138	-.113	.253	.004	-.144	-.537	-.560	-.563	-.547	-.527	.842	-.567
Slope	.636	1.000	-.104	-.078	.250	-.098	-.058	-.299	-.318	-.326	-.313	-.283	.472	-.320
Population	-.138	-.104	1.000	.975	-.091	.072	.044	.239	.226	.216	.225	.241	-.116	.225
Household	-.113	-.078	.975	1.000	-.069	.068	.034	.213	.198	.187	.197	.217	-.095	.196
NDVI	.253	.250	-.091	-.069	1.000	-.282	-.720	-.255	-.268	-.274	-.264	-.240	.209	-.285
NDBI	.004	-.098	.072	.068	-.282	1.000	-.381	-.087	-.092	-.086	-.085	-.098	-.032	-.090
MNDWI	-.144	-.058	.044	.034	-.720	-.381	1.000	.288	.295	.289	.287	.290	-.106	.312
SO₂	-.537	-.299	.239	.213	-.255	-.087	.288	1.000	.986	.967	.995	.984	-.457	.982
PM₁₀	-.560	-.318	.226	.198	-.268	-.092	.295	.986	1.000	.986	.987	.981	-.476	.996
O₃	-.563	-.326	.216	.187	-.274	-.086	.289	.967	.986	1.000	.970	.945	-.478	.977
CO	-.547	-.313	.225	.197	-.264	-.085	.287	.995	.987	.970	1.000	.972	-.464	.986
NO₂	-.527	-.283	.241	.217	-.240	-.098	.290	.984	.981	.945	.972	1.000	-.449	.978
Insolation	.842	.472	-.116	-.095	.209	-.032	-.106	-.457	-.476	-.478	-.464	-.449	1.000	-.482
Wind	-.567	-.320	.225	.196	-.285	-.090	.312	.982	.996	.977	.986	.978	-.482	1.000

Table A-5 KMO and Bartlett's Test with 14 variables in November, 2015.

Kaiser-Meyer-Olkin Measure of Sampling Adequacy.	0.677
Bartlett's Test of Sphericity	Approximate Chi-Square
	15805766.90
	Degree of freedom
	91
	Significant
	0.000

Table A-6 Correlation matrix of 16 variables before variable selection of factor analysis in December, 2015.

December (2015)	Elevation	Slope	Aspect	Distance	Population	Household	NDVI	NDBI	MNDWI	SO ₂	PM ₁₀	O ₃	CO	NO ₂	Insolation	Wind
Elevation	1.00	.636	.037	.182	-.138	-.113	.424	.014	-.380	.564	-.560	-.567	-.543	-.539	.841	-.567
Slope	.636	1.00	.038	-.074	-.104	-.078	.451	-.108	-.312	.326	-.318	-.336	-.313	-.298	.473	-.298
Aspect	.037	.038	1.00	.023	-.030	-.026	.080	.006	-.080	.083	-.084	-.082	-.080	-.083	.041	-.077
Distance	.182	-.074	.023	1.00	-.095	-.119	-.219	.215	-.019	.326	-.362	-.274	-.349	-.405	.171	-.474
Population	-.138	-.104	-.030	-.095	1.00	.975	-.094	.047	.080	-.220	.228	.205	.218	.233	-.115	.204
Household	-.113	-.078	-.026	-.119	.975	1.00	-.058	.045	.048	-.191	.200	.175	.191	.207	-.095	.173
NDVI	.424	.451	.080	-.219	-.094	-.058	1.00	-.440	-.727	.226	-.211	-.244	-.217	-.187	.357	-.199
NDBI	.014	-.108	.006	.215	.047	.045	-.440	1.00	-.194	.107	-.115	-.098	-.101	-.120	-.034	-.180
MNDWI	-.380	-.312	-.080	-.019	.080	.048	-.727	-.194	1.00	-.295	.291	.298	.286	.278	-.308	.331
SO₂	.564	.326	.083	.326	-.220	-.191	.226	.107	-.295	1.00	-.995	-.989	-.973	-.968	.477	-.936
PM₁₀	-.560	-.318	-.084	-.362	.228	.200	-.211	-.115	.291	-.995	1.00	.974	.978	.988	-.474	.940
O₃	-.567	-.336	-.082	-.274	.205	.175	-.244	-.098	.298	-.989	.974	1.00	.939	.927	-.479	.920
CO	-.543	-.313	-.080	-.349	.218	.191	-.217	-.101	.286	-.973	.978	.939	1.00	.979	-.459	.918
NO₂	-.539	-.298	-.083	-.405	.233	.207	-.187	-.120	.278	-.968	.988	.927	.979	1.00	-.457	.926
Insolation	.841	.473	.041	.171	-.115	-.095	.357	-.034	-.308	.477	-.474	-.479	-.459	-.457	1.00	-.484
Wind	-.567	-.298	-.077	-.474	.204	.173	-.199	-.180	.331	-.936	.940	.920	.918	.926	-.484	1.00

Table A-7 KMO and Bartlett's Test with 16 variables in December, 2015.

Kaiser-Meyer-Olkin Measure of Sampling Adequacy.		0.721
Approximate Chi-Square		15838341.55
Bartlett's Test of Sphericity	Degree of freedom	120
	Significant	0.000

Table A-8 Selection of variables based on communality values in December, 2015.

Variables	Description	First Communality 16 variables	Second Communality 14 variables
Elevation		.869	.909
Slope		.615	.648
Aspect		.386	
Distance	Distance to the sea (m)	.468	
Population	Population density (person/km2)	.986	.988
Household	Household density (household/ km2)	.988	.988
NDVI_1512	Normalized Difference Vegetation Index (NDVI) in December, 2015	.891	.975
NDBI_1512	Normalized Difference Built-up Index (NDBI) in December, 2015	.874	.985
MNDWI_1512	Normalized Difference Water Index (NDWI) in December, 2015	.853	.980
SO2_1512	Sulfur dioxide (SO2) in December, 2015	.983	.990
PM10_1512	Particulates Matter (PM10) in December, 2015	.989	.995
O3_1512	Ozone (O3) in December, 2015	.944	.953
CO_1512	Carbon monoxide (CO) in December, 2015	.961	.966
NO2_1512	Nitrogen dioxide (NO2) in December, 2015	.967	.967
Inso_1512	Insolation in December, 2015	.746	.803
Wind_1512	Wind speed in December, 2015	.933	.923

Table A-9 Correlation matrix of 14 Variables after variable selection of factor analysis in December, 2015.

December (2015)	Elevation	Slope	Population	Household	NDVI	NDBI	MNDWI	SO ₂	PM ₁₀	O ₃	CO	NO ₂	Insolation	wind
Elevation	1.000	.636	-.138	-.113	.424	.014	-.380	.564	-.560	-.567	-.543	-.539	.841	-.567
Slope	.636	1.000	-.104	-.078	.451	-.108	-.312	.326	-.318	-.336	-.313	-.298	.473	-.298
Population	-.138	-.104	1.000	.975	-.094	.047	.080	-.220	.228	.205	.218	.233	-.115	.204
Household	-.113	-.078	.975	1.000	-.058	.045	.048	-.191	.200	.175	.191	.207	-.095	.173
NDVI	.424	.451	-.094	-.058	1.000	-.440	-.727	.226	-.211	-.244	-.217	-.187	.357	-.199
NDBI	.014	-.108	.047	.045	-.440	1.000	-.194	.107	-.115	-.098	-.101	-.120	-.034	-.180
MNDWI	-.380	-.312	.080	.048	-.727	-.194	1.000	-.295	.291	.298	.286	.278	-.308	.331
SO₂	.564	.326	-.220	-.191	.226	.107	-.295	1.000	-.995	-.989	-.973	-.968	.477	-.936
PM₁₀	-.560	-.318	.228	.200	-.211	-.115	.291	-.995	1.000	.974	.978	.988	-.474	.940
O₃	-.567	-.336	.205	.175	-.244	-.098	.298	-.989	.974	1.000	.939	.927	-.479	.920
CO	-.543	-.313	.218	.191	-.217	-.101	.286	-.973	.978	.939	1.000	.979	-.459	.918
NO₂	-.539	-.298	.233	.207	-.187	-.120	.278	-.968	.988	.927	.979	1.000	-.457	.926
Insolation	.841	.473	-.115	-.095	.357	-.034	-.308	.477	-.474	-.479	-.459	-.457	1.000	-.484
Wind	-.567	-.298	.204	.173	-.199	-.180	.331	-.936	.940	.920	.918	.926	-.484	1.000

Table A-10 KMO and Bartlett's Test with 14 variables in December, 2015.

Kaiser-Meyer-Olkin Measure of Sampling Adequacy.	0.724
Bartlett's Test of Sphericity	Approximate Chi-Square
	15805766.90
	Degree of freedom
	91
	Significant
	0.000

Table A-11 Correlation matrix of 16 variables before variable selection of factor analysis in January, 2016.

January (2016)	Elevation	Slope	Aspect	Distance	Population	Household	NDVI	NDBI	MNDWI	SO ₂	PM ₁₀	O ₃	CO	NO ₂	Insolation	Wind
Elevation	1.000	.636	.037	.182	-.138	-.113	.436	.002	-.417	-.539	-.550	.542	.577	-.559	.828	-.815
Slope	.636	1.000	.038	-.074	-.104	-.078	.471	-.098	-.378	-.306	-.315	.304	.330	-.320	.466	-.501
Aspect	.037	.038	1.000	.023	-.030	-.026	.082	.006	-.084	-.082	-.083	.083	.076	-.084	.042	-.052
Distance	.182	-.074	.023	1.000	-.095	-.119	-.330	.236	.118	-.342	-.345	.375	.343	-.360	.168	-.489
Population	-.138	-.104	-.030	-.095	1.000	.975	-.075	.060	.051	.206	.224	-.233	-.205	.230	-.114	.195
Household	-.113	-.078	-.026	-.119	.975	1.000	-.043	.059	.024	.186	.197	-.207	-.177	.202	-.094	.173
NDVI	.436	.471	.082	-.330	-.075	-.043	1.000	-.438	-.730	-.182	-.176	.158	.184	-.177	.361	-.230
NDBI	.002	-.098	.006	.236	.060	.059	-.438	1.000	-.204	-.084	-.101	.104	.103	-.103	-.043	-.127
MNDWI	-.417	-.378	-.084	.118	.051	.024	-.730	-.204	1.000	.242	.246	-.235	-.254	.249	-.330	.315
SO₂	-.539	-.306	-.082	-.342	.206	.186	-.182	-.084	.242	1.000	.986	-.984	-.962	.976	-.450	.622
PM₁₀	-.550	-.315	-.083	-.345	.224	.197	-.176	-.101	.246	.986	1.000	-.997	-.979	.988	-.459	.646
O₃	.542	.304	.083	.375	-.233	-.207	.158	.104	-.235	-.984	-.997	1.000	.972	-.989	.453	-.651
CO	.577	.330	.076	.343	-.205	-.177	.184	.103	-.254	-.962	-.979	.972	1.000	-.965	.482	-.647
NO₂	-.559	-.320	-.084	-.360	.230	.202	-.177	-.103	.249	.976	.988	-.989	-.965	1.000	-.468	.663
Insolation	.828	.466	.042	.168	-.114	-.094	.361	-.043	-.330	-.450	-.459	.453	.482	-.468	1.000	-.673
Wind	-.815	-.501	-.052	-.489	.195	.173	-.230	-.127	.315	.622	.646	-.651	-.647	.663	-.673	1.000

Table A-12 KMO and Bartlett's Test with 16 variables in January, 2016.

Kaiser-Meyer-Olkin Measure of Sampling Adequacy.		0.783
Approximate Chi-Square		13448159.9927097
Bartlett's Test of Sphericity	Degree of freedom	120
	Significant	0.000

Table A-13 Selection of variables based on communality values in January, 2016.

Variables	Description	First Communality 16 variables	Second Communality 15 variables
Elevation		.899	.904
Slope		.600	.600
Aspect		.252	
Distance	Distance to the sea (m)	.643	.673
Population	Population density (person/km ²)	.985	.987
Household	Household density (household/ km ²)	.986	.987
NDVI_1601	Normalized Difference Vegetation Index (NDVI) in January, 2016	.894	.897
NDBI_1601	Normalized Difference Built-up Index (NDBI) in January, 2016	.875	.938
MNDWI_1601	Normalized Difference Water Index (NDWI) in January, 2016	.845	.909
SO ₂ _1601	Sulfur dioxide (SO ₂) in January, 2016	.977	.980
PM ₁₀ _1601	Particulates Matter (PM10) in January, 2016	.992	.995
O ₃ _1601	Ozone (O ₃) in January, 2016	.991	.993
CO_1601	Carbon monoxide (CO) in January, 2016	.963	.966
NO ₂ _1601	Nitrogen dioxide (NO ₂) in January, 2016	.981	.984
Inso_1601	Insolation in January, 2016	.744	.762
Wind_1601	Wind speed in January, 2016	.860	.872

Table A-14 Correlation matrix of 15 Variables after variable selection of factor analysis in January, 2016.

January (2016)	Elevation	Slope	Distance	Population	Household	NDVI	NDBI	MNDWI	SO ₂	PM ₁₀	O ₃	CO	NO ₂	Insolation	Wind
Elevation	1.000	.636	.182	-.138	-.113	.436	.002	-.417	-.539	-.550	.542	.577	-.559	.828	-.815
Slope	.636	1.000	-.074	-.104	-.078	.471	-.098	-.378	-.306	-.315	.304	.330	-.320	.466	-.501
Distance	.182	-.074	1.000	-.095	-.119	-.330	.236	.118	-.342	-.345	.375	.343	-.360	.168	-.489
Population	-.138	-.104	-.095	1.000	.975	-.075	.060	.051	.206	.224	-.233	-.205	.230	-.114	.195
Household	-.113	-.078	-.119	.975	1.000	-.043	.059	.024	.186	.197	-.207	-.177	.202	-.094	.173
NDVI	.436	.471	-.330	-.075	-.043	1.000	-.438	-.730	-.182	-.176	.158	.184	-.177	.361	-.230
NDBI	.002	-.098	.236	.060	.059	-.438	1.000	-.204	-.084	-.101	.104	.103	-.103	-.043	-.127
MNDWI	-.417	-.378	.118	.051	.024	-.730	-.204	1.000	.242	.246	-.235	-.254	.249	-.330	.315
SO₂	-.539	-.306	-.342	.206	.186	-.182	-.084	.242	1.000	.986	-.984	-.962	.976	-.450	.622
PM₁₀	-.550	-.315	-.345	.224	.197	-.176	-.101	.246	.986	1.000	-.997	-.979	.988	-.459	.646
O₃	.542	.304	.375	-.233	-.207	.158	.104	-.235	-.984	-.997	1.000	.972	-.989	.453	-.651
CO	.577	.330	.343	-.205	-.177	.184	.103	-.254	-.962	-.979	.972	1.000	-.965	.482	-.647
NO₂	-.559	-.320	-.360	.230	.202	-.177	-.103	.249	.976	.988	-.989	-.965	1.000	-.468	.663
Insolation	.828	.466	.168	-.114	-.094	.361	-.043	-.330	-.450	-.459	.453	.482	-.468	1.000	-.673
Wind	-.815	-.501	-.489	.195	.173	-.230	-.127	.315	.622	.646	-.651	-.647	.663	-.673	1.000

Table A-15 KMO and Bartlett's Test with 15 variables in January, 2016.

Kaiser-Meyer-Olkin Measure of Sampling Adequacy.	0.783
Bartlett's Test of Sphericity	Approximate Chi-Square
	13438732.6542336
	Degree of freedom
	105
	Significant
	0.000

Table A-16 Correlation matrix of 16 variables before variable selection of factor analysis in February, 2016.

February (2016)	Elevation	Slope	Aspect	Distance	Population	Household	NDVI	NDBI	MNDWI	SO ₂	PM ₁₀	O ₃	CO	NO ₂	Insolation	Wind
Elevation	1.000	.636	.037	.182	-.138	-.113	.443	.130	-.443	.492	.542	.536	-.549	-.561	.881	-.824
Slope	.636	1.000	.038	-.074	-.104	-.078	.383	.045	-.292	.301	.304	.297	-.313	-.322	.488	-.508
Aspect	.037	.038	1.000	.023	-.030	-.026	.078	.005	-.076	.073	.083	.082	-.083	-.084	.042	-.043
Distance	.182	-.074	.023	1.000	-.095	-.119	-.185	.305	-.152	.281	.376	.391	-.351	-.354	.180	-.484
Population	-.138	-.104	-.030	-.095	1.000	.975	-.062	.003	.055	-.247	-.235	-.239	.226	.227	-.121	.171
Household	-.113	-.078	-.026	-.119	.975	1.000	-.033	.008	.028	-.208	-.208	-.214	.198	.199	-.100	.149
NDVI	.443	.383	.078	-.185	-.062	-.033	1.000	-.429	-.638	.206	.204	.197	-.216	-.223	.400	-.295
NDBI	.130	.045	.005	.305	.003	.008	-.429	1.000	-.308	-.202	.181	.183	-.180	-.187	.093	-.315
MNDWI	-.443	-.292	-.076	-.152	.055	.028	-.638	-.308	1.000	-.357	-.331	-.328	.336	.345	-.394	.507
SO₂	.492	.301	.073	.281	-.247	-.208	.206	.202	-.357	1.000	.894	.893	-.894	-.883	.437	-.595
PM₁₀	.542	.304	.083	.376	-.235	-.208	.204	.181	-.331	.894	1.000	.999	-.998	-.986	.482	-.639
O₃	.536	.297	.082	.391	-.239	-.214	.197	.183	-.328	.893	.999	1.000	-.994	-.984	.477	-.639
CO	-.549	-.313	-.083	-.351	.226	.198	-.216	-.180	.336	-.894	-.998	-.994	1.000	.988	-.488	.637
NO₂	-.561	-.322	-.084	-.354	.227	.199	-.223	-.187	.345	-.883	-.986	-.984	.988	1.000	-.498	.653
Insolation	.881	.488	.042	.180	-.121	-.100	.400	.093	-.394	.437	.482	.477	-.488	-.498	1.000	-.723
Wind	-.824	-.508	-.043	-.484	.171	.149	-.295	-.315	.507	-.595	-.639	-.639	.637	.653	-.723	1.000

Table A-17 KMO and Bartlett's Test with 16 variables in February, 2016.

Kaiser-Meyer-Olkin Measure of Sampling Adequacy.		0.737
Approximate Chi-Square		15536767.543
Bartlett's Test of Sphericity	Degree of freedom	120
	Significant	0.000

Table A-18 Selection of variables based on communality values in February, 2016.

Variables	Description	First Communality 16 variables
Elevation		.876
Slope		.566
Aspect		.741
Distance	Distance to the sea (m)	.536
Population	Population density (person/km ²)	.985
Household	Household density (household/ km ²)	.987
NDVI_1602	Normalized Difference Vegetation Index (NDVI) in February, 2016	.847
NDBI_1602	Normalized Difference Built-up Index (NDBI) in February, 2016	.773
MNDWI_1602	Normalized Difference Water Index (NDWI) in February, 2016	.652
SO ₂ _1602	Sulfur dioxide (SO ₂) in February, 2016	.852
PM ₁₀ _1602	Particulates Matter (PM10) in February, 2016	.990
O ₃ _1602	Ozone (O ₃) in February, 2016	.989
CO_1602	Carbon monoxide (CO) in February, 2016	.987
NO ₂ _1602	Nitrogen dioxide (NO ₂) in February, 2016	.974
Inso_1602	Insolation in February, 2016	.744
Wind_1602	Wind speed in February, 2016	.863

Table A-19 Correlation matrix of 16 variables before variable selection of factor analysis in March, 2016.

March (2016)	Elevation	Slope	Aspect	Distance	Population	Household	NDVI	NDBI	MNDWI	SO ₂	PM ₁₀	O ₃	CO	NO ₂	Insolation	Wind
Elevation	1.000	.636	.037	.182	-.138	-.113	.370	.115	-.353	-.547	.568	.508	-.531	-.531	.954	-.889
Slope	.636	1.000	.038	-.074	-.104	-.078	.395	.056	-.334	-.310	.318	.264	-.292	-.293	.521	-.568
Aspect	.037	.038	1.000	.023	-.030	-.026	.059	.015	-.072	-.083	.083	.082	-.082	-.082	.040	-.049
Distance	.182	-.074	.023	1.000	-.095	-.119	-.372	.235	.126	-.359	.383	.457	-.402	-.393	.197	-.428
Population	-.138	-.104	-.030	-.095	1.000	.975	-.054	-.003	.035	.228	-.213	-.246	.243	.218	-.130	.198
Household	-.113	-.078	-.026	-.119	.975	1.000	-.034	.011	.016	.201	-.184	-.223	.218	.193	-.108	.179
NDVI	.370	.395	.059	-.372	-.054	-.034	1.000	-.586	-.525	-.099	.082	.037	-.075	-.077	.343	-.202
NDBI	.115	.056	.015	.235	-.003	.011	-.586	1.000	-.046	-.167	.201	.166	-.165	-.168	.105	-.206
MNDWI	-.353	-.334	-.072	.126	.035	.016	-.525	-.046	1.000	.186	-.192	-.142	.168	.172	-.330	.264
SO₂	-.547	-.310	-.083	-.359	.228	.201	-.099	-.167	.186	1.000	-.986	-.953	.993	.991	-.526	.656
PM₁₀	.568	.318	.083	.383	-.213	-.184	.082	.201	-.192	-.986	1.000	.954	-.977	-.976	.548	-.680
O₃	.508	.264	.082	.457	-.246	-.223	.037	.166	-.142	-.953	.954	1.000	-.977	-.970	.492	-.660
CO	-.531	-.292	-.082	-.402	.243	.218	-.075	-.165	.168	.993	-.977	-.977	1.000	.995	-.512	.660
NO₂	-.531	-.293	-.082	-.393	.218	.193	-.077	-.168	.172	.991	-.976	-.970	.995	1.000	-.512	.657
Insolation	.954	.521	.040	.197	-.130	-.108	.343	.105	-.330	-.526	.548	.492	-.512	-.512	1.000	-.849
Wind	-.889	-.568	-.049	-.428	.198	.179	-.202	-.206	.264	.656	-.680	-.660	.660	.657	-.849	1.000

Table A-20 KMO and Bartlett's Test with 16 variables in March, 2016.

Kaiser-Meyer-Olkin Measure of Sampling Adequacy.		0.732
Approximate Chi-Square		14552691.2839362
Bartlett's Test of Sphericity	Degree of freedom	120
	Significant	0.000

Table A-21 Selection of variables based on communality values in March, 2016.

Variables	Description	First Communality 16 variables	Second Communality 15 variables	Third Communality 14 variables
Elevation		.924	.944	.944
Slope		.612	.630	.631
Aspect		.877	.029	
Distance	Distance to the sea (m)	.516	.504	.504
Population	Population density (person/km ²)	.985	.986	.986
Household	Household density (household/ km ²)	.987	.988	.988
NDVI_1603	Normalized Difference Vegetation Index (NDVI) in March, 2016	.912	.878	.877
NDBI_1603	Normalized Difference Built-up Index (NDBI) in March, 2016	.743	.730	.741
MNDWI_1603	Normalized Difference Water Index (NDWI) in March, 2016	.473		
SO ₂ _1603	Sulfur dioxide (SO ₂) in March, 2016	.975	.975	.976
PM ₁₀ _1603	Particulates Matter (PM10) in March, 2016	.966	.966	.967
O ₃ _1603	Ozone (O ₃) in March, 2016	.965	.964	.965
CO_1603	Carbon monoxide (CO) in March, 2016	.988	.988	.989
NO ₂ _1603	Nitrogen dioxide (NO ₂) in March, 2016	.982	.983	.984
Inso_1603	Insolation in March, 2016	.845	.863	.863
Wind_1603	Wind speed in March, 2016	.891	.901	.901

Table A-22 Correlation matrix of 14 Variables after variable selection of factor analysis in March, 2016.

March (2016)	Elevation	Slope	Distance	Population	Household	NDVI	NDBI	SO ₂	PM ₁₀	O ₃	CO	NO ₂	Insolation	Wind
Elevation	1.000	.636	.182	-.138	-.113	.370	.115	-.547	.568	.508	-.531	-.531	.954	-.889
Slope	.636	1.000	-.074	-.104	-.078	.395	.056	-.310	.318	.264	-.292	-.293	.521	-.568
Distance	.182	-.074	1.000	-.095	-.119	-.372	.235	-.359	.383	.457	-.402	-.393	.197	-.428
Population	-.138	-.104	-.095	1.000	.975	-.054	-.003	.228	-.213	-.246	.243	.218	-.130	.198
Household	-.113	-.078	-.119	.975	1.000	-.034	.011	.201	-.184	-.223	.218	.193	-.108	.179
NDVI	.370	.395	-.372	-.054	-.034	1.000	-.586	-.099	.082	.037	-.075	-.077	.343	-.202
NDBI	.115	.056	.235	-.003	.011	-.586	1.000	-.167	.201	.166	-.165	-.168	.105	-.206
SO₂_1603	-.547	-.310	-.359	.228	.201	-.099	-.167	1.000	-.986	-.953	.993	.991	-.526	.656
PM₁₀	.568	.318	.383	-.213	-.184	.082	.201	-.986	1.000	.954	-.977	-.976	.548	-.680
O₃	.508	.264	.457	-.246	-.223	.037	.166	-.953	.954	1.000	-.977	-.970	.492	-.660
CO	-.531	-.292	-.402	.243	.218	-.075	-.165	.993	-.977	-.977	1.000	.995	-.512	.660
NO₂	-.531	-.293	-.393	.218	.193	-.077	-.168	.991	-.976	-.970	.995	1.000	-.512	.657
Insolation	.954	.521	.197	-.130	-.108	.343	.105	-.526	.548	.492	-.512	-.512	1.000	-.849
Wind	-.889	-.568	-.428	.198	.179	-.202	-.206	.656	-.680	-.660	.660	.657	-.849	1.000

Table A-23 KMO and Bartlett's Test with 14 variables in March, 2016.

Kaiser-Meyer-Olkin Measure of Sampling Adequacy.	0.745
Bartlett's Test of Sphericity	Approximate Chi-Square
	14302530.982
	Degree of freedom
	91
	Significant
	0.000

Table A-24 Correlation matrix of 16 variables before variable selection of factor analysis in April, 2016.

April (2016)	Elevation	Slope	Aspect	Distance	Population	Household	NDVI	NDBI	MNDWI	SO ₂	PM ₁₀	O ₃	CO	NO ₂	Insolation	Wind
Elevation	1.000	.636	.037	.182	-.138	-.113	.434	-.252	-.477	.550	.578	.539	-.523	-.378	.991	.905
Slope	.636	1.000	.038	-.074	-.104	-.078	.477	-.326	-.464	.316	.333	.290	-.284	-.210	.535	.600
Aspect	.037	.038	1.000	.023	-.030	-.026	.067	-.039	-.071	.081	.082	.083	-.082	-.057	.035	.039
Distance	.182	-.074	.023	1.000	-.095	-.119	-.396	.466	.233	.340	.319	.424	-.413	-.237	.205	.358
Population	-.138	-.104	-.030	-.095	1.000	.975	-.059	.037	.067	-.221	-.198	-.230	.232	.157	-.134	-.175
Household	-.113	-.078	-.026	-.119	.975	1.000	-.027	.019	.037	-.190	-.167	-.205	.206	.155	-.112	-.156
NDVI	.434	.477	.067	-.396	-.059	-.027	1.000	-.790	-.880	.176	.196	.138	-.141	-.133	.405	.342
NDBI	-.252	-.326	-.039	.466	.037	.019	-.790	1.000	.595	-.015	-.028	.018	-.009	.025	-.230	-.140
MNDWI	-.477	-.464	-.071	.233	.067	.037	-.880	.595	1.000	-.259	-.275	-.234	.232	.187	-.454	-.424
SO₂	.550	.316	.081	.340	-.221	-.190	.176	-.015	-.259	1.000	.971	.968	-.973	-.687	.548	.639
PM₁₀	.578	.333	.082	.319	-.198	-.167	.196	-.028	-.275	.971	1.000	.947	-.930	-.675	.575	.638
O₃	.539	.290	.083	.424	-.230	-.205	.138	.018	-.234	.968	.947	1.000	-.987	-.681	.540	.658
CO	-.523	-.284	-.082	-.413	.232	.206	-.141	-.009	.232	-.973	-.930	-.987	1.000	.694	-.523	-.641
NO₂	-.378	-.210	-.057	-.237	.157	.155	-.133	.025	.187	-.687	-.675	-.681	.694	1.000	-.378	-.440
Insolation	.991	.535	.035	.205	-.134	-.112	.405	-.230	-.454	.548	.575	.540	-.523	-.378	1.000	.893
Wind	.905	.600	.039	.358	-.175	-.156	.342	-.140	-.424	.639	.638	.658	-.641	-.440	.893	1.000

Table A-25 KMO and Bartlett's Test with 16 variables in April, 2016.

Kaiser-Meyer-Olkin Measure of Sampling Adequacy.		0.747
Approximate Chi-Square		13576058.3216348
Bartlett's Test of Sphericity	Degree of freedom	120
	Significant	0.000

Table A-26 Selection of variables based on communality values in April, 2016.

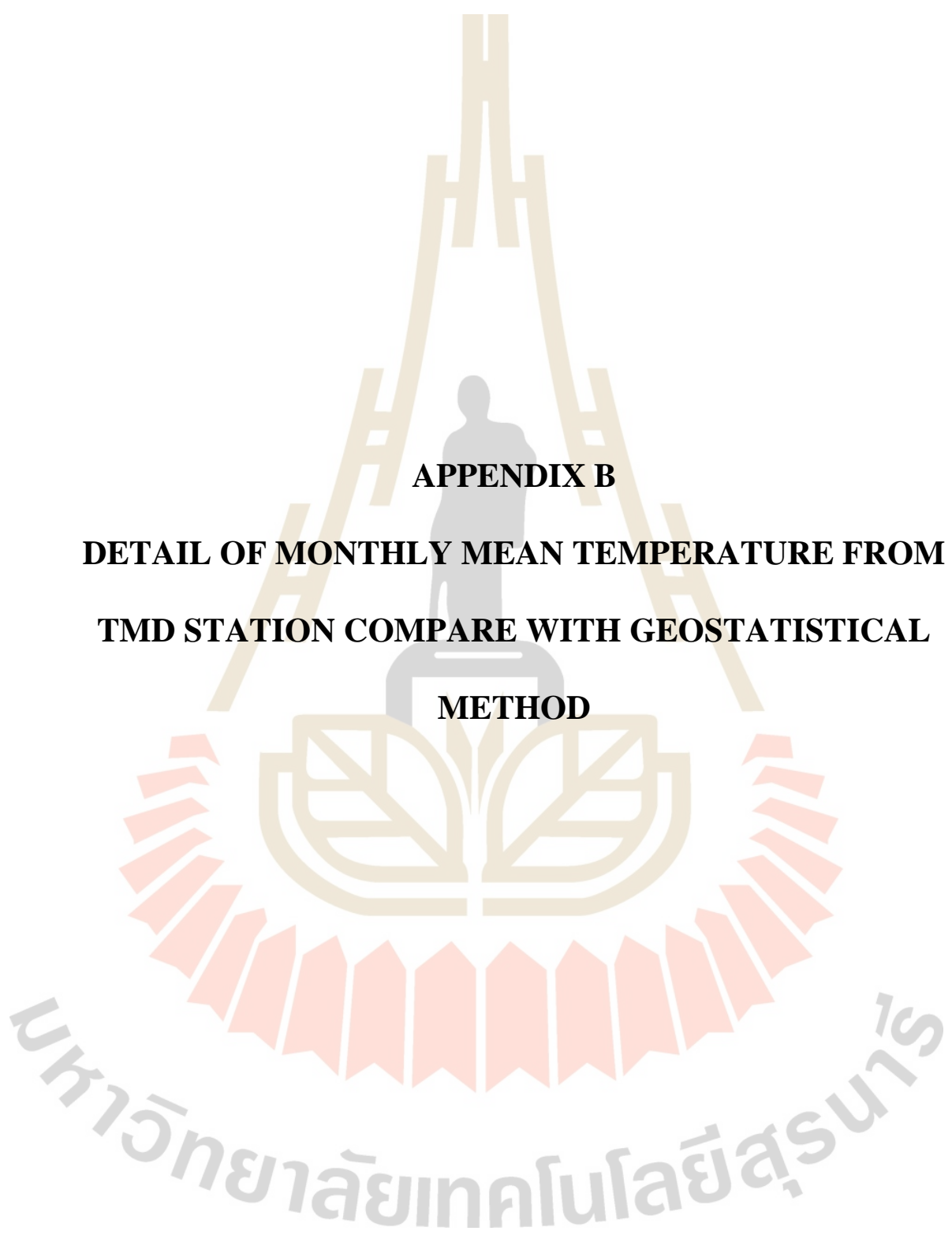
Variables	Description	First Communality 16 variables	Second Communality 15 variables
Elevation		.948	.951
Slope		.589	.591
Aspect		.063	
Distance	Distance to the sea (m)	.646	.655
Population	Population density (person/km ²)	.987	.987
Household	Household density (household/ km ²)	.988	.988
NDVI_1604	Normalized Difference Vegetation Index (NDVI) in April, 2016	.914	.915
NDBI_1604	Normalized Difference Built-up Index (NDBI) in April, 2016	.766	.770
MNDWI_1604	Normalized Difference Water Index (NDWI) in April, 2016	.765	.765
SO ₂ _1604	Sulfur dioxide (SO ₂) in April, 2016	.956	.960
PM ₁₀ _1604	Particulates Matter (PM10) in April, 2016	.927	.930
O ₃ _1604	Ozone (O ₃) in April, 2016	.960	.963
CO_1604	Carbon monoxide (CO) in April, 2016	.958	.961
NO ₂ _1604	Nitrogen dioxide (NO ₂) in April, 2016	.628	.635
Inso_1604	Insolation in April, 2016	.902	.905
Wind_1604	Wind speed in April, 2016	.927	.929

Table A-27 Correlation matrix of 15 Variables after variable selection of factor analysis in April, 2016.

April (2016)	Elevation	Slope	Distance	Population	Household	NDVI	NDBI	MNDWI	SO ₂	PM ₁₀	O ₃	CO	NO ₂	Insolation	Wind
Elevation	1.000	.636	.182	-.138	-.113	.434	-.252	-.477	.550	.578	.539	-.523	-.378	.991	.905
Slope	.636	1.000	-.074	-.104	-.078	.477	-.326	-.464	.316	.333	.290	-.284	-.210	.535	.600
Distance	.182	-.074	1.000	-.095	-.119	-.396	.466	.233	.340	.319	.424	-.413	-.237	.205	.358
Population	-.138	-.104	-.095	1.000	.975	-.059	.037	.067	-.221	-.198	-.230	.232	.157	-.134	-.175
Household	-.113	-.078	-.119	.975	1.000	-.027	.019	.037	-.190	-.167	-.205	.206	.155	-.112	-.156
NDVI	.434	.477	-.396	-.059	-.027	1.000	-.790	-.880	.176	.196	.138	-.141	-.133	.405	.342
NDBI	-.252	-.326	.466	.037	.019	-.790	1.000	.595	-.015	-.028	.018	-.009	.025	-.230	-.140
MNDWI	-.477	-.464	.233	.067	.037	-.880	.595	1.000	-.259	-.275	-.234	.232	.187	-.454	-.424
SO₂	.550	.316	.340	-.221	-.190	.176	-.015	-.259	1.000	.971	.968	-.973	-.687	.548	.639
PM₁₀	.578	.333	.319	-.198	-.167	.196	-.028	-.275	.971	1.000	.947	-.930	-.675	.575	.638
O₃	.539	.290	.424	-.230	-.205	.138	.018	-.234	.968	.947	1.000	-.987	-.681	.540	.658
CO	-.523	-.284	-.413	.232	.206	-.141	-.009	.232	-.973	-.930	-.987	1.000	.694	-.523	-.641
NO₂	-.378	-.210	-.237	.157	.155	-.133	.025	.187	-.687	-.675	-.681	.694	1.000	-.378	-.440
Insolation	.991	.535	.205	-.134	-.112	.405	-.230	-.454	.548	.575	.540	-.523	-.378	1.000	.893
Wind	.905	.600	.358	-.175	-.156	.342	-.140	-.424	.639	.638	.658	-.641	-.440	.893	1.000

Table A-28 KMO and Bartlett's Test with 15 variables in April, 2016.

Kaiser-Meyer-Olkin Measure of Sampling Adequacy.	0.747
Bartlett's Test of Sphericity	Approximate Chi-Square
	13568913.695
	Degree of freedom
	105
	Significant
	0.000



APPENDIX B

**DETAIL OF MONTHLY MEAN TEMPERATURE FROM
TMD STATION COMPARE WITH GEOSTATISTICAL
METHOD**

มหาวิทยาลัยเทคโนโลยีสุรนารี

Table B-1 Detail of monthly mean temperature from TMD station compare with geostatistical method in November.

No.	ID	NAME	Long.	Lat.	1511	2015/11					
						Univariate			Multivariate		
						OK	SK	UK	OCK	SCK	UCK
2	300202	Mae sariang meteorological station	97.97265	19.30007	26.60	26.65	27.63	26.65	26.64	28.13	26.64
3	303201	Chiangrai meteorological station	100.8133	19.12316	25.50	25.49	24.60	25.49	25.48	24.64	25.48
6	327202	Chiangmai(doi angkhang) meteorological station	104.0566	17.12527	19.25	25.65	25.96	25.65	25.64	21.25	25.64
8	328201	Lampang meteorological station	99.14025	16.87998	27.70	27.37	26.62	27.37	27.37	26.73	27.37
12	330201	Phrae meteorological station	100.2766	16.7961	28.20	27.58	28.46	27.58	27.58	27.97	27.58
13	331201	Nan meteorological station	101.1518	16.43447	27.45	26.79	27.24	26.79	26.79	27.05	26.79
14	331301	Nan meteorological station (agromet)	101.2453	16.77397	26.70	26.67	26.99	26.67	26.67	27.39	26.67
18	352201	Nong khai meteorological station	100.5302	15.34964	28.45	27.50	27.87	27.50	27.49	27.88	27.49
20	353301	Loei agrometeorological station	100.1916	15.15823	26.80	28.15	28.44	28.15	28.15	28.41	28.15
25	357301	Nakhon phanom agrometeorological station	105.0196	15.2406	26.60	27.70	28.10	27.70	27.70	28.10	27.70
27	373201	Sukhothai meteorological station	104.3271	15.08686	29.45	28.15	28.86	28.15	28.15	28.88	28.15
33	376401	Umphang hydrometeorological station	100.7249	14.53488	25.35	27.44	26.78	27.44	27.42	26.89	27.42
43	387401	Maha sarakham meteorological station	99.86128	14.30522	28.25	27.88	27.75	27.88	27.89	27.64	27.89
45	400201	Nakhonsawan meteorological station	101.1875	15.26634	29.25	28.59	28.93	28.59	28.59	29.24	28.59
47	402301	Chainat meteorological station	102.1644	14.73959	29.05	29.02	28.90	29.02	29.02	29.59	29.02
49	405201	Roi et meteorological station	103.4487	14.89255	28.30	27.60	27.52	27.60	27.60	27.55	27.60
51	407301	Ubonratchathani agrometeorological station	103.6765	15.31786	28.65	27.76	28.15	27.76	27.76	28.51	27.76
52	407501	Ubonratchathani meteorological station	102.5043	13.68894	28.75	27.75	28.17	27.75	27.75	28.76	27.75
53	409301	Sri saked agrometeorological station	99.97002	14.01186	28.35	27.68	28.25	27.68	27.68	28.44	27.68
57	424301	Ratchaburi meteorological station	100.5599	13.72639	28.70	29.15	29.14	29.15	29.15	29.57	29.15

Table B-1 (Continued).

No.	ID	NAME	Long.	Lat.	1511	2015/11					
						Univariate			Multivariate		
						OK	SK	UK	OCK	SCK	UCK
59	425301	U-thong agrometeorological station	100.5942	13.90931	28.50	29.21	29.13	29.21	29.21	29.37	29.21
75	440201	Aranya prathet meteorological station	101.1356	12.73402	29.45	28.66	28.72	28.66	28.65	29.14	28.65
78	450401	Thong pha phum meteorological station	102.1039	12.61006	28.80	27.96	27.97	27.96	27.94	28.96	27.94
79	451301	Nakhon pathom meteorological station	102.1696	12.51067	28.50	29.36	29.47	29.36	29.36	29.90	29.36
82	455301	Bang na agrometeorological station	99.81048	11.83503	29.90	29.56	30.40	29.56	29.57	30.40	29.57
84	459201	Chonburi meteorological station	99.73467	12.58927	30.35	29.42	29.19	29.42	29.42	29.48	29.42
86	459203	Pattaya meteorological station	102.8783	11.78024	28.60	29.16	29.38	29.16	29.16	29.46	29.16
89	465201	Phetchaburi meteorological station	99.18846	10.49897	29.15	29.08	28.74	29.08	29.08	29.73	29.08
93	480301	Pluei meteorological station	98.59297	9.785049	28.25	29.04	29.51	29.04	29.04	29.71	29.04
95	500202	Hua hin meteorological station	100.0333	9.451267	28.85	28.78	28.12	28.78	28.78	28.60	28.78
100	532201	Ranong meteorological station	99.93965	8.546084	27.90	27.39	27.76	27.39	27.40	27.60	27.40
101	551201	Surat thani meteorological station	99.50348	8.426408	27.25	27.15	27.26	27.15	27.15	28.24	27.15
112	566201	Ko lanta meteorological station	98.39202	7.88416	28.40	27.79	28.04	27.79	27.80	28.71	27.80
118	568502	Hatyai meteorological station	98.30754	8.104029	27.50	27.64	27.61	27.64	27.64	27.62	27.64
119	570201	Satun meteorological station	98.97984	8.100011	28.55	27.77	27.96	27.77	27.78	29.37	27.78
122	583201	Narathiwat meteorological station	100.6041	7.184278	26.75	27.78	27.82	27.78	27.79	29.46	27.79

Table B-2 Detail of monthly mean temperature from TMD station compare with geostatistical method in December.

No.	ID	NAME	Long.	Lat.	1512	2015/12					
						Univariate			Multivariate		
						OK	SK	UK	OCK	SCK	UCK
2	300202	Mae sariang meteorological station	97.97265	19.30007	24.60	24.02	26.29	26.65	24.72	26.05	24.72
3	303201	Chiangrai meteorological station	100.8133	19.12316	22.65	22.34	21.96	25.49	22.12	22.75	22.12
6	327202	Chiangmai(doi angkhang) meteorological station	104.0566	17.12527	16.75	22.72	23.28	25.65	22.87	17.70	22.87
8	328201	Lampang meteorological station	99.14025	16.87998	24.95	24.80	23.87	27.37	24.17	24.68	24.17
12	330201	Phrae meteorological station	100.2766	16.7961	25.40	24.79	25.41	27.58	25.00	26.23	25.00
13	331201	Nan meteorological station	101.1518	16.43447	24.20	23.61	23.68	26.79	23.55	25.29	23.55
14	331301	Nan meteorological station (agromet)	101.2453	16.77397	23.25	23.47	23.46	26.67	23.38	25.57	23.38
18	352201	Nong khai meteorological station	100.5302	15.34964	25.45	24.63	25.13	27.50	24.93	25.85	24.93
20	353301	Loei agrometeorological station	100.1916	15.15823	24.30	25.51	24.68	28.15	24.69	24.79	24.69
25	357301	Nakhon phanom agrometeorological station	105.0196	15.2406	24.15	25.25	25.45	27.70	25.43	25.46	25.43
27	373201	Sukhothai meteorological station	104.3271	15.08686	26.90	25.95	26.59	28.15	26.50	26.76	26.50
33	376401	Umphang hydrometeorological station	100.7249	14.53488	23.45	25.39	23.98	27.44	25.46	24.73	25.46
43	387401	Maha sarakham meteorological station	99.86128	14.30522	26.35	26.00	25.80	27.88	25.88	26.07	25.88
45	400201	Nakhonsawan meteorological station	101.1875	15.26634	27.40	26.81	27.10	28.59	27.02	28.30	27.02
47	402301	Chainat meteorological station	102.1644	14.73959	27.25	27.39	27.13	29.02	27.38	28.48	27.38
49	405201	Roi et meteorological station	103.4487	14.89255	26.55	25.77	25.94	27.60	25.89	26.02	25.89
51	407301	Ubonratchathani agrometeorological station	103.6765	15.31786	27.15	26.19	26.99	27.76	26.21	27.66	26.21
52	407501	Ubonratchathani meteorological station	102.5043	13.68894	27.35	26.05	27.01	27.75	26.35	27.40	26.35
53	409301	Sri saked agrometeorological station	99.97002	14.01186	26.70	26.13	27.03	27.68	26.44	26.91	26.44
57	424301	Ratchaburi meteorological station	100.5599	13.72639	27.75	28.08	28.45	29.15	28.03	28.94	28.03

Table B-2 (Continued).

No.	ID	NAME	Long.	Lat.	1512	2015/12					
						Univariate			Multivariate		
						OK	SK	UK	OCK	SCK	UCK
59	425301	U-thong agrometeorological station	100.5942	13.90931	26.90	27.94	27.83	29.21	27.85	28.67	27.85
75	440201	Aranya prathet meteorological station	101.1356	12.73402	28.65	27.75	28.07	28.66	28.08	28.32	28.08
78	450401	Thong pha phum meteorological station	102.1039	12.61006	27.55	26.41	26.33	27.96	26.89	27.29	26.89
79	451301	Nakhon pathom meteorological station	102.1696	12.51067	26.75	28.22	28.46	29.36	28.20	29.03	28.20
82	455301	Bang na agrometeorological station	99.81048	11.83503	28.90	28.58	29.20	29.56	29.20	29.20	29.20
84	459201	Chonburi meteorological station	99.73467	12.58927	29.15	28.58	28.56	29.42	28.56	28.49	28.56
86	459203	Pattaya meteorological station	102.8783	11.78024	28.20	28.37	28.92	29.16	28.77	28.83	28.77
89	465201	Phetchaburi meteorological station	99.18846	10.49897	28.00	28.14	28.00	29.08	27.98	28.17	27.98
93	480301	Pluei meteorological station	98.59297	9.785049	27.45	28.29	28.73	29.04	28.59	28.97	28.59
95	500202	Hua hin meteorological station	100.0333	9.451267	28.10	27.92	27.44	28.78	27.48	27.86	27.48
100	532201	Ranong meteorological station	99.93965	8.546084	27.85	27.38	27.68	27.39	27.56	28.51	27.56
101	551201	Surat thani meteorological station	99.50348	8.426408	27.50	27.32	27.71	27.15	27.33	29.20	27.33
112	566201	Ko lanta meteorological station	98.39202	7.88416	28.50	28.24	29.15	27.79	28.30	29.39	28.30
118	568502	Hatyai meteorological station	98.30754	8.104029	27.50	27.95	27.73	27.64	27.81	27.87	27.81
119	570201	Satun meteorological station	98.97984	8.100011	28.85	28.11	28.15	27.77	28.04	29.23	28.04
122	583201	Narathiwat meteorological station	100.6041	7.184278	26.95	27.88	27.32	27.78	27.66	28.41	27.66

Table B-3 Detail of monthly mean temperature from TMD station compare with geostatistical method in January.

No.	ID	NAME	Long.	Lat.	1601	2016/01					
						Univariate			Multivariate		
						OK	SK	UK	OCK	SCK	UCK
2	300202	Mae sariang meteorological station	97.97265	19.30007	21.95	21.48	22.18	21.48	21.41	24.34	21.41
3	303201	Chiangrai meteorological station	100.8133	19.12316	20.05	19.68	20.71	19.68	19.38	20.54	19.38
6	327202	Chiangmai(doi angkhang) meteorological station	104.0566	17.12527	15.20	20.87	21.07	20.87	19.82	18.08	19.82
8	328201	Lampang meteorological station	99.14025	16.87998	22.45	21.41	22.14	21.41	22.46	23.36	22.46
12	330201	Phrae meteorological station	100.2766	16.7961	23.05	22.79	22.29	22.79	22.63	24.74	22.63
13	331201	Nan meteorological station	101.1518	16.43447	22.00	22.24	21.36	22.24	21.26	23.42	21.26
14	331301	Nan meteorological station (agromet)	101.2453	16.77397	21.10	21.99	21.24	21.99	21.07	24.05	21.07
18	352201	Nong khai meteorological station	100.5302	15.34964	24.10	24.18	23.27	24.18	23.01	23.31	23.01
20	353301	Loei agrometeorological station	100.1916	15.15823	23.00	23.24	23.80	23.24	23.98	23.54	23.98
25	357301	Nakhon phanom agrometeorological station	105.0196	15.2406	23.70	24.10	24.40	24.10	24.14	23.77	24.14
27	373201	Sukhothai meteorological station	104.3271	15.08686	24.95	24.60	23.92	24.60	24.37	26.52	24.37
33	376401	Umphang hydrometeorological station	100.7249	14.53488	21.30	24.67	24.04	24.67	23.38	22.88	23.38
43	387401	Maha sarakham meteorological station	99.86128	14.30522	25.25	25.00	24.91	25.00	25.19	25.46	25.19
45	400201	Nakhonsawan meteorological station	101.1875	15.26634	26.50	25.13	25.51	25.13	26.00	27.14	26.00
47	402301	Chainat meteorological station	102.1644	14.73959	26.45	26.02	26.21	26.02	26.65	27.37	26.65
49	405201	Roi et meteorological station	103.4487	14.89255	25.85	25.30	24.89	25.30	25.15	25.43	25.15
51	407301	Ubonratchathani agrometeorological station	103.6765	15.31786	26.95	25.96	25.40	25.96	25.86	27.28	25.86
52	407501	Ubonratchathani meteorological station	102.5043	13.68894	26.95	26.14	25.42	26.14	25.80	26.93	25.80
53	409301	Sri saked agrometeorological station	99.97002	14.01186	26.60	26.40	25.45	26.40	25.79	26.75	25.79
57	424301	Ratchaburi meteorological station	100.5599	13.72639	27.20	27.39	27.18	27.39	27.38	28.08	27.38

Table B-3 (Continued).

No.	ID	NAME	Long.	Lat.	1601	2016/01					
						Univariate			Multivariate		
						OK	SK	UK	OCK	SCK	UCK
59	425301	U-thong agrometeorological station	100.5942	13.90931	26.40	27.10	26.92	27.10	27.19	27.84	27.19
75	440201	Aranya prathet meteorological station	101.1356	12.73402	28.10	26.98	26.90	26.98	27.17	27.60	27.17
78	450401	Thong pha phum meteorological station	102.1039	12.61006	26.40	26.24	25.40	26.24	24.60	25.90	24.60
79	451301	Nakhon pathom meteorological station	102.1696	12.51067	26.25	27.41	27.20	27.41	27.48	28.14	27.48
82	455301	Bang na agrometeorological station	99.81048	11.83503	28.05	28.25	27.41	28.25	27.68	27.38	27.68
84	459201	Chonburi meteorological station	99.73467	12.58927	28.10	27.56	27.42	27.56	27.66	27.42	27.66
86	459203	Pattaya meteorological station	102.8783	11.78024	27.40	27.73	27.27	27.73	27.52	27.12	27.52
89	465201	Phetchaburi meteorological station	99.18846	10.49897	27.20	27.56	27.24	27.56	27.41	26.39	27.41
93	480301	Pluei meteorological station	98.59297	9.785049	26.85	27.89	27.40	27.89	27.66	28.52	27.66
95	500202	Hua hin meteorological station	100.0333	9.451267	27.30	27.21	27.16	27.21	27.37	27.44	27.37
100	532201	Ranong meteorological station	99.93965	8.546084	28.30	27.57	27.48	27.57	27.76	28.75	27.76
101	551201	Surat thani meteorological station	99.50348	8.426408	27.70	27.61	27.73	27.61	27.64	28.76	27.64
112	566201	Ko lanta meteorological station	98.39202	7.88416	29.60	28.57	28.70	28.57	28.96	29.12	28.96
118	568502	Hatyai meteorological station	98.30754	8.104029	27.50	27.97	28.24	27.97	28.41	28.63	28.41
119	570201	Satun meteorological station	98.97984	8.100011	29.60	28.65	28.33	28.65	28.63	28.95	28.63
122	583201	Narathiwat meteorological station	100.6041	7.184278	27.25	27.99	27.79	27.99	28.24	28.01	28.24

Table B-4 Detail of monthly mean temperature from TMD station compare with geostatistical method in February.

No.	ID	NAME	Long.	Lat.	1602	2016/02					
						Univariate			Multivariate		
						OK	SK	UK	OCK	SCK	UCK
2	300202	Mae sariang meteorological station	97.97265	19.30007	23.90	24.01	24.68	24.01	24.84	25.16	21.70
3	303201	Chiangrai meteorological station	100.8133	19.12316	22.40	22.10	22.52	22.10	21.84	22.67	22.27
6	327202	Chiangmai(doi angkhang) meteorological station	104.0566	17.12527	17.70	22.84	23.42	22.84	22.95	21.18	22.49
8	328201	Lampang meteorological station	99.14025	16.87998	24.55	24.70	24.69	24.70	24.06	24.70	23.13
12	330201	Phrae meteorological station	100.2766	16.7961	25.00	24.41	24.38	24.41	24.80	25.34	26.28
13	331201	Nan meteorological station	101.1518	16.43447	23.85	23.09	22.95	23.09	23.14	23.84	25.36
14	331301	Nan meteorological station (agromet)	101.2453	16.77397	22.65	22.96	22.84	22.96	22.98	23.31	24.69
18	352201	Nong khai meteorological station	100.5302	15.34964	23.45	22.73	23.41	22.73	23.01	24.70	27.59
20	353301	Loei agrometeorological station	100.1916	15.15823	22.75	24.11	24.01	24.11	23.24	24.00	27.84
25	357301	Nakhon phanom agrometeorological station	105.0196	15.2406	21.60	22.59	23.09	22.59	22.78	23.91	25.45
27	373201	Sukhothai meteorological station	104.3271	15.08686	26.05	25.58	25.55	25.58	26.00	26.44	24.97
33	376401	Umphang hydrometeorological station	100.7249	14.53488	22.15	25.01	24.51	25.01	24.89	23.78	27.84
43	387401	Maha sarakham meteorological station	99.86128	14.30522	24.20	23.96	23.90	23.96	23.83	24.51	27.59
45	400201	Nakhonsawan meteorological station	101.1875	15.26634	27.90	26.80	27.04	26.80	27.35	27.80	26.11
47	402301	Chainat meteorological station	102.1644	14.73959	27.15	27.46	27.63	27.46	27.82	28.18	25.63
49	405201	Roi et meteorological station	103.4487	14.89255	24.30	23.59	23.61	23.59	23.52	24.24	24.28
51	407301	Ubonratchathani agrometeorological station	103.6765	15.31786	25.20	24.32	25.18	24.32	24.41	26.73	24.18
52	407501	Ubonratchathani meteorological station	102.5043	13.68894	25.50	24.02	25.04	24.02	24.44	26.69	27.06
53	409301	Sri saked agrometeorological station	99.97002	14.01186	24.75	24.23	24.80	24.23	24.55	26.13	27.62
57	424301	Ratchaburi meteorological station	100.5599	13.72639	27.05	27.44	27.34	27.44	27.30	28.00	28.05

Table B-4 (Continued).

No.	ID	NAME	Long.	Lat.	1602	2016/02					
						Univariate			Multivariate		
						OK	SK	UK	OCK	SCK	UCK
59	425301	U-thong agrometeorological station	100.5942	13.90931	27.00	27.82	27.73	27.82	27.65	28.09	28.25
75	440201	Aranya prathet meteorological station	101.1356	12.73402	28.05	27.16	27.56	27.16	27.57	27.88	27.13
78	450401	Thong pha phum meteorological station	102.1039	12.61006	27.50	25.69	25.83	25.69	26.32	26.05	27.51
79	451301	Nakhon pathom meteorological station	102.1696	12.51067	26.60	27.91	27.91	27.91	27.80	28.29	27.20
82	455301	Bang na agrometeorological station	99.81048	11.83503	28.00	27.90	28.00	27.90	28.85	28.23	27.07
84	459201	Chonburi meteorological station	99.73467	12.58927	28.50	27.82	27.77	27.82	27.48	27.94	27.33
86	459203	Pattaya meteorological station	102.8783	11.78024	27.45	27.35	27.22	27.35	27.03	27.44	28.37
89	465201	Phetchaburi meteorological station	99.18846	10.49897	27.55	27.23	27.12	27.23	27.08	27.76	26.89
93	480301	Pluei meteorological station	98.59297	9.785049	26.85	27.70	27.77	27.70	28.17	28.28	27.46
95	500202	Hua hin meteorological station	100.0333	9.451267	27.30	27.02	26.68	27.02	26.54	27.30	26.83
100	532201	Ranong meteorological station	99.93965	8.546084	28.35	27.56	27.39	27.56	27.47	28.29	27.09
101	551201	Surat thani meteorological station	99.50348	8.426408	27.35	27.43	27.28	27.43	27.29	28.06	27.57
112	566201	Ko lanta meteorological station	98.39202	7.88416	29.55	28.81	28.82	28.81	28.88	28.89	29.12
118	568502	Hatyai meteorological station	98.30754	8.104029	27.20	28.30	28.26	28.30	28.08	28.46	29.01
119	570201	Satun meteorological station	98.97984	8.100011	29.85	28.56	28.23	28.56	28.31	28.70	28.62
122	583201	Narathiwat meteorological station	100.6041	7.184278	27.30	27.97	27.41	27.97	27.72	28.52	27.95

Table B-5 Detail of monthly mean temperature from TMD station compare with geostatistical method in March.

No.	ID	NAME	Long.	Lat.	1603	2016/03					
						Univariate			Multivariate		
						OK	SK	UK	OCK	SCK	UCK
2	300202	Mae sariang meteorological station	97.97265	19.30007	28.10	28.34	29.22	28.34	29.72	29.48	29.72
3	303201	Chiangrai meteorological station	100.8133	19.12316	26.65	27.33	26.46	27.33	28.57	28.76	28.57
6	327202	Chiangmai(doi angkhang) meteorological station	104.0566	17.12527	22.25	28.37	27.51	28.37	28.59	25.72	28.59
8	328201	Lampang meteorological station	99.14025	16.87998	29.45	28.60	29.40	28.60	29.21	29.69	29.21
12	330201	Phrae meteorological station	100.2766	16.7961	30.05	29.18	29.14	29.18	29.39	29.77	29.39
13	331201	Nan meteorological station	101.1518	16.43447	28.55	28.42	27.11	28.42	28.99	29.46	28.99
14	331301	Nan meteorological station (agromet)	101.2453	16.77397	27.20	28.34	26.90	28.34	28.99	28.15	28.99
18	352201	Nong khai meteorological station	100.5302	15.34964	29.05	29.14	28.35	29.14	29.00	30.30	29.00
20	353301	Loei agrometeorological station	100.1916	15.15823	28.15	29.26	29.01	29.26	29.56	29.27	29.56
25	357301	Nakhon phanom agrometeorological station	105.0196	15.2406	28.00	29.15	28.61	29.15	29.33	30.66	29.33
27	373201	Sukhothai meteorological station	104.3271	15.08686	30.50	30.51	30.30	30.51	29.99	30.44	29.99
33	376401	Umphang hydrometeorological station	100.7249	14.53488	25.25	29.57	29.78	29.57	30.47	29.04	30.47
43	387401	Maha sarakham meteorological station	99.86128	14.30522	30.10	29.48	29.17	29.48	29.12	30.20	29.12
45	400201	Nakhonsawan meteorological station	101.1875	15.26634	32.15	30.06	30.65	30.06	30.28	30.56	30.28
47	402301	Chainat meteorological station	102.1644	14.73959	30.95	30.82	30.84	30.82	30.69	30.53	30.69
49	405201	Roi et meteorological station	103.4487	14.89255	30.10	29.22	28.96	29.22	29.56	29.73	29.56
51	407301	Ubonratchathani agrometeorological station	103.6765	15.31786	29.90	29.16	29.21	29.16	28.97	29.23	28.97
52	407501	Ubonratchathani meteorological station	102.5043	13.68894	30.45	29.60	29.22	29.60	29.45	29.74	29.45
53	409301	Sri saked agrometeorological station	99.97002	14.01186	30.05	29.51	29.32	29.51	29.48	29.89	29.48
57	424301	Ratchaburi meteorological station	100.5599	13.72639	29.95	29.99	30.05	29.99	29.97	30.37	29.97

Table B-5 (Continued).

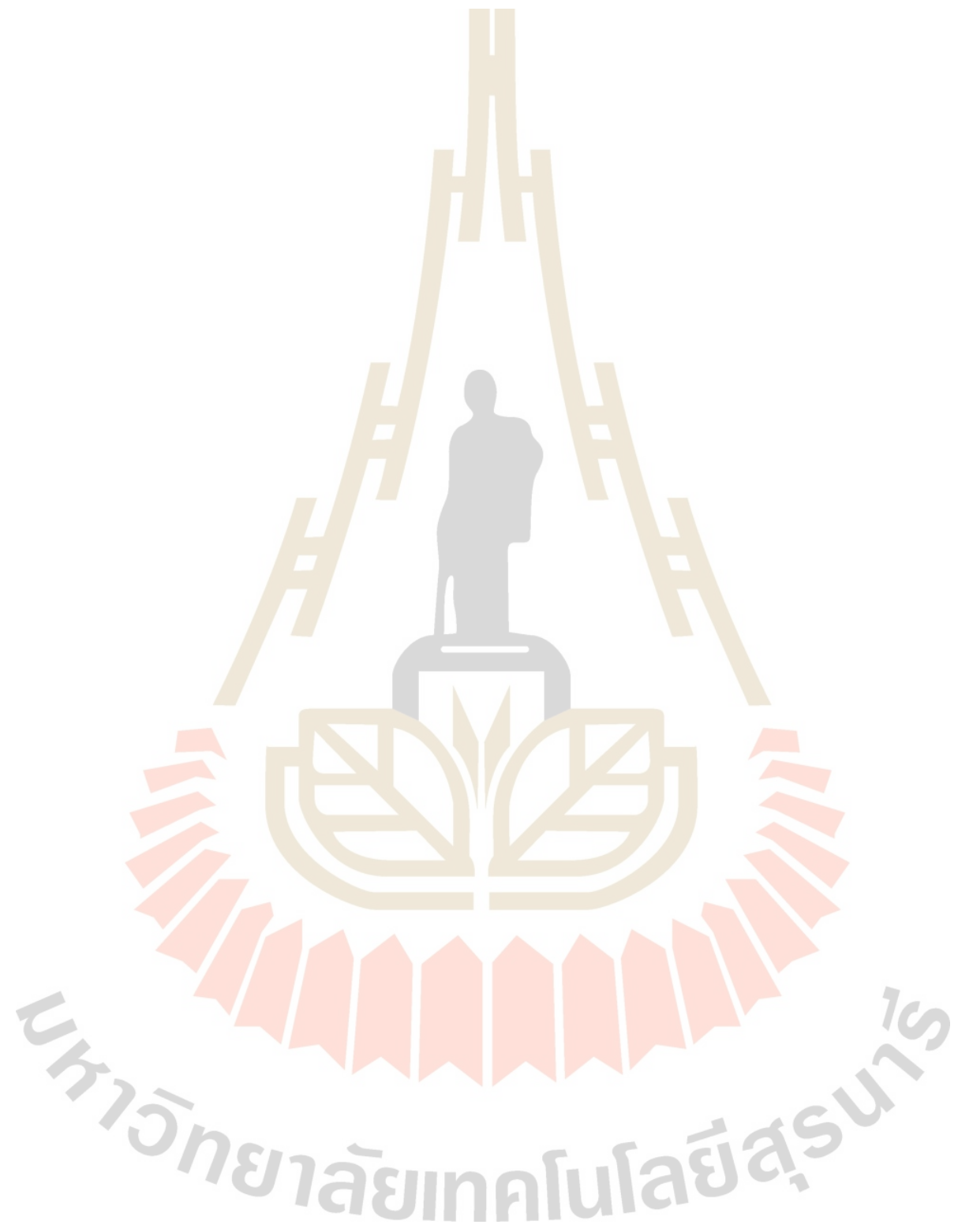
No.	ID	NAME	Long.	Lat.	1603	2016/03					
						Univariate			Multivariate		
						OK	SK	UK	OCK	SCK	UCK
59	425301	U-thong agrometeorological station	100.5942	13.90931	30.75	30.80	30.61	30.80	28.61	30.70	28.61
75	440201	Aranya prathet meteorological station	101.1356	12.73402	31.75	30.46	29.81	30.46	28.49	30.67	28.49
78	450401	Thong pha phum meteorological station	102.1039	12.61006	30.20	29.94	29.89	29.94	29.71	29.83	29.71
79	451301	Nakhon pathom meteorological station	102.1696	12.51067	30.10	30.70	30.50	30.70	28.66	30.08	28.66
82	455301	Bang na agrometeorological station	99.81048	11.83503	30.80	30.45	29.80	30.45	26.57	30.25	26.57
84	459201	Chonburi meteorological station	99.73467	12.58927	30.90	25.55	29.33	25.55	27.20	30.67	27.20
86	459203	Pattaya meteorological station	102.8783	11.78024	29.25	23.49	28.48	23.49	27.68	30.62	27.68
89	465201	Phetchaburi meteorological station	99.18846	10.49897	29.95	29.63	29.11	29.63	27.56	31.41	27.56
93	480301	Pluei meteorological station	98.59297	9.785049	28.30	29.52	29.32	29.52	25.44	29.80	25.44
95	500202	Hua hin meteorological station	100.0333	9.451267	29.00	29.12	28.42	29.12	27.43	30.55	27.43
100	532201	Ranong meteorological station	99.93965	8.546084	29.90	28.53	27.93	28.53	28.80	27.68	28.80
101	551201	Surat thani meteorological station	99.50348	8.426408	28.90	28.66	27.78	28.66	28.92	29.10	28.92
112	566201	Ko lanta meteorological station	98.39202	7.88416	30.25	29.83	29.42	29.83	29.41	28.11	29.41
118	568502	Hatyai meteorological station	98.30754	8.104029	28.50	29.38	28.90	29.38	29.37	29.33	29.37
119	570201	Satun meteorological station	98.97984	8.100011	31.10	29.68	29.07	29.68	29.49	30.13	29.49
122	583201	Narathiwat meteorological station	100.6041	7.184278	27.70	28.79	28.98	28.79	28.66	30.15	28.66

Table B-6 Detail of monthly mean temperature from TMD station compare with geostatistical method in April.

No.	ID	NAME	Long.	Lat.	1604	2016/04					
						Univariate			Multivariate		
						OK	SK	UK	OCK	SCK	UCK
2	300202	Mae sariang meteorological station	97.97265	19.30007	32.80	31.83	32.95	32.95	33.08	32.84	33.08
3	303201	Chiangrai meteorological station	100.8133	19.12316	30.15	30.97	29.40	29.40	32.30	32.19	32.30
6	327202	Chiangmai(doi angkhang) meteorological station	104.0566	17.12527	25.95	32.18	31.13	31.13	32.25	33.64	32.25
8	328201	Lampang meteorological station	99.14025	16.87998	33.65	32.27	33.25	33.25	32.78	32.97	32.78
12	330201	Phrae meteorological station	100.2766	16.7961	34.00	32.87	32.94	32.94	32.87	32.96	32.87
13	331201	Nan meteorological station	101.1518	16.43447	31.95	32.07	31.14	31.14	32.56	32.02	32.56
14	331301	Nan meteorological station (agromet)	101.2453	16.77397	30.60	31.98	30.89	30.89	32.56	31.43	32.56
18	352201	Nong khai meteorological station	100.5302	15.34964	33.00	32.83	32.06	32.06	32.59	32.51	32.59
20	353301	Loei agrometeorological station	100.1916	15.15823	31.60	32.74	32.72	32.72	32.92	32.78	32.92
25	357301	Nakhon phanom agrometeorological station	105.0196	15.2406	31.35	32.80	32.39	32.39	32.96	32.08	32.96
27	373201	Sukhothai meteorological station	104.3271	15.08686	34.05	33.98	33.79	33.79	33.21	33.18	33.21
33	376401	Umphang hydrometeorological station	100.7249	14.53488	28.10	32.42	32.93	32.93	33.17	32.93	33.17
43	387401	Maha sarakham meteorological station	99.86128	14.30522	33.45	33.03	32.89	32.89	32.60	32.71	32.60
45	400201	Nakhonsawan meteorological station	101.1875	15.26634	34.95	32.72	33.50	33.50	32.99	32.03	32.99
47	402301	Chainat meteorological station	102.1644	14.73959	33.30	33.34	33.47	33.47	33.28	32.03	33.28
49	405201	Roi et meteorological station	103.4487	14.89255	33.65	32.86	32.77	32.77	33.01	32.66	33.01
51	407301	Ubonratchathani agrometeorological station	103.6765	15.31786	33.35	31.94	32.60	32.60	32.09	32.13	32.09
52	407501	Ubonratchathani meteorological station	102.5043	13.68894	33.85	32.27	32.63	32.63	32.56	32.28	32.56
53	409301	Sri saked agrometeorological station	99.97002	14.01186	33.20	31.96	32.69	32.69	32.49	32.95	32.49
57	424301	Ratchaburi meteorological station	100.5599	13.72639	32.35	32.10	32.22	32.22	31.91	30.97	31.91

Table B-6 (Continued).

No.	ID	NAME	Long.	Lat.	1604	2016/04					
						Univariate			Multivariate		
						OK	SK	UK	OCK	SCK	UCK
59	425301	U-thong agrometeorological station	100.5942	13.90931	33.25	32.94	33.06	33.06	30.77	30.66	30.77
75	440201	Aranya prathet meteorological station	101.1356	12.73402	33.40	32.31	31.04	31.04	30.36	31.13	30.36
8	450401	Thong pha phum meteorological station	102.1039	12.61006	32.80	32.53	32.65	32.65	32.15	31.59	32.15
79	451301	Nakhon pathom meteorological station	102.1696	12.51067	32.75	32.70	32.73	32.73	30.59	30.34	30.59
82	455301	Bang na agrometeorological station	99.81048	11.83503	32.90	32.21	31.21	31.21	28.14	31.83	28.14
84	459201	Chonburi meteorological station	99.73467	12.58927	32.75	26.74	30.03	30.03	28.72	30.73	28.72
86	459203	Pattaya meteorological station	102.8783	11.78024	30.90	24.78	28.99	28.99	29.23	29.18	29.23
89	465201	Phetchaburi meteorological station	99.18846	10.49897	31.80	31.45	30.73	30.73	29.26	30.67	29.26
93	480301	Pluei meteorological station	98.59297	9.785049	29.35	30.80	29.85	29.85	26.81	20.42	26.81
95	500202	Hua hin meteorological station	100.0333	9.451267	30.90	30.93	29.56	29.56	29.04	31.34	29.04
100	532201	Ranong meteorological station	99.93965	8.546084	30.90	29.98	27.83	27.83	30.34	25.63	30.34
101	551201	Surat thani meteorological station	99.50348	8.426408	31.15	30.20	27.54	27.54	30.43	23.86	30.43
112	566201	Ko lanta meteorological station	98.39202	7.88416	30.70	31.09	29.79	29.79	30.76	21.71	30.76
118	568502	Hatyai meteorological station	98.30754	8.104029	30.15	30.66	29.60	29.60	30.74	29.65	30.74
19	570201	Satun meteorological station	98.97984	8.100011	31.10	30.82	29.75	29.75	30.80	29.57	30.80
122	583201	Narathiwat meteorological station	100.6041	7.184278	29.25	30.61	30.23	30.23	30.29	24.57	30.29



CURRICULUM VITAE

Name Wilawan Prasomsup
Date of Birth October 3, 1985
Place of Birth Kanchanaburi Province, Thailand

Education

2004-2008 Bachelor of Science in Computer Science, Faculty of Informatics, Sripatum University.
2008-2011 Master of Science in Environmental Science, Faculty of Environmental Science, Silpakorn University.
2010-2011 Graduate Diploma in Graduate diploma program of teaching profession, Bansomdejchaopraya Rajabhat University.

มหาวิทยาลัยเทคโนโลยีสุรนารี